

---

# **Interplay between plant cell walls and Jasmonate production**

---

**Dissertation**

zur Erlangung des

Doktorgrades der Naturwissenschaften (Dr. rer. nat.)

vorgelegt der

Naturwissenschaftlichen Fakultät I – Biowissenschaften

**Martin-Luther-Universität Halle-Wittenberg**

von Stefan Mielke

geboren am 13.11.1987 in Forst (Lausitz)

Gutachtende:

I: Prof. Dr. Bettina Hause

II: Prof. Dr. Marcel Quint

III: Prof. Dr. Elizabeth Haswell

eingereicht am: 15.04.2021

verteidigt am: 29.09.2021

## Summary

Plant cells are surrounded by cell walls that support, protect them and act as the immediate contact surface with the extracellular environment. Perturbations in cell walls often lead to misregulated hormonal responses, including jasmonate (JA) accumulation, a crucial regulator of plant defense and growth responses. However, it remained unclear which cellular processes arising from cell wall perturbations are involved in transducing the signal intracellularly and initiate JA production in plastids. In this thesis, I used *Arabidopsis* cellulose-deficient mutants in *KORRIGAN1* (*KOR1*) to unveil such processes.

In fact, *kor1* mutants exhibit strong induction of JA marker genes and elevated levels of the bioactive hormone conjugate (+)-7-*iso*-jasmonoyl-L-isoleucine (JA-Ile) specifically in seedling roots. I further examined the cell wall-triggered induction of JA-Ile biosynthesis in a cell type-specific context and revealed that ectopic JA-Ile signalling in endodermal and pericycle cells was caused by cell-non-autonomous signals deriving from adjacent cortex cells.

To identify components involved in initiating JA-Ile production upon cell wall alterations, I screened for suppressors of JA-Ile in *kor1*, and isolated 12 putative candidates. Among those, mutations in the putative glycosyltransferase *ESMERALDA 1* (*ESMD1*) suppressed elevated JA-Ile production in *kor1* roots, as well as reduced *kor1* root cell expansion by putatively modifying cell wall composition and properties. Consistently, restoring *KOR1* function specifically in cortex cells also restored the JA-Ile phenotype in *kor1*.

Subsequent hyperosmotic treatments phenocopied the suppression of *kor1* root morphology as well as ectopic JA-Ile production. Conversely, hypoosmotic treatments activated JA-Ile signalling in WT plants at similar locations. This ultimately led to a model in which the equilibrium of plant cell walls containing the intracellular hydrostatic water pressure is disturbed. As a consequence, altered cortex cell morphology may exert mechanical stress towards inner tissues, triggering ectopic JA-Ile production. Hence, changes in turgor pressure leading to mechanical compression may be a crucial elicitor of JA-Ile biosynthesis and could occur during other mechanical stresses such as wounding or herbivory.

Remarkably, the consequences of ectopic JA-Ile signalling in *kor1* roots were neither to affect root growth nor canonical defense responses, but included so far unidentified roles of the hormone. Specifically, JA-Ile was important to redirect root growth towards sites with higher water availability. Additionally, root-derived JA-Ile-dependent signals in *kor1* impacted shoot growth and defense responses, suggesting a root-derived signal for whole-plant coordination. Collectively, my results provide new perspectives towards understanding how plants sense and decode extracellular stimuli to initiate acclimation responses.

## Zusammenfassung

Pflanzenzellen sind von Zellwänden umgeben, die sie unterstützen, schützen und als unmittelbare Kontaktfläche mit der extrazellulären Umgebung fungieren. Störungen in Zellwänden führen häufig zu fehlregulierten hormonellen Reaktionen, einschließlich der Akkumulation von Jasmonat (JA), einem entscheidenden Regulator von Stressreaktionen und Wachstumsprozessen. Es ist jedoch unklar, welche zellulären Prozesse, die sich aus Zellwandstörungen ergeben, an der intrazellulären Signalübertragung und der Initiierung der JA-Produktion in Plastiden beteiligt sind. Um solche Prozesse aufzudecken, benutzte ich in dieser Arbeit Arabidopsis-Mutanten mit Cellulosemangel welche im Gen *KORRIGAN1* (*KOR1*) beeinträchtigt sind.

Keimlingswurzeln von *kor1*-Mutanten besitzen eine starke Induktion von JA-Markergenen und erhöhte Spiegel des bioaktiven Hormonkonjugats (+)-7-*iso*-Jasmonoyl-L-Isoleucin (JA-Ile). Ich untersuchte die durch die Zellwand ausgelöste Induktion der JA-Ile-Biosynthese in einem zelltypspezifischen Kontext und stellte fest, dass die ektopische JA-Ile-Signalübertragung in Zellen von Endodermis und Perizykel durch zellunabhängige Signale verursacht wurde, welche von benachbarten Cortexzellen stammen.

Um Komponenten zu identifizieren, die an der Initiierung der JA-Ile-Produktion bei Zellwandveränderungen beteiligt sind, suchte ich in *kor1* nach Suppressoren von JA-Ile. Mutationen in der Glycosyltransferase *ESMERALDA 1* (*ESMD1*) unterdrückten die erhöhte JA-Ile-Produktion in *kor1*-Wurzeln und wiesen eine verringerte Wurzelzellenexpansion auf, was vermutlich auf Modifizierungen der Zellwand beruht. Ebenso konnte durch die Wiederherstellung der *KOR1*-Funktion in Cortexzellen der JA-Ile-Phänotyp in *kor1* unterdrückt werden.

Hyperosmotische Behandlungen phänokopierten die Unterdrückung von *kor1*-Wurzelmorphologie und ektopischer JA-Ile-Produktion. Umgekehrt aktivierten hypoosmotische Behandlungen die JA-Ile-Biosynthese in Wurzeln von Wildtyppflanzen. Eventuell können gestörte Pflanzenzellwände dem intrazellulären hydrostatischen Wasserdruck nicht ausreichend entgegenwirken. Folglich kann die radiale Ausdehnung der Cortexzellen mechanischen Stress im inneren Gewebe ausüben und die JA-Ile-Produktion auslösen. Änderungen des Turgordrucks, die zu mechanischer Kompression führen, könnten daher ein entscheidender Auslöser der JA-Ile-Biosynthese sein und auch bei anderen mechanischen Belastungen wie Verwundung auftreten.

Erstaunlicherweise beeinflusste die ektopische JA-Ile-Signalübertragung in *kor1*-Wurzeln nicht die Wurzelelongation, sondern zeigte bisher nicht identifizierte Rollen des Hormons auf. Insbesondere war JA-Ile wichtig, um das Wurzelwachstum in Richtung höherer Wasserverfügbarkeit umzuleiten. Zusätzlich beeinflussten *kor1*-Wurzeln das Wachstum und die Abwehrreaktionen der Blattrosette in Abhängigkeit von JA-Ile, was auf ein von Wurzeln ausgehendes Signal für die Koordination der gesamten Pflanze schließen lässt. Zusammengefasst zeigen meine Ergebnisse neue Aspekte, um zu verstehen, wie Pflanzen extrazelluläre Reize wahrnehmen, dekodieren und Akklimatisierungsreaktionen auslösen.

Experimental work from this thesis was conducted at the Leibniz Institute of Plant Biochemistry (Halle, Germany), Department of Molecular Signal Processing in the research team 'Jasmonate Signaling' led by Dr. Debora Gasperini.

#### Publications arising from this Doctoral work:

- **Mielke S**, Zimmer M, Meena MK, Dreos R, Stellmach H, Hause B, Voiniciuc C, Gasperini D (2021). Jasmonate biosynthesis arising from altered cell walls is prompted by turgor-driven mechanical compression *Science Advances* 7, doi: 10.1126/sciadv.abf0356  
Contributions: For this research article I performed or supervised the majority of the research (except cell wall analysis and whole genome sequencing data). I designed the figures, wrote the first draft of results and discussion and contributed to writing the final draft.
  - Data presented in chapter 2, 5, 6, 7.1, and 7.2
- **Mielke S**, Gasperini D (2020). Plant–Insect bioassay for testing Arabidopsis resistance to the generalist herbivore *Spodoptera littoralis*. *Methods in Molecular Biology* 2085, 69-78, doi: 10.1007/978-1-0716-0142-6\_5.
  - Contributions: For this methodological book chapter I generated all data, designed the figures, wrote the complete first draft and contributed to writing the final draft.
  - Bioassay method used in chapter 7
- **Mielke S**, Gasperini D (2019). Interplay between plant cell walls and jasmonate production. *Plant & Cell Physiology* 60, 2629-2637, doi: 10.1093/pcp/pcz119.
  - Contributions: For this review article I performed the literature research and wrote the complete first draft. I designed the figures and contributed to writing the final draft.
  - Some concepts are re-presented in Section I (Introduction)
- Schulze A, Zimmer M, **Mielke S**, Stellmach H, Melnyk CW, Hause B, Gasperini D (2019). Wound-induced shoot-to-root relocation of JA-Ile precursors coordinates Arabidopsis growth. *Molecular Plant* 12, 1383-1394, doi: 10.1016/j.molp.2019.05.013.
  - Contributions: For this research article I generated parts of the data for figure 2 and designed experimental concepts for parts of figure 5. This part was in addition to my thesis and is not presented herein, but was essential for mastering micrografting.
  - Grafting method used in chapter 7

#### CONFIDENTIALITY AGREEMENT

Data presented in chapters 3, 4, and 7 is unpublished. Hence, this doctoral thesis contains proprietary and confidential information for evaluation purposes only. The information contained in this document should be kept confidential, should not be disclosed, communicated, nor divulged for any other purpose to any other person or entity.

## Table of Contents

Summary.....	III
Zusammenfassung.....	IV
Table of Contents.....	VI
List of abbreviations.....	VIII
Section I - Introduction.....	1
1. The phytohormone Jasmonate.....	1
2. Activation of the JA pathway.....	7
3. Preparatory work for this thesis.....	15
4. Aims and objectives.....	18
Section II - Results.....	20
1. Are <i>kor1</i> alleles suitable tools to study pathways linking altered cell walls to JA-Ile production?.....	20
2. Is the activation of ectopic JA-Ile signalling in <i>kor1</i> cell-autonomous or non-cell autonomous?.....	23
3. A reverse genetics approach to identify components involved in the initiation of JA-Ile biosynthesis in <i>kor1-4</i> roots.....	26
4. A forward genetic screen identified suppressors of ectopic JA-Ile signalling in <i>kor1</i> ......	35
5. Mutations in <i>ESMD1</i> suppress elevated JA-Ile signalling in <i>kor1</i> .....	41
6. Turgor-driven mechanical changes induce JA-Ile signalling.....	44
7. What are the roles of ectopic JA-Ile signalling in <i>kor1</i> ?.....	51
Section III - Discussion and future perspectives.....	61
1. Advantages of deciphering hormone functions in cell wall mutants.....	61
2. Misregulated turgor pressure in <i>kor1</i> results in mechanical compression of inner tissues leading to JA-Ile biosynthesis.....	67
3. Can osmotically- and mechanically-driven changes in turgor pressure act as general elicitors of JA-Ile biosynthesis beyond cell wall alterations?.....	74
Section IV - Material & Methods.....	77
References.....	89

Appendix .....	110
Acknowledgements .....	143
Curriculum vitae .....	145
List of publications.....	147
Eidesstattliche Erklärung (Statutory declaration) .....	148

## List of abbreviations

Throughout this thesis the amino acid three-letter or one-letter code is used according to IUPAC-IUB (recommendations 1983).

ABA	Abscisic acid
ACA <sub>13</sub>	CALCIUM-TRANSPORTING ATPase <sub>13</sub>
ACBP6	ACYL-COA-BINDING PROTEIN <sub>6</sub>
AGI	Arabidopsis gene identifier
AIR	Alcohol insoluble residue
ANOVA	Analysis of Variance
AOC	ALLENE OXIDE CYCLASE
AOS	ALLENE OXIDE SYNTHASE
ATP	Adenosine triphosphate
AVG	Aminoethoxyvinylglycine
BC	Backcross
BGLU	BETA-GLUCOSIDASE
bHLH	Basic helix-loop-helix
BiFC	Bimolecular fluorescence complementation
BGLU	BETA-GLUCOSIDASE
BRI <sub>1</sub>	BRASSINOSTEROID INSENSITIVE <sub>1</sub>
CAPS	Cleaved Amplified Polymorphic Sequences
cDNA	Complementary DNA
CesA	CELLULOSE SYNTHASE
<i>cev1</i>	<i>constitutive expression of VSP<sub>1</sub></i>
CIT	CITRINE
CML	CALMODULIN-LIKE PROTEIN
CMTA <sub>3</sub>	CALMODULIN BINDING TRANSCRIPTIONAL ACTIVATOR <sub>3</sub>
COB	COBRA
COI <sub>1</sub>	CORONATINE INSENSITIVE <sub>1</sub>
CrRLK <sub>1L</sub>	<i>Catharanthus roseus</i> RECEPTOR-LIKE KINASE <sub>1</sub> -LIKE
CSC	Cellulose synthase complex
CTL <sub>1</sub>	CHITINASE-LIKE PROTEIN <sub>1</sub>
CTS	COMATOSE
CWI	Cell wall integrity
DAD <sub>1</sub>	DEFECTIVE IN ANTHOR DEHISCENCE <sub>1</sub>
DAMP	Damage-associated molecular pattern
DEG	Differentially expressed gene
DEK <sub>1</sub>	DEFECTIVE KERNEL <sub>1</sub>
DGDG	Digalactosyldiacylglycerol
DIC	Differential interface contrast
DIR <sub>5</sub>	DIRIGENT PROTEIN <sub>5</sub>
DNA	Deoxyribonucleic acid
EDD <sub>1</sub>	EMBRYO-DEFECTIVE-DEVELOPMENT <sub>1</sub>
e.g.	<i>exempli gratia</i> – for example
EGF	Epidermal growth factor
EGTA	Ethylene glycol-bis( $\beta$ -aminoethyl ether)-N,N,N',N'-tetra acetic acid



EIL <sub>1</sub>	ETHYLENE INSENSITIVE-LIKE 1
EIN	ETHYLENE INSENSITIVE
EMS	Ethyl methanesulfonate
ER	Endoplasmatic reticulum
ERAD	Endoplasmatic reticulum-associated degradation
ERU	ERULUS
ESMD <sub>1</sub>	ESMERALDA 1
ET	Ethylene
EXT <sub>12</sub>	EXTENSIN 12
FAMT	FARNESOIC ACID CARBOXYL-O-METHYLTRANSFERASE
FER	FERONIA
Fig.	Figure
FLA6	FASCICLIN-LIKE ARABINOGALACTAN 6
FW	Fresh weight
GA <sub>2</sub> OX <sub>2</sub>	GIBBERELLIN 2-OXIDASE
GFP	Green Fluorescent Protein
GH	GLYCOSYL HYDROLASE
GLR	GLUTAMATE RECEPTOR-LIKE
GO	Gene ontology
GPI	Glycosylphosphatidylinositol
GT	GLYCOSYLTRANSFERASE
GUS	Beta-glucuronidase
HAMP	Herbivore-associated molecular pattern
HDA	HISTONE DEACETYLASE
HDC <sub>1</sub>	HISTONE DEACETYLATION COMPLEX 1
HERK	HERKULES
HG	Homogalacturonan
HORST	HYDROXYLASE OF SUBERIZED TISSUE
HPAEC-PAD	High-performance anion-exchange chromatography with pulsed amperometric detection
HSD	Honest significant difference
IAA	Indole-3-acetic acid
IAMT <sub>1</sub>	IAA CARBOXYMETHYLTRANSFERASE 1
IAR <sub>3</sub>	IAA-ALANINE RESISTANT 3
i.e.	<i>id est</i> - that is to say
IGMT <sub>1</sub>	INDOLE GLUCOSINOLATE O-METHYLTRANSFERASE 1
ILL6	IAA-LEUCINE RESISTANT-LIKE 6
IRT <sub>1</sub>	IRON-REGULATED TRANSPORTER 1
<i>ixr1</i>	<i>isoxaben resistant 1</i>
JgV	Jasg-VENUS
JA	Jasmonate
JA-Ile	(+)-7- <i>iso</i> -jasmonoyl-L-isoleucine
JAO	JASMONATE OXYGENASE
JAR <sub>1</sub>	JASMONATE RESITANT 1
JAZ	JASMONATE ZIM-DOMAIN
<i>JGP</i>	<i>JAZ1op:GUSPlus</i>
JMT	JASMONIC ACID CARBOXY METHYL TRANSFERASE
JOX	JASMONIC ACID OXIDASE

KD	Knockdown
KO	Knockout
KOR1	KORRIGAN 1
LEA4-5	LATE EMBRYOGENESIS ABUNDANT 4-5
LECRK52	CONCAVALIN A-LIKE LECTIN PROTEIN KINASE 52
logFC	Logarithmic fold change
LOQ	Limit of quantification
LOX	LIPOXYGENASE
LSM	Laser scanning microscope
MAMP	Microbe-associated molecular pattern
MCA1	MATING PHEROMONE INDUCED DEATH 1-COMPLEMENTING ACTIVITY 1
MED	MEDIATOR
MeJA	Methyl-Jasmonate
MGDG	Monogalactosyldiacylglycerol
MIK	MDIS1-INTERACTING RECEPTOR LIKE KINASE1
MIOX4	MYO-INOSITOL OXYGENASE 4
MRI	MARIS RECEPTOR KINASE
MRN1	MARNERAL SYNTHASE 1
mRNA	messenger ribonucleic acid
MS	Murashige and Skoog media
MSL	MECHANOSENSITIVE CHANNEL OF SMALL CONDUCTANCE-LIKE
mTurq	mTurquoise2
n.a.	Not analysed
NASC	Nottingham Arabidopsis Stock Centre
n.d.	Not determined
NGS	Next generation sequencing
NINJA	NOVEL INTERACTOR OF JAZ
NLS	Nuclear localisation signal
NRT	NITRATE TRANSPORTER
OG	Oligogalacturonides
OPDA	12-oxo-phytodienoic acid
OPR	OXO-PHYTODIENOIC ACID REDUCTASE
OS9	OSTEOSARCOMA-AMPLIFIED GENE 9
OSCA1	REDUCED HYPEROSMOLALITY - INDUCED CA <sub>2</sub> <sup>+</sup> INCREASE 1
PCR	Polymerase chain reaction
PDF	PLANT DEFENSIN
PE	Paired-end
PEG	Polyethyleneglycol
PEP	PLASTID ENDOPEPTIDASE
PER	PEROXIDASE
PHYB	PHYTOCHROME B
PI	Propidium iodide
PIN1	PIN-FORMED 1
PLAT	Polycystin-1, Lipoxygenase, Alpha-Toxin
PLL	PECTIN LYASE-LIKE
PME	PECTIN METHYL ESTERASE
PRR	Pattern recognition receptors
PUFA	Polyunsaturated fatty acid

qRT-PCR	Real-time quantitative reverse transcription PCR
QUA	QUASIMODO
RALF	RAPID ALKALINIZATION FACTOR
RAM	Root apical meristem
RFP	Red Fluorescent Protein
RG	Rhamnogalacturonan
RLK	RECEPTOR-LIKE KINASE
RLP	RECEPTOR-LIKE PROTEIN
RNA	Ribonucleic acid
ROS	Reactive oxygen species
SAM	Shoot apical meristem
SCF-E <sub>3</sub>	SKP, Cullin, F-box containing E <sub>3</sub> ubiquitin ligase
SCR	SCARECROW
SD	Standard deviation
<i>S. littoralis</i>	<i>Spodoptera littoralis</i>
SNP	Single nucleotide polymorphism
SQP <sub>2</sub>	SQUALENE MONOOXYGENASE 2
ST <sub>2A</sub>	SULFOTRANSFERASE 2A
SUB	STRUBBELIG
Tab.	Table
TAIR	The Arabidopsis information resource
TAT <sub>3</sub>	TYROSINE AMINOTRANSFERASE 3
TCH <sub>3</sub>	TOUCH 3
T-DNA	Transfer-DNA
TF	Transcription factor
THE <sub>1</sub>	THESEUS 1
TGN	Trans-golgi network
TPC <sub>1</sub>	TWO PORE CHANNEL 1
TPL	TOPLESS
TPS <sub>13</sub>	TERPENE SYNTHASE 13
Ub	Ubiquitin
UBC <sub>21</sub>	UBIQUITIN-CONJUGATING ENZYME 21
UDP	Uracil diphosphate
UTR	Untranslated region
VEN	VENUS
VSP <sub>2</sub>	VEGETATIVE STORAGE PROTEIN 2
WAK	WALL-ASSOCIATED KINASE
WGS	Whole-genome sequencing
WOL	WOODEN LEG
WT	Wildtype
XTH	Xyloglucan endotransglycolases/hydrolases



## Section I - Introduction

*Concepts herein were partially reviewed in (Mielke and Gasperini, 2019, Plant and Cell Physiology).*

### 1. The phytohormone Jasmonate

In response to injury or infection, animals as well as plants rapidly produce oxygenated polyunsaturated fatty acid (PUFA) derivatives (also known as oxylipins), which can function as signalling molecules and mediate stress acclimation (Dennis and Norris, 2015; Wasternack and Feussner, 2018). Plant oxylipins include the phytohormone jasmonic acid (JA), its precursors and derivatives (collectively referred to as Jasmonates, JAs), which control a wide range of developmental and stress responses (Wasternack and Feussner, 2018). Specifically, JAs are important to protect plants against herbivorous insects and necrotrophic pathogens and play a role in tolerance against abiotic stresses such as mechanical wounding, cold, drought and salt (Wasternack and Feussner, 2018). Furthermore, their important functions in plant development include growth inhibition, promotion of senescence, and reproductive organ development (Huang et al., 2017; Wasternack and Feussner, 2018).

#### JA biosynthesis and metabolism

In vascular plants such as *Arabidopsis thaliana* (*Arabidopsis*), JAs act through their bioactive amino acid conjugate (+)-7-*iso*-jasmonoyl-L-isoleucine (JA-Ile) (Fonseca et al., 2009). The biosynthesis of JA-Ile involves the orchestration of enzymes from three subcellular compartments (Fig. 1), reviewed in (Wasternack and Strnad, 2018). The pathway initiates in plant plastids from 18:3 and 16:3 polyunsaturated fatty acids, namely  $\alpha$ -linolenic acid and hexadecatrienoic acid. These compounds are bound in the form of monogalactosyldiacylglycerols (MGDGs), which are stored in the inner membrane of the plastidial envelope as well as in thylakoid membranes (Li and Yu, 2018). They are thought to be released by specific acyl-lipid hydrolases, i.e. lipases, reviewed in (Wasternack and Hause, 2013). However, to date the only lipase shown to be involved in the formation of JAs is the flower-specific DEFECTIVE IN ANther DEHISCENCE (DAD1) phospholipase A1, which de-esterifies  $\alpha$ -linolenic acid and is essential for JA-Ile biosynthesis and promotes male fertility (Ishiguro et al., 2001). Following de-esterification of 18:3 and 16:3 substrates, plastid-localized members of the 13-LIPOXYGENASE family (4 members in *Arabidopsis*: LOX2, LOX3, LOX4, and LOX6) catalyse the insertion of molecular oxygen at position 13 of the  $\alpha$ -linolenic acid and hexadecatrienoic acid carbon chains (Bannenberg et al., 2009). The resulting products from this reaction are the hydroperoxides 13(*S*)-hydroperoxy-octadecatrienoic acid (13-HPOT) and 11(*S*)-hydroperoxy-hexadecatrienoic acid (11-HPHT) that then undergo conversion to the allene oxides (13*S*)-12,13-epoxy-octadecatrienoic acid (12,13-EOT) and (11*S*)-10,11-epoxy-octadecatrienoic acid (10,11-EOT), a reaction catalysed by a single

copy gene called *ALLENE OXIDE SYNTHASE (AOS)* in *Arabidopsis* (Laudert et al., 1996). An *Arabidopsis aos* knockout mutant is completely deprived of JAs and hence does not exhibit JA-Ile mediated responses (Park et al., 2002).

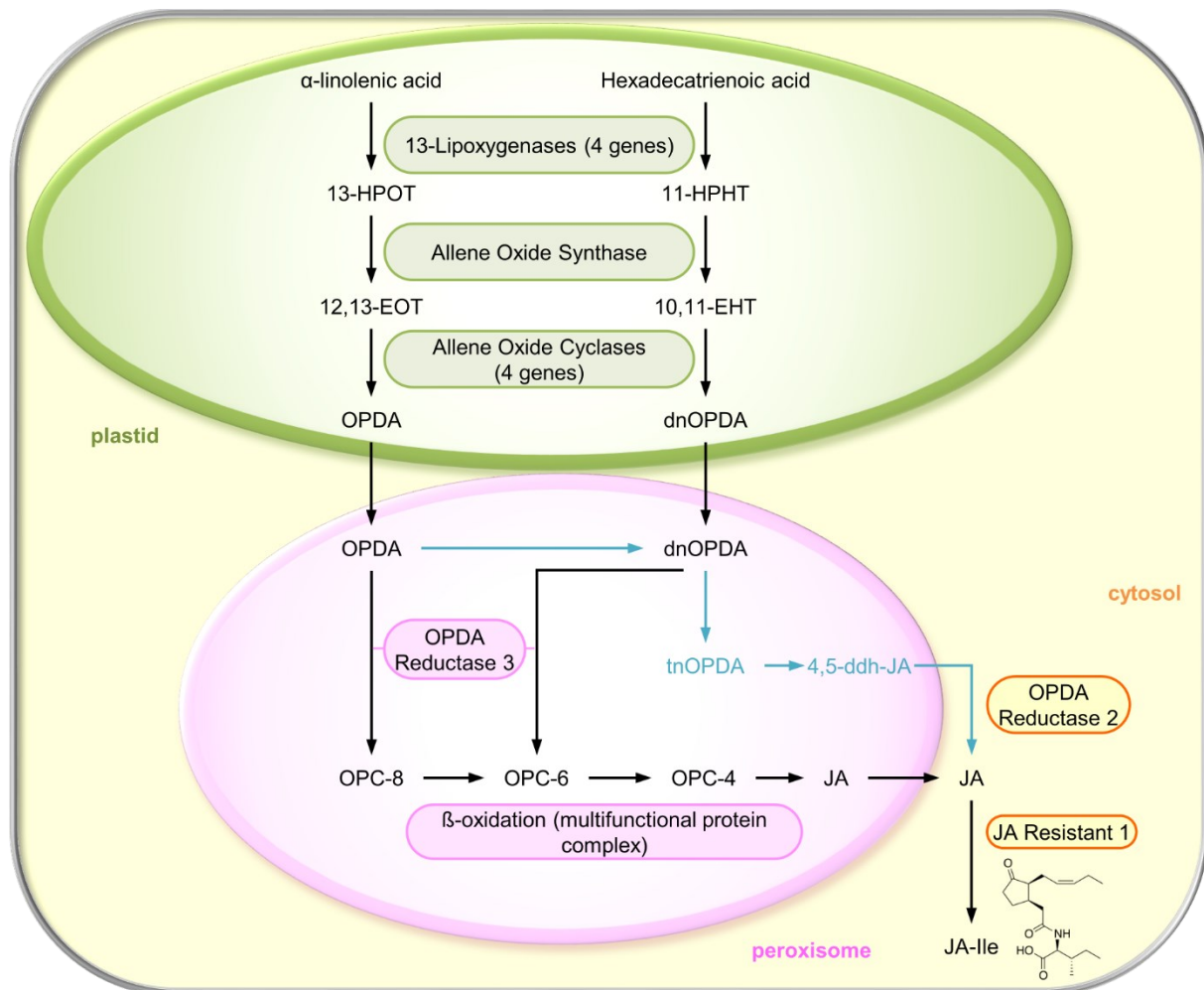


**Figure 1: JA-Ile biosynthesis in *Arabidopsis*.** The pathway initiates from de-esterification of plastidial membrane lipids (mainly galactolipids) to yield linolenic acid and hexadecatrienoic acid. Enzymes catalysing the following reactions are given in boxes. The alternative pathway yielding the formation of JA according to (Chini et al., 2018) is indicated by blue arrows. Abbreviations: 13-HPOT (13(S)-hydroperoxy-octadecatrienoic acid), 11-HPHT (11(S)-hydroperoxy-hexadecatrienoic acid), 12,13-EOT (13(S)-12,13-epoxy-octadecatrienoic acid, 10,11-EOT (11(S)-10,11-epoxy-octadecatrienoic acid), OPDA (12-oxo-phytodienoic acid), dnOPDA (dinor-oxo-phytodienoic acid), OPC-8 (3-oxo-2-(2-(Z)-pentenyl)-cyclopentane-1-octanoic acid), OPC-6 (3-oxo-2-(2-(Z)-pentenyl)-cyclopentane-1-hexanoic acid), OPC-4 (3-oxo-2-(2-(Z)-pentenyl) cyclopentane-1 butanoic acid), tnOPDA (tetranor-OPDA), 4,5-ddh-OPDA (4,5-didehydro JA), JA ((+)-7-iso-jasmonic acid), JA-Ile ((+)-7-iso-jasmonoyl-isoleucine).

As the produced allene oxides are highly unstable, they are rapidly converted by members of the ALLENE OXIDE CYCLASE (AOC) family (Stenzel et al., 2003) into 12-oxo-phytodienoic acid (OPDA) and dinor-oxo-phytodienoic acid (dnOPDA). Interestingly, dn-OPDA was recently shown to be a bioactive jasmonate in the early land plant *Marchantia polymorpha* which is unable to synthesize JA-Ile (Monte et al., 2018). In *Arabidopsis* though, dn-OPDA levels are very low and the octadecanoic pathway leading from  $\alpha$ -linolenic acid to OPDA produces the majority of precursors for JA-Ile

biosynthesis (Chini et al., 2018). OPDA and dn-OPDA are then exported from the plastid and imported into the peroxisome, presumably through the transporters JASSY (Guan et al., 2019) and COMATOSE (CTS) (Theodoulou et al., 2005), respectively. The peroxisome-localized enzyme OXO-PHYTODIENOIC ACID REDUCTASE 3 (OPR3) reduces OPDA and dn-OPDA to the cyclopentanones 3-oxo-2-(2-(Z)-pentenyl)-cyclopentane-1-octanoic (OPC-8) and hexanoic (OPC-6) acids (Breithaupt et al., 2006). A multifunctional enzyme complex then catalyses several rounds of  $\beta$ -oxidation (Li et al., 2005; Delker et al., 2007), resulting in (+)-7-*iso*-jasmonic acid (JA) production. Finally, in the cytosol, JA is conjugated to JA-Ile by the GLYCOSIDE HYDROLASE 3 (GH3) enzyme JASMONATE RESISTANT 1 (JAR1) (Staswick et al., 1992; Staswick and Tiryaki, 2004; Westfall et al., 2012). In an alternative pathway, OPDA can be directly converted to dn-OPDA, then to 4,5-didehydrojasmonate (4,5-ddh-JA), which is finally reduced to JA by the cytosolic enzyme OPR2 (Chini et al., 2018).

In addition to forming the JA-Ile conjugate, JA can undergo further metabolic routes through many enzymatic modifications, reviewed in (Koo, 2018; Heitz et al., 2019). This includes for example the conjugation to other amino acids such as JA-Val, JA-Leu, JA-Met, and JA-Ala, whose endogenous levels after wounding are much lower than JA-Ile (Staswick and Tiryaki, 2004; Yan et al., 2016). Moreover, JA can undergo hydroxylation by JASMONIC ACID OXIDASE (JOX) / JASMONATE-INDUCED OXYGENASE (JAO) to 12-hydroxy-JA (Caarls et al., 2017; Smirnova et al., 2017), sulfation by SULFOTRANSFERASE 2A (ST2A) to 12-HSO<sub>4</sub>-JA (Gidda et al., 2003) or methylation by JASMONIC ACID CARBOXY METHYL TRANSFERASE (JMT) to Methyl-JA (MeJA) (Seo et al., 2001). However, the biological activity of these JA conjugates remains disputed or unknown in Arabidopsis, suggesting they may simply be catabolites and regulate JA levels, reviewed in (Koo, 2018; Heitz et al., 2019). Indeed, a *jox* quadruple mutant accumulates more JA and higher expression levels of JA signalling marker genes at basal conditions and after wounding (Caarls et al., 2017; Smirnova et al., 2017).

The bioactive JA-Ile hormone can also be further metabolized by cytochrome P<sub>450</sub> monooxygenases of the CYP9<sub>4</sub> family, which generate 12-hydroxy-JA-Ile and 12-carboxy-JA-Ile in successive oxidation reactions (Kitaoka et al., 2011; Koo et al., 2011; Heitz et al., 2012). Another JA-Ile catabolic route is characterized by the deconjugation of JA-Ile into JA through amidohydrolases IAA-ALANINE RESISTANT 3 (IAR3) and IAA-LEUCINE RESISTANT-LIKE 6 (ILL6) (Widemann et al., 2013). Although these metabolic routes were initially thought to be important for control of JA-Ile signalling only, recent studies also propose an independent signalling activity of certain catabolites such as 12-hydroxy-JA-Ile (Jimenez-Aleman et al., 2019; Poudel et al., 2019; Marquis et al., 2020).

## JA-Ile perception and signalling

The activation of JA-Ile-dependent transcriptomic, proteomic, and metabolic changes is energetically costly (Baldwin, 1998; Havko et al., 2016) and is hence kept being repressed at basal conditions when endogenous JA-Ile levels are low such as in vegetative tissues (Glauser et al., 2009; Schulze et al., 2019). In the absence of JA-Ile, JA-Ile-dependent transcription factors (TFs) of the basic helix-loop-helix (bHLH) family, the most prominent being MYC<sub>2</sub>, <sub>3</sub>, and <sub>4</sub> (Lorenzo et al., 2004; Fernandez-Calvo et al., 2011), are kept repressed by a modular repressor complex. This complex is composed of JASMONATE ZIM-DOMAIN (JAZ) proteins, which form a group of transcriptional modulators with thirteen members in Arabidopsis (Chini et al., 2007; Thines et al., 2007; Yan et al., 2007; Thireault et al., 2015) that can suppress target TFs by recruiting the transcriptional repressor TOPLESS (TPL) or TPL-related proteins (TPRs) either directly or through the adaptor protein NOVEL INTERACTOR OF JAZ (NINJA, Fig. 2) (Pauwels et al., 2010; Shyu et al., 2012). TPL in turn recruits histone deacetylases like HDA6 or HDA19, leading to a reduced chromatin accessibility and repression of gene expression (Pauwels et al., 2010; Zhu et al., 2011).

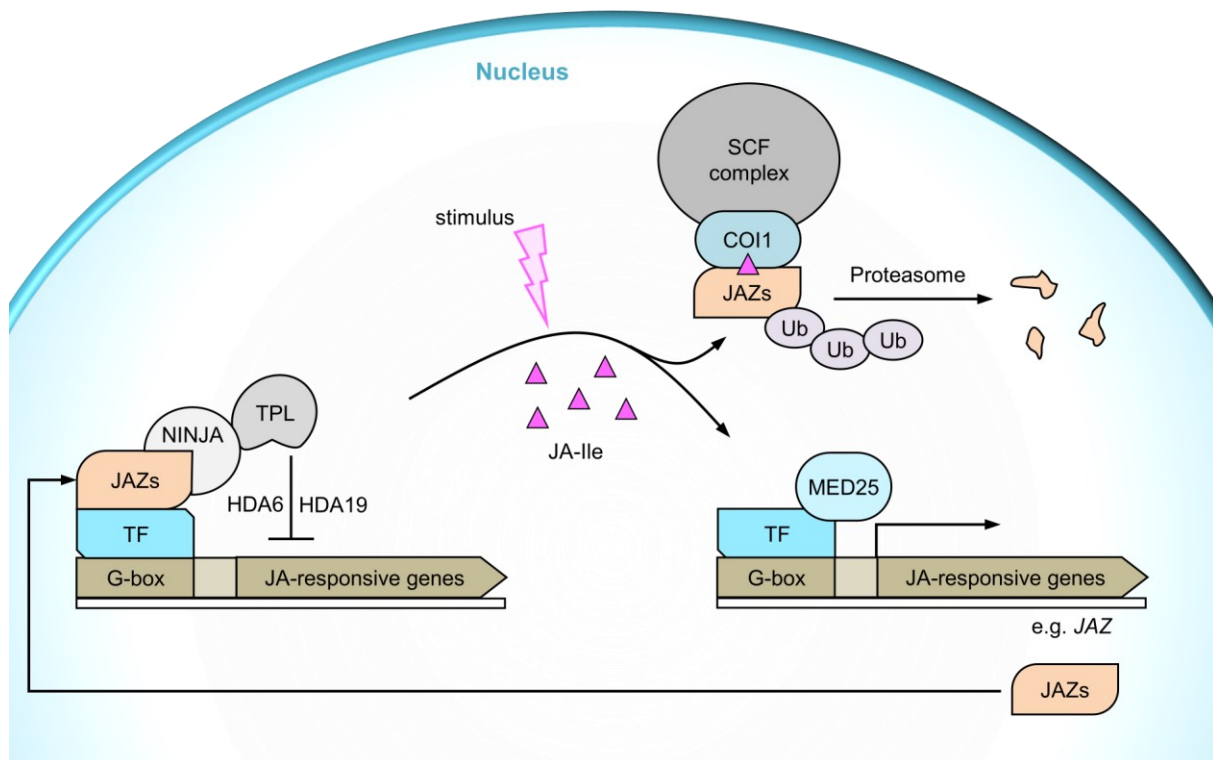


**Figure 2: Scheme of JA-Ile perception and signalling.** At low JA-Ile levels, the JAZ-NINJA-TPL repressor complex inhibits G-Box binding TFs, such as MYC<sub>2</sub>, MYC<sub>3</sub>, and MYC<sub>4</sub>, by recruiting HISTONE DEACETYLASES like HDA6 and HDA19. Upon developmental or environmental stimuli, JA-Ile levels increase and promote the direct interaction between JAZs and the F-Box protein COI<sub>1</sub> which is part of an SCF-type E<sub>3</sub> Ubiquitin ligase. As a consequence, JAZs are polyubiquitylated (Ub) and degraded by the proteasome, and the expression of JA responsive genes is mediated by the released TFs in cooperation with the MEDIATOR COMPLEX (e.g. MED25).

Upon a JA-inducing stimulus, the bioactive hormone JA-Ile facilitates the preferential binding of JAZs to the F-box protein CORONATINE INSENSITIVE 1 (COI<sub>1</sub>), which is part of an SKP, Cullin, E<sub>3</sub> (SCF-E<sub>3</sub>)



ubiquitin ligase (Xie et al., 1998), leading to the formation of the JAZ-CO1 co-receptor complex (Fig. 2) (Sheard et al., 2010). As a consequence, JAZs are polyubiquitylated and targeted for degradation by the proteasome (Chini et al., 2007; Thines et al., 2007; Blazquez et al., 2020). This in turn liberates TFs to recruit transcriptional mediator complexes like MED25 and hence activate JA-Ile-responsive gene expression (Cevik et al., 2012; Zhang et al., 2015a). As JAZs are early JA-Ile-responsive genes (Yan et al., 2007; Chung et al., 2008), the intracellular pool of transcriptional regulators is replenished and provides a negative feedback loop for control of JA-Ile signalling.

The expression levels of early JA-Ile responsive genes, which in addition to *JAZ* transcripts also include *MYC2*, start increasing 5 minutes following wounding or exogenous MeJA treatment and reach their highest expression level within 1 h (Chung et al., 2008; Hickman et al., 2017). They are followed by mid-term transcripts such as the JA biosynthesis genes *AOS*, *LOX3*, *LOX4*, and *OPR3*, which reach their peak around 2 - 4 h after the initial stimulus (Chung et al., 2008). At longer time points (> 4 h after wounding or MeJA treatment), several canonical JA-Ile-dependent defense response genes such as *VEGETATIVE STORAGE PROTEIN 1* and *2* (*VSP1*, *VSP2*), or *PLANT DEFENSIN 1.2* (*PDF1.2*) reach their maxima (Kilian et al., 2007; Chung et al., 2008; Shin et al., 2012). In general, JA-Ile-dependent signalling is tightly regulated and normally induced only when required.

### **JA-Ile function**

JA-Ile-mediated signalling is essential to regulate plant responses against insect herbivores, necrotrophic pathogens and mechanical wounding (Wasternack and Feussner, 2018). In fact, *Arabidopsis* mutants deficient in JA-Ile production or signalling are more susceptible to a variety of herbivorous insects, which either have dietary preferences and feed on a specific set of plant species (specialist herbivores) or endure on a variety of plant species (generalist herbivores). This includes lepidopteran caterpillars like *Pieris rapae* or *Spodoptera littoralis* (Reymond et al., 2004; Zhang et al., 2015b), spider mites like *Tetranychus urticae* (Zhurov et al., 2014), and thrips such as *Frankliniella occidentalis* (Abe et al., 2008). Similar susceptibility phenotypes in JA mutants were also observed in other plant species like tobacco and tomato (Li et al., 2004; Paschold et al., 2007; Kallenbach et al., 2012). Even vertebrate herbivores like the cottontail rabbit (*Sylvilagus nuttallii*) and the Eastern Hermann's tortoise (*Eurotestudo boettgeri*) preferentially eat material from JA-deficient plants over wild-type (WT) plants, suggesting a general role of JA-Ile in defense responses against herbivory (Mafli et al., 2012; Machado et al., 2016). Moreover, the detritivorous crustaceans *Porcellio scaber* and *Armadillidium vulgare* changed to a herbivorous lifestyle in presence of JA-deficient plants (Farmer and Dubugnon, 2009), further emphasizing that animals of different classes can sense JA-mediated defenses. Interestingly, when comparing the transcriptomes of *Arabidopsis* WT and JA-insensitive

plants subjected to insect herbivory, transcripts involved in secondary defense compound production were identified, including genes associated to indolic glucosinolate metabolism (Reymond et al., 2004). Indeed, the production of several groups of secondary metabolites in various plant species is dependent on JA-Ile signalling, reviewed in (Goossens et al., 2017), with glucosinolates in *Arabidopsis*, nicotine in tobacco and the anti-cancer drug paclitaxel in *Taxus* being prominent examples involved in defense responses (Yukimune et al., 1996; Mewis et al., 2006; Shoji et al., 2008; Lenka et al., 2015). In addition to herbivory, JA-Ile also controls defense responses after mechanical wounding. When comparing the transcriptome between mechanically wounded *Arabidopsis* plants and plants that were subjected to insect herbivory, gene expression profiles were very similar (Reymond et al., 2000). Moreover, JA and JA-Ile levels rapidly increase within minutes after mechanical wounding (Glaser et al., 2009; Koo et al., 2009), rendering mechanical wounding an excellent elicitor to study JA responses. The JA pathway is also crucial in mediating defense responses against necrotrophic pathogens, which kill their host cells to acquire nutrients from dying tissues (Yan and Xie, 2015). Mutants deficient in JA biosynthesis or signalling are more susceptible to necrotrophic fungi like *Alternaria brassicicola* (Thomma et al., 1998), *Fusarium oxysporum* (Thatcher et al., 2016) and *Verticillium dahlia* (Thaler et al., 2004) as well as to oomycetes from the *Pythium* genus (Staswick et al., 1998; Vijayan et al., 1998).

The initiation of JA-Ile signalling in response to wounding or herbivory is usually accompanied by an inhibition of vegetative growth (Yang et al., 2012). In fact, exogenously supplied JA as well as repetitive wounding are known to inhibit root and shoot growth (Zhang and Turner, 2008; Chen et al., 2011; Gasperini et al., 2015). Growth inhibition through JA-Ile signalling can be caused by reducing root meristem activity and cell elongation (Chen et al., 2011), by inhibiting cell expansion and delaying the onset of endoreduplication in leaves (Noir et al., 2013), and by executing changes in carbon partitioning (Havko et al., 2016; Guo et al., 2018b). These trade-offs between growth and defense were recently challenged by the identification of mutants that exhibit elevated defense responses without showing growth alterations. Specifically, the introgression of a photoreceptor mutant in *PHYTOCHROME B* (*phyb*) resulted in the restoration of the reduced growth phenotype of a *jaz* quintuple mutant (*jazQ: jaz1 jaz3 jaz4 jaz9 jaz10*) exhibiting constitutive JA-Ile signalling (Campos et al., 2016). In this case, light and JA-Ile signalling act in parallel to regulate overall growth and defense phenotypes.

Contrary to their negative growth effects in vegetative tissues, JAs are crucial for the development of reproductive organs. In *Arabidopsis*, JA-Ile-deficient or insensitive mutants are male sterile, due to compromised stamen elongation and anther dehiscence, as well as pollen unviability, reviewed in (Browse and Wallis, 2019). Exogenous application of JAs can rescue male sterility in JA biosynthesis

but not in signalling mutants (Feys et al., 1994; Park et al., 2002). The JA pathway also participates in promoting stamen development and pollen viability in tomato (Dobritsch et al., 2015; Schubert et al., 2019a), where it is essential for the development of the female organs (Li et al., 2004; Schubert et al., 2019b). Interestingly, the role of JA-Ile in regulating fertility was co-opted later in evolution, as JA-signalling mutants in the early land plant *Marchantia polymorpha* are unaffected in reproductive organ development but still exhibit canonical growth and defense phenotypes (Monte et al., 2018). Taken together, JAs regulate multiple aspects in development and stress responses and are hence essential for plant fitness and survival.

## 2. Activation of the JA pathway

Although steps in JA-Ile biosynthesis and signalling are well characterized, reviewed in (Wasternack and Feussner, 2018), it is still unknown how cells sense damage signals and which intracellular events lead to the activation of JA biosynthesis enzymes to initiate JA-Ile production. Numerous lines of evidence across multiple plant species indicate that JA biosynthesis enzymes are present under basal conditions (Bachmann et al., 2002; Strassner et al., 2002; Stenzel et al., 2003; Swain et al., 2017). However, their overexpression did not lead to an increase in basal hormone levels (Staswick and Tiryaki, 2004; Sharma et al., 2006; Chen et al., 2018), suggesting that JA-Ile biosynthesis is initiated through post-translational activation of plastidial enzymes. Indeed, such an activation mechanism was speculated for LOX enzymes, which carry a putative Ca<sup>2+</sup> binding Polycystin-1, Lipoxygenase, Alpha-Toxin (PLAT) domain (Farmer et al., 2014). Intriguingly, an increase in Ca<sup>2+</sup> ions leads to PLAT-domain binding of mammalian 5-LOX enzymes, leading to their re-localization from soluble to membrane-bound enzymes where they can presumably access their substrates (Hammarberg et al., 2000; Kulkarni et al., 2002). Ca<sup>2+</sup> was also hypothesized to be involved in triggering JA-Ile biosynthesis, as mutations in Ca<sup>2+</sup> signalling components caused alterations in JA biosynthesis and / or signalling (Scholz et al., 2014; Matschi et al., 2015). Additionally, a gain of function mutant of the vacuolar cation channel TWO PORE CHANNEL 1 (TPC1) resulted in increased basal expression of JA-Ile-responsive genes, elevated JA and OPDA levels after wounding and a higher oxygenation efficiency of  $\alpha$ -linolenic acid (Bonaventure et al., 2007b; Bonaventure et al., 2007a; Lenglet et al., 2017). Furthermore Ca<sup>2+</sup> fluxes are important to facilitate distal JA-Ile production, which is mediated by members of the clade 3 GLUTAMATE-RECEPTOR-LIKE (GLR) proteins (Mousavi et al., 2013; Nguyen et al., 2018; Toyota et al., 2018). Despite the underlying indications, it is still unknown how Ca<sup>2+</sup> changes activate JA-Ile biosynthesis upon different stresses such as wounding or herbivory. Moreover, it is also unclear whether Ca<sup>2+</sup> is directly activating plastidial enzymes, and if so, how are Ca<sup>2+</sup> changes transmitted into the plastid.

Given that tissue damage causes a rapid (<30') increase in JA and JA-Ile levels (Glauser et al., 2009), it was also proposed that JA and JA-Ile may derive from various hormone precursors that are then rapidly converted to bioactive JA-Ile rather than from MGDG directly (Stelmach et al., 2001; Dave and Graham, 2012). A similar mechanism is present for auxin, where several storage forms exist that can be rapidly converted into indole-3-acetic acid (IAA) (Korasick et al., 2013). However, in *Arabidopsis* JA-Ile precursors (e.g OPC-4, OPC-6, OPC-8, and JA) are present in low quantities at basal conditions, and their levels increase after a stimulus (Glauser et al., 2008; Kienow et al., 2008; Glauser et al., 2009; Schulze et al., 2019). Similar response levels were also observed for other JA metabolites such as 12-hydroxy-JA and 12-hydroxy-JA-Ile (Glauser et al., 2008; Poudel et al., 2019). Contrarywise, OPDA levels are relatively high at basal conditions, but the possibility of its rapid conversion to JA remains debated (Grebner et al., 2013). The most abundant pool of JAs in *Arabidopsis* are arabidopsides, which are galactolipids containing esterified *cis*-OPDA and *dn*-OPDA (Glauser et al., 2009; Genva et al., 2019). In contrast to other JAs, arabidopside levels are not affected in distal systemic leaves after wounding (Glauser et al., 2009; Koo et al., 2009), which contradicts their putative contribution to JA-Ile biosynthesis. Hence, the most accepted hypothesis is that JA-Ile production relies upon the activation of the whole pathway starting from MGDG precursors.

Nevertheless, it remains unclear how are JA biosynthesis enzymes activated to initiate JA-Ile production and what are the upstream signalling events sensing damage. A wide-range of exogenous and endogenous signals have been proposed as elicitors of *de novo* JA-Ile biosynthesis, reviewed in (Campos et al., 2014). Among the exogenous elicitors, herbivore- and microbial-associated molecular patterns (HAMPs and MAMPs) derived from pathogenic organisms can be recognized by putative pattern recognition receptors (PRR), which consequently activate defense responses (Zhang et al., 2017). Several of these elicitors, such as flagellin and elongation factor-Tu from bacterial pathogens, chitin from fungal pathogens or fatty acid-amino acid conjugates from lepidopteran herbivores, were reported to activate multiple defense pathways including JA (Schmelz et al., 2009; Campos et al., 2014; Kim et al., 2014; Steinbrenner et al., 2020). However, although some of their receptors are known, the downstream signalling events leading to the induction of the JA pathway remain obscure. Furthermore, there is no reported evidence that mutants in the PRR receptors are affected in JA-Ile production and signalling following wounding.

Endogenous elicitors, such as damage-associated molecular patterns (DAMPs), are instead derived from the plant and are produced during tissue wounding as well as attacks from herbivores and pathogens (Hou et al., 2019; Li et al., 2020b). They are considered danger signals and have been proposed to elicit JA-Ile production (Campos et al., 2014). One example is the peptide AtPep1, which

is released upon wounding and pathogen attack and can stimulate the expression of JA-Ile-dependent defense genes such as *PDF1.2* (Huffaker et al., 2013). Interestingly, the degradation of plant cell walls by enzymes produced by pathogens may generate cell wall fragments, of which some are also considered DAMPs that can trigger the JA pathway, reviewed in (Mielke and Gasperini, 2019). Among them, pectin-derived breakdown fragments called  $\alpha$ -(1,4)-linked oligogalacturonides (OGs) can be putatively perceived by WALL-ASSOCIATED KINASE 1 and 2 (WAK1, WAK2) receptors in Arabidopsis (Decreux et al., 2006; Kohorn et al., 2009; Brutus et al., 2010). In fact, treatment with OGs of certain chain length (degree of polymerization of 10 - 25) induce the production of JA in tomato (Doares et al., 1995) and exhibit elevated expression levels of JA-Ile-responsive genes including *AOS*, *LOX2*, *LOX3*, and *LOX4* (Moscatiello et al., 2006; Souza et al., 2017). Recently, the cellulose-derived fragment cellobiose was also reported to elicit specific defense responses and caused elevated expression of JA biosynthesis genes *AOS*, *LOX3*, and *LOX4* (Souza et al., 2017), although the respective cellobiose receptor has not been identified yet. Therefore, although several elicitors are capable of triggering JA production, the molecular mechanisms mediating the initiation of JA biosynthesis remains obscure.

### **Cell wall alterations can trigger the JA pathway**

Mechanical wounding, herbivory and pathogen infection, which all can lead to JA-Ile production, have in common that they breach the cell wall. In fact, a number of chemical and genetic alterations within the plant cell wall can induce JA-Ile biosynthesis and / or signalling, reviewed in (Mielke and Gasperini, 2019). Plant cell walls are polysaccharide-rich structures, which provide mechanical strength while allowing flexibility for cell growth and proliferation. They can be categorized into primary and secondary walls, depending on their structural and functional differences. Primary cell walls are mainly comprised of cellulose (Fig. 3), hemicelluloses and pectic polysaccharides and are synthesized during cell division at the cell plate, where they encase newly formed cells and increase their area during cell growth, reviewed in (Lampugnani et al., 2018). Once plant tissues cease growing, they may be additionally surrounded by lignified secondary walls adding further compressive and tensile strength, reviewed in (Cosgrove and Jarvis, 2012).

Cellulose chains (unbranched poly  $\beta$ -1,4-D-glucan chains) are synthesized by a hexameric cellulose synthase complex (CSC) at the plasma membrane which uses cytosolic uracil-diphosphate glucose (UDP-glucose) as a substrate (Fig. 3), reviewed in (Carpita, 2011). The CSC is composed of proteins of the CELLULOSE SYNTHASE (*CesA*) family, which are inserted into the plasma membrane. Three *CesAs* form a rosette, and six rosettes ultimately form a CSC that spans the plasma membrane and synthesizes cellulose microfibrils at the cell wall (Kimura et al., 1999; Polko and Kieber, 2019). For primary cell wall biosynthesis in Arabidopsis, proteins *CesA1*, *CesA3*, and *CesA6* proteins are

necessary to form a functional CSC (Persson et al., 2005). Mutations in some of the *CesA* genes, like *CesA1* and *CesA3*, lead to severely stunted growth phenotypes due to impaired cellulose production (Cano-Delgado et al., 2000; Gillmor et al., 2002).

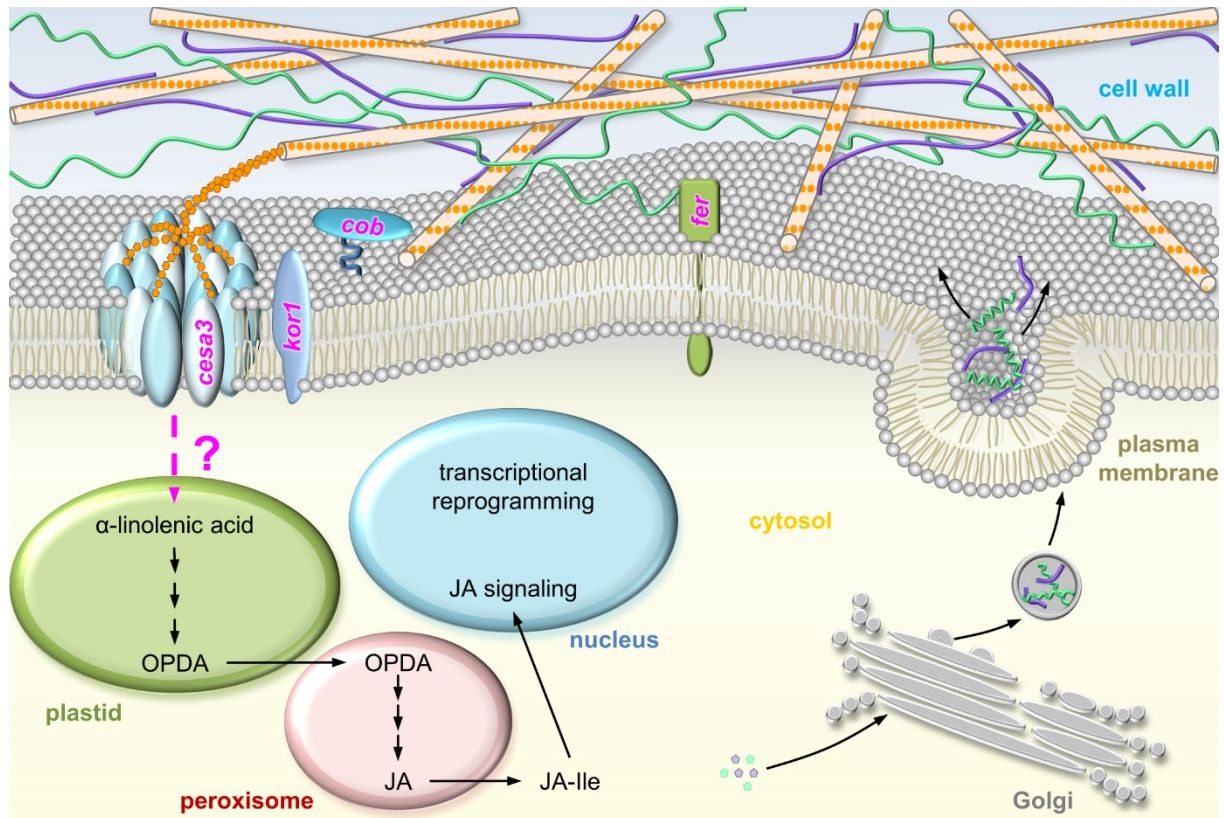


**Figure 3: Genetic mutations in specific cell wall biosynthesis and sensing components activate the JA pathway.** The plant cell wall represents the extracellular barrier and is mainly composed of complex polysaccharides including cellulose (schematically represented by orange rods), hemicelluloses (by purple lines), and pectins (by green ribbons). Cell wall biosynthesis and sensing components whose loss of function results in the activation of the JA pathway are highlighted in magenta and include: *CELLULOSE SYNTHASE 3* (*cesa3*), *KORRIGAN1* (*kor1*), *COBRA* (*cob*), and *FERONIA* (*fer*). Nevertheless, intracellular components linking alterations in cell wall biosynthesis to JA-Ile production are still unknown. The Figure is a modified version from (Mielke and Gasperini, 2019).

Cellulose microfibrils are cross-linked by hemicellulose chains through hydrogen bonds in order to form a complex network, reviewed in (Park and Cosgrove, 2015). Unlike cellulose, hemicelluloses are branched polymers, which have a cellulose-like backbone but couple different monosaccharides, such as glucose, xylose, arabinose, and mannose, by  $\beta$ -(1,4)-links, reviewed in (Pauly et al., 2013). The most abundant hemicellulose in *Arabidopsis* is xyloglucan. Other hemicelluloses include glucomannan, galactomannan or arabinoxylan (Pauly and Keegstra, 2016). Hemicellulose oligomers are synthesized in the Golgi and are afterwards delivered to the wall via the secretory pathway where they are further assembled into longer chains by members of the glucan endo-transglucosylase/hydrolase family (Park and Cosgrove, 2015; Anderson and Kieber, 2020).

The complex network of cellulose microfibrils and hemicelluloses is embedded in a gel-like pectin matrix. Pectins are galacturonic acid-containing multiblock polymers which eventually carry complex side chains, reviewed in (Atmodjo et al., 2013). Similarly to hemicelluloses, these polysaccharides are synthesized in the Golgi and reach the cell wall through secretory vesicles (Toyooka et al., 2009). The most abundant form of pectin in primary walls is homogalacturonan (HG), which is composed of unbranched  $\alpha$ -1,4-linked galacturonic acid chains that can be decorated with xylose to form xylogalacturonan or apiose to form apiogalacturonan (Anderson, 2016). HG is delivered to the wall in a methylesterified neutral state, but can then be de-esterified by pectin methyl esterases (PME), which leads to the exposure of negative charges that can form strong cross-links with  $\text{Ca}^{2+}$  (Senechal et al., 2014). Other important pectins include rhamnogalacturonan-I (RG-I) and rhamnogalacturonan-II (RG-II). RG-I and RG-II possess a backbone of alternating rhamnose and galacturonic acid subunits or a HG-like backbone respectively, and are both decorated by structurally complex side chains (Atmodjo et al., 2013). Moreover, specific side chains of RG-II can form borate diester linkages to crosslink RG-II molecules (Funakawa and Miwa, 2015).

Cellulose, hemicelluloses, and pectins are thought to have a number of functional interactions which are crucial for determining the mechanical characteristics of plant cell walls. Indeed, physical interactions between all components have been described, and the list of identified covalent linkages between them is constantly growing (Anderson and Kieber, 2020). Although the major components of primary cell walls are well known and intensively studied, much research is still required to understand these dynamic structures whose composition and architecture changes during plant growth and development. Especially the signalling components driving this communication system are still poorly understood and have only recently started to emerge, reviewed in (Voxeur and Hofte, 2016).

The first evidence that genetic alterations in plant cell walls might exhibit altered JA-Ile responses was provided by the isolation and characterization of the *CesA3* mutant *constitutive expression of VSP1* (*cev1*), which ectopically produces JA and ethylene (ET) and exhibits higher basal expression levels of JA-Ile-dependent defense genes *VSP1*, *VSP2*, and *PDF1.2* (Ellis and Turner, 2001; Ellis et al., 2002). Constitutive expression of these defense-related genes was furthermore observed in other mutant alleles of *CesA3*, such as *ectopic lignification 1* (*eli1*) (Cano-Delgado et al., 2003) and *isoxaben resistant 1* (*ixr1*) (Hernandez-Blanco et al., 2007). Moreover, a mutant in *COBRA*, which encodes a glycosylphosphatidylinositol (GPI)-anchored protein that modulates cellulose deposition, constitutively overexpresses JA biosynthesis genes *AOS*, *LOX2*, and *OPR3* and exhibits a basal overproduction of JA levels (Ko et al., 2006). Additionally, chemical inhibition of cellulose biosynthesis

by treating plants with the herbicide isoxaben, triggers the degradation of the negative JA biosensor Jas9-VENUS (J9V) (Larrieu et al., 2015) and induces high JA levels (Denness et al., 2011; Engelsdorf et al., 2018). Nevertheless, intracellular signalling steps that link defects in cell walls to the activation of JA biosynthesis remain largely unknown (Fig. 3).

### **Plant cell wall surveillance signalling**

The plant cell wall is a highly responsive and dynamic structure whose composition and properties need to be coordinated with developmental and environmental stimuli to ensure proper growth and stress responses (Bacete and Hamann, 2020; Rui and Dinneny, 2020). Thus, cell wall properties are constantly monitored at the plasma membrane and their status is transmitted intracellularly to signalling cascades aimed at readjusting growth. The existence of a pathway, constantly monitoring the integrity and status of plant cell walls regarding developmental and stress signals was first proposed by (Somerville et al., 2004), based on an equivalent pathway present in yeast (Heinisch et al., 1999). In *Arabidopsis*, a loss-of-function mutant of the *Catharanthus roseus Receptor-Like Kinase 1-like* (*CrRLK1L*) *THESEUS 1* (*THE1*), suppresses the short hypocotyl phenotype of a *cesa6* mutant without restoring its low cellulose content (Hematy et al., 2007). Members of the *CrRLK1L* family harbour a cytoplasmic kinase domain and an ectodomain exposed towards the plant cell wall, and several have been implicated in sensing and transducing cell wall-derived signals (Wolf, 2017). Specifically, they were found to integrate developmental and environmental cues by binding to secreted peptides of the RAPID ALKALINIZATION FACTOR (RALF) family leading to the regulation of immune and growth responses (Haruta et al., 2014; Ge et al., 2017; Stegmann et al., 2017). Moreover, the malectin-like domains in the *CrRLK1L* FERONIA (FER) facilitate direct binding to pectins in the cell wall (Feng et al., 2018). FER can also directly interact with extracellular leucine-rich repeat extensin proteins, allowing cells to sense mechanical constraints in the cell wall and consequently adjust vacuolar size and cell elongation (Dunser et al., 2019). Interestingly, *fer* loss of function mutants accumulate high basal levels of JA-Ile precursors (Fig. 3) (Guo et al., 2018a). Specifically, FER inhibits JA-Ile signalling by phosphorylating and destabilizing MYC2, while upon RALF<sub>23</sub> elicitation FER stabilizes MYC2 and promotes JA-Ile-dependent responses (Guo et al., 2018a).

In addition to *CrRLK1L*, stretch-activated ion channels, other receptor-like kinases (RLKs), leucine-rich-repeat extensins, mechanosensors and osmosensors are thought to be involved in maintaining cell wall integrity in *Arabidopsis* (Wolf, 2017; Bacete and Hamann, 2020). In conclusion, there is growing evidence that cell wall surveillance pathways are essential for maintaining the communication between the extracellular matrix and the cell interior in order to orchestrate responses upon developmental and stress signals.



### **Turgor pressure and plant mechanoperception**

Plant cells can maintain a high internal hydrostatic water pressure (turgor pressure), that can reach values of around 20 atmospheres (Beauzamy et al., 2014). It is generated by osmotic water uptake that leads to vacuolar expansion and pushes the plasma membrane against the cell wall (Fig. 4). The wall is counteracting the internal pressure and prevents cells from bursting, and is set under mechanical tension as a consequence. In growing plant cells, cell wall biosynthesis and remodelling co-ordinately give in to the turgor, thus allowing the cell to expand. Hence, turgor pressure is considered as the driving force of growth (Hamant and Traas, 2010).

However, turgor pressure is nondirectional, meaning that anisotropic growth can only be achieved by modifying the cell wall as a counteracting force. In fact, directional growth is controlled by several mechanisms. Numerous cell wall-modifying enzymes, such as expansin, PMEs, xyloglucan endotransglycosylases/hydrolases (XTHs), and endo-(1,4)- $\beta$ -D-glucanases, are capable of loosening the wall at specific sites to allow for directional growth (Cosgrove, 2018). In addition, cortical microtubules, which guide the deposition of load-bearing cellulose microfibrils (Paredes et al., 2006), predominantly align transversally to the growth axis and hence along the direction of maximal tension (Colin et al., 2020).

Turgor pressure decreases or increases according to the water pressure within the cell (Fig. 4). As a consequence, environmental conditions can have a strong impact on turgor. Hyperosmotic conditions during low water availability or high salinity can reduce turgor and even plasmolyze the cell, while hypoosmotic conditions during flooding or mechanical compression increase the pressure and hence the mechanical tension of the wall (Fig. 4) (Beauzamy et al., 2014). Therefore, in order to maintain turgor within tissues, plant cells rely on the movement of water and water-attracting osmotically active substances (osmolytes). The intra- and intercellular movement of water is mainly accomplished by gated water channels called aquaporins. They are localized at the plasma membrane as well as membranes of other cellular compartments and seem to mediate the majority of water transport between symplast and apoplast (Chaumont and Tyerman, 2014). Another mode of water transport within the symplast is mediated by plasmodesmata. Depending on the size exclusion limit of these symplasmic connections, also the passive transport of osmolytes is warranted (Sager and Lee, 2018). Osmoregulation through the transport of osmolytes is key to control the internal turgor. The major classes of molecules used for osmoregulation in plant cells are ions, sugars, and amino acids, which can be directionally relocated by specific transporters (Beauzamy et al., 2014).

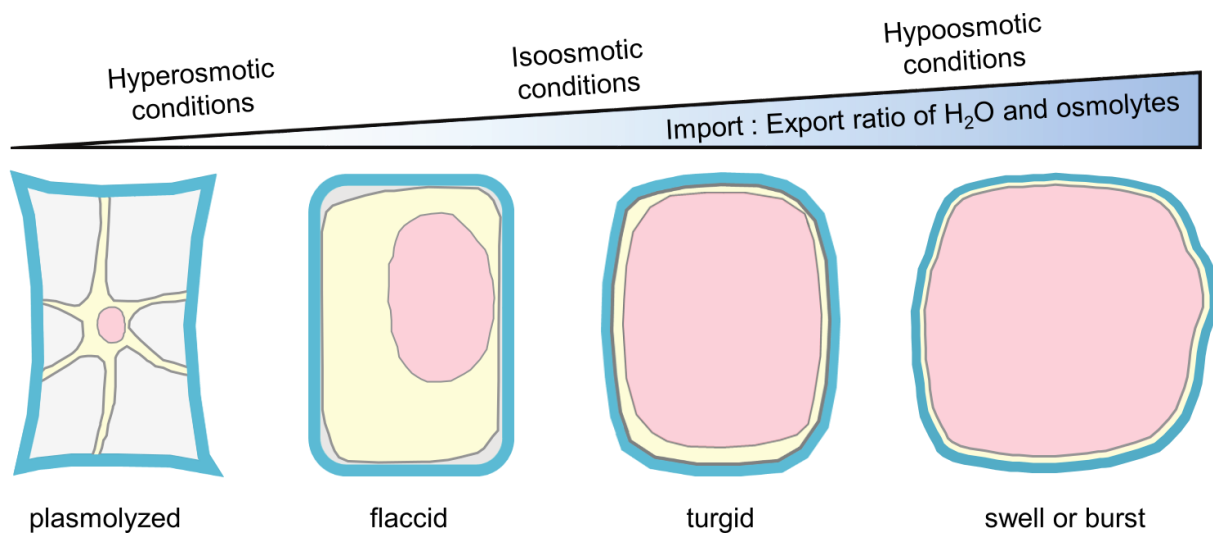


**Figure 4: Simplified scheme of the cellular adjustment of turgor pressure in plants.** Depending on water availability and osmotic conditions, passive and active transport of water and osmolytes regulate internal turgor pressure. Hyperosmotic treatments result in increased water export and volume loss of vacuole (red) and cytoplasm (yellow). In contrast, hypoosmotic conditions lead to increased water uptake and result into the expansion of the vacuole and subsequent loss of cytoplasmic volume and compression of the plasma membrane (grey) against the cell wall (blue), which as a consequence is set under mechanical tension. Depending on the strength of hypo- and hyperosmotic conditions, plant cells might experience morphological changes in their volume.

As turgor pressure is directly linked to the extracellular osmotic conditions, plants evolved means to sense osmotic cues and their mechanical consequences in order to initiate internal responses (Hamant and Haswell, 2017). For instance, members of the MECHANOSENSITIVE CHANNEL OF SMALL CONDUCTANCE-LIKE (MSL) family were shown to be important for osmoregulation as they mediate responses to hypoosmotic stress in plant cells and organelles (Veley et al., 2012; Basu and Haswell, 2020). Another example is the channel MATING PHEROMONE INDUCED DEATH 1 (MID1)-COMPLEMENTING ACTIVITY 1 (MCA1) which enhances  $Ca^{2+}$  influx in response to hypoosmotic shock and mechanical stimuli (Nakagawa et al., 2007). Intriguingly, MCA1 was also found to be required for the induction of JA biosynthesis upon osmosensitive alterations in the cell wall triggered by isoxaben (Engelsdorf et al., 2018). Indeed, osmotic changes can lead to alterations in cell morphology such as cell swelling (Basu and Haswell, 2020), which in turn might activate mechanical stress within tissues (Hamant and Haswell, 2017). Additionally, mechanical wounding can lead to the formation of hydraulic pressure waves (Huber and Bauerle, 2016), which are hypothesized to play a role in the activation of JA-Ile biosynthesis in distal tissues (Farmer et al., 2014; Farmer et al., 2020). Nevertheless, the molecular mechanisms linking turgor changes and mechanical stress remain largely unknown and have yet to be connected to the JA pathway.

### 3. Preparatory work for this thesis

In a genetic screen designed to identify negative regulators of JA-Ile signalling, (Acosta et al., 2013) searched for ethyl methanesulfonate (EMS)-mutagenized  $M_2$  seedlings with constitutive activation of the JA-Ile-responsive reporter *JAZ10p:GUSPlus* (*JGP*). Whereas basal *JGP* activity in the WT as well as in JA-deficient *aos* plants is very weak and limited to the hypocotyl, cotyledon wounding triggers robust reporter induction across the wounded cotyledon as well as in the unwounded hypocotyl, cotyledon, and root of the WT but not of *aos* (Fig. 5A). Hence, *JGP* represents an excellent reporter to reveal sites of increased JA-Ile production or signalling (Acosta et al., 2013). The screen isolated two allelic mutants with ectopic *JGP* activation in the primary root that did not extend into aerial organs (Fig. 5B). Whole genome sequencing of twice backcrossed (BC)  $BC_2F_2$  bulk segregants mapped the putative causative mutations to single nucleotide polymorphism (SNPs) in *KORRIGAN1* (*KOR1*). The mutants were named *kor1-4* and *kor1-5* and correspond to L573F and P172L amino acid exchanges, respectively (Fig. 5C).

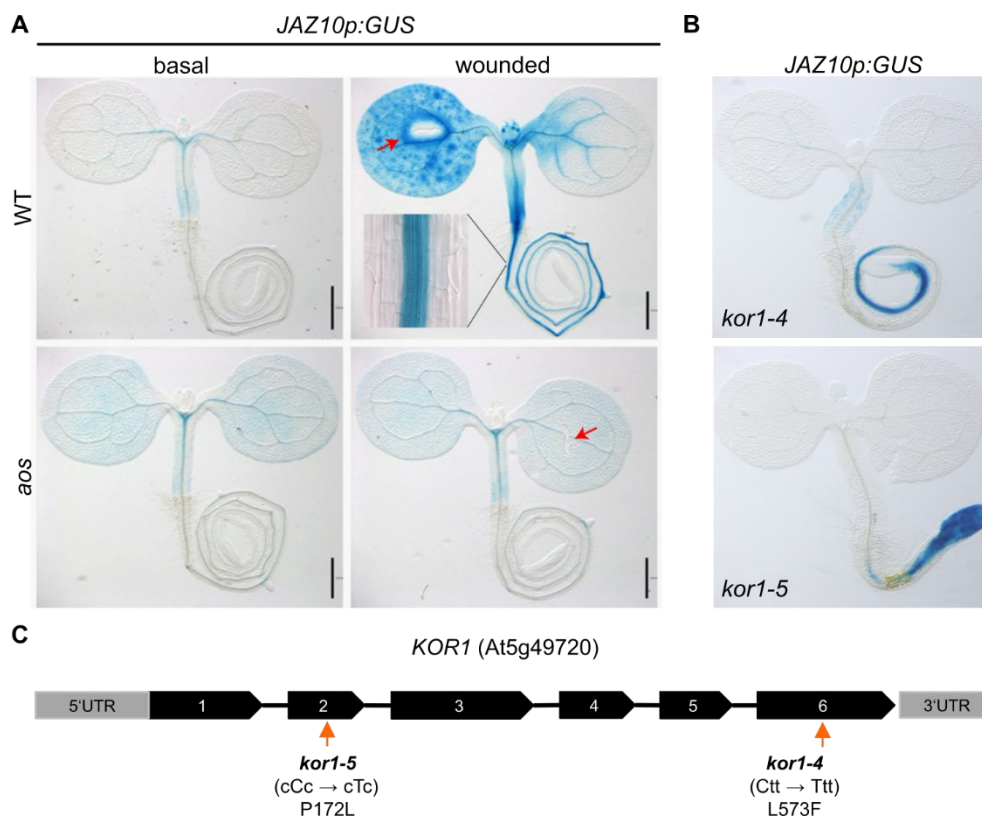


**Figure 5: A forward genetic screen to identify negative regulators of JA-Ile signalling yielded two novel *kor1* alleles.** (A) Representative *JAZ10p:GUS* reporter activity in 5-do seedlings of WT and *aos* at basal conditions and 2 h after cotyledon wounding (red arrow). Note the increase of reporter activity in the WT but not in the mutant. (B) Representative *JAZ10p:GUS* reporter activity in 5-do seedlings of *kor1-4* and *kor1-5* at basal conditions. Note the constitutive reporter expression in the primary root of both mutants. (C) Schematic representation of *KOR1* gene structure describing the 2 novel *kor1* alleles found in the screen. Black boxes depict exons and lines introns. Scale bars in (A) and (B) = 0.5 mm. Data from (A) was taken from (Acosta et al., 2013).

*KOR1* is a member of putative plasma membrane-bound endoglucanases (GLYCOSYL HYDROLASE 9A1, GH9A1) and is comprised of an N-terminal cytosolic tail domain, a transmembrane domain and

a C-terminal extracellular endo-1,4- $\beta$ -glucanase catalytic domain (Fig. 6A) (Nicol et al., 1998; Urbanowicz et al., 2007). Partial loss-of-function and knock-down alleles of *kor1* exhibit a variety of phenotypes in Arabidopsis including dwarfism, elongation defects, organ swelling, an altered cell wall architecture and decreased cellulose content (Fig. 6B and C, Tab. S1) (Nicol et al., 1998; Lane et al., 2001; Sato et al., 2001; Szyjanowicz et al., 2004; Lei et al., 2014). Stronger alleles cause cytokinesis defects, early growth arrest and calli formation (Zuo et al., 2000; Krupkova et al., 2007). In addition, several *kor1* alleles are temperature-sensitive and exhibit exacerbated phenotypes at elevated temperatures (Lane et al., 2001). However, a true knockout-allele of *kor1* has not been described yet and is thought to be lethal (Lei et al., 2014). As KOR1 is conserved throughout different plant species, dwarf phenotypes of knockdown-alleles were also observed in poplar and spruce (Maloney and Mansfield, 2010; Maloney et al., 2012).

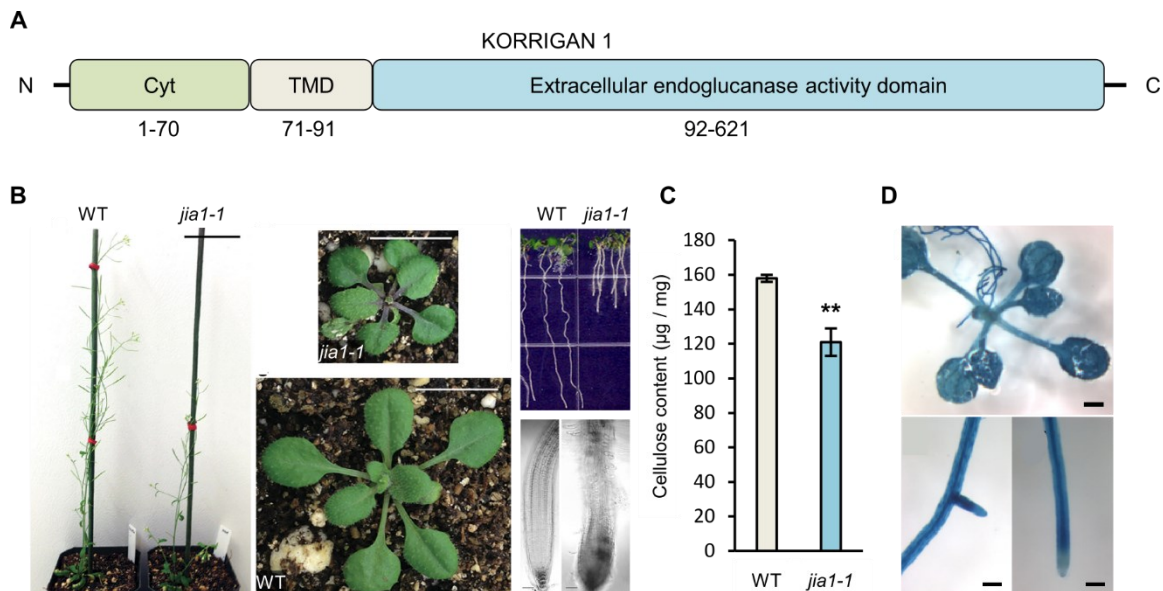


**Figure 6: Structure of KOR1 and mutant phenotypes.** (A) Schematic representation of Arabidopsis KOR1. Specific domains include a cytosolic tail domain (Cyt, green, amino acids 1-70), a transmembrane domain (TMD, grey, amino acids 71-91) and an extracellular endoglucanase activity domain (blue, amino acids 92-621). (B) Morphology of the *kor1* mutant allele *jia1-1* in comparison to the WT. Images show 7-week-old flowering plants, 4-week-old rosettes, root elongation as well as primary root tip morphology. Note the overall dwarfism of *jia1-1* in comparison to the WT. (C) Crystalline cellulose content of 4-d-old, dark-grown WT and *jia1-1* plants. Double asterisks indicate significant differences from the WT at the same data point ( $P < 0.01$ , Student's t test). Error bars represent standard deviation. (D) Expression of *KOR1p:GUS-KOR1* in Col-o. Note that KOR1 is expressed throughout the plant body. Scale bars = 1 mm (top image); 0.1 mm (bottom images). Images and data in (B) and (C) are from (Lei et al., 2014) and images in (D) from (Rips et al., 2014).

Co-localization of Green Fluorescent Protein (GFP)-KOR1 with specific plasma membrane- and organelle markers revealed, that the protein is predominately localized at the plasma membrane and the trans-Golgi network (TGN) and undergoes constant intracellular cycling (Robert et al., 2005; Nagashima et al., 2020b). The ectodomain of KOR1 carries 8 N-Glycosylation sites, which are processed in the endoplasmic reticulum (ER) and are important for the subcellular localization and hence proper function of the protein (Liebminger et al., 2009; Rips et al., 2014). Most likely KOR1

*N*-glycans are important for proper ectodomain folding, as lack of glycoprotein quality control in the ER as well as underglycosylation lead to KOR1 accumulation and presumably degradation in the tonoplast (Rips et al., 2014; Nagashima et al., 2020a).

The importance of KOR1 on cellulose biosynthesis was further substantiated by uncovering its interaction with CesAs involved in primary and secondary cellulose biosynthesis via *in vitro* affinity chromatography, yeast-two-hybrid screens, and bimolecular fluorescence complementation (BiFC) experiments in tobacco (Lei et al., 2014; Mansoori et al., 2014; Vain et al., 2014). These interaction studies corroborate the evidence on KOR1 co-localization with components of the CSC at the plasma membrane and the TGN (Lei et al., 2014; Vain et al., 2014). Consistently, loss of *KOR1* leads to defective motility of CesA6 and CesA3 trajectories at the plasma membrane (Paredes et al., 2008; Lei et al., 2014). The enzymatic activity of KOR1 has been thus far been analysed only *in vitro* where recombinant KOR1 variants from poplar or Arabidopsis hydrolysed the cellulose derivate carboxymethylcellulose (Master et al., 2004; Liebminger et al., 2009; Lei et al., 2014). However, the precise function of KOR1 in cellulose biosynthesis, the exact molecular mechanism of the enzyme and its *in vivo* substrates are still unknown. An early study proposed that KOR1 is necessary for the cleavage of sterol-linked primers during cellulose elongation (Peng et al., 2002). Other hypotheses state that KOR1 may reduce cellulose crystallinity and hence relieve the tension of cellulose microfibrils (Takahashi et al., 2009), or that KOR1 may hydrolyse  $\beta$ -glucoside primers in the apoplast during initiation of cellulose biosynthesis or even cleave cellulose chains to reduce fibril length (Ding and Himmel, 2006). Nevertheless, KOR1 is broadly expressed throughout the plant and across all developmental stages, reinforcing its pivotal role in plant cell wall biosynthesis and remodelling (Fig. 6D) (Rips et al., 2014).

Interestingly *kor1-1* knock-down plants showed reduced susceptibility to the necrotrophic fungus *Botrytis cinerea* (Finiti et al., 2013) and an increased susceptibility to the hemibiotrophic bacteria *Pseudomonas syringae* pv *tomato* (Lopez-Cruz et al., 2014). Upon infection, *kor1-1* leaves exhibited increased levels of JA and JA-Ile, as well as a potentiated expression of defense-related transcripts compared to WT plants (Lopez-Cruz et al., 2014). Additionally, KOR1 localization in the TGN is important for proper root growth during salt stress (Nagashima et al., 2020b). Nevertheless, it is still unclear how KOR1 impacts plant stress and defense responses at the molecular level.

The newly identified *kor1-4* and *kor1-5* alleles were the founding genetic material for this thesis and provided the basis to decipher the link between plant cell wall alterations and the initiation of JA-Ile biosynthesis.

#### 4. Aims and objectives

Although JA-Ile biosynthesis and signalling are fairly well understood, knowledge on what signals stimulate the initiation of JA-Ile biosynthesis in plastids and how plastids sense these signals is still completely missing. In fact, insect herbivory and mechanical wounding trigger the initiation of several concomitant signalling pathways in addition to JA-Ile production, with the consequence of being unable to dissect molecular signals lying upstream of JA-Ile biosynthesis (Campos et al., 2014). We therefore hypothesized that specific cell wall perturbations stimulate JA-Ile production in plastids via an unknown signalling pathway, and that the elucidation of such pathway(s) could lead to the understanding on how JA-Ile biosynthesis is initiated more broadly. These putative pathways could include sensors or channels at the plasma membrane which sense cell wall-derived cues and transduce the information intracellularly and to plastids where JA-Ile biosynthesis is initiated (Fig. 3). To test my hypothesis, I had the following objectives:

##### **Objective I: Are *kor1* alleles suitable tools to study pathways linking altered cell walls to JA-Ile production?**

First, I aimed to determine if the constitutive upregulation of JA-Ile signalling in my *kor1* allele was indeed caused by the absence of a functional KOR<sub>1</sub> by evaluating complementation lines. I next evaluated if the *JGP* phenotype was dependent on hormone production by generating *kor1 aos* double mutants and by measuring endogenous hormone levels. I also wanted to define how do *kor1* mutants respond to other JA-Ile inducing stimuli, and which of the two *kor1* alleles is most suitable for further studies.

##### **Objective II: Is the activation of ectopic JA signalling in *kor1* cell-autonomous or non-cell autonomous?**

Although *KOR1* is expressed throughout the plant and *kor1* mutants are cell wall mutants everywhere (Rips et al., 2014), activation of JA-Ile signalling in *kor1* alleles was restricted to specific root portions (Fig. 5B). As JA-Ile precursors are mobile (Schulze et al., 2019; Li et al., 2020a), ectopic *JGP* reporter activity in *kor1* could be a result of either cell-autonomous or cell non-autonomous signals. To discriminate between these possibilities and identify the tissue responsible for triggering JA-Ile biosynthesis, I aimed to generate a detailed cellular map of where is ectopic JA-Ile signalling occurring in *kor1*. I then expressed a functional CIT-KOR<sub>1</sub> fusion protein in specific cell layers of the root to evaluate which tissue is responsible for triggering JA-Ile production in *kor1*.

**Objective III: What are the genetic components involved in initiation of JA-Ile biosynthesis in *kor1*?**

For this aim, I used a combination of reverse and forward genetic approaches. First, I analysed the *kor1* root transcriptome to search for possible upstream regulators of JA-Ile production. Mutants from potential candidates acting upstream of JA-Ile, as well as reported cell wall integrity sensors were crossed into *kor1*, and resulting double mutants combinations were analysed for their capacity to abolish increased JA-Ile signalling. In parallel, I have also performed an unbiased forward genetic screen on an EMS mutagenized *kor1* population for *JGP* suppression. One of the identified suppressors was functionally characterized and provided evidence on the physiological trigger of the JA-Ile pathway in *kor1*.

**Objective IV: What are the roles of ectopic JA-Ile signalling in *kor1* mutants?**

As the activation of JA-Ile signalling normally triggers defense responses at the expense of plant growth (Yang et al., 2012), it is likely that the root activation of JA-Ile signalling in *kor1* mutants could contribute to the reduction of growth and activation of defense responses of cellulose-deficient *kor1* plants. It is also possible that ectopic JA-Ile signalling may impact other less-known JA-Ile-regulated processes, or that JA-Ile production in *kor1* is physiologically insignificant. To test this multitude of possibilities, I aimed to characterize a variety of *kor1* phenotypes and compare them with the JA-deficient *kor1 aos* background.

## Section II - Results

### 1. Are *kor1* alleles suitable tools to study pathways linking altered cell walls to JA-Ile production?

Data from this chapter is published in (Mielke et al., 2021, *Science Advances*).

Before starting to further characterize *kor1* mutants with respect to the JA pathway, I first confirmed whether the causative mutations of the observed *JGP* phenotype are *kor1*-dependent. An allelism test between *kor1-4* and the T-DNA insertion mutant *kor1-6* in the *JGP* background did not abolish constant activation of JA-Ile signalling in the primary root (Fig. 7A).

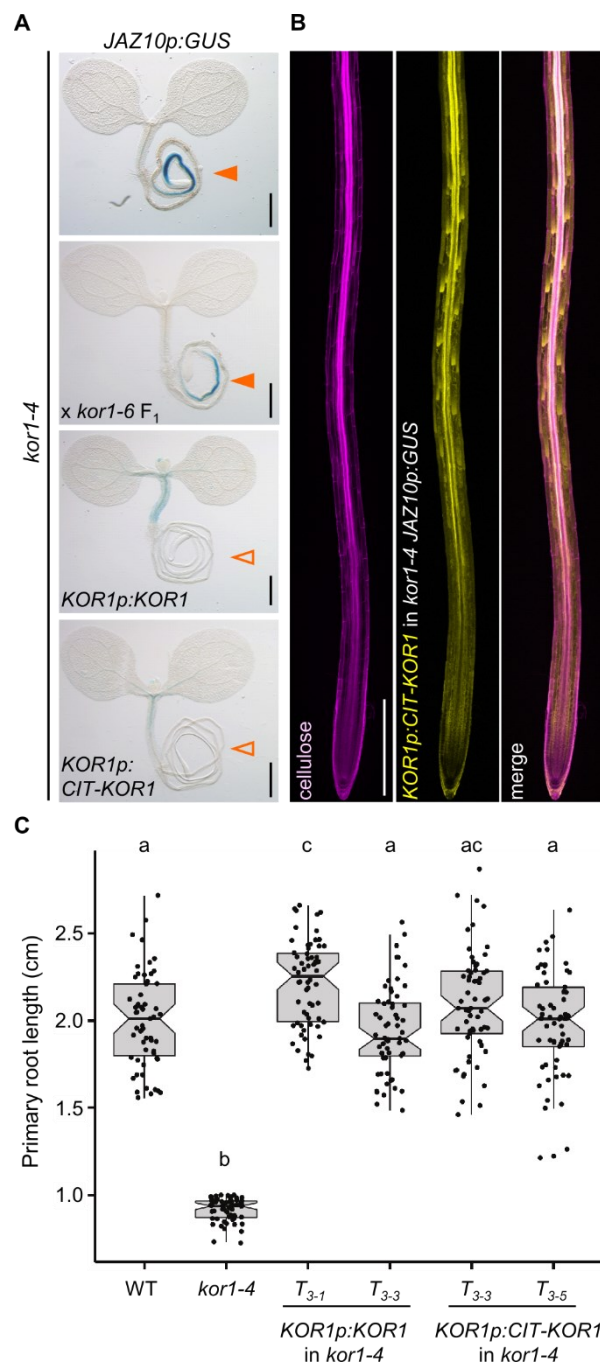


**Figure 7: Untagged and tagged KOR1 versions fully restore the *kor1* mutant phenotype.** (A) Representative *JAZ10p:GUS* reporter activity in 5-do seedlings of *kor1-4*, *kor1-4* x *kor1-6* F<sub>1</sub> (allelism test), and *kor1-4* complemented with *KOR1p:KOR1* and *KOR1p:CIT-KOR1*. Note the increased *JAZ10p:GUS* reporter activity in *kor1-4* and allelism test (orange arrowheads), and its absence from complementation lines (empty arrowheads). (B) CIT-KOR1 expression in 5-do *kor1-4 JGP* seedling roots under the control of its native *KOR1* promoter (*KOR1p:CIT-KOR1*). Samples were cleared in ClearSee and counterstained with the cellulose (cell wall) dye Direct Red 23. (C) Primary root length box plot summary of 7-do seedlings in indicated genotypes. Medians are represented inside the boxes by solid lines, circles depict individual measurements (n = 51-61). Letters denote statistically significant differences among samples as determined by ANOVA followed by Tukey's HSD test (P < 0.05). Scale bars (A) = 0.5 mm, (B) = 200  $\mu$ m.

Furthermore, expressing untagged (*KOR1p:KOR1*) or N-terminal CITRINE (CIT)-tagged *KOR1* (*KOR1p:CIT-KOR1*) constructs in *kor1-4* fully complemented ectopic *JGP* activity and the mutant's short root length (Fig. 7A and C). As expected, CIT-KOR1 expressed under its endogenous promoter was localized across the entire root (Fig. 7B) (Rips et al., 2014).



This verified that mutations in *KOR1* trigger the constant activation of JA-Ile signalling in mutant roots and that the CIT-KOR1 fusion protein is functional. Interestingly, the strength of the *JGP* phenotypes in the three *kor1* alleles clearly differed (Fig. 8A). While *kor1-5* showed *JGP* activity in the whole primary root, *kor1-4* and *kor1-6* had milder phenotypes with GUS staining localizing predominantly in the root early differentiation zone, but not in the root division zone nor at older root portions (Fig. 8A). Despite *KOR1* being expressed everywhere and the occurrence of stunted shoot growth of characterized mutants (Rips et al., 2014), constitutive *JGP* activation was not detected in aerial tissues of *kor1* alleles (Fig. 8A). I further confirmed the activation of JA-Ile signalling in *kor1* alleles by quantifying transcript levels of *JAZ10* and an additional JA-Ile-dependent gene *JASMONATE OXYGENASE 3 (JOX3)*. The data confirmed elevated basal levels of JA-Ile marker transcripts in roots but not in shoots (Fig. 8B and C). In addition, shoot wounding and exogenous treatment with MeJA induced *JGP* reporter expression in *kor1* shoots and roots (Fig. 8A), further validating the root specificity of basal *JGP* activity.

I next determined whether the *JGP* phenotype is dependent on bioactive hormone production. I hence generated JA-deficient *kor1-4 aos* and *kor1-5 aos* double mutants, in which basal *JGP* reporter activity was indeed fully abolished (Fig. 8A). Similar to *aos*, *kor1 aos* mutants only displayed *JGP* activation upon treatment with exogenous MeJA but not after wounding (Fig. 8A). Likewise, *JAZ10* transcript levels in *kor1-4 aos* were similar to the WT at basal conditions and did not increase after shoot wounding, further confirming that constitutive JA-Ile signalling in *kor1* mutants was dependent on increased JA-Ile biosynthesis (Fig. 8D and E). Consistently, bioactive hormone JA-Ile levels, as well as its precursors OPDA and JA, were significantly increased in *kor1-4* roots (Fig. 8F to H). A typical phenotype frequently observed in cellulose mutants is the ectopic lignification of the primary root, which is considered to be a compensatory mechanism due to the lack of proper cellulose biosynthesis (Zhong et al., 2002a; Cano-Delgado et al., 2003; Hematy et al., 2007). By performing phloroglucinol-HCl staining of seedlings I could also observe ectopic lignin patches in *kor1-4* roots in comparison to the WT, that were still present in the absence of JA-Ile (Fig. 8I).

To determine which of the *kor1* alleles is the most suitable tool for my further studies, I next investigated their morphological phenotypes. The *kor1-5* allele showed the most severe impairment in shoot growth and root elongation, while *kor1-4* and *kor1-6* had milder phenotypes (Fig. S1A and B). Hence, root length of *kor1* alleles correlated with the activation of JA. Because of its severe stunted growth, *kor1-5* plants barely produced seeds and were hard to propagate or to transform.

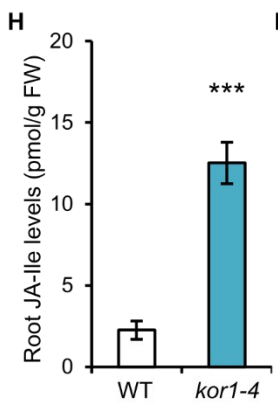
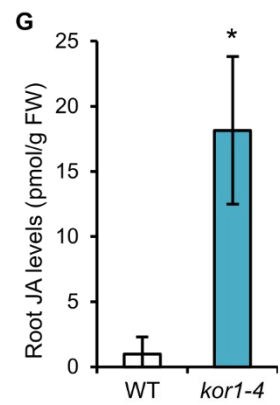
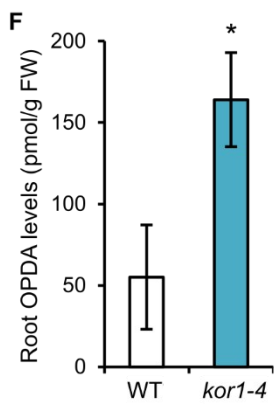
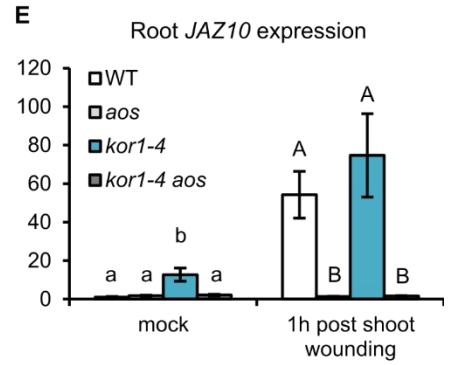
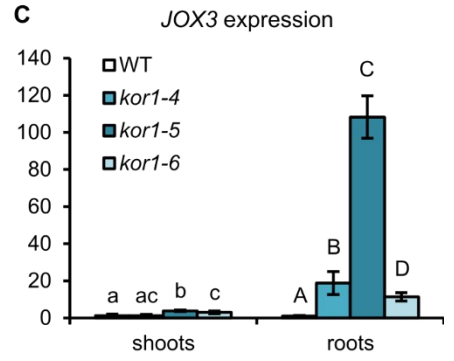
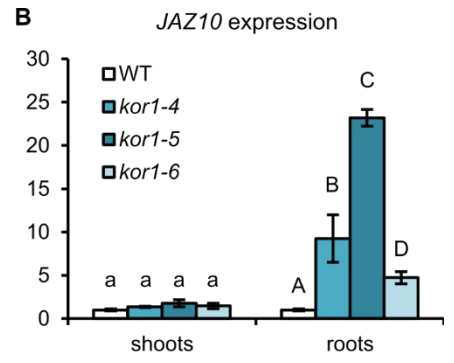
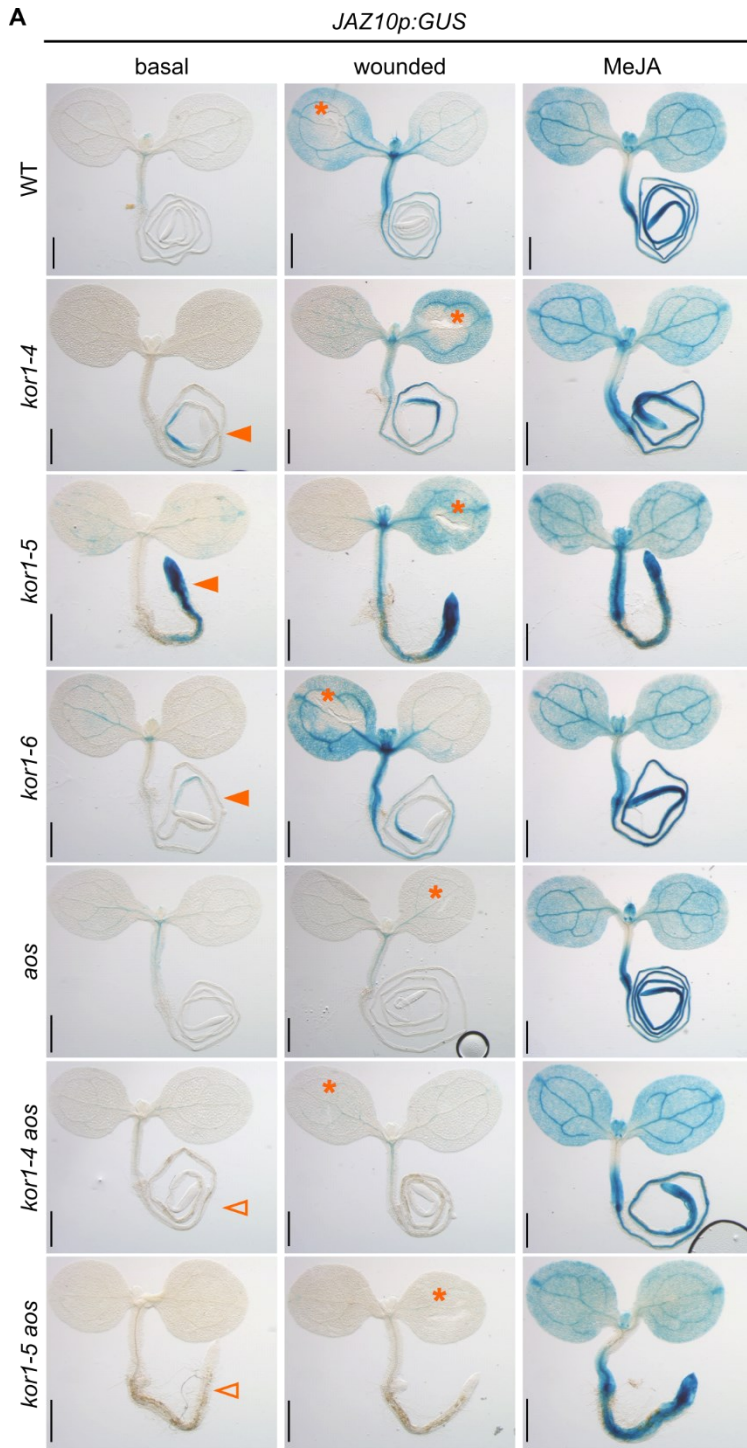


**Figure 8: Mutations in *KOR1* exhibit constitutive root JA-Ile production and signalling.** (A) Representative *JAZ1op:GUS* reporter activity in 5-do seedlings of indicated genotypes at basal conditions, 2 h after cotyledon wounding (orange asterisks) and 2 h after 10  $\mu$ M MeJA treatment. Note the presence of *JAZ1op:GUS* reporter activity in roots of *kor1* mutants at basal conditions (orange arrowheads), and its absence in *kor1 aos* mutants (empty arrowheads). Scale bars = 0.5 mm. (B and C) qRT-PCR of basal (B) *JAZ1o* and (C) *JOX3* expression in shoots and roots of indicated genotypes. *JAZ1o* and *JOX3* transcript levels were normalized to those of *UBC21*. (D and E) qRT-PCR of *JAZ1o* expression basally and 1 h after shoot wounding in (D) aerial organs and (E) roots of WT, *aos*, *kor1-4*, and *kor1-4 aos*. *JAZ1o* transcript levels were normalized to those of *UBC21*. Bars in (B to E) represent the means of three biological replicates ( $\pm$ SD), each containing a pool of ~60 organs from 5-do seedlings. (F to H) Absolute (F) OPDA, (G) JA, and (H) JA-Ile content in WT and *kor1-4* roots. Bars represent the means of three biological replicates ( $\pm$ SD), each containing a pool of ~600 roots from 5-do seedlings. (I) Representative phloroglucinol-HCl stainings showing lignin deposition (fuchsia color) in primary roots of indicated genotypes. Scale bars = 200  $\mu$ m. Letters and asterisks denote statistically significant differences among samples as determined by (B to E) ANOVA followed by Tukey's HSD test ( $P < 0.05$ ), or by (F to H) Student's t-test ( $P * \leq 0.05$ ,  $*** \leq 0.001$ ).

Given that *kor1-4* exhibited milder growth defects but still displayed a robust JA phenotype, I employed this allele for all further analyses. Collectively, my data indicate that *KOR1* is a negative regulator of root JA-Ile biosynthesis. Therefore, *kor1* mutants represent valuable genetic tools to study how cell-wall derived signals are linked to intracellular hormone production.

## 2. Is the activation of ectopic JA-Ile signalling in *kor1* cell-autonomous or non-cell autonomous?

*Data from this chapter is published in (Mielke et al., 2021, Science Advances).*

### Constitutive activation of JA-Ile signalling in *kor1-4* roots occurs predominantly in endodermis and pericycle cells of the root early differentiation zone

Given that ectopic *JGP* reporter activity was confined to specific *kor1-4* root portions (Fig. 8A), I wanted to identify the precise cell types displaying increased JA-Ile signalling. However, this question could not be addressed with the *JGP* reporter as it is secreted into the apoplast and is therefore not suitable for detailed cellular analysis (Acosta et al., 2013). I therefore generated a transcriptional reporter line expressing 3x-VENUS coupled to a nuclear localisation signal (NLS-3xVEN) under the control of *JAZ1op* (*JAZ1op:NLS-3xVEN*), which could be visualized by *in vivo* live cell imaging. Similar to the *JGP* reporter, *JAZ1op:NLS-3xVEN* expression was not present basally in primary roots of WT or *aos* plants, but was strongly induced after MeJA treatment in both WT and *aos* roots (Fig. S2). Consistently mechanical wounding of cotyledons triggered the reporter induction in roots of the WT but not in *aos* (Fig. S2).

In contrast to the WT, primary roots of *kor1-4* exhibited basal reporter expression chiefly in the early differentiation zone of the primary root, where optical confocal sections revealed the presence of the signal mainly in endodermis and pericycle cell files (Fig. 9B and C). I then quantified the presence of

the reporter along longitudinal cell files of epidermis, cortex, endodermis, and pericycle cells from 20 roots and generated a frequency map for each cell layer (Fig. 9D). On average, the reporter was weakly activated around the onset of cell elongation and proceeded to show more frequent activation in the early differentiation zone, before ceasing approximately 30 cells after the onset of elongation. The reporter was present only sporadically in a few epidermal or cortex cells, and the predominant site of its activation was observed in a stretch of 10 to 15 cells in endodermis and pericycle after the onset of differentiation (Fig. 9D).

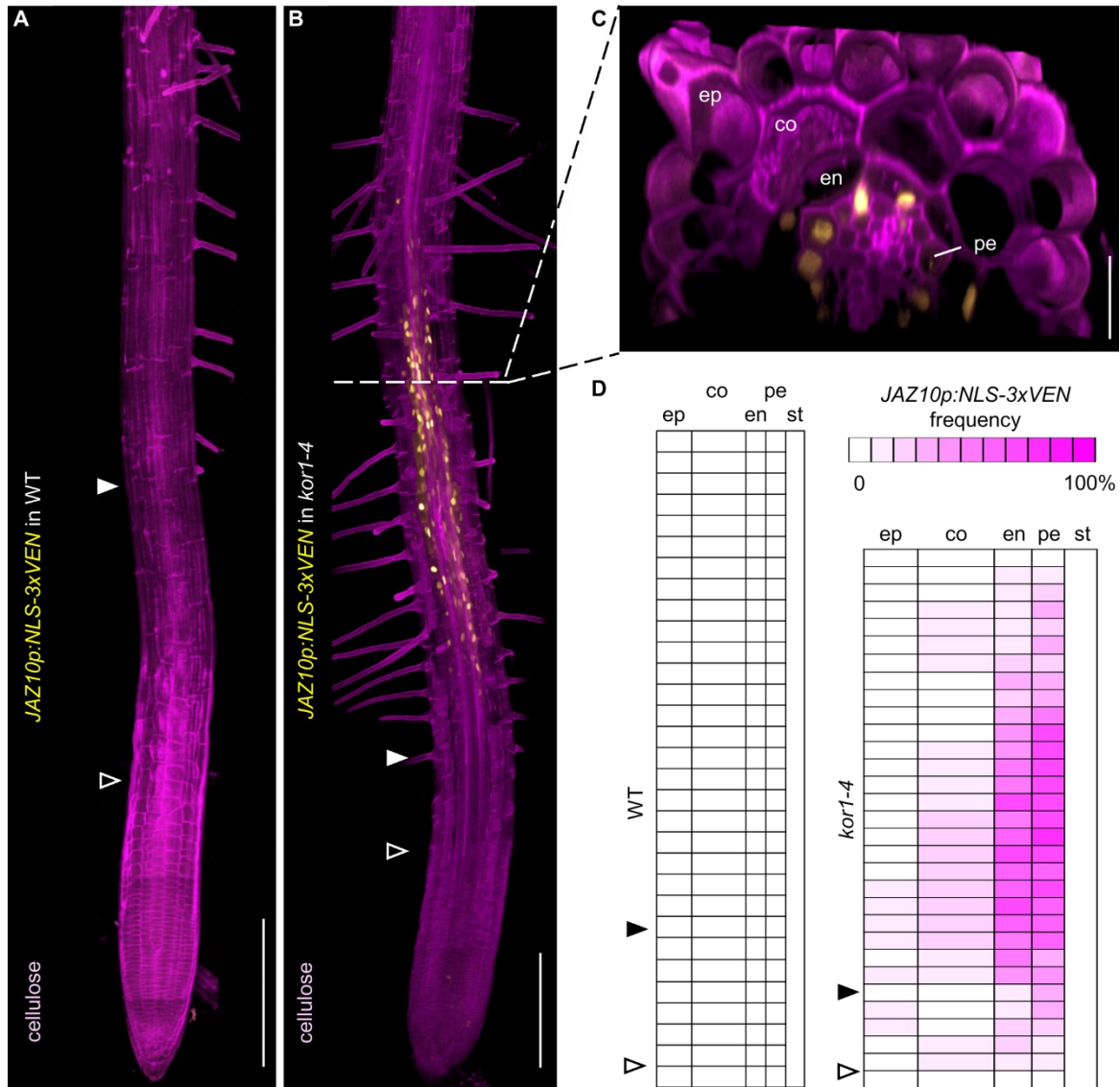


**Figure 9: *kor1-4* roots exhibit increased JA-Ile signalling in endodermis and pericycle cells.** (A to C) *JAZ10p:NLS-3xVEN* expression in (A) WT and (B and C) *kor1-4* 5-do roots cleared with ClearSee, counterstained with the cellulose dye Direct Red 23 and visualized as a 3D texture based volume renderings from Z-stacks. (C) Orthogonal view from of an optical *kor1-4* root section. The onset of elongation is indicated by empty arrowheads (first elongated cortex cell), and that of differentiation by filled arrowheads (presence of root hairs). ep, epidermis; co, cortex; en, endodermis; pe, pericycle. Scale bars (A and B) = 200  $\mu$ m, (C) = 30  $\mu$ m. (D) Heatmap of *JAZ10p:NLS-3xVEN* frequency in individual cells from WT and *kor1-4* primary roots (n = 21). Presence or absence of the reporter was evaluated from the onset of elongation in individual cells along consecutive longitudinal files for each tissue layer. Reporter expression was not observed in the WT nor in *kor1-4* vascular tissues of the stele (st). The onset of elongation is indicated by an empty arrowhead and that of differentiation by a filled arrowhead.

### Cortex-specific CIT-KOR1 expression complements ectopic JA-Ile signalling in inner *kor1* tissues

As JA signals can travel from cell to cell and JA-Ile precursors are mobile (Schulze et al., 2019; Li et al., 2020a), the activation of JA-Ile signalling in *kor1-4* endodermal and pericycle cells could be a result of either cell-autonomous or cell non-autonomous signals.

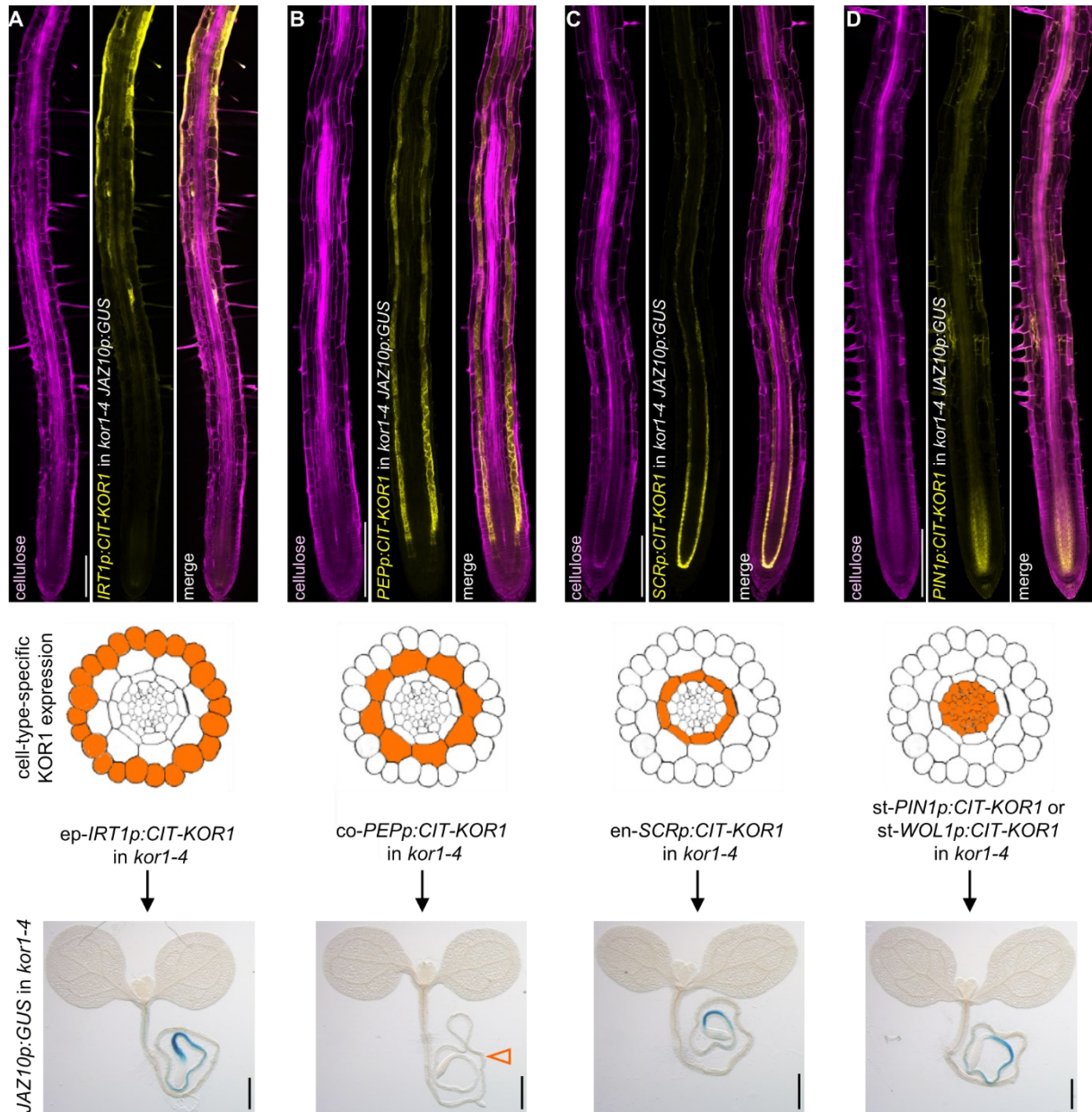


**Figure 10: Cortical-specific KOR1 expression complements the constitutive JA-Ile signalling in *kor1-4*.** (A to D) Representative images of cell-type specific CIT-KOR1 expression in 5-day *kor1-4* seedling roots and respective *JAZ10p:GUS* reporter activity in these lines. CIT-KOR1 expression was driven by either (A) the epidermal *IRT1* promoter (*ep-IRT1p:CIT-KOR1*), (B) the cortex *PEP* promoter (*co-PEPp:CIT-KOR1*), (C) the endodermal *SCR* promoter (*en-SCRp:CIT-KOR1*), or (D) the pericycle- and stele-specific *PIN1* or *WOL1* promoters (*st-PIN1p:CIT-KOR1*, *st-WOL1p:CIT-KOR1*). Samples for CIT-KOR1 visualization were cleared with ClearSee and counterstained with the cellulose dye Direct Red 23. Note that cortex-expressed CIT-KOR1 complements *JAZ10p:GUS* activity in *kor1-4* roots (empty orange arrowhead). Scale bars (A to D) = 200  $\mu$ m (fluorescence images) and 0.5 mm (GUS-stained seedlings).

To determine which tissue is the source of JA-Ile biosynthesis, I generated lines for cell-specific expression of CIT-KOR1 in epidermis, cortex, endodermis or stele by using promoters *IRON-REGULATED TRANSPORTER 1 (IRT1p)*, *PLASTID ENDOPEPTIDASE (PEPp)*, *SCARECROW (SCRp)*, or *WOODEN LEG 1 (WOL1p)*, respectively (Marques-Bueno et al., 2016). When expressed under its endogenous promoter, which led to full complementation of JA-Ile signalling and root growth, CIT-KOR1 was visualized in all root tissues (Fig. 7A to C). Similarly, CIT-KOR1 expressed under cell-type-specific promoters was localized to the expected cell types in the primary root (Fig. 10A to C). Because the WOL1p:CIT-KOR1 construct displayed very weak fluorescence signals at the intended locations, I used an additional promoter (*PIN-FORMED 1, PIN1p*) to drive CIT-KOR1 in the stele, which includes the pericycle (Marques-Bueno et al., 2016) (Fig. 10D). After ensuring CIT-KOR1 localized to the expected tissue-types, I then analysed whether any of these constructs were able to complement the ectopic JA-Ile signalling in *kor1-4 JGP*. Remarkably, JA-Ile signalling in *kor1-4* roots was complemented only when CIT-KOR1 was expressed in the cortex, but not when expressed in the epidermis, nor in endodermis or pericycle cells which exhibited ectopic *JGP* expression (Fig. 10A to D). Primary root length was also partially restored in cortex-complemented transformants only, while it remained unchanged when expressing the construct in the epidermis, or got even more stunted by cell-specific expression in endodermis and pericycle (Fig. S3). This suggests that ectopic JA-Ile production in *kor1-4* is cell non-autonomous, and triggered by a yet unknown mechanism originating from the cortex.

### 3. A reverse genetics approach to identify components involved in the initiation of JA-Ile biosynthesis in *kor1-4* roots

*Data from this chapter is unpublished. Manuscript in preparation.*

To identify cellular genetic components regulating JA-Ile production in *kor1-4* roots, I undertook a reverse genetic approach based on candidate genes differentially expressed in *kor1-4* roots, and on plasma membrane localized cell wall integrity sensors known from the literature.

#### The *kor1-4* root transcriptome

To gain a global overview on the transcriptional changes occurring in *kor1-4* roots, we performed an RNA-seq analysis of WT, *aos*, *kor1-4*, and *kor1-4 aos* roots. The study was performed on four genotypes with the aim to categorize differentially expressed genes (DEG) in *kor1-4* as being JA-dependent or JA-independent. The transcriptome of each genotype was first normalized to values found in the WT, revealing that 769 transcripts were mis-regulated in *kor1-4* roots, with 439 genes being upregulated and 330 downregulated [cutoff of 2.5-fold-change (FC), i.e.  $\log_{2}FC = \pm 1.32$ ].

Hierarchical clustering then classified DEG transcripts in *kor1-4* according to their differential expression pattern across the three normalized genotypes in 7 groups (Fig. 11A). DEGs in *kor1-4* that were not in common with *kor1-4 aos* were classified as JA-dependent, with *kor1-4 aos* suppressing DEG levels found in *kor1-4* by at least 50% logFC (classes 1, 2, 5, and 6).

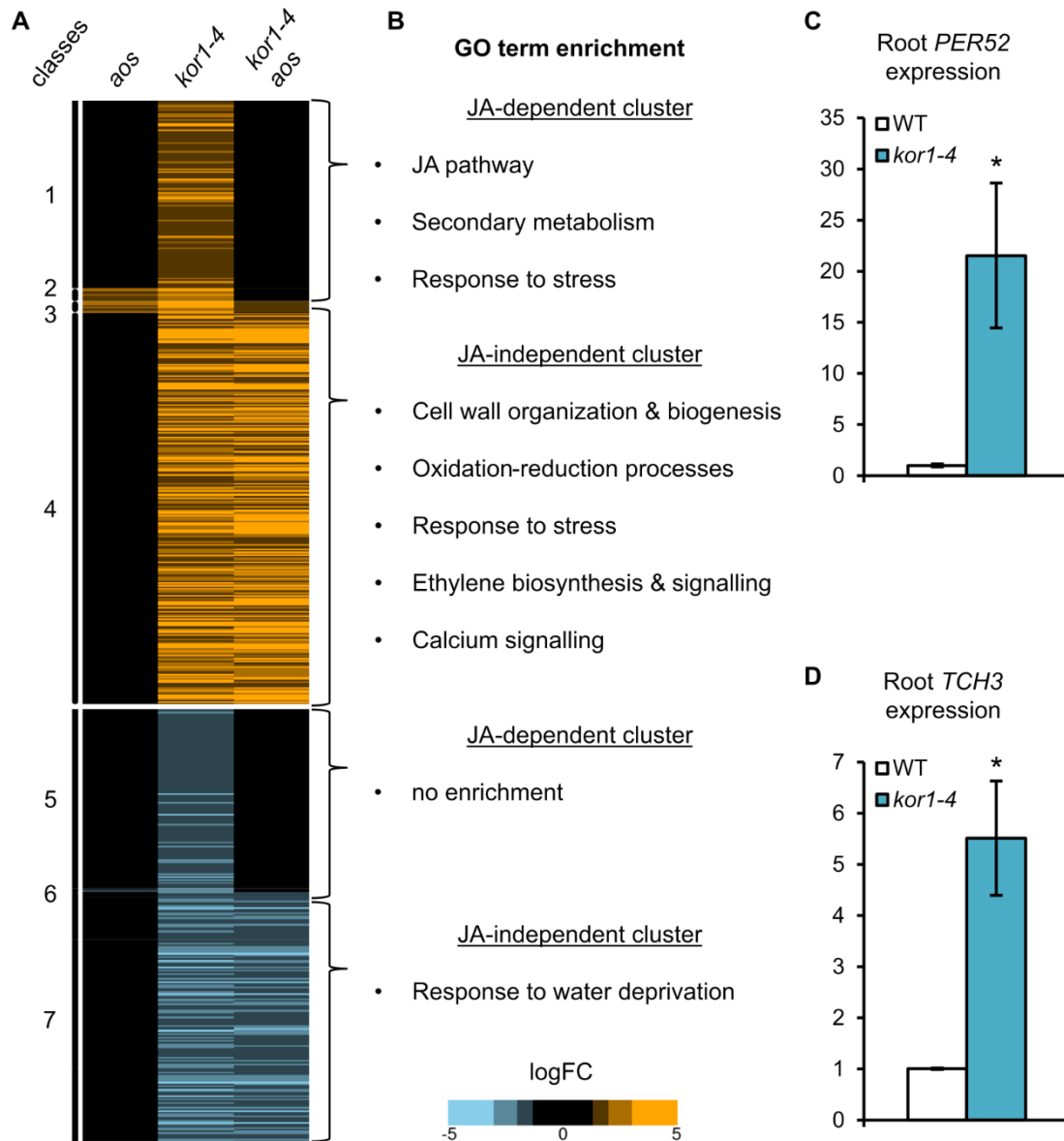


**Figure 11: Global RNA-seq root transcriptome identifies JA-dependent and JA-independent differentially expressed genes (DEGs) in *kor1-4*.** (A) Heat map representing the expression of 769 differentially expressed genes (DEGs) in 5-do *kor1-4* roots with respect to the WT identified by RNA-seq. Indicated genotypes were first normalized to the WT, and then organized in 7 classes according to hierarchical clustering analysis. Upregulated transcripts are coloured in orange, downregulated ones in blue, and unchanged values with respect to the WT are shown in black (cutoff: logFC =  $\pm 1.32$ , p-value < 0.01). Transcripts were considered as JA-dependent (up- or downregulated in *kor1-4* but not in *kor1-4 aos*, classes 1, 2, 5, and 6) or JA-independent (up- or down-regulated in both *kor1-4* and *kor1-4 aos*, classes 3, 4, and 7). (B) Examples of Gene ontology (GO) enriched terms from JA-dependent and JA-independent DEGs in *kor1-4* roots (aspect 'biological process'; false discovery rate < 0.05). Full dataset is available in Supplementary Tables S2 & S3. (C and D) qRT-PCR of basal (C) *PER52* and (D) *TOUCH3* (*TCH3*) expression in WT and *kor1-4* roots. Transcript levels were normalized to those of *UBC21* and displayed relative to the WT control. Bars represent the means of three biological replicates ( $\pm$ SD), each containing a pool of ~60 roots from 5-do seedlings. Asterisks denote statistically significant differences among samples as determined by Student's t-test (p < 0.05).

The JA-dependent group specifies transcripts downstream of the JA pathway and is critical to validate the upregulation of JA-mediated responses in *kor1-4* roots (Fig. 11A, Tab. S2). Conversely, shared DEGs between *kor1-4* and *kor1-4 aos* roots were considered as JA-independent when the logFC in *kor1-4 aos* remained at least 51% of values found in *kor1-4*, i.e. when *kor1-4 aos* did not drastically alter the DEG levels found in *kor1-4*. This group can potentially reveal processes that are upstream of JA-Ile production (classes 3, 4, and 7).

### **JA-dependent DEGs in *kor1-4* roots**

In the JA-dependent cluster, we found a total of 241 DEG genes in *kor1-4* roots, of which 123 were upregulated (classes 1 and 2) and 118 were downregulated (classes 5 and 6). Among these, Gene ontology (GO) enrichment analysis for 'biological process' revealed the upregulation of terms involved in the JA pathway, secondary metabolism and stress responses. No specific enrichment was found for downregulated transcripts and hence I focussed on the upregulated cluster (Tab. S2).

The global transcriptome analysis revealed the upregulation of the JA biosynthesis gene *LIPOXYGENASE 3 (LOX3)* and the 12-OH-JA catabolizing enzyme *SULFOTRANSFERASE 2A (ST2A)* (Gidda et al., 2003; Wasternack and Strnad, 2018), in addition to confirming elevated *JAZ10* and *JOX3* levels in *kor1-4* roots (Fig. 8B and C, Tab. S2). Other typical JA-Ile marker genes such as *JAZ3*, *JAZ9*, *LOX6*, and *JOX2* were also significantly upregulated in *kor1-4* in comparison to the WT, but were below the chosen cut-off value. Stronger JA-Ile-inducing stimuli such as mechanical wounding or insect herbivory typically result in a higher and larger induction of JA-Ile marker genes, including the majority of the 13 *JAZs*, *MYC2*, *LOX3*, *LOX4*, *AOS*, and *OPR3* (Reymond et al., 2004; Chung et al., 2008; Zhang et al., 2020). Overall, our results strengthen our observation on the activation of JA-Ile signalling in *kor1-4* mutant roots, and suggest that a specific subset of JA-Ile-dependent genes may be activated upon cell wall alterations or that JA-Ile responses are activated in a root restricted zone and hence the effect is diluted in a whole-root transcriptome (Fig. 9B).

Among the other GO clusters we found further genes that are known to be regulated by JA, which for instance includes transcripts from secondary metabolism (e.g. *MARNERAL SYNTHASE 1 [MRN1]*, upregulated in *jazQ* [Major et al., 2017] or *SQUALENE MONOOXYGENASE 2 [SQP2]*, upregulated in *ninja* [Gasperini et al., 2015]), amino acid metabolism (e.g. *TYROSINE AMINOTRANSFERASE 3 [TAT3]*, *MYC2/3/4*-dependent expression after MeJA treatment [Song et al., 2014]), oxidation-reduction processes (e.g. *At3g59710*, upregulated in *ninja* [Gasperini et al., 2015]) and nutrient transporters (*NITRATE TRANSPORTER 1.8 [NRT1.8]*, *COL1*-dependent upregulation during salt and cadmium stress [Zhang et al., 2014a]).



In contrast, it was rather unexpected that the highest upregulated JA-dependent transcript in the *kor1-4* roots transcriptome (*FARNESOIC ACID CARBOXYL-O-METHYLTRANSFERASE* [FAMT]) was not present in other transcriptomic analyses of MeJA-treated seedlings (Sasaki-Sekimoto et al., 2005) or in a *ninja* mutant that exhibits ectopic root JA-Ile signalling (Gasparini et al., 2015). Hence, our transcriptomic data set might be important to better understand JA responses specific to roots and could reveal novel physiological roles of JA-Ile-mediated signalling.

#### **JA-independent DEGs in *kor1-4* roots**

Among the 528 DEGs found in the *kor1-4* JA-independent cluster, 316 were upregulated (classes 3 and 4) and 212 were downregulated (class 7). A GO term enrichment analysis for 'biological process' revealed an enrichment for genes involved in cell wall organization and biogenesis, oxidation-reduction processes, stress, ET and calcium signalling as well as response to water deprivation (Fig. 11B, Tab. S3).

It is well described that defects in cellulose biosynthesis result in compensatory mechanisms from other cell wall components which are reflected both in terms of cell wall composition and transcriptional changes (Peng et al., 2000; Manfield et al., 2004; Denness et al., 2011). Consistently, *kor1-4* roots showed a conspicuous increase in transcripts involved in pectin (e.g. *PECTIN LYASE-LIKE 6* [PLL6], *PME17*), hemicellulose (e.g. *XYLOGLUCAN ENDOTRANSGLUCOSYLASE/HYDROLASE 26* and *22* [XTH26; XTH22]) and lignin metabolism (e.g. *DIRIGENT PROTEIN 5* [DIR5]), as well as transcripts involved in cell wall organization (e.g. *FASCICLIN-LIKE ARABINOGALACTAN 6* [FLA6]; *EXTENSIN 12* [EXT12]) (Tab. S3). Likewise, alterations in hemicellulose and pectin composition have been described for different alleles of *kor1* (Peng et al., 2000; His et al., 2001; Sato et al., 2001), and ectopic lignification is present in *kor1* primary roots (Fig. 8I). It is likely that the cell wall structural changes occurring in *kor1-4* give rise to intracellular signalling processes reflected in an upregulation of transcripts involved in oxidation-reduction processes (e.g. *PEROXIDASE 52* [PER52]; *MYO-INOSITOL OXYGENASE 4* [MIOX4], secondary metabolism (e.g. *BETA GLUCOSIDASE 27* [BGLU27]), membrane receptors, and ligands sensing events (e.g. *CONCANAVALIN A-LIKE LECTIN PROTEIN KINASE 52* [LECRK52]), response to water deprivation (e.g. *LATE EMBRYOGENESIS ABUNDANT 4-5* [LEA4-5]), regulation in gene transcription (e.g. *WRKY DNA-BINDING PROTEIN 28* [WRKY28]), as well as other stress responses (e.g. *PDF1.4*).

33 differentially expressed transcripts were found in the GO cluster of oxidation-/reduction processes, including several *PEROXIDASE* (*PER*) genes. This is not surprising as PERs are potent scavengers of reactive oxygen species (ROS) (Huang et al., 2019), which are known to increase upon cell wall

perturbations, reviewed in (Bacete et al., 2018). Moreover, several PERs like *PER52*, which's transcript was among the highest upregulated genes in the *kor1-4* transcriptome, are also involved in shaping the secondary plant cell wall as they participate in lignin biosynthesis (Fernandez-Perez et al., 2015; Hoffmann et al., 2020). The upregulation of *PER52* in *kor1-4* roots was validated in independent samples by qRT-PCR (Fig. 11C).

Similarly to heightened ET levels found in cellulose deficient mutants such as *cev1* and *chitinase-like protein 1* (Ellis and Turner, 2001; Ellis et al., 2002; Zhong et al., 2002b), the *kor1-4* root transcriptome revealed an upregulated gene cluster enriched for GO terms in ET biosynthesis and signalling indicating that this pathway is strongly upregulated in the mutant (Tab. S3). The ET pathway is a major mediator of many developmental and stress responses (Muller and Munne-Bosch, 2015; Dubois et al., 2018), including growth regulation and pathogen resistance, and can result in both synergistic and antagonistic crosstalk interactions with the JA pathway, reviewed in (Zhu and Lee, 2015). Several JAZ repressors can interact with and suppress ET-related transcription factors ETHYLENE INSENSITIVE 3 (EIN3) and EIN3 LIKE 1 (EIL1) to regulate pathogenesis-related genes upon necrotrophic fungal infection (Zhu et al., 2011). Although, several other transcripts involved in other phytohormones were misregulated in *kor1-4* roots (e.g. *GIBBERELLIN 2-OXIDASE [GA2OX2]*; *INDOLE-3-ACETIC ACID CARBOXYMETHYLTRANSFERASE 1 [IAMT1]*) the transcriptome indicated that the major perturbations in hormonal responses occur in ET and JA pathways (Tab. S3).

In addition to having an upregulated ET pathway, *kor1-4* roots displayed an increase in transcripts involved in Ca<sup>2+</sup> signalling, such as *CALMODULIN-LIKE* proteins (*TCH3*, *CML25*, *CML46*, and *CML47*), a calmodulin binding transcription activator (*CMTA3*) and a calcium-transporting ATPase (*ACA13*, Tab. S3). Calmodulins are principal sensors of Ca<sup>2+</sup> signals that decode and relay information via interactions with a wide spectrum of targets to modulate their biochemical activities, reviewed in (Zeng et al., 2015). Several studies have shown that increases in Ca<sup>2+</sup> levels correlate with the activation of JA-Ile biosynthesis and signalling (Scholz et al., 2014; Matschi et al., 2015; Lenglet et al., 2017). These observations were further substantiated by the identification of clade 3 GLR proteins as regulators of Ca<sup>2+</sup> fluxes that stimulate distal JA-Ile production (Mousavi et al., 2013; Nguyen et al., 2018; Toyota et al., 2018). The strong upregulation of *TCH3* in *kor1-4* roots was validated in independent samples by qRT-PCR (Fig. 11D). Hence, upregulated Ca<sup>2+</sup> signalling may be upstream of JA-Ile production in *kor1-4*.

## A candidate gene approach based on JA-independent DEGs in *kor1-4* roots did not identify regulators of constitutive JA-Ile production

All *kor1-4* DEG genes belonging to the JA-independent cluster (Tab. S3) could be putative regulators of JA-Ile production in mutant roots. To test this assumption, I selected a subset of highly upregulated genes belonging to this cluster across several GO terms, ordered relative T-DNA insertion mutants and crossed them to *kor1-4* to assess if JA-Ile signalling is suppressed in resulting double mutants. Selected genes and relative results are summarized in Table 1.

**Table 1: Reverse genetics screen to identify suppressors of JA-Ile production in *kor1-4* roots**

Gene (AGI code)	Mutant	Mutation	Reference	Current cross to <i>kor1-4</i>	JA phenotype in double mutant
<b>Selected JA-independent upregulated genes from <i>kor1-4</i> root transcriptome</b>					
<i>ETHYLENE INSENSITIVE 2, EIN2</i> (At5g03280)	<i>ein2-1</i>	Q556*	(Alonso et al., 1999)	F <sub>3</sub>	no suppression ( <i>JGP</i> reporter activity & <i>JAZ10</i> qPCR)
<i>TOUCH 3, TCH3</i> (At2g41100)	<i>tch3-2</i>	T-DNA insertion (SALK_090554)	(Wang et al., 2011)	F <sub>3</sub>	no suppression ( <i>JGP</i> reporter activity)
<i>CALCIUM-TRANSPORTING ATPase 13, ACA13</i> (At3g22910)	<i>aca13</i>	T-DNA insertion (SAIL_878_Bo6)	(Iwano et al., 2014)	F <sub>3</sub>	no suppression ( <i>JGP</i> reporter activity)
<i>PEROXIDASE 52, PER52</i> (At5g05340)	<i>per52-1</i>	T-DNA insertion (SALK_081257)	(Pourcel et al., 2013)	F <sub>3</sub>	no suppression ( <i>JGP</i> reporter activity)
<i>XYLOGLUCAN ENDOTRANSGLUCOSYLASE/HYDROLASE 26, XTH26</i> (At4g28850)	<i>xth26-2</i>	T-DNA insertion (SALK_055758)	u.a.	F <sub>3</sub>	no suppression ( <i>JGP</i> reporter activity)
<i>EXTENSIN 12, EXT12</i> (At4g13390)	<i>ext12</i>	T-DNA insertion (SAIL_1249_F11)	(Velasquez et al., 2011)	F <sub>1</sub>	n.a.
<i>PUTATIVE PECTATE LYASE-LIKE 6, PLL6</i> (At1g11920)	<i>pll6-1</i>	T-DNA insertion (GK_033D05)	u.a.	F <sub>3</sub>	no suppression ( <i>JGP</i> reporter activity)
<i>LIPOXYGENASE 4</i> (At1g72520)	<i>lox4A</i>	T-DNA insertion (SALK_071732)	(Caldelari et al., 2011)	F <sub>3</sub>	no suppression ( <i>JGP</i> reporter activity)
<i>RECEPTOR-LIKE PROTEIN 38</i> (At3g23120)	<i>rlp38-1</i>	T-DNA insertion (SALK_017819)	(Wang et al., 2008)	F <sub>1</sub>	n.a.
<b>Cell wall integrity sensing</b>					
<i>THESEUS1, THE1</i> (At5g54380)	<i>the1-1</i>	G37D	(Hematy et al., 2007)	F <sub>3</sub>	partial suppression ( <i>JAZ10</i> qPCR)
<i>RHO-RELATED PROTEIN FROM PLANTS 2, ROP2</i> (At1g20090)	<i>rop2-12</i>	T-DNA insertion (WiscDsLox441B8)	u.a.	F <sub>3</sub>	no suppression ( <i>JGP</i> reporter activity)
<i>ERULUS, ERU</i> (At5g61350)	<i>eru-2</i>	T-DNA insertion (SALK_083442)	(Bai et al., 2014)	F <sub>3</sub>	no suppression ( <i>JAZ10</i> qPCR)
<i>WALL-ASSOCIATED KINASE 1, WAK1</i> (At1g21250)	<i>wak1-1</i>	T-DNA insertion (SALK_107175)	(Zarattini et al., 2017)	F <sub>3</sub>	no suppression ( <i>JGP</i> reporter activity)
<i>WALL-ASSOCIATED KINASE 2, WAK2</i> (At1g21270)	<i>wak2-12</i>	T-DNA insertion (SAIL_12_Do5)	(Engelsdorf et al., 2018)	F <sub>2</sub>	n.a.
<i>HERKULES 1, HERK1</i> (At3g46290)	<i>herk1-1</i>	T-DNA insertion (SALK_008043)	(Guo et al., 2009)	F <sub>3</sub>	no suppression ( <i>JAZ10</i> qPCR)
<i>HERKULES 2, HERK2</i> (At1g30570)	<i>herk2-1</i>	T-DNA insertion (SALK_105055)	(Guo et al., 2009)	F <sub>3</sub>	no suppression ( <i>JGP</i> reporter activity)

**Table 1 (continued)**

Gene (AGI code)	Mutant	Mutation	Reference	Current cross to <i>kor1-4</i>	JA phenotype in double mutant
<i>MARIS</i> , <i>MRI</i> (At2g41970)	<i>mri-2</i>	T-DNA insertion (GK_820D05)	(Boisson-Dernier et al., 2015)	F <sub>2</sub>	n.a.
<i>RECEPTOR-LIKE PROTEIN 44</i> , <i>RLP44</i> (At3g49750)	<i>rlp44-3</i>	T-DNA insertion (SAIL_596_E12)	(Wolf et al., 2014)	F <sub>3</sub>	no suppression ( <i>JAZ10</i> qPCR)
<i>MDIS1-INTERACTING RECEPTOR LIKE KINASE1</i> , <i>MIK1</i> (At4g28650)	<i>mik1</i>	T-DNA insertion (SALK_095005)	(Wang et al., 2016)	F <sub>2</sub>	n.a.
<i>MDIS1-INTERACTING RECEPTOR LIKE KINASE2</i> , <i>MIK2</i> (At4g08850)	<i>mik2-1</i>	T-DNA insertion (SALK_061769)	(Wang et al., 2016)	F <sub>2</sub>	n.a.
<i>STRUBBELIG</i> , <i>SUB</i> (At1g11130)	<i>sub-9</i>	T-DNA insertion (SAIL_1158_D09)	(Vaddepalli et al., 2011)	F <sub>3</sub>	no suppression ( <i>JGP</i> reporter activity)
<b>Mechano- / Osmo-sensitive channels and receptors</b>					
<i>MID1-COMPLEMENTING ACTIVITY 1</i> , <i>MCA1</i> (At4g3592)	<i>mca1-3</i>	T-DNA insertion (SALK_206846)	u.a.	F <sub>2</sub>	n.a.
<i>MECHANOSENSITIVE CHANNEL OF SMALL CONDUCTANCE-LIKE 10</i> , <i>MSL10</i> (At5g12080)	<i>msl10-1</i>	T-DNA insertion (SALK_076254)	(Haswell et al., 2008)	F <sub>2</sub>	n.a.
<i>DEFECTIVE KERNEL 1</i> , <i>DEK1</i> (AT1G55350)	<i>dek1-4</i>	C2106R	(Roeder et al., 2012)	F <sub>2</sub>	n.a.
<i>REDUCED HYPEROSMOLALITY, INDUCED CA<sup>2+</sup> INCREASE 1</i> , <i>OSCA1</i> (At4g04340)	<i>osca1-2</i>	T-DNA insertion (SAIL_607_F09)	(Yuan et al., 2014)	F <sub>3</sub>	no suppression ( <i>JAZ10</i> qPCR)
	<i>osca1-4</i>	T-DNA insertion (SAIL_1172_D02)	u.a.	F <sub>3</sub>	no suppression ( <i>JGP</i> reporter activity)

n.a. = not analyzed

u.a. = uncharacterized allele

Upregulated ET signalling may in principle sequester JAZ repressors via their engagement with ET-dependent TF, and thus result in increased JA-Ile signalling (Zhu et al., 2011). To test if heightened ET responses are upstream of JA-Ile production in *kor1-4* roots, I generated an ET insensitive double mutant by crossing *kor1-4 JGP* to a mutant in *ETHYLENE INSENSITIVE 2 (EIN2)*, *ein2-1*, required for ET signalling (Alonso et al., 1999). The resulting *kor1-4 ein2-1* double mutant still displayed constitutive *JGP* reporter activity and elevated *JAZ10* transcript levels, similar to *kor1-4* roots (Fig. 12A and B). Furthermore, when *kor1-4 JGP* seedlings were grown on media supplemented with inhibitors of ET biosynthesis or signalling, aminoethoxyvinylglycine (AVG) or AgNO<sub>3</sub> respectively (Schaller and Binder, 2017), they still exhibited constitutively elevated JA-Ile signalling levels (Fig. 12A). Collectively, these results indicated that the upregulated ET pathway does not act upstream of JA-Ile production in *kor1-4* roots.

Although it is still unclear how Ca<sup>2+</sup> changes may impact JA-Ile biosynthesis (Mielke and Gasperini, 2019), it was proposed that the PLAT domain of 13-LOX enzymes may bind Ca<sup>2+</sup> ions leading to their activation (Hammarberg et al., 2000; Kulkarni et al., 2002; Farmer et al., 2014). Interestingly, unlike *LOX3* that was upregulated in the JA-dependent cluster of *kor1-4* roots, *LOX4* was upregulated in a JA-independent manner (Tab. S3 GO cluster: "Response to stress"). I hence hypothesized that

elevated  $\text{Ca}^{2+}$  signalling (or ions) in *kor1-4* may specifically activate the  $\text{LOX}_4$  enzyme to produce JA-Ile and hence increase signalling and upregulate  $\text{LOX}_{3/4}$  and  $\text{JAZ}$  transcripts. However, abolishing  $\text{LOX}_4$  function in *kor1-4* did not reduce heightened  $\text{JGP}$  levels, indicating that  $\text{LOX}_4$  is not upstream of JA-Ile production in the mutant (Fig. 12D).

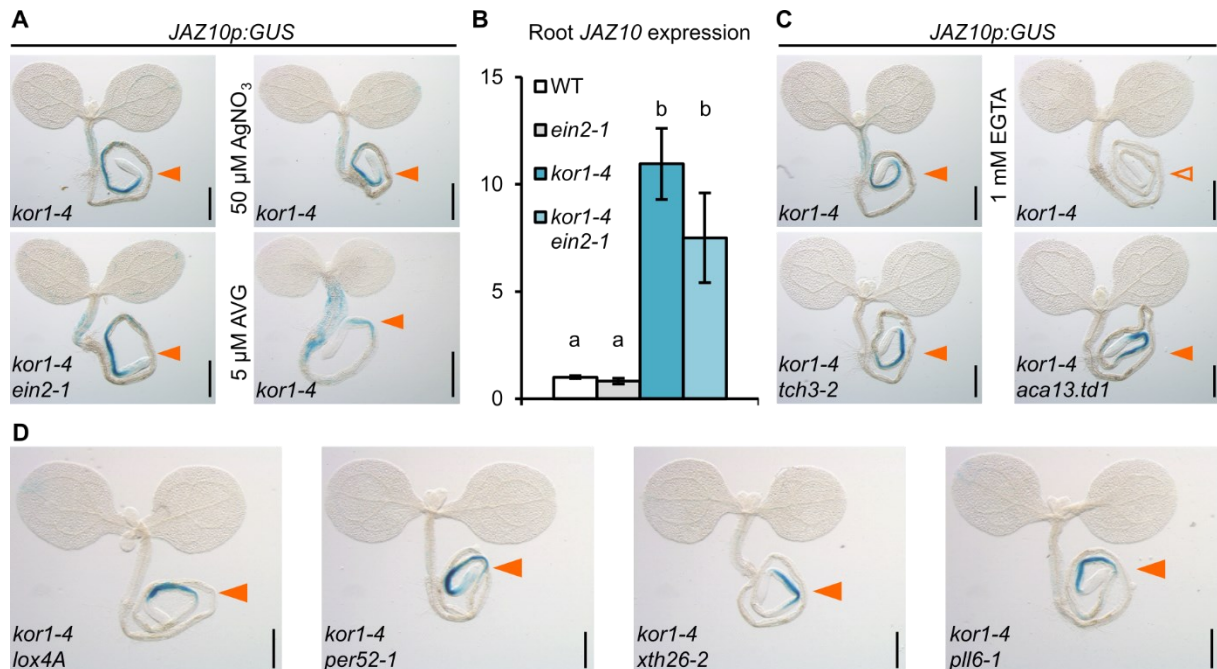


**Figure 12: A reverse genetics approach did not identify suppressors of ectopic JA-Ile production in *kor1-4*.** (A and B) Inhibition of ET biosynthesis or signalling does not suppress the high JA-Ile signalling levels in *kor1-4*. (A) Representative images of  $\text{JGP}$  expression in *kor1-4* and *kor1-4 ein2-1* grown under control conditions, and of *kor1-4* grown in the presence of ET biosynthesis inhibitors 50  $\mu\text{M}$   $\text{AgNO}_3$  or 5  $\mu\text{M}$  Aminoethoxyvinylglycine (AVG). The  $\text{JGP}$  reporter was active in all conditions (B) qRT-PCR of basal  $\text{JAZ}10$  expression in roots of WT, *ein2-1*, *kor1-4*, and *kor1-4 ein2-1*.  $\text{JAZ}10$  transcript levels were normalized to those of  $\text{UBC}21$  and displayed relative to the WT controls. Bars represent the means of three biological replicates ( $\pm\text{SD}$ ), each containing a pool of ~60 organs from 5-day seedlings. Letters denote statistically significant differences among samples as determined by ANOVA followed by Tukey's HSD test ( $P < 0.05$ ). (C and D) Representative images of  $\text{JGP}$  expression in (C) *kor1-4*, *kor1-4 tch3-2*, *kor1-4 aca13*, and *kor1-4* grown on 1 mM ethylene glycol-bis( $\beta$ -aminoethyl ether)-N,N,N',N'-tetra acetic acid (EGTA) and (D) *kor1-4 lox4A*, *kor1-4 per52-1*, *kor1-4 xth26-2*, and *kor1-4 pll6-1*. Note that basal  $\text{JGP}$  reporter activity in *kor1-4* roots was not suppressed in any double mutant combinations but was abolished upon EGTA treatment (empty arrowhead). Scale bars (A, C and D) = 0.5 mm.

Similarly, *kor1-4* double mutant combinations with  $\text{TCH}_3$  or  $\text{ACA}13$  (Tab. 1) did not suppress ectopic JA-Ile signalling in *kor1-4* roots (Fig. 12C).  $\text{TCH}_3$  was proposed to be involved in mechanosignalling (Benjamins et al., 2003; Lee et al., 2005; Hamant and Haswell, 2017) while  $\text{ACA}13$  belongs to a group of membrane-bound ATPases that mediate  $\text{Ca}^{2+}$  efflux during stress and developmental processes (Frei dit Frey et al., 2012; Iwano et al., 2014). To question whether  $\text{Ca}^{2+}$  could be involved in regulating JA-Ile biosynthesis in *kor1-4* more generally, I grew *kor1-4 JGP* seedlings in the presence of the  $\text{Ca}^{2+}$  chelator ethylene glycol-bis( $\beta$ -aminoethyl ether)-N,N,N',N'-tetra acetic acid (EGTA), which hampers  $\text{Ca}^{2+}$  signalling by chelating free  $\text{Ca}^{2+}$  (De Vriese et al., 2018). The treatment totally suppressed  $\text{JGP}$  reporter activity in mutant roots (Fig. 12C). However, EGTA treatments are very harsh and often result

in many pleiotropic consequences due to the chelating effects of multiple divalent cations (De Vriese et al., 2018), precluding accurate results interpretations. Nevertheless, these preliminary studies indicate that  $\text{Ca}^{2+}$  ions may be involved in JA-Ile production in *kor1-4* roots, although the reverse genetics screen approach did not identify any specific component.

The transcriptomics data also revealed many genes involved in cell wall biogenesis and organization as being misregulated in *kor1-4* in a JA-independent manner (Tab. S3). It has been proposed that specific cell wall fragments may act as DAMPs to initiate intracellular signalling, including a direct or indirect upregulation of JA (Campos et al., 2014). I therefore generated several double mutants with *kor1-4* which are involved in hemicelluloses, pectins, and lignin metabolism (*XYLOGLUCAN ENDOTRANSGLUCOSYLASE/HYDROLASE 26* [*XTH26*], *PECTATE LYASE-LIKE 6* [*PLL6*], and *PER52* respectively [Tab. 1]), but none of these suppressed basal *JGP* reporter activity (Fig. 12D).

### **A second reverse genetics approach did not identify regulators of constitutive JA-Ile production in *kor1-4* roots**

In a complementary reverse genetic approach aimed at identifying upstream components regulating JA-Ile biosynthesis in *kor1-4* roots, I investigated whether known cell wall integrity sensors, mechano- and osmo-sensors located at the plasma membrane are involved in this process, reviewed in (Hamant and Haswell, 2017; Wolf, 2017; Bacete and Hamann, 2020). In line with my hypothesis, (Engelsdorf et al., 2018) found isoxaben-induced JA production was partly dependent on the CrRLK proteins *THE1* and *FEI2*, and the ion channel *MCA1*.

Therefore, I crossed knockout alleles of 11 RLKs (*FER*, *THE1*, *WAK1*, *WAK2*, *HERCULES RECEPTOR KINASE 1* [*HERK1*], *HERK2*, *ERULUS RECEPTOR KINASE* [*ERU*], *MARIS RECEPTOR KINASE* [*MRI*], *MDIS1-INTERACTING RECEPTOR LIKE KINASE1* [*MIK1*], *MIK2*, and *STRUBBELIG* [*SUB*]), one receptor-like protein (*RLP44*), a Rho GTPase involved in signal transduction (*ROP2*) and 4 genes implicated in the perception of mechanical or osmotic cues (*MCA1*, *MSL10*, *DEFECTIVE KERNEL 1* [*DEK1*], and *REDUCED HYPEROSMOLALITY - INDUCED  $\text{Ca}^{2+}$  INCREASE 1* [*OSCA1*]) to *kor1-4 JGP*. The specific alleles used and the current state of the double mutants are summarized in Table 1. I then assessed if JA signalling was compromised in the resulting double mutants. Basal *JGP* reporter activity in *kor1-4* roots was not abolished in mutant backgrounds of *herk2-1*, *sub-9*, *osca1-4*, *rop2-12*, and *wak1-1* (Fig. 13A). Likewise, elevated *JAZ10* transcript levels were not suppressed in double mutants with *eru-2*, *herk1-1*, *osca1-2*, and *rlp44-3* (Fig. 13C). However, the absence of functional *THE1* in *kor1-4 the1-1* double mutant was able to partially diminish constitutive root *JAZ10* levels, indicating that *THE1* might act as a positive regulator of ectopic JA-Ile production in *kor1* (Fig. 13B).

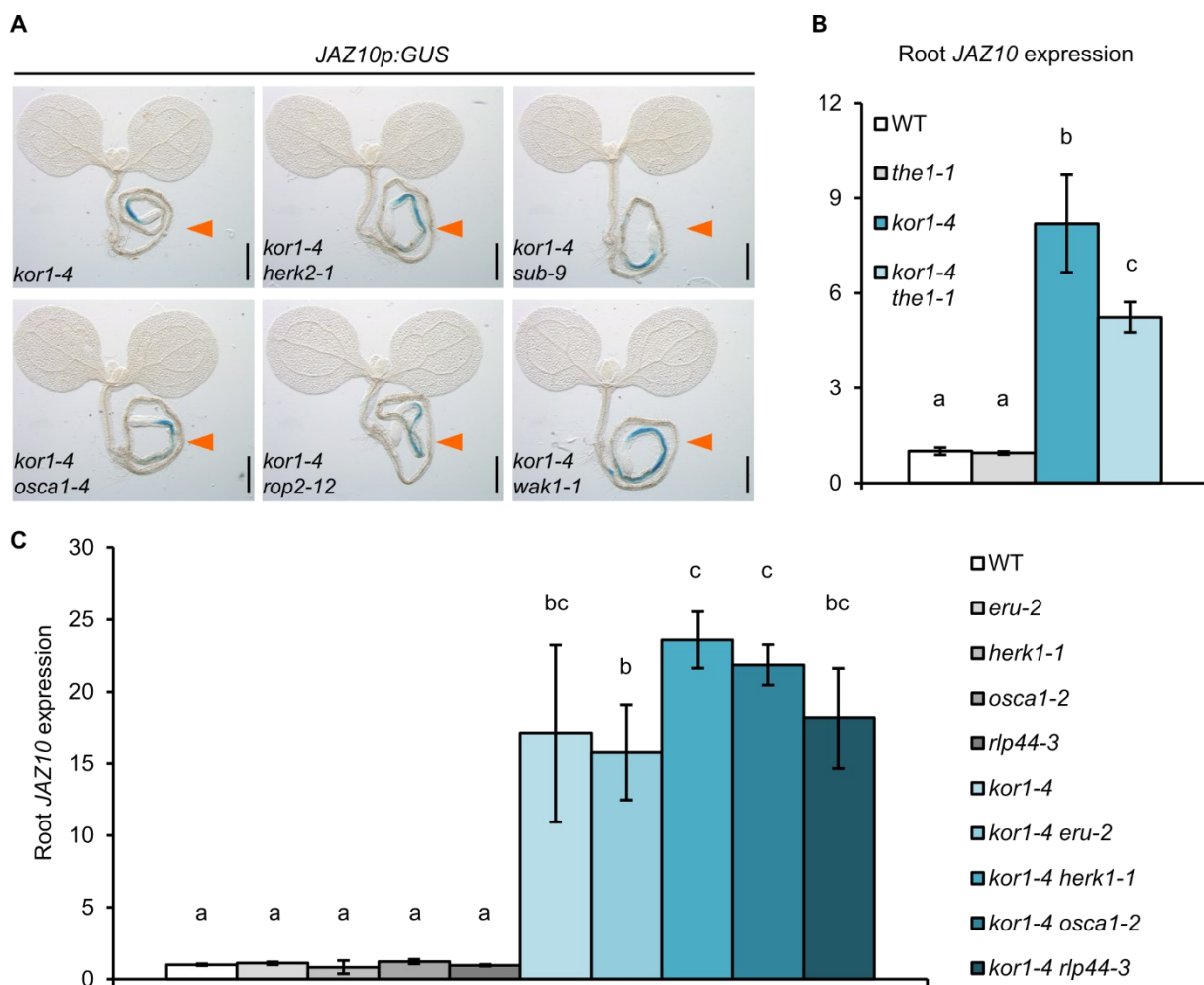


**Figure 13: Second site mutations in genes involved in cell wall integrity-, mechano- or osmo-signalling do not fully abolish constitutive JA-Ile signalling in *kor1-4* roots.** (A) Representative images of *JAZ10p:GUS* expression in *kor1-4* and indicated double mutants. For allele information see Table 1. (B and C) qRT-PCR of basal *JAZ10* expression in roots of indicated genotypes. *JAZ10* transcript levels were normalized to those of *UBC21* and displayed relative to WT controls. Bars represent the means of three biological replicates ( $\pm$ SD), each containing a pool of ~60 organs from 5-do seedlings. Letters denote statistically significant differences among samples as determined by ANOVA followed by Tukey's HSD test ( $P < 0.05$ ). Scale bars in (A) = 0.5 mm

#### 4. A forward genetic screen identified suppressors of ectopic JA-Ile signalling in *kor1*.

*The description of the suppressor screen and the identification of the esmd1 mutant were published in (Mielke et al., 2021, Science Advances). All other data are unpublished.*

Given that the reverse genetics approach did not identify genes that could completely abolish the elevated JA-Ile levels in *kor1-4* roots, I performed an untargeted forward genetics screen. The suppressor screen consisted of searching an EMS-mutagenized  $M_2$  population of *kor1-4* for the absence of ectopic *JGP* reporter expression (Fig. 14A). Importantly, GUS from the *JGP* reporter is targeted to the plant apoplast, allowing a fast and non-destructive "GUS live-staining" (Acosta et al., 2013) and recovery of viable putative suppressors. However, live-GUS staining exhibited a weaker reporter intensity than the usual destructive GUS staining, which increased the chances of recovering

false-positive mutants. Hence, I first optimized the live-GUS staining conditions. Several *kor1* alleles have been reported to exhibit temperature-sensitivity, with more severe growth phenotypes at increased temperatures (Lane et al., 2001). Given that the phenotype severity of our *kor1* alleles correlated with the intensity of basal *JGP* reporter expression in the root, I tested if *kor1-4* is also temperature sensitive and whether this could enhance *JGP* reporter activity. Indeed, when *kor1-4* seedlings were grown at 26°C instead of the usual 21°C, their primary root length was reduced by an average of 52% as opposed to WT plants which increased their root length by 31% (Fig. S4A). Consistently, 5-do *kor1-4* seedlings that were shifted to 26°C 24 h prior live-staining displayed a stronger *JGP* expression that could even extend to the meristematic division zone of the primary root (Fig. S4B). Therefore, to increase the screens' stringency and diminish the recovery of false positives, I used the 24 h temperature shift before performing live-GUS staining of M<sub>2</sub> seedlings.

To enlarge both the screening breadth and depth, 20 M<sub>2</sub> plants were screened from 1,243 M<sub>1</sub> plants harvested individually, and 480 M<sub>2</sub>s were screened from 230 M<sub>2</sub> plants harvested in pools of 12 individuals. A total of 135,260 seedlings (from 4,003 M<sub>1</sub> plants) were assayed for lack of *JGP* activity in 5-do *kor1-4* seedlings by live-GUS staining as described (Acosta et al., 2013). From the screen, 190 putative suppressors were recovered and backcrossed twice to *kor1-4 JGP* to remove EMS-induced background mutations and to assess inheritance and segregation (Fig. 14A, Tab. 2). All retrieved suppressors were then further analysed in secondary screens (Fig. 14B), which included:

1. *JGP* reporter expression after wounding and MeJA treatment to exclude reporter silencing;
2. Allelism tests with known JA-biosynthesis and signalling mutants *aos* (Park et al., 2002), *opr3-2* (Acosta et al., 2013), *jar1-1* (Staswick et al., 1998), and *coi1-34* (Acosta et al., 2013), which were expected to be found in the screen as they would inhibit basal *JGP* expression;
3. Allelism tests among the identified suppressors to determine complementation groups;
4. Phloroglucinol-HCl staining for ectopic lignification as well as primary root length measurements, to assess if recovered mutants could suppress typical cell wall mutant features of *kor1*.

**Table 2: Suppressor screen summary**

M <sub>2</sub> screened	Putative suppressors	M <sub>3</sub> confirmed	BC <sub>1</sub> F <sub>1</sub> inheritance	Mendelian segregation	NGS*
135,260 (from 4,003 M <sub>1</sub> )	190	33	33 recessive	16	12

\* Next Generation Sequencing

Allelism tests with known JA mutants identified a novel allele in *COI1* and two novel alleles in *OPR3* as suppressors of JA-Ile signalling in *kor1-4*, which were designated as *coi1-43* (Caa to Gaa transversion,



resulting in a premature stop codon Trp183\*), *opr3-4* (aAt to aCt transversion, resulting in a Gly187Arg mutation), and *opr3-5* (cCg to cTg transition, resulting in a Pro350Leu mutation) that further substantiated the specificity of the screen.

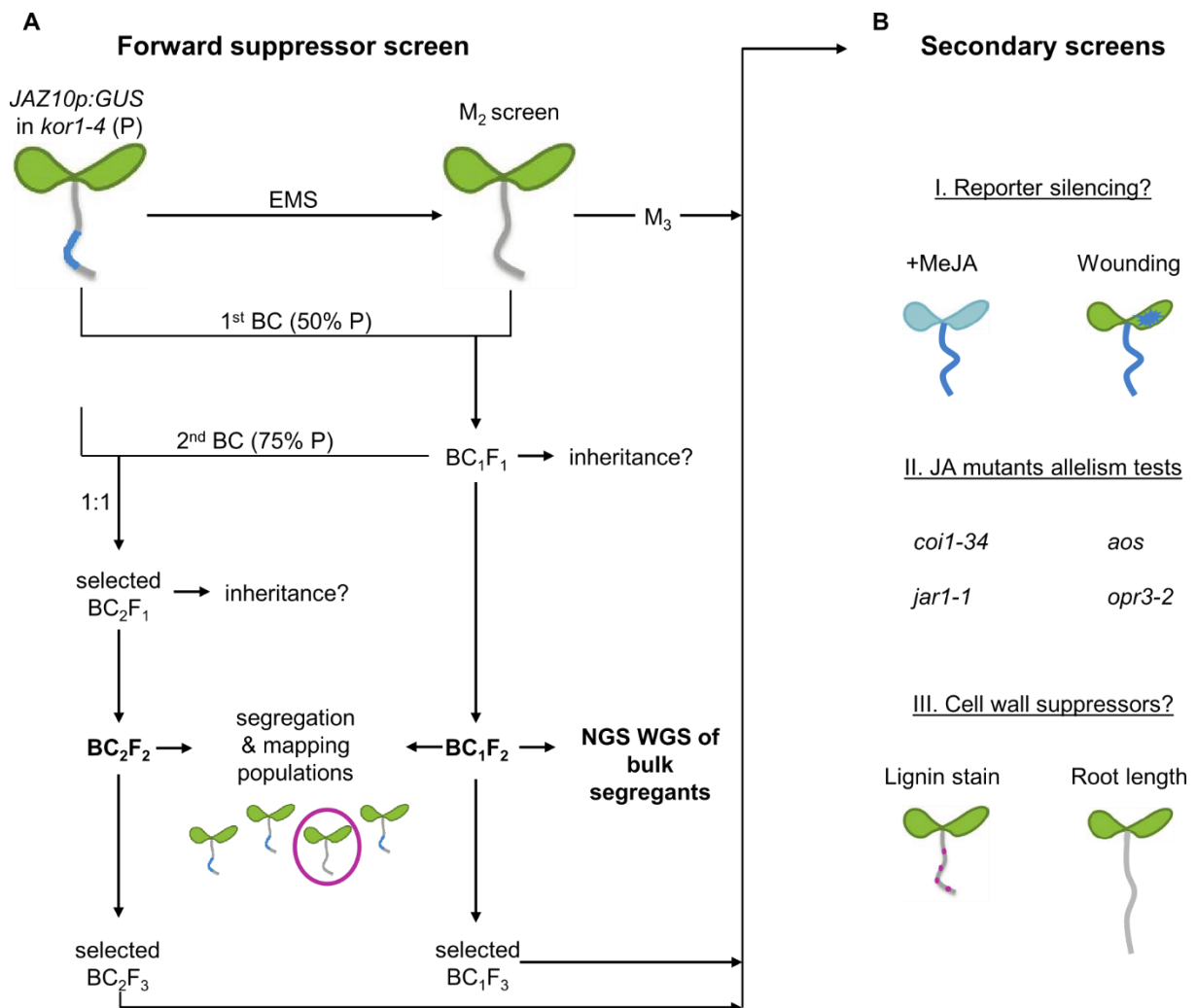


**Figure 14: A forward genetic screen to identify novel components involved in the initiation of JA-IIe biosynthesis in *kor1-4*.** (A) Overview of the screening and mapping pipeline. Parental (P) *kor1-4 JGP* seeds were EMS mutagenized and resulting  $M_2$  seedlings were screened for the lack of constitutive *JGP* reporter activity. Recovered putative  $M_2$  mutants were backcrossed (BC<sub>1</sub>) to the parental line to remove 50% of the EMS-induced mutations. Inheritance was assessed in BC<sub>1</sub>F<sub>1</sub> heterozygous progeny, which was backcrossed (BC<sub>2</sub>) again to the parental line to further clean the genetic background. Mendelian segregation was assessed in BC<sub>1</sub>F<sub>2</sub> and selected BC<sub>2</sub>F<sub>2</sub> populations. Mutants displaying segregation ratios compatible with single-gene inheritance were selected for next generation whole-genome sequencing (NGS WGS) by pooling approximately 120 suppressor individuals for genomic DNA extraction (bulk segregants). (B) Concomitantly, the phenotypes of recovered putative mutants were verified across several stages of mapping population development via secondary screens.  $M_3$ , BC<sub>1</sub>F<sub>3</sub>, and BC<sub>2</sub>F<sub>3</sub> plants were assessed for their reporter activity upon wounding and MeJA treatment to exclude *JGP* reporter silencing.  $M_3$  plants were also crossed to JA biosynthesis and signalling mutants predicted to suppress the *JGP* phenotype (*coi1-34*, *jar1-1*, *aos*, *opr3-2*), and resulting F<sub>1</sub> were analysed in allelism tests. To assess if recovered mutants could suppress typical cell wall features of *kor1*, seedlings were analysed for ectopic root lignification as well as root length. Mutants in this category could potentially be involved in cell wall integrity sensing or signalling.

After performing secondary screens and confirming the phenotypes across different generations, it was possible to group 12 distinct suppressors in three different phenotypic classes according to their

phenotypes (Fig. 15). Seven suppressors were represented in “Class I” and exhibited no basal *JGP* expression in the root, responded to wounding and MeJA-treatment, showed ectopic lignification and had a root as short or shorter than *kor1-4*. The three mutants in “Class II” differed in respect to the lignin phenotype as they did not exhibit ectopic lignification, indicating that compensatory mechanisms following cellulose deficiency were not triggered. The two mutants grouped in “Class III” had the same features as “Class II” but displayed longer roots.

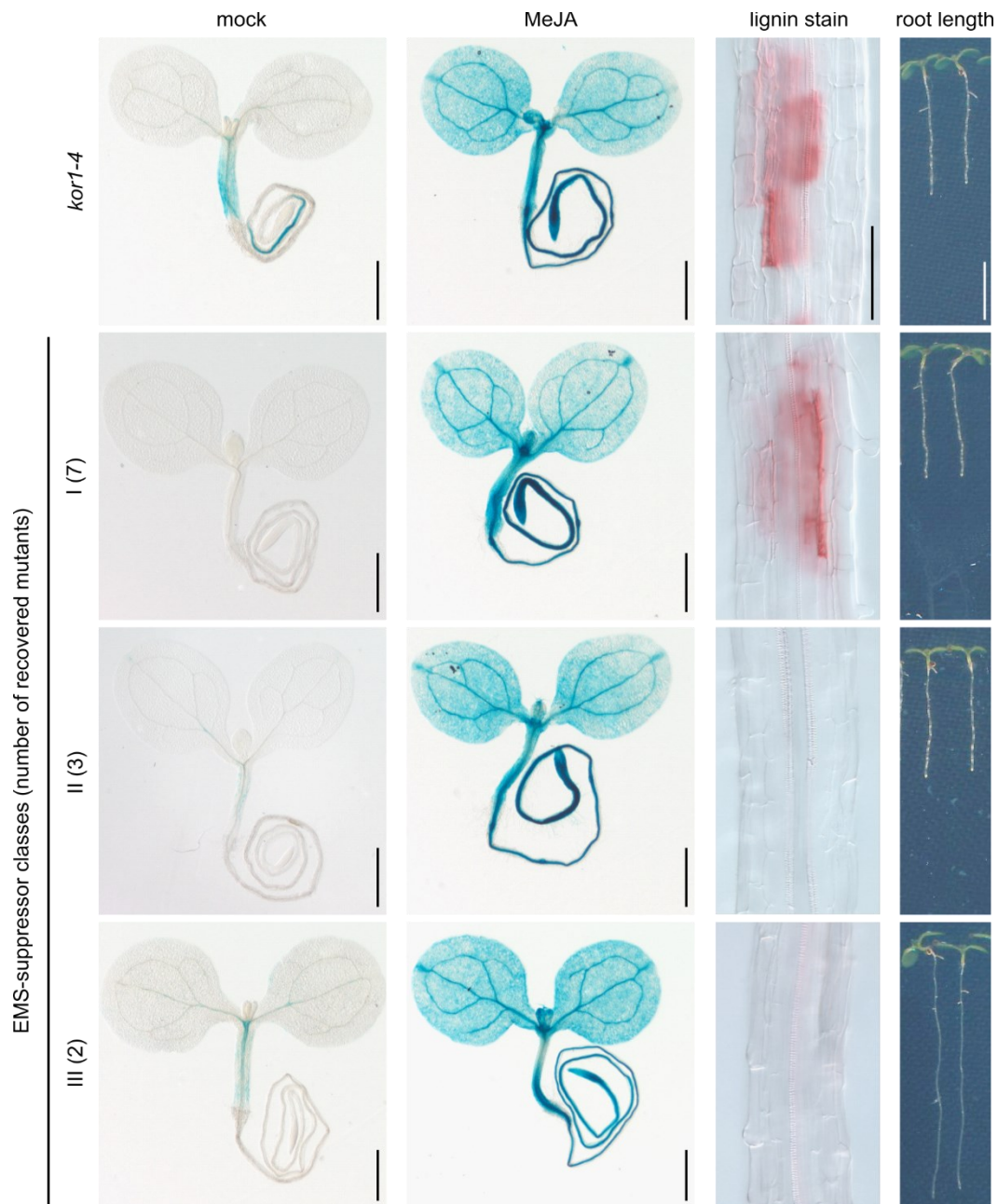


**Figure 15: Identified suppressors were categorized in three phenotypic classes, according to basal and MeJA-induced *JGP* reporter activity, ectopic root lignification (phloroglucinol stain) and root length. Scale bars (GUS stains, root length) = 0.5 mm, (lignin stains) = 100  $\mu$ m.**

This full suppression of morphological phenotypes suggests a putative role of the suppressors in CWI signalling, as a similar full suppression of the cellulose mutant *cesa6* is caused by a *the1* loss-of-function mutant (Hématy et al., 2007).

Candidate mutations responsible for the 12 mutant phenotypes were identified by Whole Genome Illumina sequencing of bulk segregants from 100-150 selected suppressor plants deriving from respective BC<sub>2</sub>F<sub>2</sub> mapping populations. Illumina sequencing reads for all suppressor mutants were aligned to the TAIR10 reference genome and mutations were mapped and identified by comparing single nucleotide polymorphism (SNP) frequencies to *kor1-4 JGP* (in collaboration with R. Dreos; University of Lausanne, Switzerland). Candidate genes responsible for the suppressors' phenotypes are listed in Table 3.

**Table 3: Candidate suppressor genes identified by Whole Genome Illumina Sequencing**

Mutant name	Phenot. class <sup>a</sup>	Candidate gene (AGI code)	SNP freq. <sup>b</sup>	Function (localization)	Complem. by cross <sup>c</sup>	Complem. by transf. <sup>d</sup>
475A	I	<i>THO COMPLEX SUBUNIT 1</i> ( <i>THO1</i> , At5g09860)	79/85 (93%)	mRNA export and splicing (nucleus)	NC	-
		<i>FORMIN-LIKE PROTEIN 20</i> ( <i>FH20</i> , At5g07740)	51/54 (94%)	putative actin binding protein (cytoplasm)	NA	-
487D	I	<i>ESMERALDA 1</i> ( <i>ESMD1</i> , At2g01480)	66/66 (100%)	putative O-fucosyl transferase (Golgi)	yes	yes
565A	I	<i>HISTONE DEACETYLATION COMPLEX 1</i> ( <i>HDC1</i> , At5g08450)	103/103 (100%)	Component of histone deacetylase complexes (nucleus)	yes	-
739A	I	<i>EMBRYO-DEFECTIVE-DEVELOPMENT 1</i> ( <i>EDD1</i> , At3g48110)	101/101 (100%)	Glycine-tRNA-ligase (chloroplast stroma)	yes	-
1843B	I	<i>NUCLEAR RNA POLYMERASE C2</i> ( <i>NRPC2</i> , At5g45140)	102/106 (96%)	Subunit of RNA polymerase III (nucleus)	-	-
1939C	I	At3g49490	111/119 (93%)	Hypothetical nuclear protein (nucleus)	NC	-
2767A	I	<i>ELONGATOR PROTEIN 2</i> ( <i>ELP2</i> , At1g49540)	75/77 (97%)	Transcriptional elongation (nucleus)	-	-
		<i>RECEPTOR-LIKE PROTEIN 7</i> ( <i>RLP7</i> , At1g47890)	87/92 (94%)	Receptor like protein (plasma membrane)	NC	-
1135A	II	<i>ROOT UVB SENSITIVE 1</i> ( <i>RUS1</i> , At3g45890)	100/100 (100%)	Contains domain of unknown function 647 (chloroplast membrane)	yes	-
1237D	II	<i>PLEIOTROPIC REGULATORY LOCUS 1</i> ( <i>PRL1</i> , At4g15900)	106/107 (99%)	WD40 protein (nucleus)	yes	yes
1315A	II	<i>PHOTOSENSITIVE 1</i> ( <i>PHS1</i> , At3g47390)	93/107 (87%)	Pyrimidine reductase (chloroplast)	-	-
2455B	III	<i>OSTEOSARCOMA-AMPLIFIED GENE 9</i> ( <i>OS9</i> , At5g35080)	106/107 (99%)	Involved in degradation of glycoproteins (ER)	yes	yes
3211A	III	<i>MEDIATOR 23</i> ( <i>MED23</i> , At1g23230)	90/90 (100%)	Mediator/transcriptional coactivator (nucleus)	-	-
		<i>RNA POLYMERASE II SUBUNIT 3</i> ( <i>NRPB3</i> , At2g15430)	86/86 (100%)	Subunit of RNA polymerases II, IV & V (nucleus)	-	-

<sup>a</sup> Phenotypic classes according to Fig. 15

<sup>b</sup> SNP frequency

<sup>c</sup> was the suppressor confirmed by crossing *kor1* mutants to an allele of the putative suppressor (e.g. T-DNA)?, NA (no suppressor allele available), NC not complementing

<sup>d</sup> was the suppressor confirmed by transformation with the WT candidate?, - (not done)

Two strategies were used to verify if the candidate genes are indeed responsible to suppress *JGP* expression in *kor1-4*. On the one hand, available T-DNA insertion alleles for putative suppressors were crossed to *kor1-4 JGP* and *kor1-6 JGP* to test whether ectopic JA-Ile signalling can be suppressed by independent allele combinations in resulting double mutant combinations. This option was chosen as opposed to a standard allelism test (e.g. crossing the 475A suppressor to a *tho1* KO mutant allele and

analysing the  $F_1$  for presence or absence of constitutive *JGP* expression) due to the resulting heterozygosity of the *kor1-4* allele in  $F_1$  progeny. On the other hand, WT coding sequences (CDS) of each candidate suppressor under control of their own promoters were cloned and transformed into the relative suppressor mutants to verify their ability to complement *JGP* expression. Due to lack of available T-DNA alleles, technical issues during cloning and time restriction, it was not possible to verify the gene identity for all suppressors (Tab. 3). Nevertheless, in the time available, I successfully confirmed the causative mutations governing the *JGP* phenotype in *kor1* for 6 of the newly identified suppressors.

Among the 6 confirmed suppressors, 2 are localized in the nucleus (HISTONE DEACETYLATION COMPLEX 1 [HDC1] and PLEIOTROPIC REGULATORY LOCUS [PRL1]). HDC1 is a component of histone deacetylase complexes that facilitates histone deacetylation and hence regulates gene transcription (Perrella et al., 2013; Perrella et al., 2016). *PRL1* encodes for a WD40 repeat protein, which is involved in a plethora of processes related to plant growth, responses to sugars and multiple hormones including auxin, abscisic acid (ABA), cytokinin, and ET, through either transcriptional or post-translational regulation (Nemeth et al., 1998; Bhalerao et al., 1999; Zhang et al., 2014b; Ji et al., 2015). Their nuclear localization might indicate that these suppressors may be involved in regulating gene transcription in *kor1*, such as JA-Ile biosynthesis or signalling genes, or they might affect *JGP* activity through indirect pathways. As the *JGP* reporter in all suppressor mutants responds to wounding, these nuclear suppressors can provide valuable tools to identify subsets of JA-Ile-regulated genes following cell wall alterations. Interestingly, EMBRYO-DEFECTIVE-DEVELOPMENT 1 (EDD1) and ROOT UVB SENSITIVE 1 (RUS1), both localize to plastids, the organelles where JA-Ile biosynthesis initiates. EDD1 is a glycyl-tRNA ligase, which is required for normal development during embryogenesis and organ formation (Uwer et al., 1998; Moschopoulos et al., 2012). RUS1 encodes for a protein carrying a domain with unknown function that mediates root UV-B sensing, starch metabolism, and chloroplast development (Tong et al., 2008; Zou et al., 2021). These candidates might directly control or influence the very first steps of JA-Ile biosynthesis, regulate the activity or abundance of plastidial JA biosynthesis enzymes, affect JA substrate levels (e.g. MGDG, linolenic acid), or affect organellar morphology and functionality and hence indirectly influence JA-Ile production. Another confirmed suppressor was a mutant in *OSTEOSARCOMA-AMPLIFIED GENE 9* (*OS9*), which fully suppressed all JA- and cell wall-related phenotypes in *kor1-4* (Fig. 15, Tab. 3). *OS9* is a lectin localized in the Golgi lumen that is important for the degradation of misfolded glycoproteins (Huttner et al., 2012). Hence it is possible, that the target of *OS9* might be our mutant version of KOR1. A striking confirmed suppressor identified in the screen was *ESMERALDA 1* (*ESMD1*) with

known functions in cell wall homeostasis (Verger et al., 2016). I therefore decided to characterize this suppressor mutant (487D) in greater detail.

## 5. Mutations in *ESMD1* suppress elevated JA-Ile signalling in *kor1*

*Data from this chapter is published in Mielke et al, 2021, Science Advances.*

Specifically, mutant alleles of *ESMD1* fully suppressed the morphological growth phenotypes of pectin biosynthesis mutants in *QUASIMODO1* (*qua1-1*) and *QUASIMODO2* (*qua2-1*) (Verger et al., 2016). *QUA1* and *QUA2* encode for a galacturonyltransferase and a pectin methyltransferase respectively, and mutants exhibit impaired cell adhesion as well as reduced contents in the major pectin constituent HG (Bouton et al., 2002; Mouille et al., 2007). However, *esmd1* restored the growth phenotypes of these mutants without altering HG levels or cell wall composition in general, an observation that is reminiscent to mutants involved in CWI signalling (Hematy et al., 2007; Verger et al., 2016). Hence and based on protein sequence similarity, *ESMD1* was proposed to have an *O*-fucosyltransferase activity with which it might modify target proteins involved in CWI (Verger et al., 2016).

The isolated allele from the genetic screen, hereafter named *esmd1-3* carries an Arg373Cys mutation, fully suppressed the elevated JA-Ile signalling in *kor1-4* roots (Fig. 16A, B and D), while still retaining the capacity to induce *JAZ10* transcripts after wounding (Fig. S5A to C). A tagged mTurquoise2 (mTurq)-*ESMD1* fusion protein expressed under the control of the *ESMD1* native promoter fully reverted the *kor1-4 esmd1-3* phenotype back to *kor1-4* (Fig. 16A, Fig. S5A).

Consistently, introgressing another mutant allele *esmd1-1* (Verger et al., 2016) into *kor1-4* also led to partial suppression of *JAZ10* expression levels (Fig. 16B). As I could not retrieve homozygous mutants from a segregating F<sub>2</sub> *esmd1* population (*esmd1-4*, GABI\_216D03, Fig. 16D), and *esmd1-1* was a weaker JA-Ile suppressor than *esmd1-3* (Fig. 16B), it is likely that full *ESMD1* knockouts lead to lethality and that both alleles used herein have a partial loss-of-function. Because *esmd1* mutants were able to suppress growth phenotypes of *qua1* and *qua2* mutants without altering cell wall composition (Verger et al., 2016), I verified which other *kor1* phenotypes are reverted by *esmd1-3*. In contrast to *qua* mutants, *esmd1-3* did not impact the short root growth of *kor1-4* plants while it affected its cell wall composition (Fig. 16C).

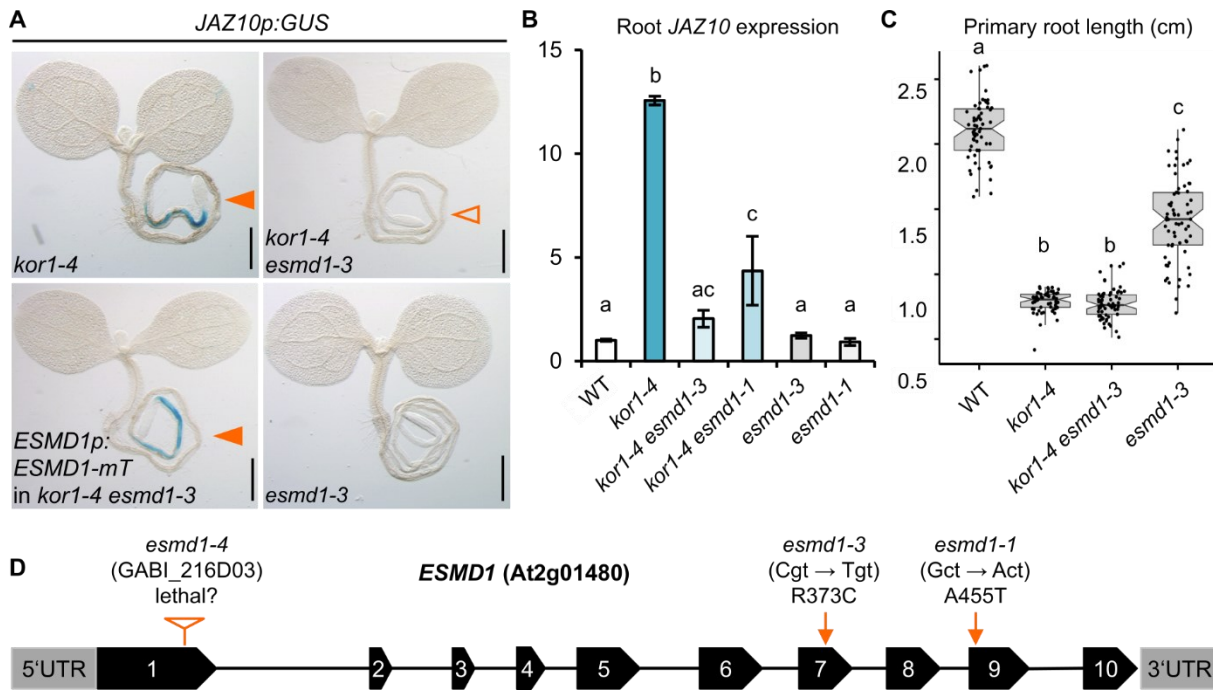


**Figure 16: Mutations in *ESMD1* suppress elevated JA-Ile signalling levels in *kor1*.** (A) Representative images of *JAZ10p:GUS* reporter expression in *kor1-4*, its suppressor *kor1-4 esmd1-3*, its *ESMD1p:ESMD1-mTurquoise(mT)* complementation line, and in *esmd1-3*. Note the lack of *JAZ10p:GUS* reporter activity in roots of *kor1-4 esmd1-3* (empty arrowhead), and its presence in *kor1-4* and the complemented line (orange arrowhead). Scale bars = 0.5 mm. (B) qRT-PCR of basal *JAZ10* expression in roots of indicated genotypes. *JAZ10* transcript levels were normalized to those of *UBC21*. Bars represent the means of three biological replicates ( $\pm$ SD), each containing a pool of ~60 organs from 5-do seedlings. (C) Primary root length box plot summary in 7-do WT, *kor1-4*, *kor1-4 esmd1-3*, and *esmd1-3* seedlings. Medians are represented inside the boxes by solid lines, circles depict individual measurements ( $n = 58-66$ ). (D) Schematic representation of *ESMD1* (At2g01480) gene structure describing the *esmd1* alleles used in this study (orange arrows). Grey boxes indicate untranslated regions (UTRs), black boxes depict exons and lines introns. Letters in (B and C) denote statistically significant differences among samples as determined by ANOVA followed by Tukey's HSD test ( $P < 0.05$ ).

### Loss of *ESMD1* impacts cell wall composition

In line with *KOR1* role in cellulose biosynthesis and in agreement with previous reports (Peng et al., 2000; Szyjanowicz et al., 2004; Lei et al., 2014), cellulose content was reduced in *kor1-4* roots and shoots (Fig. 17A and B). However, cellulose levels were not affected by *esmd1-3*, and were still low in *kor1-4 esmd1-3* and similar to WT in *esmd1-3* (Fig. 17A and B). According to previous reports from *esmd1* etiolated hypocotyls (Verger et al., 2016), we expected no major changes caused by *esmd1* in terms of monosaccharide composition analysis, which determines the abundance of hemicellulose and pectin constituents. Instead, several minor changes were detected with a conspicuous decrease in rhamnose abundance that was detected in *esmd1-3* and *kor1-4 esmd1-3* genotypes with respect to the WT, accounting for a reduction of 32-38% in roots and 15% in shoots (Fig. 17C and D). The analysis of cell wall constituents was performed in collaboration with Cătălin Voiniciuc (Leibniz Institute of Plant Biochemistry Halle, Germany). I also found that ectopic lignification in *kor1-4* roots, which putatively is produced as a compensation for the lack of cellulose (Cano-Delgado et al., 2003), was totally abolished in *kor1-4 esmd1-3* (Fig. 17E). Overall, the analysis of the *kor1-4 esmd1-3* double

mutant suggests a complex compensatory network, in which some phenotypes were epistatic to *kor1-4* (short root length, cellulose deficiency) and others to *esmd1-3* (lack of increased JA-Ile signalling, reduced rhamnose abundance, lack of ectopic lignification). The results therefore indicate that constant activation of the JA pathway in *kor1* may be due to indirect consequences of cellulose deficiency.

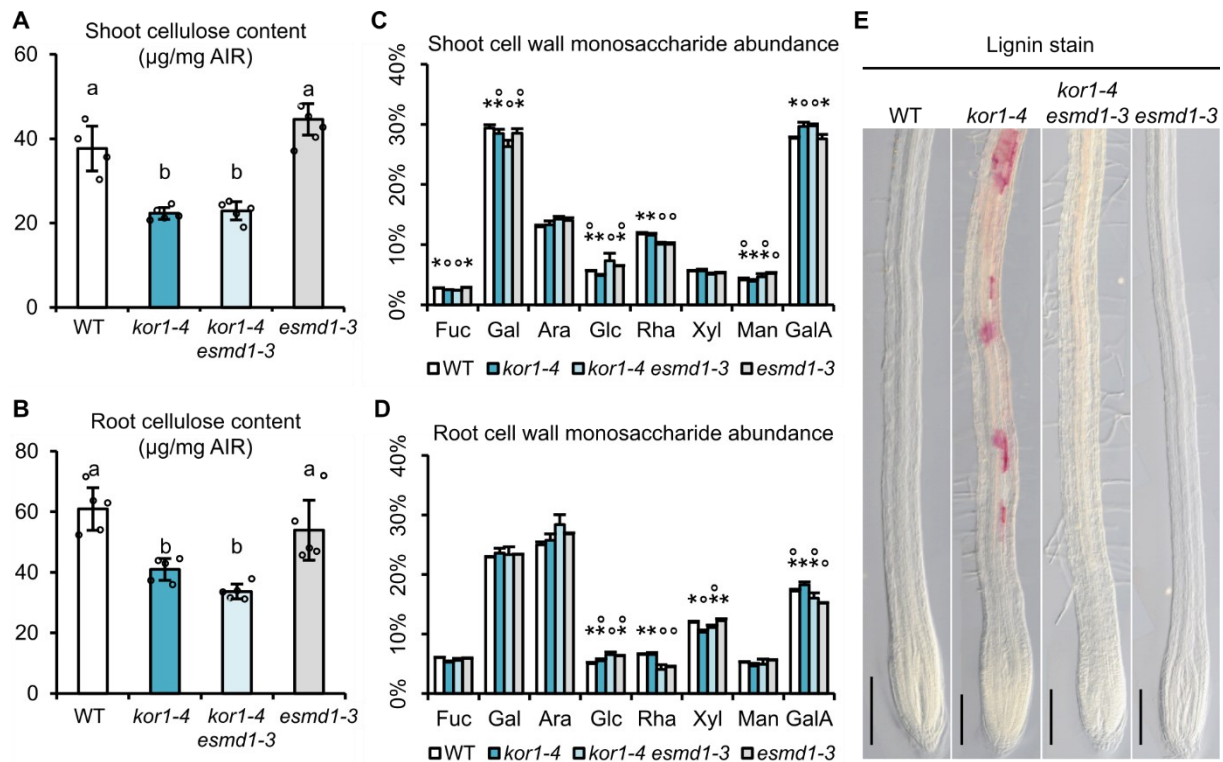
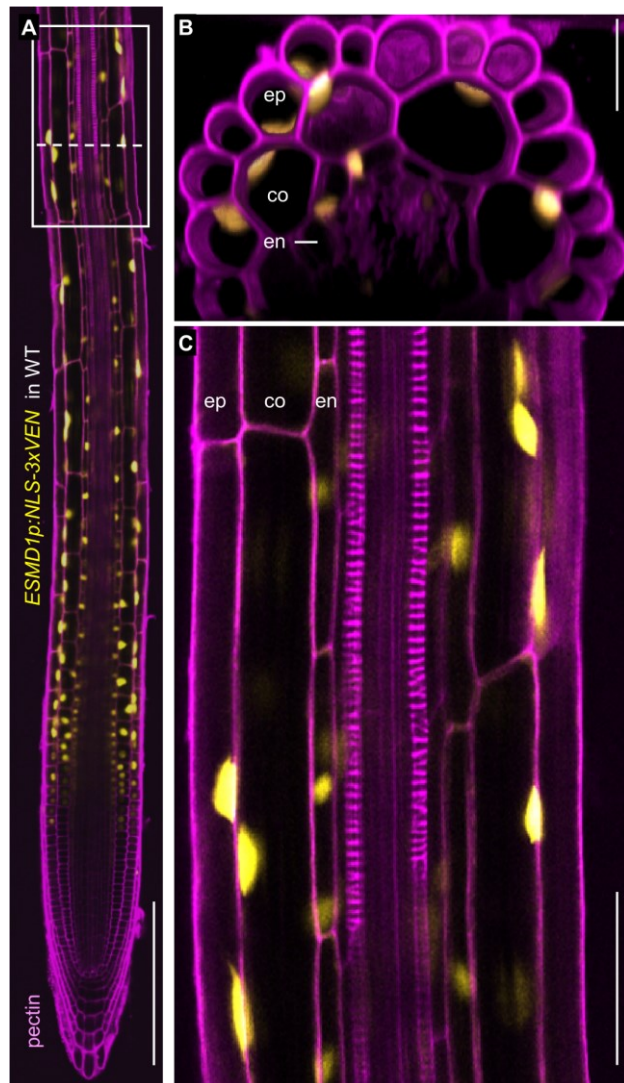


**Figure 17: Mutations in *ESMD1* alter the composition of the cell wall.** (A and B) Crystalline cellulose content from alcohol insoluble residue (AIR) extracted from (A) shoots and (B) roots of indicated genotypes. Bars represent means of five biological replicates depicted as dots ( $\pm$ SD), each consisting of pools from (A) ~100 shoots or (B) ~300 roots from 12-do seedlings. (C and D) Cell wall monosaccharide composition analysis from AIR extracted from (C) shoots or (D) roots of indicated genotypes. Bars represent the means of (C) four or (D) three biological replicates ( $\pm$ SD), each containing a pool of (C) ~100 shoots or (D) ~300 roots from 12-do seedlings. Fuc, fucose; Gal, galactose; Ara, arabinose; Glc, glucose; Rha, rhamnose; Xyl, xylose; Man, mannose; GalA, Galacturonic acid. Letters in (A and B) and asterisk and circle symbols in (C and D) denote statistically significant differences among samples or individual sugars as determined by ANOVA followed by Tukey's HSD test ( $P < 0.05$ ) in (A) and (B); ( $P < 0.001$ ) in (C) and (D). Absence of symbols in (C and D) indicates that no statistically significant differences were present. (E) Lignin deposition visualized by phloroglucinol-HCl stain (in fuchsia) in 5-do primary roots of indicated genotypes. Scale bars = 200  $\mu$ m.

### ***ESMD1* expression domains coincide with sites of elevated JA-Ile signalling in *kor1***

As knowing *ESMD1* localization sites might be informative to further hypothesize how *ESMD1* regulates JA-Ile biosynthesis in *kor1* roots, I analysed its expression sites with transcriptional and translational reporters in the primary root. Although an *ESMD1*-GFP fusion protein was expressed in the Golgi when transiently overexpressed in leaf epidermal cells of *Nicotiana benthamiana* (Verger et al., 2016), I was unable to visualize the functional *ESMD1p:ESMD1-mT* construct nor an alternative

*ESMDp:ESMD1-CIT* variant in WT Arabidopsis roots. This suggests that *ESMD1* levels are either too low to be detected and/or tightly regulated. I thus generated and mapped a transcriptional reporter driving NLS-3xVEN expression under control of the native *ESMD1p* promoter.



*ESMD1p* promoter activity was detected in the elongation and differentiation zone of the primary root, but not in the division zone (Fig. 18A). Transverse optical sections in my zone of interest (early differentiation zone) then allowed me to narrow the signal down to the epidermis, cortex, and endodermis cell files (Fig. 18B and C), hence partially overlapping with the sites of constitutive JA-Ile signalling in *kor1-4* (Fig. 9B and C).

**Figure 18: *ESMD1* is expressed in outer tissues of the root elongation and differentiation zone.** (A to C) *ESMD1p:NLS-3xVEN* expression in 5-d-old WT primary roots. Cell wall pectins were counterstained with propidium iodide. (B) Orthogonal view of a section in the early differentiation zone through (A, dotted line) visualized as 3D texture based volume rendering from a Z-stack. (C) Increased magnification in the early differentiation zone from (A, boxed). Note that the transcriptional reporter is present only in outer tissues of epidermis (ep), cortex (co), and endodermis (en). Scale bars: (A) = 200  $\mu\text{m}$ , (B) = 25  $\mu\text{m}$ , and (C) = 50  $\mu\text{m}$ .

## 6. Turgor-driven mechanical changes induce JA-Ile signalling.

*Data from this chapter is published in (Mielke et al., 2021, Science Advances).*

### Loss of *ESMD1* reduces *kor1-4* root swelling

After determining that *ESMD1* promoter activity coincides with sites of elevated JA-Ile production in *kor1-4* roots (Fig. 18), I noticed that the radially swollen root of *kor1-4*, a phenotype also described in other *kor1* alleles (Lane et al., 2001; Lei et al., 2014), was significantly thinner in *kor1-4 esmd1-3* (Fig. 19A). Specifically, root diameter at the onset of differentiation was 47% thicker in *kor1-4* in comparison to the WT (Fig. 19A and B). While root width in *esmd1-3* was not affected, *esmd1-3* effectively reduced the root diameter of *kor1-4* (Fig. 19A and B).



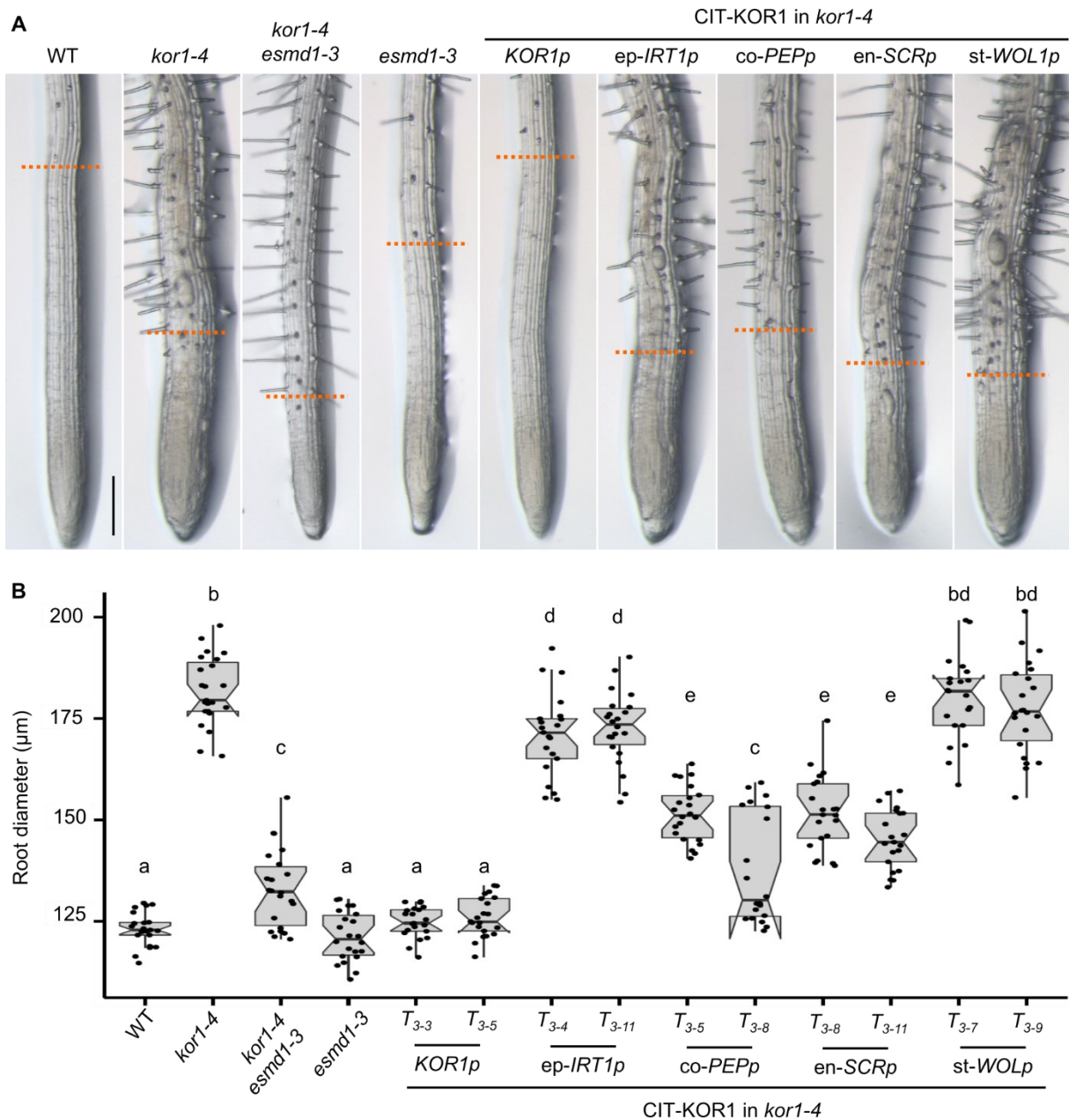


**Figure 19: *kor1* root swelling is alleviated in *esmd1* and different cell-type-specific CIT-KOR1 expression lines.** (A) Representative primary root images in 7-day seedlings of WT, *kor1-4*, *kor1-4 esmd1-3*, *esmd1-3*, and *kor1-4* complemented with CIT-KOR1 under the control of its native *KOR1p* promoter, or epidermis- (*ep-IRT1p*), cortex- (*co-PEPp*), endodermis- (*en-SCRp*), or stele-specific (*st-WOL1p*) promoters. Orange dashed lines denote the beginning of the differentiation zone, as indicated by the appearance of root hairs. Scale bar = 200  $\mu$ m. (B) Box plot summary of primary root diameter at the onset of differentiation as specified in (A). Medians are represented inside the boxes by solid lines and circles depict individual measurements ( $n = 22-23$ ). Letters denote statistically significant differences among samples as determined by ANOVA followed by Tukey's HSD test ( $P < 0.05$ ).

To characterize the morphological differences occurring between *kor1-4* and *kor1-4 esmd1-3* that might affect JA-Ile production, I analysed root transversal sections across the early differentiation zone (Fig. 20A to F). In agreement with root diameter, *kor1-4* total root area was twice that of the WT and resulted from enlarged areas of all examined cell-types (Fig. 20A and C, Fig. S6A to E). *kor1-4* epidermal cells had the smallest expansion in cell area compared to the WT (1.1-fold), but exhibited a

significant increase in their cell number that was not present in cortex or endodermis (Fig. 20B and C, Fig. S6B).

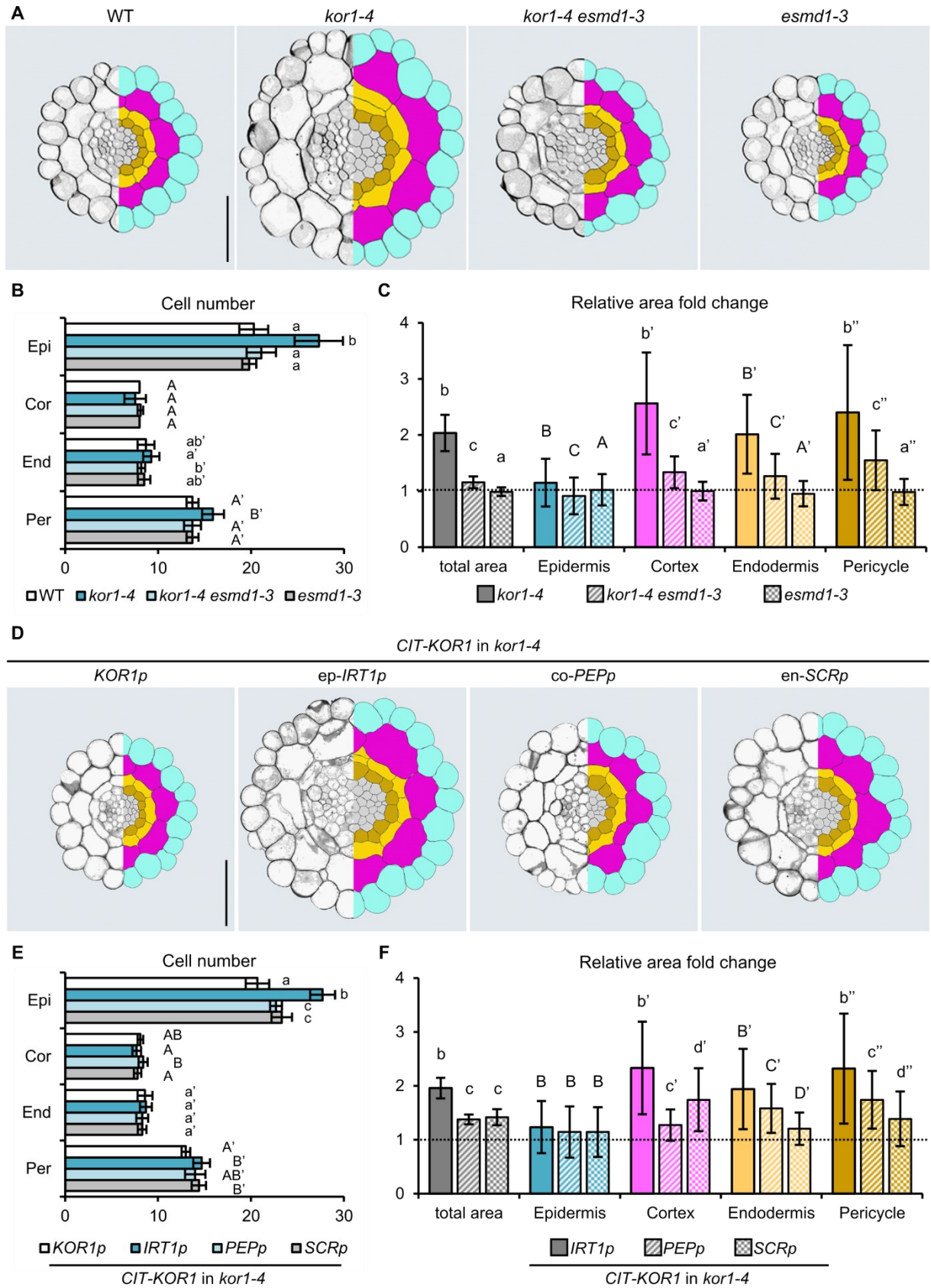


**Figure 20: Enlargement of cortex cells correlates with ectopic JA-Ile signalling in *kor1* roots.** (A to F) Anatomy, cell number and cell size comparisons from transverse sections across the early differentiation zone of the primary root in (A to C) WT, *kor1-4*, *kor1-4 esmd1-3*, and *esmd1-3*, and in (D to F) *kor1-4* complemented with CIT-KOR1 expressed under cell-type-specific promoters. (A and D) Representative split images from cross sections (left panels) and respective cell segmentations (right panels). Segmented cell-types are color-coded as: epidermis, turquoise; cortex, magenta; endodermis, yellow; pericycle, mustard; stele, grey. (B and E) Cell number in epidermis (Epi), cortex (Cor), endodermis (End), and pericycle (Per) of the early differentiation zone of primary roots in indicated genotypes. (C and F) Fold change in total and cell-specific areas from segmented transversal root sections in indicated genotypes. Measurements were normalized to those of the (C) WT or (F) *KOR1p:CIT-KOR1*, indicated by dashed lines (individual measurements are available in Fig. S5). Letters in (B, C, E and F) denote statistically significant differences among samples as determined by ANOVA followed by Tukey's HSD test ( $P < 0.05$ ). Note that WT in (C) and the full complementation line driving expression under *KOR1p* in (F), as indicated by the dashed line are always considered as letter 'A' in the statistical analyses. All data represent the means of  $n = 10-11$  roots. Scale bars (A and D) = 50  $\mu\text{m}$ .

The largest increase in *kor1-4* cell area was found for cortex cells (2.6-fold), while endodermis and pericycle cells were 2- and 2.4-fold larger than the WT, respectively (Fig. 20C, Fig. S6C to E). In contrast, area measurements in *esmd1-3* were not altered in comparison to the WT. However, all the observed *kor1-4* phenotypes were restored to a large extent in *kor1-4 esmd1-3*, which exhibited a full complementation of epidermal cell number as well as reduced cell areas in all tissues (Fig. 20B and C, Fig. S6A to E). Remarkably, the biggest area reduction (50%) was observed for the cortex file (Fig. 20C, Fig. S6 C), leading to the hypothesis that enlarged cortex cells might exert mechanical pressure towards the inner cell files and thus prompt JA-Ile biosynthesis.

### Enlarged *kor1* cortex cells impact JA-Ile production in inner tissues

To test the above hypothesis, I measured root diameter and cellular areas in root cross sections of *kor1-4* transgenic lines expressing CIT-KOR1 under cell-type-specific promoters. As expected, when complemented with CIT-KOR1 expressed under the native *KOR1p* promoter, *kor1-4* root thickness was completely reverted to WT levels (Fig. 19A and B). Furthermore, while expressing CIT-KOR1 in either epidermis or stele did not have a major impact on *kor1-4* root diameter, its expression in cortex or endodermis resulted in a substantial decrease of *kor1-4* root thickness (Fig. 19 A and B).

To verify if loss of JA-Ile signalling in *kor1-4* correlated with size reduction of cortex cells, I next analysed cell areas in the *kor1-4* transgenic lines expressing CIT-KOR1 under cell-type-specific promoters (Fig. 20D to F). Because stele-specific CIT-KOR1 expression neither affected overall *kor1-4* root diameter nor restored constitutive JA-Ile signalling (Fig. 19A and B, Fig. 10D), I did not expect cellular differences and excluded these lines from further analyses. As anticipated, expressing CIT-KOR1 under its native promoter fully restored *kor1-4* root phenotypes (cell numbers and cell areas) to WT levels (Fig. 20E and F, Fig. S6 F to J). Epidermis-specific CIT-KOR1 expression still resulted in a typical *kor1-4* morphology, with a 2-fold increase in root area and increased epidermal

cell number (Fig. 20E and F, Fig. S6F). In agreement with root diameter measurements Fig. 19, expressing CIT-KOR1 in either cortex or endodermis cell layers rendered *kor1-4* phenotypes more similar to the *KOR1p:CIT-KOR1* complemented *kor1-4* line by showing a 1.4-fold increase in total root area, and only a milder enlargement of cortex, endodermis, and pericycle cells (Fig. 20F, Fig. S6F to J). While the most pronounced consequence of CIT-KOR1 expression in cortex or endodermis was the decrease of area in cells where the fusion protein was localized, the strongest correlation between JA-Ile signalling and cell-type area was again found for the cortex cell layer. In fact, expressing CIT-KOR1 in the cortex abolished *JGP* expression in *kor1-4* (Fig. 10B) and restored cortex cell area to almost WT levels (1.2-fold) without fully recovering cellular enlargement of endodermal and pericycle cells which persisted being 1.6- and 1.7-fold larger than the *KOR1p:CIT-KOR1* complemented line (Fig. 20F). In turn, endodermal CIT-KOR1 expression did not abolish elevated JA-Ile signalling in *kor1-4* nor led to a drastic reduction in cortex expansion which remained 1.7-fold larger, albeit almost completely restoring endodermal and pericycle cell areas (Fig. 20F). As KOR1 activity in cortex cells is important to regulate their size and *JGP* expression in adjacent inner tissues, and *ESMD1* is expressed in both cortex and endodermal cells, it is conceivable that the cortex-endodermis interface is critical for governing constitutive JA-Ile production in *kor1*.

### **Manipulation of turgor pressure abolishes constitutive JA-Ile signalling in *kor1***

JA-Ile production can be induced by exogenous applications of specific pectin- and cellulose-derived fragments acting as putative cell wall-derived elicitors (Moscatiello et al., 2006; Souza et al., 2017; Mielke and Gasperini, 2019). More notoriously, JA-Ile biosynthesis is readily triggered by mechanical stress (Farmer et al., 2014). To test our hypothesis that increased JA-Ile levels in *kor1-4* resulted from expanded cortex cells that 'squeeze' spatially constrained inner tissues, I grew *kor1-4* plants under hyperosmotic conditions to withdraw water from their cells and hence reduce their cellular enlargement. In fact, cellular expansion is mainly regulated by the interplay of internal turgor pressure and the external cell wall restraining it, reviewed in (Guerriero et al., 2014; Anderson and Kieber, 2020). Furthermore, changes in osmotic potential are known to influence turgor pressure and were shown to revert cell expansion as well as isoxaben-triggered JA production (Engelsdorf et al., 2018; Basu and Haswell, 2020). I hence expected that reducing cortex cell enlargement with hyperosmotic treatments would alleviate the compression on inner tissues and abolish JA-Ile production in *kor1-4*. Indeed, all tested substances acting as osmotica (mannitol, sorbitol, polyethyleneglycol, and hard agar) completely abolished ectopic JA-Ile signalling in *kor1-4* roots (Fig. 21A and B). This was not due to the inability of activating the *JGP* reporter, as WT seedlings grown on mannitol-containing media still responded to wounding (Fig. 21C). Furthermore, while WT root growth was compromised in

hyperosmotic conditions, *kor1-4* roots exhibited a significant amelioration in root growth, as the mutant root length was longer than in mock conditions (Fig. 21D).

We then analysed cellular parameters by segmenting transversal root sections of the early differentiation zone in mock- and mannitol-grown seedlings of WT and *kor1-4* (Fig. 21E to G). Consistent with our hypothesis, mannitol-grown *kor1-4* seedlings restored their total area as well as their epidermal cell number back to WT levels (Fig. 21F and G, Fig. S7A). Remarkably, although cell size was reduced in all analysed cell types, cortex cell size was fully reverted to the extent of WT while endodermal and pericycle cells were still 1.2-fold larger (Fig. 21G, Fig. S7B to E). Hence, this further strengthens the assumption that the activation of JA-Ile production in *kor1* is consistent with inner tissues being mechanically stressed by enlarged cortex cells in a turgor-dependent manner.

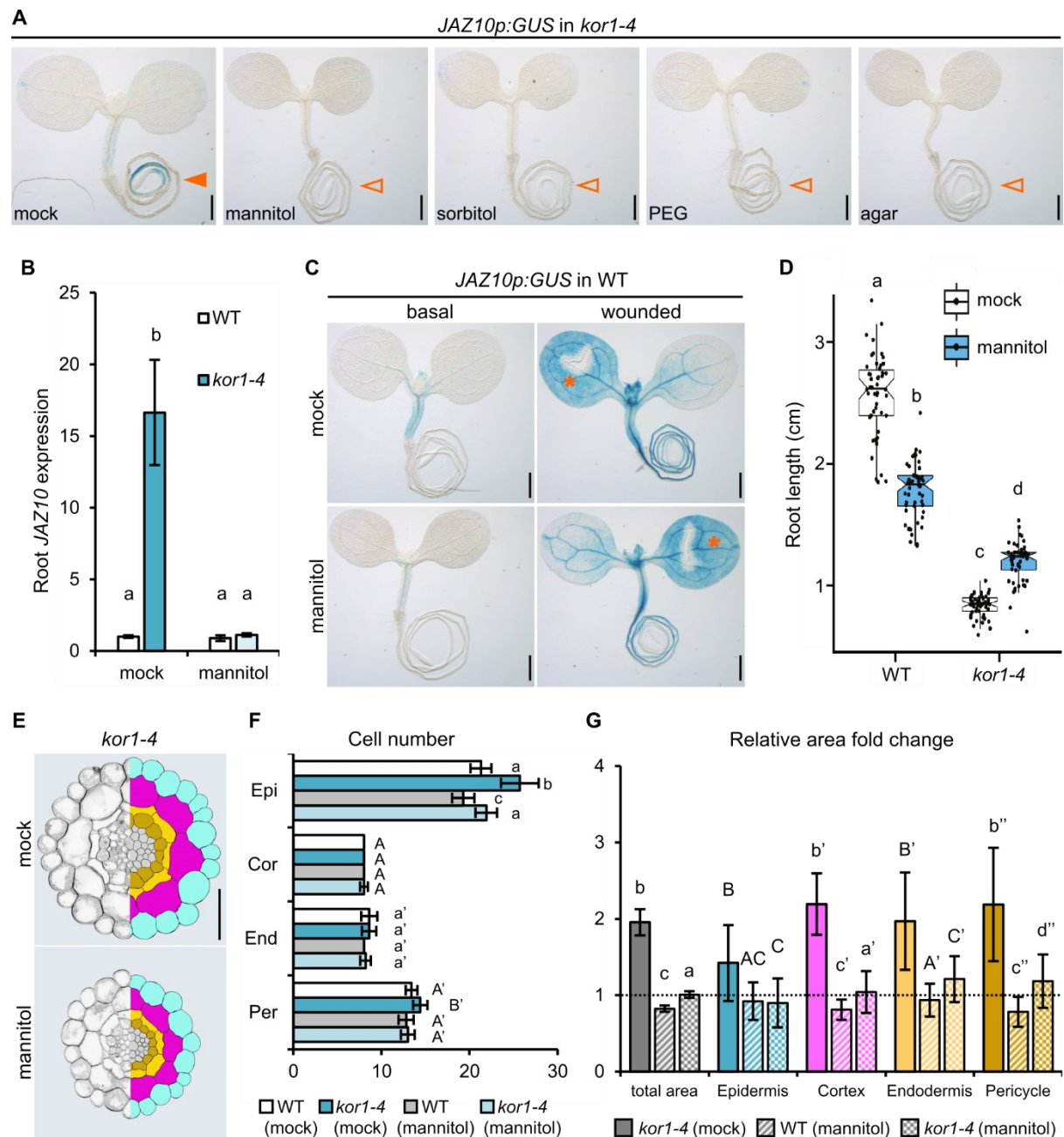


**Figure 21: Hyperosmotic treatments alleviate cortex cell swelling and abolish ectopic JA-Ile signalling in *kor1*.** (A) Representative images of basal *JAZ1op:GUS* reporter activity in 5-do *kor1-4* seedlings grown in the absence (mock) or presence of 3% sorbitol, 3% Polyethylenglycol (PEG), or 3% agar. Note the presence of reporter activity in mock conditions (orange arrowhead) and its abolishment in hyperosmotic conditions (empty arrowheads). (B) qRT-PCR of *JAZ10* expression in roots of indicated genotypes grown in basal (mock) or hyperosmotic (3% mannitol) conditions. *JAZ10* transcript levels were normalized to those of *UBC21*. Bars represent the means of three biological replicates ( $\pm$ SD), each containing a pool of ~60 roots from 5-do seedlings. (C) *JAZ1op:GUS* reporter activity in 5-do WT seedlings grown in the absence (mock) or presence of 3% mannitol under basal conditions, and 2 h after cotyledon wounding (orange asterisks). (D) Box plot summary of primary root length from 7-do seedlings of WT and *kor1-4* grown in basal (mock) or hyperosmotic (3% mannitol) conditions. Medians are represented inside the boxes by solid lines, circles depict individual measurements ( $n = 59-61$ ). Letters denote statistically significant differences as determined by a linear model for differences in responsiveness between the two genotypes. (E to G) Anatomy, cell number and cell size comparisons from transverse sections across the early differentiation zone of the primary root in WT and *kor1-4* roots grown in basal (mock) or hyperosmotic (3% mannitol) conditions. (E) Representative split images from transversal sections (left panels) and respective cell segmentations (right panels) across the early differentiation zone of primary *kor1-4* roots grown in basal (mock) or hyperosmotic conditions. Segmented cell-types are color-coded as: epidermis, turquoise; cortex, magenta; endodermis, yellow; pericycle, mustard; stele, grey. (F) Cell number in epidermis (Epi), cortex (Cor), endodermis (End), and pericycle (Per) of the early differentiation zone of primary WT and *kor1-4* roots grown in basal (mock) or hyperosmotic conditions. Bars represent the means of  $n = 10$  roots ( $\pm$ SD). (G) Fold change in total and cell-specific areas from segmented transversal root sections of WT and *kor1-4* grown in basal (mock) or hyperosmotic conditions. Measurements were normalized to those of the mock-treated WT indicated by a dashed line (individual measurements can be found in Fig. S6). Letters in (C, D, F, and G) denote statistically significant differences among samples as determined by ANOVA followed by Tukey's HSD test ( $P < 0.05$ ). Analyses in (F and G) were performed for each cell file individually. Note that mock-treated WT in (F), as indicated by the dashed line, is always considered as letter 'A' in the statistical analysis. Scale bars (A and B) = 0.5 mm, (E) = 50  $\mu$ m. Data in this Figure were generated by Dr. Mukesh Meena under my supervision.

### Hypoosmotic treatment triggers JA-Ile signalling in the WT

As hyperosmotic treatments abolished cortex cell enlargement and JA-Ile signalling in *kor1-4*, we then hypothesised that opposite growth conditions (hypoosmotic treatments causing cellular water influx) might cause mechanical stress within tissues and result in JA-Ile biosynthesis even in WT plants. Hence, we transferred WT plants to de-ionized water and analysed *JGP* reporter expression, which was activated within 6 h in the root and the shoot apical meristem and increased over a time course of 24 h (Fig. 22A). Because the *JGP* reporter is suited to reveal JA-Ile signalling in tissues but not to map cellular expression sites (Acosta et al., 2013), I verified which cells activated JA-Ile signalling with the *JAZ1op:NLS-3xVEN* reporter. A transfer of 24 h into isotonic mock solution did neither activate the reporter nor impact root morphology (Fig. 22B). In contrast, hypoosmotic treatment severely affected the root apical meristem as indicated by the cellular penetration of propidium iodide (Fig. 22C). Moreover, we detected *JAZ1op:NLS-3xVEN* reporter expression in inner tissues starting at the root early differentiation zone, which was predominantly confined to endodermal and pericycle cells (Fig. 22C to E). Our data thus indicate that osmotically-driven turgor changes have a general impact on JA-Ile production.

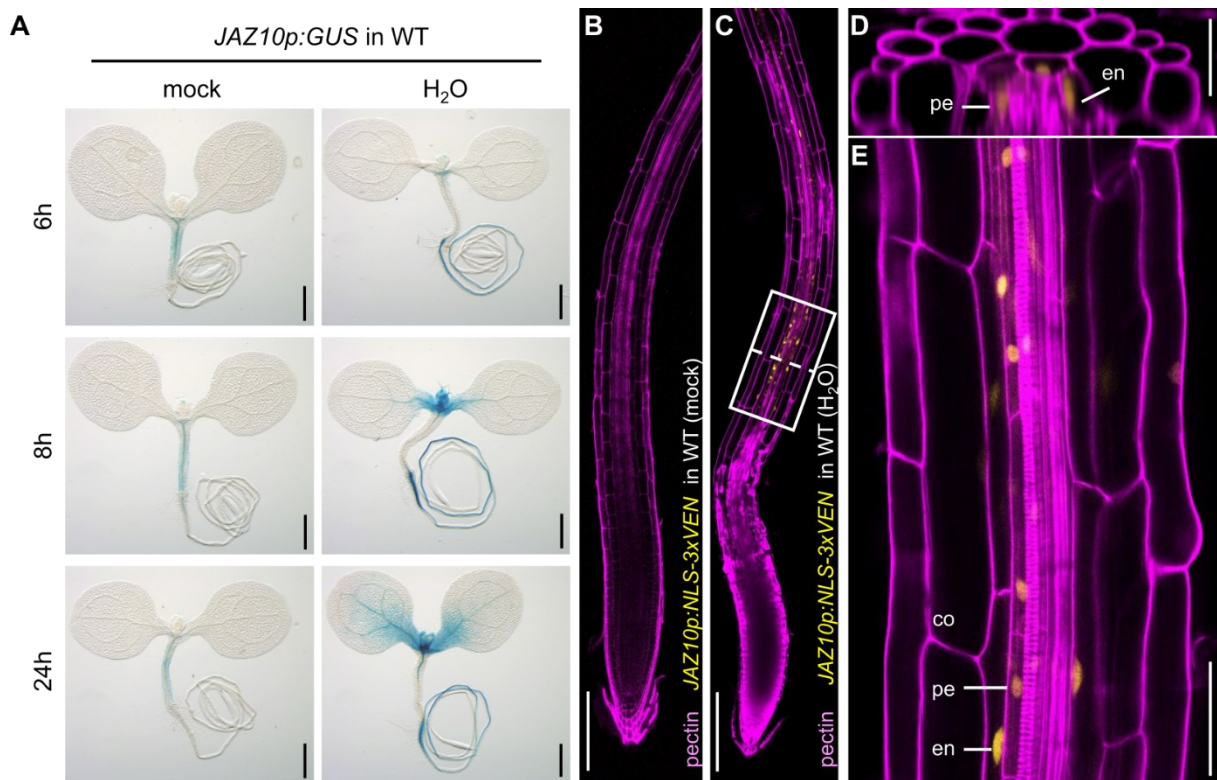


**Figure 22: Hypoosmotic treatment of WT seedlings activates JA-Ile signalling.** (A) Representative images of *JAZ10p:GUS* (*JGP*) reporter activity in WT seedlings submerged in isotonic solution (liquid MS, mock) or deionized water (H<sub>2</sub>O) for 6, 8, and 24 h. (B to E) *JAZ10p:NLS-3xVEN* expression in WT roots submerged in (B) liquid MS or (C to E) H<sub>2</sub>O for 24 h and counterstained with propidium iodide. (G) Orthogonal and (H) longitudinal view from epidermis to vascular cylinder in the early differentiation zone. co, cortex; en, endodermis. Scale bars, 200 µm (B and C), 30 µm (D) and 50 µm (E). Data in (B to E) were generated by Dr. Mukesh Meena under my supervision.

## 7. What are the roles of ectopic JA-Ile signalling in *kor1*?

*Data presented in Figures 23 and 24 and relative sections are published in (Mielke et al., 2021, Science Advances). Data presented in Figures 25 to 27 are unpublished, manuscript in preparation.*

Endogenous JA-Ile levels are normally very low in vegetative tissues of unchallenged plants, often below the limit of detection (Glaser et al., 2008; Schulze et al., 2019). In contrast, *kor1* roots constitutively produce the bioactive hormone and exhibit persistent activation of downstream signalling. As JA-Ile is an important regulator of stress and growth responses, reviewed in (Wasternack and Feussner, 2018), I next investigated what is the impact of activated JA-Ile signalling in *kor1-4* by comparing it with the JA-deficient *kor1-4 aos* double mutant.

### Elevated JA-Ile levels in *kor1-4* roots do not trigger canonical growth or defense responses

The initiation of JA-Ile signalling in response to wounding or herbivory triggers transcriptional changes necessary to activate defense responses at the expense of plant growth (Yang et al., 2012). In fact, exogenous JA treatment as well as endogenous increases in hormone levels inhibit root

growth by reducing root meristem cell number and cell elongation (Chen et al., 2011; Gasperini et al., 2015). Hence it is possible that the constant activation of JA-Ile signalling in *kor1* roots contributes to restrain root growth as the mutant has reduced cellulose content. Indeed, dwarf phenotypes, including a stunted primary root growth, were already described for *kor1* mutants, but were usually attributed to impaired cellulose biosynthesis (Nicol et al., 1998; Lei et al., 2014). Consistently, our *kor1* alleles displayed reduced root growth phenotypes (Fig. S1B). To define whether the short root phenotype is caused by a defect in cell proliferation in the root apical meristem (RAM) or by a defect in cell elongation, I performed cellular measurements in roots of *kor1-4* and WT plants. Although RAM cortex cell number was unaltered between *kor1-4* and WT, the overall meristem length was significantly shorter in *kor1-4*, suggesting an impairment in longitudinal cell elongation (Fig. 23A to C). This was further substantiated as cortex cell length in the differentiation zone of *kor1-4* was on average 50% shorter than in the WT (Fig. 23D and E), which confirmed the inability of root *kor1-4* cortex cells to undergo elongation. To test if constitutive JA-Ile signalling contributed to stunt *kor1-4* root growth, I compared *kor1-4* root elongation rates to those of the JA-Ile deficient *kor1-4 aos* double mutant. In agreement with previous reports (Gasperini et al., 2015), there were no differences in root length between WT and *aos* plants and also their root growth rate over a duration of six days was similar (Fig. 23F). However, and contrary to the expectation that activated JA-Ile signalling may inhibit root growth (Acosta et al., 2013; Gasperini et al., 2015), I found no difference in root growth rates between *kor1-4* and *kor1-4 aos* as well (Fig. 23F). This indicates that constant JA-Ile production in *kor1-4* roots is unlikely regulating root growth.

I next tested if JA-Ile-dependent defense signalling may be activated in *kor1-4* roots in an *aos*-dependent manner. In the *kor1-4* root transcriptome we found several upregulated JA-Ile-dependent genes involved in stress responses (Tab. S2). However, among them there were no canonical defense transcripts such as *VSP2* or *PDF1.2*, which are induced upon wounding or herbivory (Penninckx et al., 1998; Liu et al., 2005; Mielke and Gasperini, 2019). To confirm this, I analysed basal root expression levels of *VSP2* and *PDF1.2* in *kor1-4* roots, in which the levels of both transcripts were indeed not altered in comparison to the WT nor *kor1-4 aos* (Fig. 23G and H). Collectively, the data suggest that constitutive JA-Ile production in *kor1-4* roots is not contributing to canonical JA-Ile-regulated growth phenotypes, but might trigger root-specific defense phenotypes that still need to be assessed.



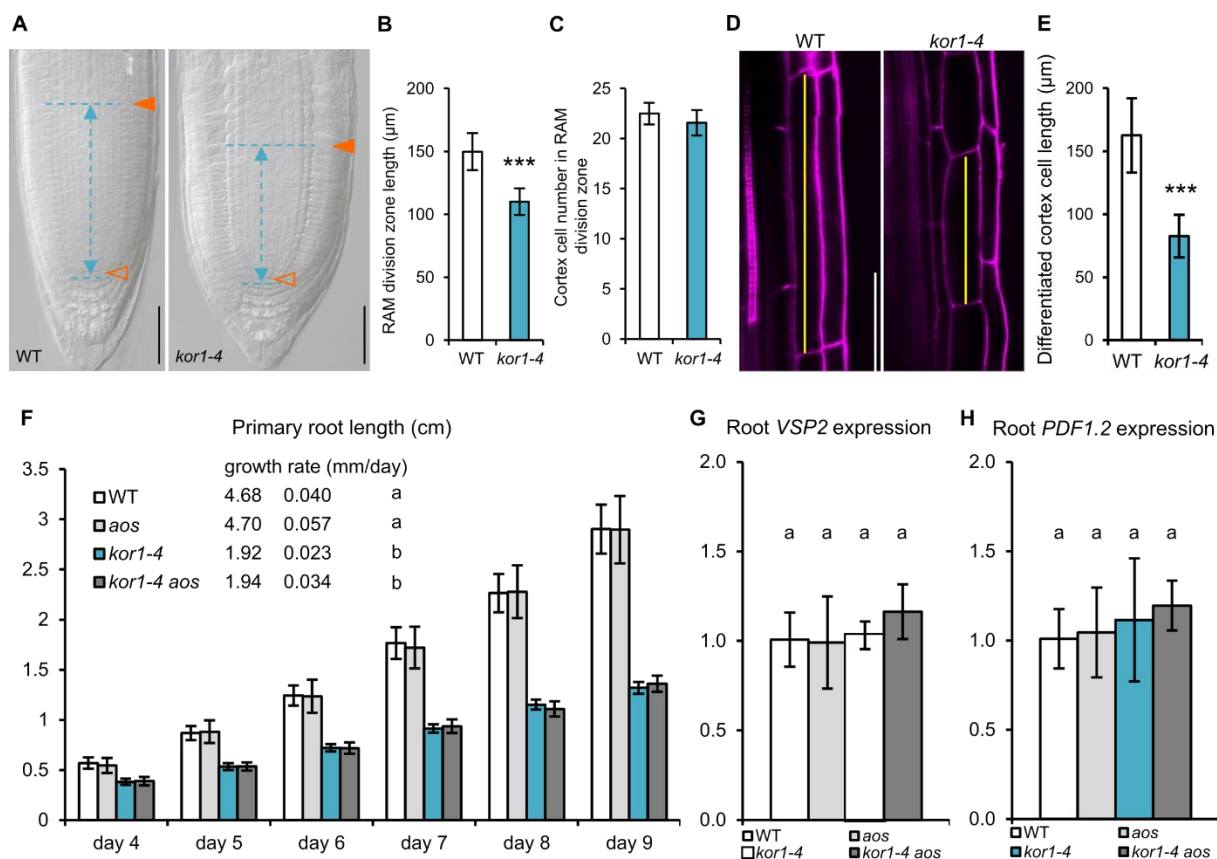


**Figure 23: Constitutive JA-Ile production in *kor1-4* roots does not regulate canonical growth and defense responses.** (A) Representative differential interference contrast (DIC) images of 5-do WT and *kor1-4* primary root meristems. Empty orange arrowheads point to the quiescent center, and full orange arrowheads indicate the beginning of the elongation zone. Blue arrows indicate the distance measured for meristem length. (B and C) Root apical meristem (RAM) (B) length (from quiescent center to elongation zone) and (C) cortex cell number in the division zone in 5-do seedlings of WT and *kor1-4*. Cortex cell number in the RAM was determined by counting all cells in the cortex file until the onset of elongation. Data shown are means from  $n = 10$  plants. (D and E) Representative cortex cells in the root differentiation zone of (D) WT and *kor1-4* plants. Yellow bars indicate cell length measured in (E). (E) Quantification of cortex cell length in 5-do seedlings of WT and *kor1-4* plants. Data shown are means from  $n = 10$  plants, each consisting of 40 cellular measurements along the same longitudinal cell file starting from the onset of differentiation. Scale bars (A) = 100  $\mu\text{m}$ , (D) = 50  $\mu\text{m}$ . (F) Primary root length of indicated genotypes between 4- and 9-days post germination. Bars represent the means of 40-50 plants. Data were used to determine the root growth rate in mm per day by linear regression. (G and H) qRT-PCR of basal (G) *VSP2* and (H) *PDF1.2* expression in roots of indicated genotypes. *VSP2* and *PDF1.2* transcript levels were normalized to those of *UBC21*. Bars represent the means of three biological replicates ( $\pm$ SD), each containing a pool of ~60 roots from 5-do seedlings. Letters and asterisks in (B and E to H) denote statistically significant differences among samples as determined by ANOVA followed by Tukey's HSD test ( $P < 0.05$ ) in (F to H) or Student's t-test ( $P < 0.001$ ) in (B and E).

### Heightened JA-Ile levels facilitate *kor1* response to root hydrotropism

Although typical JA-dependent growth and defense phenotypes did not differ between *kor1-4* and *kor1-4 aos* (Fig. 23), the short *kor1-4* root growth phenotype was alleviated when continuously grown in hyperosmotic mannitol media (Fig. 21D). I hence verified if the mutant might preferentially grow towards hyperosmotic conditions to ameliorate its root length, and if this may be influenced by constant root JA-Ile signalling. This process can be tested in split-agar assays used for measuring root hydrotropic responses (Antoni et al., 2016; Dietrich et al., 2017). Root hydrotropism describes the

directional growth of roots towards media with greater water availability, a process that requires signalling by the hormone ABA in cortical cells of the root elongation zone (Takahashi et al., 2002; Dietrich et al., 2017). As root hydrotropism assays are only comparable among genotypes with similar root growth rates, lines with normal root growth (WT and *aos*) and stunted root growth (*kor1-4* and *kor1-4 aos*) were assessed independently. As expected, when transferring seedlings to mock (MS/MS) conditions, seedlings of all genotypes were growing gravitropically without bending at the media boundary (Fig. 24A and B, Fig. S8A and B).

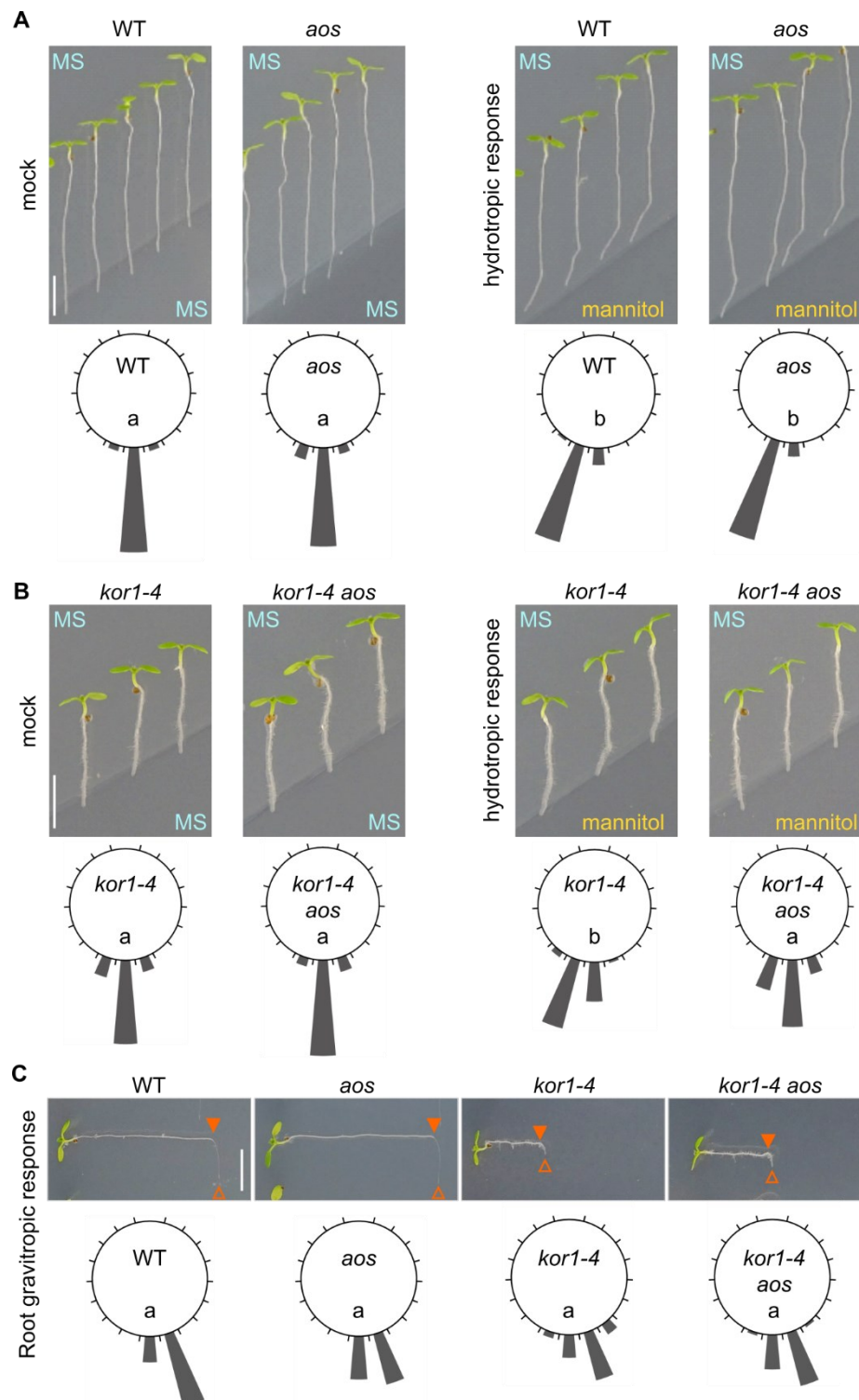


**Figure 24: Ectopic JA-Ile production facilitates *kor1-4* root growth towards greater water availability.** (A and B) Determination of root hydrotropic response of (A) WT and *aos*, and (B) *kor1-4* and *kor1-4 aos* seedlings. Representative images and circular histograms summarizing root curvatures of indicated genotypes 24 h after transfer to split-agar Murashige and Skoog (MS) plates under mock (MS/MS) or hydrotropism-inducing (MS/400 mM mannitol) conditions. Bars indicate the percentage of seedlings exhibiting a root bending angle assigned to one of the 18 20° sectors on the circular diagram from a total of n = 42 plants. Raw data are in Fig. S8. (C) Root gravitropic response in indicated genotypes. Representative images depict seedlings grown vertically for 5-d in the 1<sup>st</sup> gravity direction (full orange arrowheads indicate initial root tip position), turned by 90° and grown for additional 24 h in the 2<sup>nd</sup> gravity vector (root tip indicated by empty orange arrowhead) before measuring the gravitropic bending angle. Circular histograms summarize root growth curvatures with bars indicating the percentage of seedlings exhibiting a root bending angle assigned to one of the 18 20° sectors on the circular diagram from a total of n = 31-35 plants. Raw data are in Fig. S8. Letters denote statistically significant differences as determined by (C) One-Way-ANOVA or (A and B) Two-Way-ANOVA followed by Tukey's HSD test (P < 0.05). Scale bars = 5 mm.

Following transfer to split-agar plates harbouring asymmetric water availability (MS/mannitol), both WT and *aos* seedlings redirected their root growth towards MS and away from mannitol with a positive root curvature (Fig. 24A, Fig. S8A and B). Similarly, *kor1-4* seedlings did not grow into the mannitol media as hypothesized and also readjusted their growth towards higher water availability exhibiting a positive hydrotropic root curvature (Fig. 24B, Fig. S8C). Unexpectedly, the JA-deficient *kor1-4 aos* double mutant did not redirect its root growth towards isotonic conditions and instead grew into the mannitol media (Fig. 24B, Fig. S8C). Consistently, while *esmd1-3* roots showed a normal root hydrotropic response, the *kor1-4 esmd1-3* double mutant with abolished constitutive root JA-Ile production did not redirect its root growth away from the mannitol media (Fig. S8F to I). To test whether this JA-dependent effect represented a specific insensitivity towards root hydrotropism, or was caused by a general inability of *kor1-4 aos* to undergo root bending, I analysed root bending responses upon sudden changes in gravity direction known as gravitropism (Su et al., 2017). All genotypes tested (WT, *aos*, *kor1-4*, and *kor1-4 aos*) effectively redirected their root growth in response to a gravitropic stimulus with comparable gravitropic bending angles (Fig. 24C, Fig. S8D and E). Overall, data thus revealed that the constitutive activation of JA-Ile production facilitates the directional growth of *kor1-4* roots towards water.

### **JA-Ile-dependent root-derived signal(s) impact *kor1* shoot growth**

Although elevated JA-Ile signalling in *kor1* roots did not influence root elongation in young seedlings (Fig. 23F), I noticed that rosette size of 5-weeks-old short-day grown plants is considerably larger in JA-Ile-deficient *kor1-4 aos* plants compared to *kor1-4*, while WT and *aos* exhibited comparable shoot size (Fig. 25A). Interestingly, although *kor1-4* had a lower leaf number and overall smaller leaves than WT and *aos* rosettes, *kor1-4* and *kor1-4 aos* did not differ in terms of leaf number but only in terms of leaf size with *kor1-4* having 37% smaller leaves than *kor1-4 aos* (Fig. 25B and D). These results suggest that enhanced JA-Ile signalling in *kor1-4* is unlikely slowing leaf emergence and may rather affect leaf expansion.

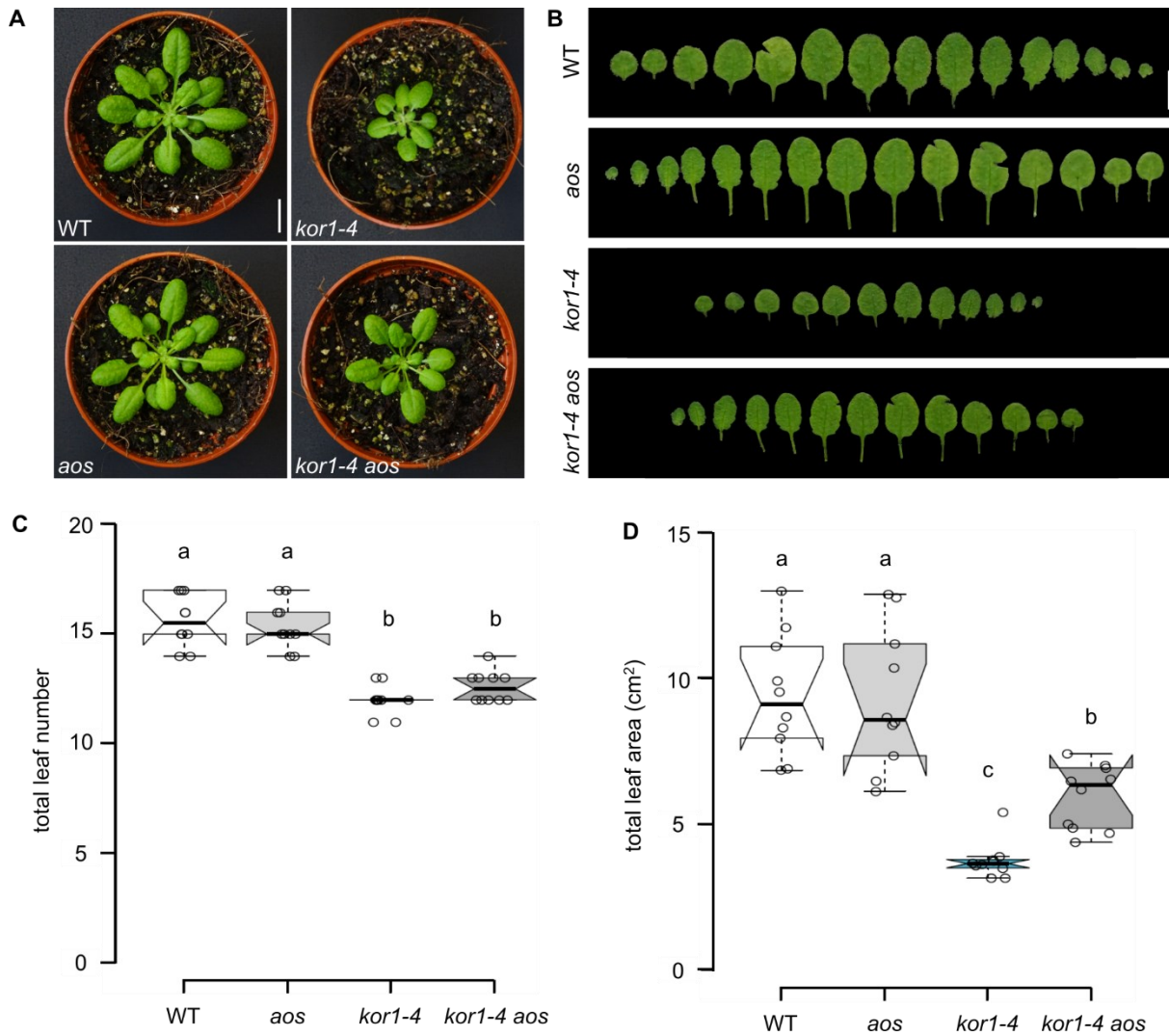


**Figure 25: Absence of JA-Ile in *kor1-4* increases shoot growth.** (A to D) Impact of JA-Ile on *kor1-4* rosette phenotypes. (A) Representative rosette images of 5-week-old plants from indicated genotypes grown under short day conditions. (B) True leaves excised from plants in (A). Scale bars (A and B) = 1 cm. (C and D) Box plot summary of (C) total leaf number, and (D) total leaf area in plants from (A). Medians are represented by a solid line inside the boxes. Circles depict individual data points (n = 10 plants). Letters in (C and D) denote statistically significant differences among samples as determined by ANOVA followed by Tukey's HSD test (P < 0.05). The assays were repeated two times with similar results.

Since increased *JGP* signalling is still persisting only in roots even in adult *kor1-4* plants (Fig. S9), I hypothesized that root-derived signals arising from activated JA-Ile may be responsible for the observed differences in rosette size between *kor1-4* and *kor1-4 aos*. To test this possibility, I generated chimeric plants with varying genotypes between scions (shoots) and rootstocks (roots) via micrografting (Schulze et al., 2019). The evaluation of leaf number and rosette size in *kor1-4(scion)/kor1-4(rootstock)* and the JA-Ile deficient *kor1-4 aos/kor1-4 aos* counterparts confirmed that the self-grafts behaved similarly to the un-grafted controls (Fig. 26A to D). Specifically, leaf number between *kor1-4/kor1-4* and *kor1-4 aos/kor1-4 aos* remained unchanged while rosette size was 69% larger in the JA-Ile deficient genotype (Fig. 26C and D).

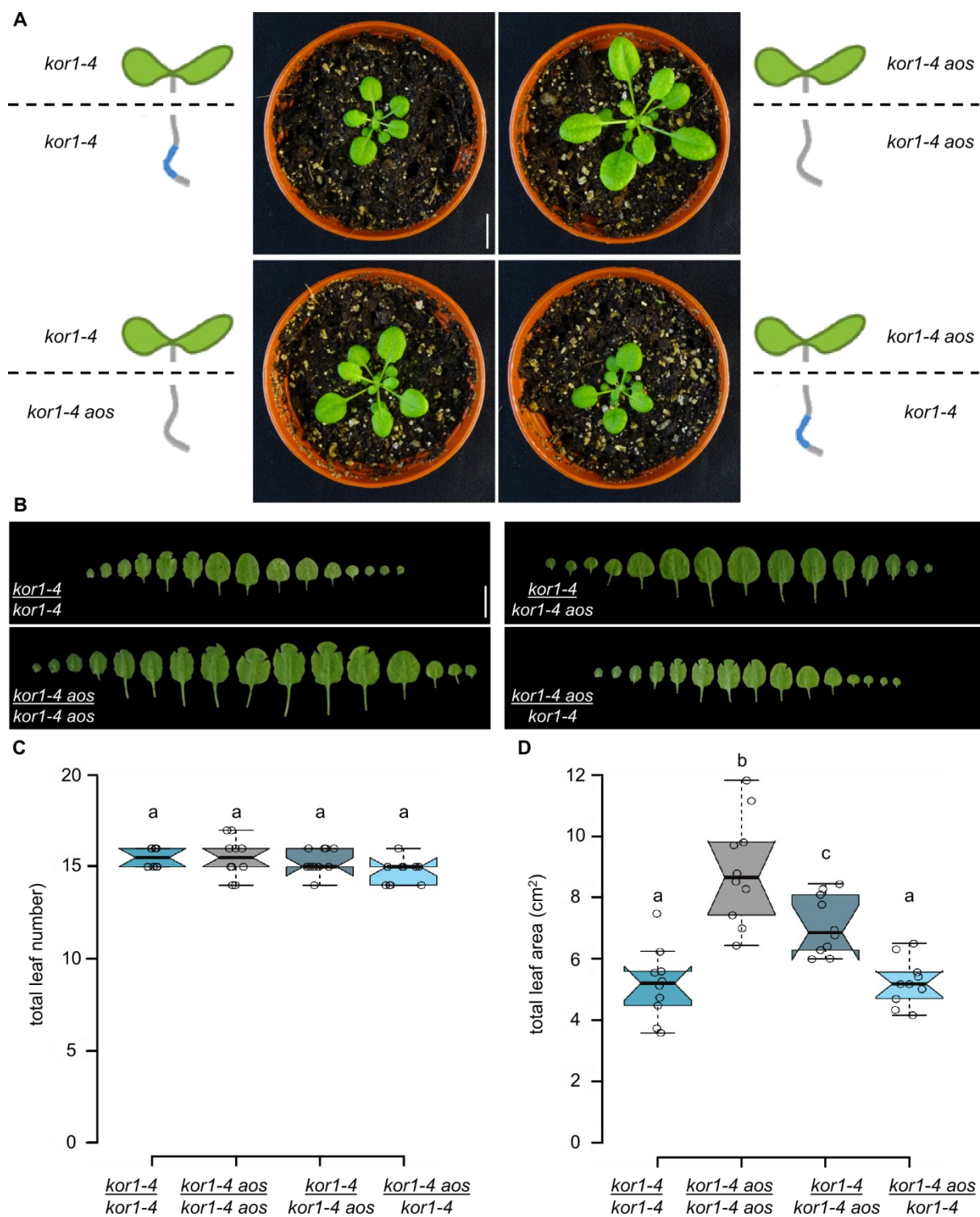


**Figure 26: *kor1-4* leaf expansion is regulated by increased JA-Ile levels in the root.** (A to D) Grafting experiments showing that ectopic JA-Ile production in *kor1-4* roots affects shoot growth. (A) Representative rosette images from 6-week-old grafted plants of indicated genotypes grown in short day conditions. (B) True leaves from 7-week-old grafted plants from (A). Scale bars (A and B) = 1 cm. (C and D) Box plot summary of (C) total leaf number and (D) total leaf area in plants from (B). Medians are represented by solid lines inside the boxes. Circles depict individual data points from n = 10 plants. Letters in (C and D) denote statistically significant differences among samples as determined by ANOVA followed by Tukey's HSD test (P < 0.05). The assays were repeated two times with similar results.

Consistently, leaf number did not differ in rosettes from self-grafts nor chimeric *kor1-4/kor1-4 aos* and *kor1-4 aos/kor1-4* plants, but total rosette size was 37% larger in *kor1-4/kor1-4 aos* with respect to *kor1-4/kor1-4*, and diminished by 41% in *kor1-4 aos/kor1-4* compared to *kor1-4 aos/kor1-4 aos* plants (Fig. 26A, B and D). In other words, constitutive JA-Ile production in *kor1-4* roots reduced rosette size in *kor1-4 aos*, and blocking ectopic JA-Ile signalling with a *kor1-4 aos* rootstock ameliorated *kor1-4* rosette size. These results indicate that constitutive JA-Ile signalling in *kor1-4* roots negatively regulates leaf expansion.

### **JA-Ile-dependent root-derived signal(s) warrant *kor1* increased rosette protection against herbivorous insects**

The intriguing finding of putative JA-Ile-dependent root-derived signals regulating shoot growth led me to hypothesize that such signals may also impact defense phenotypes in rosettes. To test this assumption, I first optimized a plant-insect bioassay to measure insect performance of the generalist herbivore *Spodoptera littoralis* (*S. littoralis*) on Arabidopsis genotypes compromised in the JA pathway (Mielke and Gasperini, 2020). The bioassay was then used to assess insect larvae performance in WT, *aos*, *kor1-4*, and *kor1-4 aos* plants. As WT and *aos* plants exhibited a higher leaf number and were thus developmentally ahead compared to genotypes harbouring the *kor1-4* allele (Fig. 25C), I synchronized plant growth for the bioassays by growing *kor1-4* mutants one week longer. Hence, at the start of the bioassay all genotypes had the same leaf number (15 to 16 true leaves) with WT and *aos* being 5-week old and *kor1-4* genotypes being 6-week old. *S. littoralis* larvae were then allowed to feed until they consumed the shoot apical meristem (SAM) of the first and hence most susceptible genotype, i.e. for 10 days. In agreement with previous reports (Mielke and Gasperini, 2020), larval weight was greatly enhanced in JA-deficient *aos* compared to WT plants (Fig. 27A and B). Similar to *aos*, *kor1-4 aos* plants were also completely eaten and larvae were comparably heavy (Fig. 27A and B). Conversely, *kor1-4* plants were able to defend themselves even better than the WT, as indicated by a significantly lower weight of *S. littoralis* larvae (Fig. 27A and B). These results suggest that constitutive JA-Ile production in *kor1-4* may also impact insect performance.

Following results obtained in intact plants, I next evaluated whether activation of the JA pathway in roots could contribute to shoot defense by performing bioassays in chimeric plants generated via micrografting. First, I carried out bioassays in reciprocal grafts between WT and *aos* plants. Although WT plants in comparison to *kor1* show no basal JA-Ile production in the roots, shoot wounding triggers the translocation of JA-Ile precursors into the root (Schulze et al., 2019), which might in turn activate defense-related root-to-shoot signals.

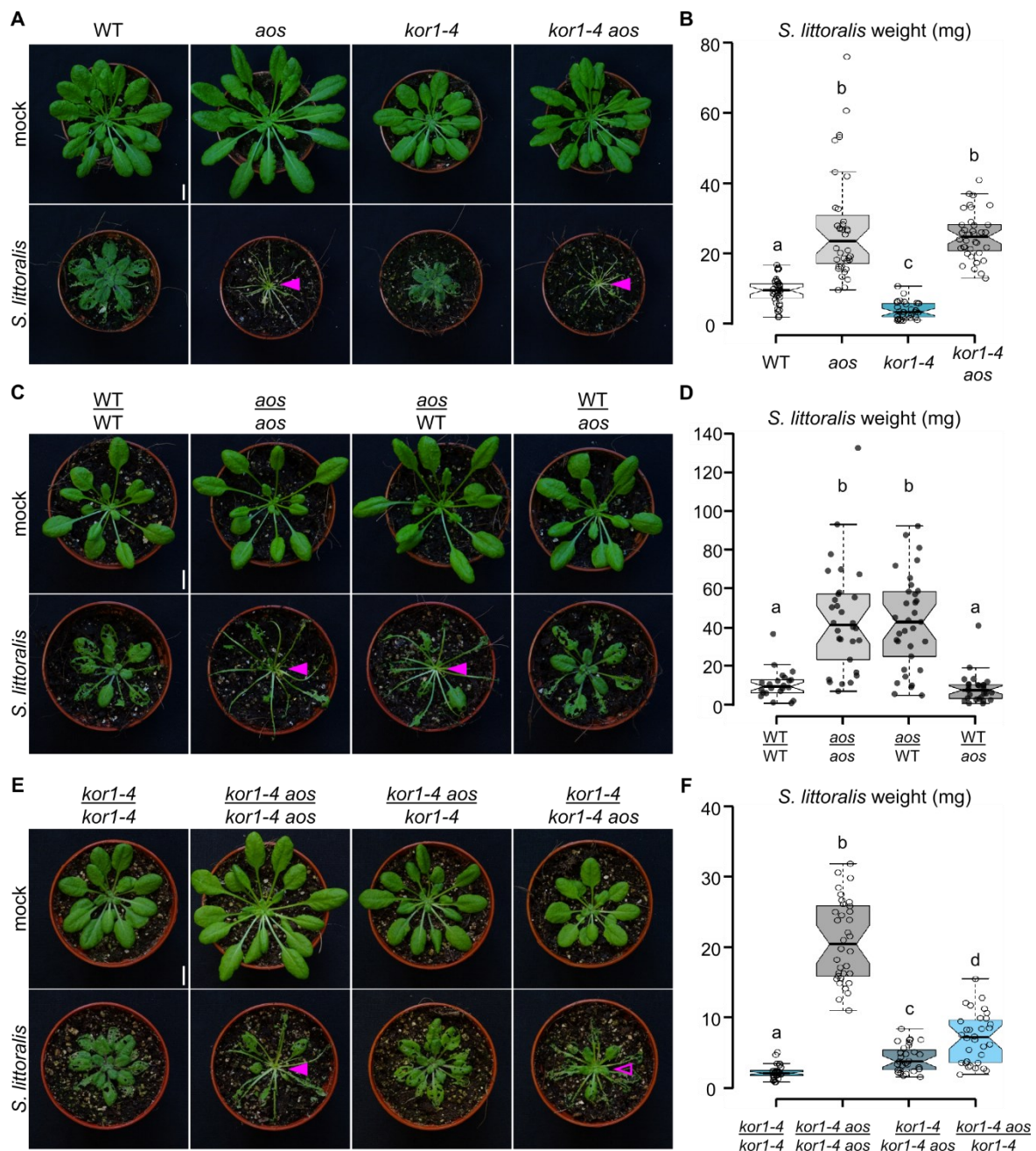


**Figure 27: Constitutive JA-Ile production in *kor1* roots impacts shoot resistance against herbivorous insects.** (A and B) Plant resistance against the generalist herbivore *S. littoralis*. (A) 5-week old (WT and *aos*) and 6-week old (*kor1-4* and *kor1-4 aos*) rosettes 10 days after mock treatment or after challenge by *S. littoralis* larvae. Note that JA-deficient genotypes were eaten down to the meristem (magenta arrowheads). (B) Box plot summary of *S. littoralis* larval weights after feeding from plants in (A). Medians are represented by solid lines inside the boxes. Circles depict individual data points (n = 33-36). (C to F) Contribution of the root genotype towards shoot performance against the insect herbivore *S. littoralis*. (C) 6-week old rosettes of indicated grafted plants after 10 days of mock or challenge by *S. littoralis*. Note that meristems of JA-deficient grafts in the scions (*aos/aos* and *aos/WT*) were fully eaten (full magenta arrowhead). (D) Box plot summary of *S. littoralis* larval weights after feeding for 10 days on indicated genotypes. Medians are represented by solid lines inside boxes. Circles depict individual data points (n = 23-33). (E) 7-week old rosettes of indicated grafted plants after 9 days of mock or challenge by *S. littoralis*. Note that meristems of JA-deficient grafts (*kor1-4 aos/kor1-4 aos*) were fully eaten (full magenta arrowhead), while meristems of JA-deficient *kor1-4 aos* shoots were not fully consumed from grafts harboring *kor1-4* rootstocks with constitutive root JA-Ile production (empty magenta arrowhead). (F) Box plot summary of *S. littoralis* larval weights after feeding for 10 days on indicated genotypes. Medians are represented by solid lines inside boxes. Circles depict individual data points (n = 29-31). Letters in (B, D, and F) denote statistically significant differences among samples as determined by ANOVA followed by Tukey's HSD test (P < 0.05). Bioassays in (B, D, and F) were repeated 3 times and showed similar results. Scale bars (A, C and E) = 1 cm.

However, there was no difference in insect weight between grafts from WT or *aos* rootstock, as all grafts with *aos* scions were consumed down to the SAM and yielded larvae with high weights, while all grafts with WT scions could defend better and led to larvae with decreased weight (Fig. 27 C and D). These results suggest that WT roots are unlikely contributing to mount shoot defense responses under our bioassay conditions.

I next tested if constitutive root JA-production may affect insect performance by conducting bioassays in reciprocal grafts between *kor1-4* and *kor1-4 aos* which exhibit similar leaf numbers (Fig. 26C). Comparable to their un-grafted variants (Fig. 27B), larval weight on *kor1-4/kor1-4* self-grafts were lower than JA-deficient *kor1-4 aos/kor1-4 aos* plants (Fig. 27E and F). In fact, all leaf material was consumed down to the SAM in *kor1-4 aos/kor1-4 aos* plants (Fig. 27E). Remarkably, abolishing root JA-Ile production from *kor1-4* scions in *kor1-4/kor1-4 aos* combinations led to a significant 42% increase in larval weight (Fig. 27F). Consistently, larvae feeding on *kor1-4 aos/kor1-4* plants with constitutive root JA-Ile signalling were 40% lighter than when feeding on *kor1-4 aos/kor1-4 aos* plants (Fig. 27F). Notably, larvae avoided to feed on the SAM and the younger leaves of *kor1-4 aos/kor1-4* plants (Fig. 27E), indicating that there may be a JA-dependent root-derived signal reaching young leaf tissues contributing to leaf defense.



## Section III - Discussion and future perspectives

Despite the essential roles of JA-Ile in mediating plant growth and environmental responses, it is still unclear what intracellular processes lead to the activation of JA-Ile biosynthesis. Perturbations in plant cell walls have frequently been associated with the activation of the JA pathway. However, the variety of stressors altering wall properties, including mechanical rupture, enzymatic degradation or inhibition of cell wall biosynthesis, as well as the emergence of cell wall-derived elicitors yielded in heterogenic evidence on the initiation of the JA pathway as well as its consequences. In this thesis I utilized mutants in *KOR1* that are impaired in cellulose biosynthesis, and revealed a turgor-driven misregulation of cell expansion in the root cortex, which likely mechanically compromises inner tissues leading to enhanced JA-Ile production (Fig. 28). I abolished enhanced JA-Ile production by restoring cortex cell size via cell type-specific *KOR1* complementation, by isolating a genetic suppressor likely modulating cell wall properties and by lowering turgor pressure with hyperosmotic treatments (Fig. 28). Furthermore, hypoosmotic treatments activated JA-Ile signalling in WT plants at similar sites. To our surprise JA-Ile did not exert its expected functions in altering growth rate and canonical defense responses in the root, but was rather crucial to guide root growth into the direction of water (Fig. 28). Additionally, root-derived JA-dependent signals in *kor1* were able to shape shoot growth and defense (Fig. 28). Collectively, my results provide new perspectives on how plants sense and decode extracellular stimuli to initiate acclimation responses.

### 1. Advantages of deciphering hormone functions in cell wall mutants

Wounding and insect herbivory are potent triggers of JA-Ile production and are often used to study the impact and physiological consequences of elevated JA-Ile signalling. Both treatments induce similar transcriptional changes (Reymond et al., 2000), involving the upregulation of typical JA marker genes in JA biosynthesis and signalling such as *JAZs*, *MYC2*, *LOX3*, *LOX4*, *AOS*, *AOC1* and *3*, *JOX2*, *3* and *4*, and *OPR3* (Reymond et al., 2004; Chung et al., 2008; Zhang et al., 2020). Contrariwise, constitutive JA-Ile production in *kor1-4* roots resulted in a much weaker JA response, which comprised only a subset of typical JA markers (*JAZ10*, *JAZ9*, *JAZ3*, *LOX3*, *LOX6*, *JOX2*, *JOX3*, and *ST2A*). This may be due to a dilution-effect of sampling the entire root, whereas JA-Ile signalling was activated only in specific cells of the early differentiation zone, or to the activation of a subset of JA markers in cell-specific contexts. Similarly, although not checked for JA-dependency, the *CesA3* mutant *ixr1* also exhibits upregulation of a smaller subset of JA marker genes such as *LOX3*, *LOX4*, *JAZ1*, *JAZ4*, *JAZ5*, *JAZ6*, *JAZ7*, and *JAZ10* (Engelsdorf et al., 2018). However, there is only a small overlap between the *kor1* root transcriptome and the transcriptome of *ninja-1* roots, which exhibit elevated basal JA-Ile signalling (Acosta et al., 2013; Gasperini et al., 2015). Among the JA-related transcripts that are found

upregulated in both transcriptomes are *JAZ10* and *ST2A* only (Tab. S2) (Gasperini et al., 2015). Hence, our transcriptomic data suggest that JA-Ile responses arising from cell wall alterations are distinct to those triggered by other or stronger elicitors.

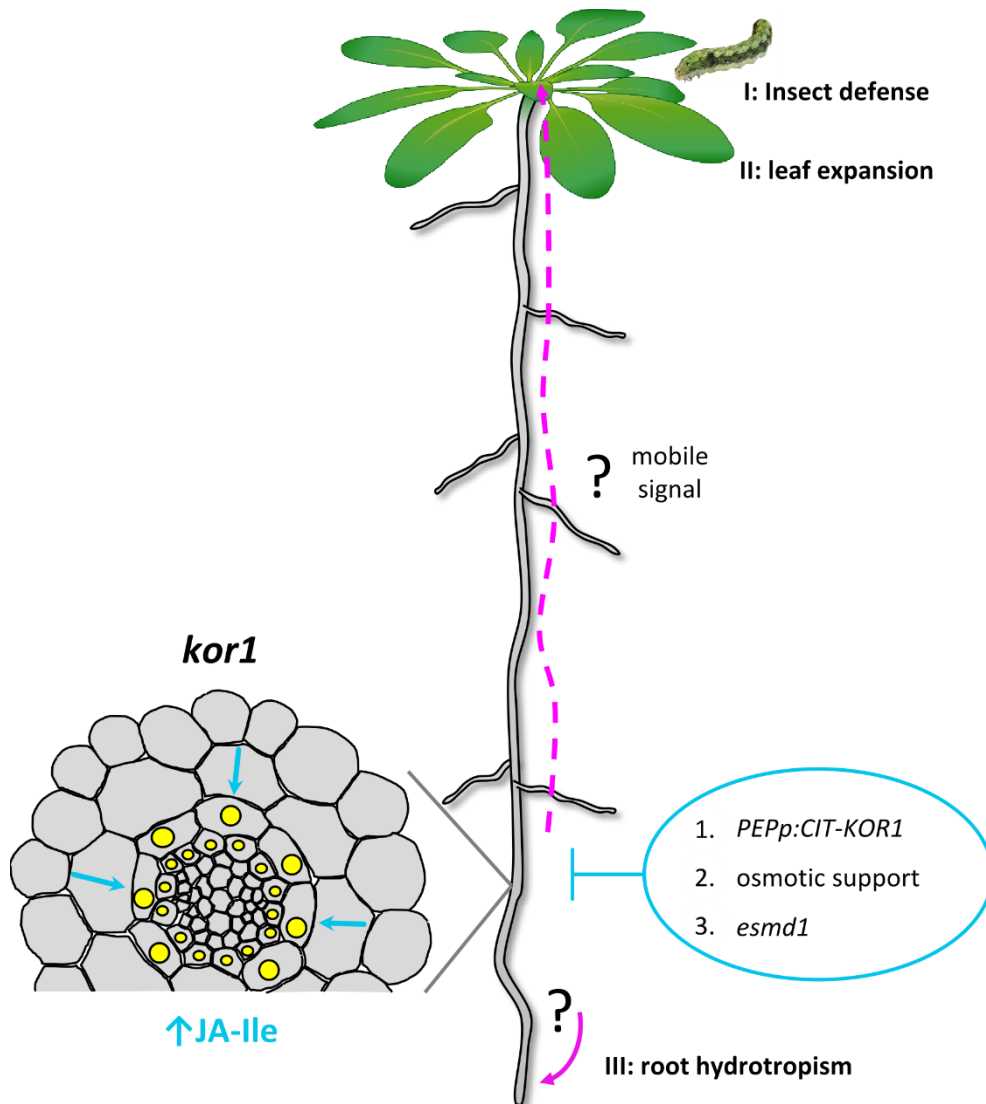


**Figure 28: Final model summarizing causes and consequences of ectopic JA-Ile production in cellulose-deficient *kor1* mutants.** *kor1* mutants exhibit basal induction of JA marker genes and elevated levels of JA-Ile predominantly in endodermis and pericycle cells of the root early differentiation zone (yellow dots). This is caused by cell-non-autonomous signals deriving from adjacent cortex cells, which are enlarged and likely mechanically compromise inner tissues (blue arrows). The JA phenotype was abolished by restoring cortex cell size via cell type-specific *KOR1* complementation (*PEPp:CIT-KOR1*), by lowering turgor pressure with hyperosmotic treatments (osmotic support) and by isolating a genetic suppressor likely modulating cell wall properties (*esmd1*). Via an unknown mechanism, ectopic JA-Ile can act locally to allow root hydrotropism. Moreover, yet unidentified JA-Ile-dependent mobile signals hamper leaf expansion and increase defense against a generalist herbivore in *kor1* rosettes.

Hypothetically, breeding plants with constitutively elevated JA-dependent defense responses could be beneficial for agriculture. However, this strategy has so far proven to be challenging due to the concomitant negative impact of JA on growth (Campos et al., 2016; Major et al., 2020). Ectopic JA-Ile

production in *kor1* roots did not influence root growth rate as expected, and similarly, it did not regulate the expression of typical JA-dependent defense marker genes *PDF1.2* and *VSP2*. More notably, constitutive JA-Ile signalling in *kor1* was important for the root hydrotropic response, and for regulating growth and defense responses in the shoots. These findings highlight the benefit of using cell wall mutants as genetic tools to characterize subtler or cell-specific JA-Ile functions, which can be potentially masked by strong JA-Ile-inducing stimuli such as wounding and herbivory. This strategy might also be useful to reveal potentially new roles of other hormonal pathways, as a variety of perturbations in plant cell walls can lead to altered hormonal responses such as upregulation of ET in *cev1* and *chitinase-like protein 1 (ctl1)* (Ellis and Turner, 2001; Zhong et al., 2002b; Sanchez-Rodriguez et al., 2010). Moreover, even though canonical defense marker genes were not upregulated in *kor1* roots, the RNA-seq revealed a big cluster of stress- and defense-related genes that are differentially expressed in *kor1* roots in a JA-Ile-dependent manner (Tab. S2). It is thus possible that upregulated JA-Ile signalling in *kor1* may mediate root-specific defense responses which await further characterization. For example, it would be interesting to ascertain defense responses between *kor1* and the JA-deficient *kor1 aos* double mutant against root pathogens such as *Pythium irregulare*, *Fusarium oxysporum*, or nematodes (Bohlmann and Wieczorek, 2015; Sohrabi et al., 2015; Kesten et al., 2019).

#### **How does constitutive JA-Ile production in *kor1* influence root hydrotropism?**

Surprisingly, root hydrotropism assays revealed that constitutive JA-Ile signalling in *kor1* guided root growth towards greater water availability. While the root hydrotropic response did not differ between WT and *aos*, the lack of constitutive JA production in *kor1 aos* and *kor1 esmd1-3* rendered plants unable to redirect their roots away from hyperosmotic conditions containing mannitol. These findings indicate that JA-Ile signalling is dispensable for the hydrotropic response in WT plants, but ectopic JA activation in precise cell types can be beneficial. Signalling mechanisms guiding WT hydrotropic responses might be inactive and overridden by the JA pathway in *kor1* roots. A possibility is that ABA signalling or biosynthesis is altered in *kor1* as a consequence of cell wall perturbations. In fact, the cellulose-deficient mutant *kobito1* displays altered ABA signalling and fails to exhibit normal ABA responses (Brocard-Gifford et al., 2004). Specifically, ABA signalling in cortex cells of the root elongation zone is important for perceiving and acclimating to water potential gradients in WT plants (Dietrich et al., 2017). However, the *kor1* root transcriptome did not detect changes in genes involved in ABA signalling or metabolism under basal conditions. To further study the mechanisms of how constitutive JA-Ile signalling guides *kor1* root hydrotropism, ABA levels and hydrotropism-related marker gene expression should be evaluated at control and hyperosmotic conditions. Relevant

changes between *kor1-4* and *kor1-4 aos* plants might only occur during low water availability, which could explain why we see no obvious targets in the basal *kor1* root transcriptome.

Hyperosmotic mannitol treatments are also used to mimic drought and study plant performance under water deficiency. It is therefore tempting to speculate that elevated root JA-Ile levels might be advantageous during drought conditions. Accordingly, exogenous JA treatments confer enhanced drought tolerance in various plant species, reviewed in (Ruan et al., 2019). Moreover, *Arabidopsis* mutants deficient in either JA-Ile biosynthesis (*aos*) or signalling (*coi1*) display a lower survival rate after experiencing prolonged drought (Kim et al., 2017). Monitoring plant performance during drought conditions by accessing and comparing parameters such as survival rate, biomass, leaf expansion or total water content in plants and soil (Bouزيد et al., 2019) could reveal whether JA-Ile-guided root hydrotropism is increasing plant performance under water limiting conditions. Perhaps, activating JA-Ile production in specific root cell types by manipulating cell wall properties could eventually yield plants with enhanced drought resistance without hampering overall root growth. Although the underlying signalling mechanisms that either activate JA-Ile production under drought or improve water foraging when JA-Ile signalling is activated are unknown, their elucidation could have beneficial impacts on breeding programs aimed at increasing plant drought tolerance.

### **How does constitutive root JA-Ile signalling impact shoot growth and defense?**

Interestingly, although activated JA-Ile signalling in *kor1* roots did not impact local organ growth nor the root expression of canonical defense-marker genes, reciprocal grafts between *kor1-4* and *kor1-4 aos* revealed that constitutively heightened root JA-Ile levels restricted shoot growth and mediated enhanced resistance against the generalist herbivore *S. littoralis*. Despite JA-Ile precursors OPDA and JA can travel across tissues and organs (Schulze et al., 2019; Li et al., 2020a), it is unlikely that their translocation is responsible for the observed shoot phenotypes in grafted plants. First, neither *JGP* reporter activity nor JA-Ile-dependent marker gene expression (*JAZ10*, *JOX3*) were induced in shoots of *kor1* mutants. Second, although phytohormones such as strigolactones and cytokinines can translocate from roots to shoots (Kohlen et al., 2011; Ko et al., 2014), JA-Ile precursors relocate through the phloem and the putative OPDA transporter ACYL-COA-BINDING PROTEIN6 (ACBP6) localizes to phloem companion cells (Ye et al., 2016; Schulze et al., 2019; Li et al., 2020a). Third, unlike shoot wounding that triggers JA-Ile marker gene expression in undamaged roots, root wounding induces JA-Ile signalling only locally and does not lead to *JAZ10* upregulation in shoots (Acosta et al., 2013; Schulze et al., 2019).

A possibility for the observed root-derived JA-dependent shoot phenotypes in *kor1*, may reside in nutrient uptake. Apart from carbon which is assimilated during photosynthesis, plants rely on their roots to forage the soil for other nutrients and to distribute them across the whole plant by active and passive transport (Ramakrishna and Barberon, 2019). Insufficient supply of important macronutrients such as nitrogen, phosphorus or potassium leads to detrimental growth and developmental phenotypes in shoots and roots (Gruber et al., 2013; Forieri et al., 2017). Our *kor1* root transcriptome did not identify major changes in phosphate nor potassium transporters or associated marker genes. Instead it identified a JA-dependent upregulation of *NITRATE TRANSPORTER 1.8 (NRT1.8)* (Tab. S2). In contrast to *NRT1.5* which facilitates nitrate shoot transport by loading it into root xylem vessels (Lin et al., 2008), *NRT1.8* transports nitrate in the opposite direction thus keeping it in the root (Li et al., 2010). This equilibrium is abolished by certain stress conditions such as high cadmium, high salt and drought stress, during which *NRT1.8* expression is highly upregulated to keep nitrate locked in the root and mediate stress acclimation and proper root growth (Li et al., 2010; Zhang et al., 2014a). This process is under the control of JA and ET (Zhang et al., 2014a), which might be also reflected in the *kor1* root transcriptome, where *NRT1.8* levels are still slightly upregulated in *kor1-4 aos* in comparison to the WT (Tab. S3). Interestingly, *NRT1.8* localizes to pericycle cells (Li et al., 2010), thus coinciding with sites of ectopic JA-Ile production in *kor1-4* roots. Whether constant root-locking of nitrate by *NRT1.8* affects shoot growth has not been investigated so far, but would be conceivable as nitrogen limitation also affects shoot growth (Konishi et al., 2017). Hence this transporter represents a promising candidate to explain the regulation of root-derived JA-dependent inhibition of shoot growth. Specifically, phenotypic comparisons between *kor1-4*, *kor1-4 aos*, and *kor1-4 nrt1.8* could reveal if suppressing *NRT1.8* function of sequestering nitrate to the roots alleviates the reduced *kor1* rosette size as in *kor1 aos*. Similarly, measuring nitrate levels in shoots and roots of *kor1-4* and *kor1-4 aos* might also reveal differences in nitrogen allocation. Interestingly, nitrogen is also an important component of plant defense compounds such as glucosinolates (Chhajed et al., 2020).

*S. littoralis* insect weight was greater when caterpillars fed on JA-deficient *kor1 aos/kor1 aos* than *kor1 aos/kor1* plants. Vice versa, larval weight was lighter when feeding on *kor1/kor1* plants with respect to *kor1 aos/kor1* grafts. Although reciprocal grafts involving *aos* also caused a general increase in leaf area available to the caterpillars (but not in leaf number as a proxy for comparable developmental stages), rosette size is unlikely to be a prominent factor influencing insect performance. First, rosette tissue from smaller *kor1/kor1* as well as larger *kor1/kor1 aos* plants was still available at the end of the bioassay, and insect larvae were slightly but significantly heavier in *kor1/kor1 aos* with respect to *kor1/kor1* controls, indicating that tissue availability was not limiting in this comparison. Second, although insects were considerably heavier in *kor1 aos/kor1 aos* compared to *kor1 aos/kor1* plants,

meristematic tissue in the shoot apical meristem was entirely consumed in the first genotype, while it still remained available in the second, implying that the observed bioassay phenotypes are due to plant defense responses rather than plant size.

A possible explanation for the rosette defense phenotypes arising from constitutive JA-Ile root signalling in the grafting experiments may be the root-to-shoot translocation of (a) JA-dependent molecule(s) synthesized in *kor1* roots. For instance, 9-LOX oxylipins are transported from the root to the shoot and participate in defense against aphids (Nalam et al., 2012). The most prominent example for JA-dependent root-to-shoot translocation is the secondary metabolite nicotine, which is produced in *Nicotiana tabacum* and is a potent anti-herbivore compound (Steppuhn et al., 2004; Fragoso et al., 2014). Although I did not have the time to explore possible mobile candidates explaining the rosette growth phenotype from the JA-dependent misregulated genes in *kor1* roots, I identified several genes involved in secondary metabolite production which could explain the defense phenotype (Tab. S2).

Several transcripts involved in glucosinolates and terpene metabolism were upregulated in *kor1* roots (Tab. S2). Glucosinolates are important defense compounds against herbivorous insects, as they can be degraded to toxic isothiocyanates and thiocyanates (Chhajed et al., 2020). Specifically, *INDOLE GLUCOSINOLATE O-METHYLTRANSFERASE 1 (IGMT1)* and *BETA-GLUCOSIDASE 30 (BGLU30)* were strongly upregulated in *kor1* roots with respect to the WT (Tab. S2). IGMT1 regulates the production of 4-methoxy-indole-3-yl-methyl glucosinolate, which is an important defense compound against aphids (Pfalz et al., 2009). BGLU30 is a myrosinase involved in glucosinolate catabolism (Morikawa-Ichinose et al., 2020), which mediates the release of toxic breakdown fragments of glucosinolates that can repel herbivorous insects (Chhajed et al., 2020). Importantly, glucosinolates are root-to-shoot mobile, as indicated by feeding experiments with labelled glucosinolates and the abundance of endogenous glucosinolates in the xylem sap (Andersen et al., 2013; Madsen et al., 2014). Hence, an increased production of 4-methoxy-indole-3-yl-methyl glucosinolate or its breakdown products in *kor1-4* roots, which are then transported to the shoot, might mediate the increased resistance against *S. littoralis* in graft combinations with *kor1-4* rootstocks. To test this hypothesis, glucosinolate levels could be measured in shoots and roots of *kor1* and *kor1 aos* graft combinations. If shoot glucosinolate levels decrease in *kor1 aos* rootstocks, successive *kor1* double mutants with *bglu30* or *igmt1* could reveal the relative contribution of these genes to insect herbivory.

In contrast to glucosinolates, so far not much is known on root-to-shoot translocation of terpenes in Arabidopsis. However, in gymnosperms such as Norway spruce, terpenes are present in the xylem sap and are thought to be mobile (Martin et al., 2002; Duan et al., 2020). Among the JA-Ile-dependent upregulated genes in *kor1-4* roots involved in terpene metabolism, *TERPENOID SYNTHASE 13*

(*TPS13*), *FAMT*, and *FAMT-LIKE* were the highest upregulated candidates (Tab. S2). *TPS13* converts (2E,6E)-farnesyl diphosphate to (Z)- $\gamma$ -bisabolene, which was reported to be a potent larvicide and deterrent against mosquitos (Ro et al., 2006; Govindarajan et al., 2018). *FAMT* represented the highest upregulated gene in *kor1-4* roots in comparison to the WT (logFC = 8.27). It encodes for a protein that catalyses the methylation of the sesquiterpene farnesoic acid to methyl farnesoate (Yang et al., 2006). Methyl farnesoate is a member of the insect juvenile hormone family, which can be metabolized by insects and inhibits larval development (Tsang et al., 2020). Hence, *FAMT* is suspected to be important during plant defense against insects (Yang et al., 2006). Remarkably, *FAMT* mRNA was reported to be root-to-shoot mobile (Thieme et al., 2015), rendering it a promising candidate in explaining the elevated shoot defense of *kor1-4* against *S. littoralis*.

As for glucosinolates, to test if root-produced terpenes are influencing shoot defense phenotypes, specific compounds like (Z)- $\gamma$ -bisabole and methyl farnesoate, as well as *FAMT* transcripts could be measured from roots and shoots of our grafting combinations, and if promising, *kor1* double mutants with *tps13* or *famt* could determine the contribution of the specific genes under analysis to shoot defences. As also other genes in terpene metabolism are misregulated in a JA-dependent manner *kor1* roots (Tab. S2), and in case a targeted candidate search proves unsuccessful, one could use a combined transcriptomics / metabolomics approach in reciprocal grafts between *kor1-4* and *kor1-4 aos*. This could identify putative shoot-to-root mobile mRNAs or metabolites, which are dependent on constitutive JA-Ile production in *kor1-4* rootstocks. Once putative candidates are identified, their contribution could be analysed by generating double mutants with *kor1-4* and subjecting them in bioassays. Although reciprocal grafts between WT and *aos* did not reveal a JA-dependent contribution of the rootstock to *S. littoralis* defense, different conditions that trigger root JA-production (e.g. hypoosmotic treatments) might help to identify general mechanisms in which roots contribute towards shoot defenses.

## **2. Misregulated turgor pressure in *kor1* results in mechanical compression of inner tissues leading to JA-Ile biosynthesis.**

Plant cells are pressurized and can reach an internal hydrostatic pressure of about 2 MPa, which is around 20 times that of the atmospheric pressure (Beauzamy et al., 2014). This high internal pressure is in part sustained by cell walls, which surround each plant cell. Hence, cells with weakened cell walls might experience morphological changes which could result in mechanical imbalances within tissues. Here we described cellulose-deficient *kor1* mutants, which displayed elevated JA-Ile levels in seedling roots. We show on a cellular resolution level that JA-Ile production specifically occurs in endodermis

and pericycle cells of the early differentiation zone and is triggered by a cell non-autonomous mechanism occurring in the cortex cell layer. As cortex cells in *kor1* roots were dramatically enlarged, we hypothesized that increased JA-Ile levels in *kor1* result from cortex cells 'squeezing' inner tissues. We furthermore propose that this is caused by a misregulation of turgor pressure arising from weakened cell walls, and provided chemical and genetic evidence supporting our hypothesis.

First, by using hyperosmotic treatments we reduced turgor pressure and hence abolished cortex cell swelling and ectopic JA-Ile signalling in inner tissues of *kor1* roots. This indicates that JA-Ile production is triggered by turgor-driven processes rather than cell-wall derived elicitors and is in line with available evidence that isoxaben-mediated cellulose depletion leads to slow activation of the JA pathway (Larrieu et al., 2015) and is also osmo-sensitive (Engelsdorf et al., 2018). Vice versa, we show that without having a cell wall mutant, we can reconstitute the JA-Ile signalling phenotype in the same cell types by hypoosmotic treatments in WT, which putatively increase internal turgor pressure. Second, with *esmd1* we found a suppressor of ectopic JA-Ile signalling in *kor1*, which reduced cortex cell swelling likely by counteracting turgor misregulation through cell wall modifications. Additionally, an RNA-seq dataset of *kor1* roots revealed ten misregulated genes involved in water deprivation response. Expression of genes in this GO cluster is usually upregulated during drought conditions (Kilian et al., 2007; Benny et al., 2019). However, in *kor1* roots, transcripts of these genes were significantly downregulated in comparison to the WT (Tab. S3), which might indicate changes in water potential that could affect turgor pressure. Moreover, the upregulation of marker genes involved in response to mechanical stimuli like *TCH3* or *XTH22* (Braam and Davis, 1990; Lee et al., 2005) are putative indicators of mechanical stress occurring in *kor1* roots.

Although our data point towards a scenario where inner tissues experience mechanical stress caused by cortex cells that cannot contain turgor pressure, we still miss experimental ways that would allow us to provide direct evidence for these phenomena. Either desirable tools, such as genetically encoded sensors for mechanical properties, are not available or present techniques, such as atomic force microscopy, are not suitable for analysing inner tissues (Routier-Kierzkowska et al., 2012; Peaucelle, 2014; Hamant and Haswell, 2017). However, the recent design of fluorophore-based mechanoprobes targeted to the cell wall or plasma membrane might provide valuable tools to map changes in zones of interest in our mutants (Michels et al., 2020). The fluorescence lifetime of these probes serves as a proxy for cell wall mesh size or plasma membrane lipid packing, which are indicators of mechanical stress parameters (Michels et al., 2020).



Another goal of this thesis was to identify genetic regulators of ectopic JA-Ile production in *kor1*. We employed two reverse genetic approaches, including a targeted approach focusing on known components involved in cell wall integrity-, osmo- and mechano-signalling, and a transcriptomic approach focussed on selected differentially expressed candidates in *kor1* roots. However, so far none of the generated double mutants with *kor1-4* displayed a complete suppression of constitutive JA-Ile signalling. Only *kor1-4 the1-1* mutants showed a significant 25% reduction of basal root *JAZ10* expression in comparison to *kor1-4*. This again coincides with a report that osmosensitive alterations in the cell wall triggered by isoxaben also require THE1 for proper JA production (Engelsdorf et al., 2018).

Our search for mutants with abolished *JGP* reporter expression in *kor1-4* by a forward genetic screen yielded, in addition to *esmd1*, eleven other suppressors exhibiting WT-like responses to wounding and exogenous MeJA treatment. This suggests that we targeted specific signalling pathways leading to the initiation of JA-Ile biosynthesis and signalling following cell wall alterations. Although not all candidate suppressors are confirmed yet (Tab. 3), three of them encode for proteins localized to plastids. Hence, these mutants represent interesting candidates that might regulate JA-Ile biosynthesis, which is initiated in these organelles. Another interesting suppressor candidate is the mutant *2455B*, which we confirmed to be affected in the gene *OS9*. *OS9* encodes for a lectin localized in the Golgi lumen and is involved in endoplasmic reticulum-associated degradation (ERAD) of glycoproteins (Huttner et al., 2012). There, it is organized in a protein complex and putatively recognizes a specific glycan code of misfolded proteins, which are then either ubiquitylated and degraded via the 26S proteasome or undergo trafficking to the vacuole (Vembar and Brodsky, 2008; Shin et al., 2018). An *OS9* loss of function line suppressed the severe growth phenotypes of brassinosteroid receptor mutants *bri1-5* and *bri1-9* (Huttner et al., 2012). These mutant proteins are theoretically functional but misfolded, and are therefore retained in the ER and degraded, a quality control process which is inactive in an *os9* mutant background (Huttner et al., 2012; Su et al., 2012). The *OS9* mutant *2455B* fully suppressed the phenotypes of *kor1-4*, including ectopic *JGP* expression, ectopic lignification and short root growth (Fig. 15, Tab.3). It is therefore plausible that the KOR1<sup>L573F</sup> protein variant in *kor1-4* is also partially functional but misfolded, and hence an ERAD substrate and *OS9* target. This is consistent with a recent report, where the lack of glycoprotein quality control in the ER led to KOR1 accumulation in the tonoplast (Nagashima et al., 2020a). Interestingly, our *kor1-4* is a temperature-sensitive allele, which upon exposure to slightly elevated temperatures (26°C) exhibited more drastic phenotypes. As temperature-sensitive alleles in many cases are caused by misfolding (Zhang et al., 2018), this provides an additional argument for KOR1<sup>L573F</sup> being an ERAD substrate.

Despite finding twelve interesting candidate genes, the suppressor screen did not retrieve known components involved in osmo- and mechanosensing nor cell wall integrity sensors such as THE1. First, this might be due to the screen not being saturated, although we retrieved two novel *opr3* alleles. Second, the screen was designed to assess the absence of *JGP* reporter activity, which would be difficult to observe in case of genetic redundancy or only partial *JGP* suppression. This limitation should also be considered for the reverse genetic screen, where so far several of the generated double mutants with *kor1-4* were analyzed for qualitative *JGP* expression only.

As this thesis revealed that misregulated turgor pressure in *kor1* might cause mechanical compression of inner tissues leading to JA-Ile biosynthesis, the future search for genetic players involved in this pathway should focus on putative osmo- and mechanosensitive components. Promising candidates include MSL10, which mediates responses to cell swelling initiated by cell wall softening and hypoosmotic treatments (Basu and Haswell, 2020). Interestingly, an *msl10* gain-of-function mutant exhibits elevated JA levels after wounding (Zou et al., 2016). Moreover one should focus on MCA1, which next to THE1 was required to initiate JA production upon isoxaben treatment (Engelsdorf et al., 2018). The generation of respective double mutants with *kor1-4* was already initiated (Tab. 1), which will then be characterized for *JGP* reporter expression as well as *JAZ10* expression levels. Moreover, analysing JA-Ile responses in mutants like *msl10* and *mca1*, might also reveal whether these players are involved in initiating JA-Ile biosynthesis upon misregulation of turgor pressure.

#### **How come ectopic JA-Ile signalling is present in specific cell types of a restricted *kor1* root portion?**

Mechanical stress is known to be an excellent trigger of JA-Ile biosynthesis (Koo and Howe, 2009), but how come hormone increase caused by cortex cell swelling was only observed in inner but not outer tissues? One possibility is that epidermal cells could disperse the mechanical pressure by expanding towards the outer space. In fact, *kor1-4* roots displayed an increased number of epidermal cells in comparison with the WT, which could indeed account for mechanical stress reduction. In general, mechanical cues are known to affect cell cycle progression in animals (Fernandez-Sanchez et al., 2015). Although this has not yet been demonstrated in plants, mechanical forces are important in guiding the orientation of plant cell division planes (Sampathkumar et al., 2014; Louveaux et al., 2016). In contrast to the epidermis, endodermal and pericycle cells are physically constrained within the root and may get "squeezed" by enlarged cortex cells without being able to dissipate the mechanical pressure. Remarkably, hypoosmotic treatments of WT roots activate JA-Ile signalling in the same cell types, indicating that the mechanisms might be more general and not specific to cell wall mutants lacking cellulose.

Strikingly, the activation of JA-Ile-signalling did not encompass the entire root along its longitudinal axis: it started at the onset of elongation and proceeded for about 30 consecutive cells into the early differentiation zone before ceasing. One could hypothesize that a parallel trigger of JA-Ile production includes mechanical tension generated during cell elongation that could cause stretching imbalances in growing cells. In *kor1* this could either be explained by cortex cells being more vulnerable towards cell swelling during elongation, or vice versa, endodermis and pericycle cells being more sensitive towards mechanical tension. Nevertheless, constitutive JA-Ile production arrests in older parts of the root, suggesting that mechanical stress may be alleviated or compensated. Interestingly, the equivalent part of the root in WT plants (~ 30 cells after onset of elongation) coincides with the completed deposition of a full apoplastic and transcellular diffusion barrier composed of lignified casparian strips and suberin lamellae in the secondary cell walls of endodermal cells (Naseer et al., 2012; Wang et al., 2019). Perhaps, these and other secondary cell wall modifications of endodermal and pericycle cells are able to counteract the mechanical compression exerted by adjacent cortex cells. Alternatively, as these compounds form a diffusion barrier, this might also lead to changes in internal turgor pressure in older parts of *kor1* roots. Importantly, the effect of cellulose deficiency on activating JA-Ile biosynthesis seems to be dose-dependent, as indicated by the isolation of a stronger *kor1-5* allele that exhibits *JGP* reporter activation across broader root tissues. Here, the consequences of partial *KOR1* loss are probably so severe that all cells exhibiting *JGP* activation are under mechanical stress and hence the phenotypes are greatly exacerbated.

Deepening our understanding on the cellular specificities of JA-Ile production in *kor1* could advance our knowledge on the consequences of mechanical stress. To verify whether secondary wall deposition in older parts of *kor1* roots indeed fortifies endodermal and pericycle cell walls, lignin and suberin deposition could be analysed with the use of specific dyes such as Basic Fuchsin and Nile Red, respectively (Ursache et al., 2018). Similarly, delaying the formation of casparian strips or suberin deposition in *kor1-4* double mutants with *schengen 1 (sgn1)* or *hydroxylase of root suberized tissue (horst)* (Naseer et al., 2012; Alassimone et al., 2016) could reveal if sites of JA-Ile production increase acropetally towards the shoot or remain the same.

Another interesting question is why turgor-driven mechanical compression first predominantly affects inner tissues of endodermis and pericycle? In order to find key molecular players that might regulate the cellular sensitivity towards these mechanical cues and lead to a differential dose-dependent activation of JA-Ile production in different cell types, it would be desirable to study the transcriptome of different cell types individually. This can be achieved by single cell transcriptome

analysis. However, established protocols often require protoplasting of the desired tissue (Shaw et al., 2021), which will remove our targeted mechanical cues. Hence, an alternative approach using laser-capture-microdissection of single cells followed by transcriptome analysis might be more informative (Sakai et al., 2018; Berkowitz et al., 2020).

### **What is the contribution of the cell wall towards constitutive JA-Ile biosynthesis in *kor1* roots?**

The cell wall physically constrains plant cells and is important for growth by providing mechanical stability and containing the internal turgor pressure (Hamant and Traas, 2010). Thus, it is likely that misregulated turgor in *kor1* roots is caused by cell wall alterations leading to a weakened external resistance towards the internal pressure. As a consequence, anisotropic growth cannot be fully maintained and cells rather expand radially leading to a swollen root. In fact, in addition to other *kor1* alleles (Tab. S1) (Lane et al., 2001), cellulose-deficient mutants in *cesa1*, *cesa3*, and *cesa6* exhibit root cell swelling phenotypes, indicating that they are unable to fully contain their turgor during anisotropic growth (Baskin et al., 1992; Williamson et al., 2001; Burn et al., 2002; Hu et al., 2018). Similar observations of tissue swelling can also be caused by inhibiting cellulose biosynthesis using isoxaben (Engelsdorf et al., 2018). Cellulose microfibrils are a main load-bearing component of the plant cell wall and usually align perpendicularly to the growth axis with the help of cortical microtubule arrays that guide CSC trajectories at the plasma membrane (Paredez et al., 2006). In addition to their reduced cellulose content, *kor1* and *cesa* mutants also display altered CSC trajectories and cellulose microfibril orientation (Fujita et al., 2013; Lei et al., 2014). This furthermore strengthens the hypothesis that misregulated turgor in *kor1* roots is a direct consequence of cellulose deficiency.

However, cellulose deficiency can also lead to secondary alterations of other cell wall components such as hemicelluloses and pectins (Manfield et al., 2004). Similarly, roots of *kor1* and *cesa1* alleles exhibited altered pectin-derived uronic acid levels (Peng et al., 2000; His et al., 2001). Our *kor1* root transcriptome identified a large GO cluster of misregulated genes involved in cell wall biogenesis and organization (Tab. S3). Among them there are several genes encoding for extensins, xyloglucan endotransglucosylases / hydrolases, pectate lyases, and PMEs, which are enzyme classes thought to be important for cell wall loosening and / or softening (Cosgrove, 2016b) and could therefore also be candidates that mediate cell wall changes leading to the misregulation of turgor in cells of *kor1* roots. Nevertheless, when determining the cell wall composition in roots of *kor1-4* and WT, the most striking difference was the lack of cellulose in *kor1-4*, while monosaccharide analysis of hemicellulose and pectin fractions resulted in only a minor reduction of xylose in *kor1-4*. These results were also in contrast to another report that identified major changes in pectin and hemicellulose composition in *kor1* roots grown on glucose-supplemented media (Peng et al., 2000). It is also possible that changes

in hemicelluloses and pectins reflected in our transcriptome, affect cross-links among different polysaccharides rather than their overall abundance (Pettolino et al., 2012; Cosgrove, 2016a), which could explain why we were unable to detect them.

Mutant alleles of *ESMD1* suppressed cell-adhesion defects of pectin-deficient mutants *qua1* and *qua2* (Verger et al., 2016), and were identified in my screen to suppress cortex cell swelling and consequently ectopic JA-Ile signalling in *kor1-4* roots. The exact function of *ESMD1* is still unknown and despite encoding for a glycosyltransferase, cell wall composition was not altered in dark-grown hypocotyls of *esmd1* (Verger et al., 2016). Based on conserved motifs and previous classifications *ESMD1* was then postulated to act as an *O*-fucosyl-transferase on target proteins involved in cell wall integrity signalling that carry an Epidermal growth factor (EGF)-like repeat domain such as WAKs and WAK-like proteins (Hansen et al., 2009; Verger et al., 2016). In contrast to these previous reports we identified a significant decrease in rhamnose levels in *esmd1* root cell walls of >30%. As most of rhamnose detected in Arabidopsis is assigned to RG-I (Pettolino et al., 2012), and related members of the glycosyltransferase family GT106 were identified as pectin RG-I rhamnosyltransferases (Takenaka et al., 2018; Wachananawat et al., 2020), a direct effect of *ESMD1* on pectin composition should be considered. This further suggests an altered pectin status in *kor1* mutants that is then counterbalanced in *kor1 esmd1*. Intriguingly, an antibody raised against a component of RG-I resulted in increased labelling densities in epidermal cells of elongated *kor1* hypocotyls in comparison to the WT (His et al., 2001). Alternatively, the lack of cellulose might also indirectly affect pectin properties, as especially RG-I was shown to have significant and specific contacts with cellulose microfibrils (Wang et al., 2015).

Future studies addressing the role of the plant cell wall in triggering constitutive JA-Ile biosynthesis in *kor1* roots could focus on a more detailed characterization of cell wall composition. One option is to perform linkage analysis of cell wall polysaccharides (Pettolino et al., 2012), which might reveal differences in *kor1* in comparison to the WT. Alternatively, the employment of immunohistochemistry methods targeting different cell wall components in root sections of WT and *kor1* is also an option to tackle this question, and would furthermore allow for a cell-specific characterization of cell wall composition. To this end, antibodies recognizing the methylesterification status of pectins such as LM19 and LM20 would be of high interest (Verhertbruggen et al., 2009), as the esterification status can alter the mechanical properties of the cell wall and could therefore indicate softer and stronger wall regions (Cosgrove, 2016b). Similar approaches could also be employed to detect differences in cell wall composition between *kor1* and *kor1 esmd1*. As *esmd1* might affect RG-I polysaccharides, respective antibodies like LM16 (Verhertbruggen et al., 2009) and especially the anti-RGI antibody

described in (His et al., 2001) should be tested. To address ESMD1 function and substrate specificity, its expression and purification could be performed in line with successful methods optimized for other GT106 family members (Takenaka et al., 2018). Similarly to assessing mechanical properties of the plasma membrane, (Michels et al., 2020) also described a fluorescent molecular rotor targeted to the plant cell wall. The fluorescence lifetime of this probe is changed depending on the mesh size of the cell wall, which could be used to identify mechanical cell wall changes at the cortex-endodermis interface of my mutants.

### **3. Can osmotically- and mechanically-driven changes in turgor pressure act as general elicitors of JA-Ile biosynthesis beyond cell wall alterations?**

Hypoosmotic treatments in WT roots, putatively causing cell swelling due to water uptake, triggered JA-Ile signalling in the same cells as in *kor1*. This implies that mechanical stress arising from turgor pressure changes might be a general elicitor of JA-Ile production. Mechanical stress is known to be a potent trigger of JA-Ile biosynthesis (Reymond et al., 2004; Glauser et al., 2008; Koo and Howe, 2009; Schulze et al., 2019). However, JA-Ile hormone production is not restricted to wounded sites only, but usually comprises a wide area in local tissues of the wounded organ (e.g. a leaf), and even distal tissues in other organs as indicated by *JGP* reporter activation upon wounding (Acosta et al., 2013; Mousavi et al., 2013). JA production upon mechanical wounding can be measured within seconds in local and distal tissues (Glauser et al., 2009; Chauvin et al., 2013), meaning that a rapid propagation of the damage signal is transmitted to distal unwounded sites. Clade 3 GLR proteins are essential to propagate the rapid wound signals over long-distances between leaves that share vascular connections as they mediate alterations in electrical surface potentials (caused by membrane depolarization) and ensure JA-Ile production at distal sites (Mousavi et al., 2013). Additionally, they regulate axial and radial  $\text{Ca}^{2+}$  fluxes, which follow after membrane depolarization and could present an elicitor of JA-Ile biosynthesis (Nguyen et al., 2018; Toyota et al., 2018). However, local JA-Ile production in the wounded leaf of *glr* mutants is unaffected and similar to the WT (Mousavi et al., 2013). Furthermore, JA-Ile formation precedes the cytosolic  $\text{Ca}^{2+}$  maximum (Nguyen et al., 2018), making a correlation between those rather unlikely.

Taking turgor pressure changes into account, however, could explain the incongruity of the current available data. Mechanical wounding, whether caused by biotic or abiotic stressors, squashes tissues and possibly compresses spatially constrained adjacent cells. As cells are connected through their cell walls (apoplastic connection) and through plasmodesmata (symplastic connection), mechanical stress may propagate over distances through turgor pressure changes. Indeed, mechanical wounding generates hydrostatic pressure changes (Malone and Stanković, 1991; Stahlberg and Cosgrove, 1992;

Shimmen, 2001) that can also travel as 'hydraulic pressure waves' over long distances through the plant vasculature (Stahlberg and Cosgrove, 1997; Lopez et al., 2014). The speed of hydraulic waves may even exceed these of electrical and chemical signals, and hence hydraulic pressure changes are proposed to induce electrical signals through depolarization of the plasma membrane (Huber and Bauerle, 2016; Evans and Morris, 2017). Specifically, pressure sensors placed in the xylem of different tree species almost simultaneously responded towards mechanical stem bending when placed directly at / or ~50cm distal to the bending site (Lopez et al., 2014). Moreover, pressure transducers monitoring thickness of distal leaves upon wounding suggested hydraulic wave velocities of up to 20 cm/s in different plant species (Boari and Malone, 1993). In contrast, electrical signals usually travel at speeds in the low cm/min range, reviewed in (Farmer et al., 2020). Consistently, transmitted pressure changes are suggested as possible initiators of JA-Ile biosynthesis in the vasculature distal to wounds (Farmer et al., 2014; Farmer et al., 2020). In the so called 'squeeze cell hypothesis', wound-induced axial hydraulic pressure waves in the vascular tissue are converted into radial pressure changes that squeeze cells bordering xylem vessels or phloem sieve tubes, which may activate mechanosensitive components to initiate JA-Ile production. This model indeed reflects a similar situation as present in *kor1*, where putative radial turgor pressure changes in the cortex squeeze inner tissues and lead to constitutive JA-Ile biosynthesis. Remarkably, proteins involved in JA-Ile production are strongly expressed along the vasculature (Hause et al., 2003; Stenzel et al., 2003; Chauvin et al., 2013).

Nevertheless, the question still remains: how is turgor-mediated mechanical stress sensed in order to initiate JA-Ile production? Does turgor pressure-mediated mechanical stress require mechanosensitive components at the plasma membrane to initiate JA-Ile biosynthesis in the plastids? Contrary to this assumption is the subcellular localization of members of the GLR family, which are important for long-distance JA-Ile production upon wounding. GLR3.3 is localized to the ER of phloem companion cells, while GLR3.6 is present on the vacuole tonoplast in xylem contact cells (Nguyen et al., 2018). Therefore, it is conceivable that plastids could sense mechanical and osmotic stress directly, and that they could serve as stress sensors (Virdi et al., 2016; Beltran et al., 2018). Although it is still largely unclear how osmotic balance across organellar membranes is maintained, it is known that organelles such as plastids have the capacity of osmosensing (Haswell and Meyerowitz, 2006). For example, in plastids the mechanosensitive ion channels MSL2 and MSL3 serve to maintain osmotic homeostasis as well as normal plastid size and shape, as an *msl2 msl3* double mutant is under constant hypoosmotic stress and exhibits enlarged spherical plastids (Haswell and Meyerowitz, 2006; Velez et al., 2012; Wilson et al., 2014). Transcriptomic data of this mutant show the basal upregulation of the JA-Ile-dependent gene *PDF1.2* (Luesse et al., 2015), hence it would be interesting to further evaluate the JA status. Intriguingly, another mutant exhibiting enlarged plastids with an altered shape called

*crumpled leaf*, displays ectopic JA-Ile signalling as expression of several JA-Ile-dependent transcripts (*AOC1/2/3*, *JAZ5/6/8/10*, *VSP2*, and *PDF1.2*) is upregulated (Luesse et al., 2015). Plastid shape can also be altered by the composition of the plastidial membranes. The major lipid components of plastidial membranes are the galactolipids monogalactosyldiacylglycerol (MGDG) and digalactosyldiacylglycerol (DGDG). Remarkably, a *DGDG SYNTHASE 1* mutant (*dgd1*) that exhibits a higher MGDG:DGDG ratio, contains plastids that are more spherical and displays constitutive JA-Ile signalling as indicated by higher transcript levels of *AOS*, *AOC1 LOX2/3/4*, *PDF1.2*, *VSP2*, but not *JAZs* (Yu et al., 2020). MGDG is the main galactolipid used as substrate for JA-Ile biosynthesis, serving as putative target of plastid lipases releasing  $\alpha$ -linolenic acid, reviewed in (Li and Yu, 2018). However, overall MGDG levels are not altered in a *dgd1* mutant, indicating that it is unlikely that increased substrate availability leads to elevated JA-Ile biosynthesis (Yu et al., 2020). As plastid shape is changed, could it be that MGDG as a substrate is just better accessible by target enzymes such as lipases or 13-LOXs? In fact, in comparison to DGDG which has a cylindrical shape common for packed bilayer membranes, MGDG is a conical-shaped non-bilayer lipid (Seiwert et al., 2017; Li and Yu, 2018). As a consequence, a higher MGDG:DGDG ratio might create spaces within the bilayer allowing enzymes to gain easier accessibility towards MGDG as a substrate. Similarly, hypoosmotic or mechanical stress acting on the plastids may also alter membrane topology allowing the initiation of JA-Ile biosynthesis, without the requirement of osmo- or mechanosensors. Among the enzymes that catalyse this initial step could be plastid lipases like DAD1. However, although DAD1 is required for male fertility, the wound-response of a *dad1* mutant is not affected (Ishiguro et al., 2001; Ellinger et al., 2010). Alternatively, 13-LOXs could directly act on MGDG to initiate JA-Ile production. Even though *in vitro* most LOXs prefer free fatty acids, some of them might also act on esterified fatty acids *in vivo* (Feussner et al., 2001; Stelmach et al., 2001).

Taken together my data lead to the new hypothesis that turgor pressure changes generating mechanical compression may be a crucial elicitor of JA-Ile biosynthesis in circumstances extending beyond cell wall perturbations. To test this, it will be of high interest to elucidate the amount and velocity of JA-Ile production in different osmotic conditions. Can plants produce JA-Ile when overall turgor pressure is low or when cells experience drastic loss of hydrostatic pressure like during plasmolysis? Additionally, one should focus on the mechanical features of the plastid membrane to determine whether JA-Ile biosynthesis is initiated by sterical accessibility of substrates. For this, the generation of plastidial membrane-targeted fluorescent molecular rotors, similar to the ones available for the plasma membrane (Michels et al., 2020), which exhibit a different fluorescent lifetime depending on their sterical freedom might be promising in order to assess conditions that favour JA-Ile biosynthesis.



## Section IV - Material & Methods

### Key resources

Table 4: Key resources table.

REAGENT or RESOURCE	SOURCE	IDENTIFIER
<i>Bacterial Strains</i>		
<i>Escherichia coli</i> Dh5 $\alpha$	Thermo Fisher	18265017
<i>Agrobacterium tumefaciens</i> Gv3101	GoldBio	CC-207-A
<i>Chemicals, Peptides, and Recombinant Proteins/Enzymes</i>		
Murashige & Skoog (MS) basal salt mix	Duchefa	Mo221.0025
2-(N-morpholino)ethanesulfonic acid (MES)	Sigma	M8250
Plant agar	Applichem	A2111
Propidium Iodide (PI)	Sigma	P4864
Direct Red 23	Sigma	212490
Xylitol	Sigma	X3375
Urea	Sigma	U5378
Sodiumdeoxycholate	Sigma	D6750
Paraformaldehyde	Merck	8.18715
X-Gluc	Biomol	AG-CN2-0023-M001
Phloroglucinol	Sigma	79330
Mannitol	J&K Scientific	351126
Sorbitol	Roth	6213.1
EGTA	Sigma	E3889
AgNO <sub>3</sub>	Sigma	209139
AVG	Sigma	32999
Polyethylenglycol (PEG6000)	Serva	33137
Technovit 7100	Morphisto	64709003
Methyl Jasmonate (MeJA)	Sigma	392707
Ethyl methanesulfonate (EMS)	Sigma	Mo880
Taq DNA Polymerase	Thermo Fisher	10342020
Phusion High-Fidelity DNA Polymerase	Life Technologies	F530
<i>Hinfl</i> restriction enzyme	New England Biolabs	R0155S
<i>NcoI</i> restriction enzyme	New England Biolabs	R0193S
<i>ApeKI</i> restriction enzyme	New England Biolabs	R0643S
<i>HaeIII</i> restriction enzyme	New England Biolabs	R0108S
<i>BsrBI</i> restriction enzyme	New England Biolabs	R0102S
<i>BsaAI</i> restriction enzyme	New England Biolabs	R0531S
<i>DdeI</i> restriction enzyme	New England Biolabs	R0175S
BP Clonase	Thermo Fisher	11789-100
LR Clonase	Thermo Fisher	11791-100
LR Plus Clonase	Thermo Fisher	12176590
<i>Critical Commercial Assays</i>		
DNeasy Plant Mini Kit	Qiagen	69106
RNeasy Plant Mini Kit	Qiagen	74904
NucleoSpin Gel and PCR CleanUp	Marchery & Nagel	740609.25
QIAprep Spin MiniPrep Kit	Qiagen	27106

**Table 4 (continued)**

REAGENT or RESOURCE	SOURCE	IDENTIFIER
<i>Experimental Models: Organisms/Strains</i>		
<i>Spodoptera littoralis</i> : eggs	Syngenta Crop Protection AG (kind gift by O. Kindler & R. Reist)	N/A
<i>Arabidopsis thaliana</i> : aos	(Park et al., 2002)	N/A
<i>Arabidopsis thaliana</i> : coi1-34	(Acosta et al., 2013)	N/A
<i>Arabidopsis thaliana</i> : jar1-1	(Staswick et al., 1998)	N/A
<i>Arabidopsis thaliana</i> : opr3-2	(Acosta et al., 2013)	N/A
<i>Arabidopsis thaliana</i> : kor1-4	(Acosta et al., 2013)	N/A
<i>Arabidopsis thaliana</i> : kor1-5	(Acosta et al., 2013)	N/A
<i>Arabidopsis thaliana</i> : kor1-6	NASC	SALK_075812
<i>Arabidopsis thaliana</i> : esmd1-1	(Verger et al., 2016)	N/A
<i>Arabidopsis thaliana</i> : esmd1-3	This study; (Mielke et al., 2021)	N/A
* <i>Arabidopsis thaliana</i> : the1-1	(Hematy et al., 2007)	N/A
* <i>Arabidopsis thaliana</i> : rop2-12	NASC	WiscDsLox441B8
* <i>Arabidopsis thaliana</i> : eru-2	NASC; (Bai et al., 2014)	SALK_083442
* <i>Arabidopsis thaliana</i> : wak1-1	NASC; (Zarattini et al., 2017)	SALK_107175
* <i>Arabidopsis thaliana</i> : wak2-12	NASC; (Engelsdorf et al., 2018)	SAIL_12_D05C
* <i>Arabidopsis thaliana</i> : herk1-1	NASC; (Guo et al., 2009)	SALK_008043
* <i>Arabidopsis thaliana</i> : herk2-1	NASC; (Guo et al., 2009)	SALK_105055
* <i>Arabidopsis thaliana</i> : mri-2	NASC; (Boisson-Dernier et al., 2015)	GK_820D05
* <i>Arabidopsis thaliana</i> : rlp44-3	NASC; (Wolf et al., 2014)	SAIL_596_E12
* <i>Arabidopsis thaliana</i> : mik1	NASC; (Wang et al., 2016)	SALK_095005
* <i>Arabidopsis thaliana</i> : mik2-1	NASC; (Wang et al., 2016)	SALK_061769
* <i>Arabidopsis thaliana</i> : sub-9	NASC; (Vaddepalli et al., 2011)	SAIL_1158_D09
* <i>Arabidopsis thaliana</i> : mca1-3	NASC	SALK_206846
* <i>Arabidopsis thaliana</i> : msl10-1	NASC; (Haswell et al., 2008)	SALK_076254
* <i>Arabidopsis thaliana</i> : dek1-4	(Roeder et al., 2012)	N/A
* <i>Arabidopsis thaliana</i> : osca1-2	NASC; (Yuan et al., 2014)	SAIL_607_F09
* <i>Arabidopsis thaliana</i> : osca1-4	NASC	SAIL_1172_D02
* <i>Arabidopsis thaliana</i> : ein2-1	ABRC; (Alonso et al., 1999)	CS3071
* <i>Arabidopsis thaliana</i> : tch3-2	NASC; (Wang et al., 2011)	SALK_090554

**Table 4 (continued)**

REAGENT or RESOURCE	SOURCE	IDENTIFIER
* <i>Arabidopsis thaliana: aca13</i>	NASC; (Iwano et al., 2014)	SAIL_878_Bo6
* <i>Arabidopsis thaliana: per52-1</i>	NASC; (Pourcel et al., 2013)	SALK_o81257
* <i>Arabidopsis thaliana: xth26-2</i>	NASC	SALK_055758
* <i>Arabidopsis thaliana: ext12</i>	NASC; (Velasquez et al., 2011)	SAIL_1249_F11
* <i>Arabidopsis thaliana: ppl6-1</i>	NASC	GK_033D05
* <i>Arabidopsis thaliana: lox4A</i>	NASC; (Caldelari et al., 2011)	SALK_071732
<i>Arabidopsis thaliana: kor1-4 aos</i>	This study; (Mielke et al., 2021)	N/A
<i>Arabidopsis thaliana: kor1-5 aos</i>	This study; (Mielke et al., 2021)	N/A
<i>Arabidopsis thaliana: kor1-4 esmd1-1</i>	This study; (Mielke et al., 2021)	N/A
<i>Arabidopsis thaliana: kor1-4 esmd1-3</i>	This study; (Mielke et al., 2021)	N/A
All mutants designated with an asterisk (*) were cossed to <i>kor1-4</i> in this study to receive the respective double mutant. The current state of these mutants is listed in Table S4		
<i>Arabidopsis thaliana: JAZ1op:GUS (JGP) in Col-o</i>	(Acosta et al., 2013)	N/A
<i>Arabidopsis thaliana: JAZ1op:GUS (JGP) in kor1-4</i>	This study; (Mielke et al., 2021)	N/A
<i>Arabidopsis thaliana: JAZ1op:GUS (JGP) in kor1-5</i>	This study; (Mielke et al., 2021)	N/A
<i>Arabidopsis thaliana: JAZ1op:GUS (JGP) in kor1-6</i>	This study; (Mielke et al., 2021)	N/A
<i>Arabidopsis thaliana: JAZ1op:GUS (JGP) in esmd1-3</i>	This study; (Mielke et al., 2021)	N/A
<i>Arabidopsis thaliana: JAZ1op:GUS (JGP) in aos</i>	This study; (Mielke et al., 2021)	N/A
<i>Arabidopsis thaliana: JAZ1op:GUS (JGP) in kor1-4 aos</i>	This study; (Mielke et al., 2021)	N/A
<i>Arabidopsis thaliana: JAZ1op:GUS (JGP) in kor1-5 aos</i>	This study; (Mielke et al., 2021)	N/A
<i>Arabidopsis thaliana: JAZ1op:GUS (JGP) in kor1-4 esmd1-3</i>	This study; (Mielke et al., 2021)	N/A
<i>Arabidopsis thaliana: JAZ1op:NLS3xVEN in Col-o</i>	This study; (Mielke et al., 2021); similar to (Marhavy et al., 2019; Mielke et al., 2021)	N/A
<i>Arabidopsis thaliana: JAZ1op:NLS3xVEN in aos</i>	This study; (Mielke et al., 2021); similar to (Marhavy et al., 2019)	N/A
<i>Arabidopsis thaliana: JAZ1op:NLS3xVEN in kor1-4</i>	This study; (Mielke et al., 2021); similar to (Marhavy et al., 2019)	N/A

**Table 4 (continued)**

REAGENT or RESOURCE	SOURCE	IDENTIFIER
<i>Arabidopsis thaliana</i> : KOR1p:KOR1 in kor1-4 JGP	This study; (Mielke et al., 2021)	N/A
<i>Arabidopsis thaliana</i> : KOR1p:CIT-KOR1 in kor1-4 JGP	This study; (Mielke et al., 2021)	N/A
<i>Arabidopsis thaliana</i> : IRT1p:CIT-KOR1 in kor1-4 JGP	This study; (Mielke et al., 2021)	N/A
<i>Arabidopsis thaliana</i> : PEP1p:CIT-KOR1 in kor1-4 JGP	This study; (Mielke et al., 2021)	N/A
<i>Arabidopsis thaliana</i> : SCR1p:CIT-KOR1 in kor1-4 JGP	This study; (Mielke et al., 2021)	N/A
<i>Arabidopsis thaliana</i> : WOL1p:CIT-KOR1 in kor1-4 JGP	This study; (Mielke et al., 2021)	N/A
<i>Arabidopsis thaliana</i> : PIN1p:CIT-KOR1 in kor1-4 JGP	This study; (Mielke et al., 2021)	N/A
<i>Arabidopsis thaliana</i> : ESMD1p:NLS3xVEN in Col-o	This study; (Mielke et al., 2021)	N/A
<i>Arabidopsis thaliana</i> : ESMD1p:ESMD1-mTurquoise2 in kor1-4 esmd1-3 JGP	This study; (Mielke et al., 2021)	N/A
<i>Arabidopsis thaliana</i> : ESMD1p:ESMD1-CIT in kor1-4 esmd1-3 JGP	This study; (Mielke et al., 2021)	N/A
<b>Oligonucleotides</b>		
primers used for cloning, genotyping, RT-PCR & qRT-PCR can be found in Table S4		
<b>Recombinant DNA</b>		
Plasmid: pUC57 ( <i>KpnI</i> - <i>XmaI</i> )	(Chauvin et al., 2013)	N/A
Plasmid: pDONR221	Invitrogen	Cat# 12536017
Plasmid: pDONR-P2R-P3	Invitrogen	Cat# 12537023
Plasmid: pEDO 097	(Chauvin et al., 2013)	N/A
Plasmid: pR7m34gw	Invitrogen, but then modified and gifted by Ivan Acosta	N/A
Plasmid: pEN-4-KOR1p-1	This study; (Mielke et al., 2021)	N/A
Plasmid: pEN-4-ESMD1p-1	This study; (Mielke et al., 2021)	N/A
Plasmid: pEN-4-IRT1p-1	NASC; (Marques-Bueno et al., 2016)	NASC ID: N2106366
Plasmid: pEN-4-PEPp-1	NASC; (Marques-Bueno et al., 2016)	NASC ID: N2106366
Plasmid: pEN-4-SCRp-1	NASC; (Marques-Bueno et al., 2016)	NASC ID: N2106366
Plasmid: pEN-4-WOL1p-1	NASC; (Marques-Bueno et al., 2016)	NASC ID: N2106366
Plasmid: pEN-4-PIN1p-1	NASC; (Marques-Bueno et al., 2016)	NASC ID: N2106366
Plasmid: pEN-1-CIT(no*)-2	(Gasparini et al., 2015)	N/A
Plasmid: pEN-1-NLS-3x-VEN*-2	(Marhavy et al., 2019)	N/A
Plasmid: pEN-1-KOR1*-2	This study; (Mielke et al., 2021)	N/A

**Table 4 (continued)**

REAGENT or RESOURCE	SOURCE	IDENTIFIER
Plasmid: <i>pEN-1-ESMD1_no*<sup>-2</sup></i>	This study; (Mielke et al., 2021)	N/A
Plasmid: <i>pEN-2-KOR1*<sup>-3</sup></i>	This study; (Mielke et al., 2021)	N/A
Plasmid: <i>pEN-2-mTurquoise2*<sup>-3</sup></i>	This study; (Mielke et al., 2021)	N/A
Plasmid: <i>pEN-2-CIT*<sup>-3</sup></i>	(Gasperini et al., 2015)	N/A
Plasmid: <i>pDEST-1-KOR1p:KOR1*<sup>-3</sup></i>	This study; (Mielke et al., 2021)	N/A
Plasmid: <i>pDEST-1-ESMD1p:NLS-3x-VEN*<sup>-3</sup></i>	This study; (Mielke et al., 2021)	N/A
Plasmid: <i>pDEST-1-KOR1p:CIT-KOR1*<sup>-4</sup></i>	This study; (Mielke et al., 2021)	N/A
Plasmid: <i>pDEST-1-IRT1p:CIT-KOR1*<sup>-4</sup></i>	This study; (Mielke et al., 2021)	N/A
Plasmid: <i>pDEST-1-PEPp:CIT-KOR1*<sup>-4</sup></i>	This study; (Mielke et al., 2021)	N/A
Plasmid: <i>pDEST-1-SCR1p:CIT-KOR1*<sup>-4</sup></i>	This study; (Mielke et al., 2021)	N/A
Plasmid: <i>pDEST-1-WOL1p:CIT-KOR1*<sup>-4</sup></i>	This study; (Mielke et al., 2021)	N/A
Plasmid: <i>pDEST-1-PIN1p:CIT-KOR1*<sup>-4</sup></i>	This study; (Mielke et al., 2021)	N/A
Plasmid: <i>pDEST-1-ESMD1p:ESMD1-mTurquoise2*<sup>-4</sup></i>	This study; (Mielke et al., 2021)	N/A

N/A = not available

\* = stop codon

NASC = Nottingham Arabidopsis Stock Centre

## Plant material and growth conditions

The *Arabidopsis thaliana Columbia-o (Col-o)* accession was the genetic background used in this study to generate all transgenic and mutant plant lines. A list of the genetic material used is presented in Table 4. For assays on solid plant growth media, seeds were sterilized and stratified 2 days at 4 °C in the dark as described (Acosta et al., 2013). Seedlings were grown on 0.5x solid Murashige and Skoog (MS) media supplemented with 0.5 g/L 2-(N-Morpholino)ethanesulfonic acid (MES) hydrate and 0.7% or 0.85% plant agar for horizontal or vertical growth, respectively. Horizontally grown seedlings were germinated on a nylon mesh (Lanz-Anliker AG, Rohrbach, Switzerland) with 200 µm pore size placed on top of the MS media as described (Acosta et al., 2013). Controlled growth conditions were set at 21°C under 100 µE m<sup>-2</sup> s<sup>-1</sup> light, with a 14 h light/10 h dark photoperiod. For bioassays and determination of total leaf area plants were grown on soil (Einheitserde Classic Kokos (45% (w/w) white peat, 20% (w/w) clay, 15% (w/w) block peat, 20% (w/w) coco fibers; Balster Einheitserdewerk, Germany) with the same temperature (T) and light intensity, but with a short-day 8 h light/16 h dark

photoperiod. For propagation, transformation and crossing, plants were also grown on soil at the same conditions but under continuous light.

## Genotyping

Genomic DNA was extracted and purified with the DNeasy Plant Mini Kit (Quiagen) according to the manufacturer's protocol. Genotyping of T-DNA insertion lines was performed in 20  $\mu$ L PCR reactions [20 ng genomic DNA, 500 nM each of specific forward and reverse primers, 500 nM of the general T-DNA primer left border primer, 200  $\mu$ M Deoxynucleotide Triphosphates, 1 $\times$  PCR buffer (Invitrogen), and 0.1 U of Taq DNA polymerase (Invitrogen) on a Thermocycler (Eppendorf™ Mastercycler™ PRO) with 95°C x 5' of initial denaturation and 35 amplification cycles consisting of 95°C x 30" denaturation, 58°C x 30" annealing, and 72°C x 60" extension. Single nucleotide polymorphisms (SNPs) were genotyped with Cleaved Amplified Polymorphic Sequences (CAPS) or derived Cleaved Amplified Polymorphic Sequences (dCAPS) markers (<http://helix.wustl.edu/dcaps/>). Briefly, PCR products were amplified as above but without a T-DNA primer and then digested with restriction enzymes according to the manufacturer specifications. Specific primers and restriction enzymes are listed in Table S4. PCR products >300bp were separated by electrophoresis on 0.9% agarose gels, while <300bp products were separated on 2% agarose gels.

## Histochemical detection of GUS activity and lignin deposition

GUS stainings were performed as described (Gasperini et al., 2015) and seedlings were mounted in chloral hydrate : glycerol : water solution (8:2:1) and photographed with a Leica M165 FC stereomicroscope fitted with a Leica MC170 HD camera. Lignin deposition was visualized by submerging seedlings in acidified phloroglucinol solution (1% phloroglucinol in 18% HCl) for 5 min, washing in 1x Phosphate Buffered Saline (PBS) buffer, mounting in 10% glycerol, and imaging using Differential Interference Contrast (DIC) optics on a Leica DM6B microscope fitted with a Leica DMC6200 camera.

## Plant treatments

Single cotyledon wounding of seedlings and MeJA treatments to assess *JGP* reporter activity were performed as described (Acosta et al., 2013). To evaluate JA responses in *JAZ1op:NLS-VEN* reporter plants, primary roots from vertically-grown seedlings were mounted in mock or 10  $\mu$ M MeJA 0.5x MS with 30  $\mu$ g/ml propidium iodide (PI) solution, imaged immediately (t=0) and after 2 h, or 2 h following cotyledon wounding on a Zeiss confocal laser scanning microscope LSM880 (n = 10). For hyperosmotic treatments, plant growth media was supplemented and autoclaved with either 3% mannitol (165mM), 3% sorbitol (165mM), 3% PEG6000 or 3% plant agar. For hypoosmotic treatments,

seedlings were grown vertically for 5 or 7 days on MS media and then transferred to liquid isotonic solution (MS) or deionized water for the indicated times before GUS staining ( $n = 20$ ) or confocal laser scanning microscopy (LSM880) imaging ( $n = 10$ ). For treatments with EGTA, plant growth media was supplemented and autoclaved with 1 mM EGTA. For treatments with AgNO<sub>3</sub> or AVG, filter-sterilized stock solutions in water (100 mM AgNO<sub>3</sub>; 5 mM AVG) were prepared and added to growth media for a final concentration of 5 μM AVG or 50 μM AgNO<sub>3</sub>.

### Gene expression analyses

RNA extraction and qRT-PCR conditions were performed as in (Gasparini et al., 2015; Schulze et al., 2019) on transcripts with primers listed in Table S4. Primer efficiency was optimized for each primer pair with a dilution series and kept with a 1.9 - 2.1 range.

For RNAseq analysis, WT, *aos*, *kor1-4*, and *kor1-4 aos* seedlings, all in the *JGP* background, were grown vertically in aseptic conditions as described above. Total RNA was extracted from 5-do roots and purified with an RNeasy Plant Mini Kit (Qiagen). Two biological replicates were sequenced per genotype, each consisting of 120 roots. 3 μg of total RNA was precipitated with 0.1 volumes of NaOAc and 2 volumes of EtOH (i.e. 50 μL sample + 5 μL NaOAc + 110 μL EtOH) and sent for sequencing at Macrogen ([www.macrogen.com](http://www.macrogen.com)). After verifying RNA quality on an Agilent 2100 Bioanalyzer (Agilent) and preparing an Illumina TruSeq stranded mRNA library, samples were sequenced on an Illumina HiSeq4000 instrument with 150 bp paired-end (PE) read length resulting in an output of 9.4 - 13.8 Gb of total read bases. RNAseq analysis was performed in R by René Dreos (University of Lausanne, Switzerland). Reads were quality filtered using PrinSeq (v. 0.20.4) (Schmieder and Edwards, 2011) and mapped to the *A. thaliana* genome (TAIR10) using tophat (v. 2.1.1) (Trapnell et al., 2009). Read quantification per gene locus was performed using htseq-count (v. 0.12.4) (Anders et al., 2015). Differential gene expression analysis was performed in R using DESeq2 package (Love et al., 2014), whereas GO analysis was performed using ReactomePA package (Yu and He, 2016).

### Hormone quantification

5-do roots from vertically-grown seedlings were excised beneath the collet region and flash frozen to yield approximately 50 mg of fresh weight (FW), corresponding to ~300 roots for each biological replicate. Extraction and quantitative measurements were performed as described (Schulze et al., 2019). The limit of quantification (LOQ = 3x limit of detection) was determined from an Arabidopsis matrix as 7 pmol/g FW for OPDA, 13.2 pmol/g FW for JA, and 0.49 pmol/g FW for JA-Ile. Measurements below these values were not considered for statistical analyses.

## Cloning and generation of transgenic lines

All transcriptional and translational reporter constructs were generated by double or triple Multisite Gateway Technology (Thermo Fisher). ENTRY plasmids containing cell-type specific promoters (pEN-L4-*IRT1p*-L3, pEN-L4-*PEPp*-L3, pEN-L4-*SCRp*-L3, pEN-L4-*PIN1p*-L3, and pEN-L4-*WOLp*-L3) were described in (Marques-Bueno et al., 2016) and obtained from NASC. pEN-L4-*JAZ1op*-R1, pEN-L1-*NLS-3xVEN*-L2 and pEN-R2-*CIT*-L3 were as in (Acosta et al., 2013; Gasperini et al., 2015). CIT and mTurquoise (mT) fluorophores were subcloned into pDONR221 or pDONR-P2R-P3 to obtain pEN-L1-*CIT*-L2 and pEN-R2-*mT*-L3. Promoters were amplified from WT genomic DNA with Phusion High-Fidelity DNA Polymerase (Thermo Fisher) and oligonucleotides containing adequate restriction sites for *KOR1p* (primers MST-093 and MST-094, 2.132 kb) and *ESMD1p* (primers MST-151 and MST-152, 2.168 kb) and cloned into pUC57 to create pEN-L4-*promoter*-R1 clones, as described (Gasperini et al., 2015). Coding DNA sequences of *KOR1* (primers MST-095 and MST-096, or primers MST-097 and MST-098, amplifying *KOR1* with and without the stop coding, respectively) and *ESMD1* (primers MST-149 and MST-150) were amplified from WT cDNA with oligonucleotides specified in parenthesis containing appropriate *att* sites and recombined with pDONR221 or pDONR-P2R-P3 to obtain pEN-L1-*KOR1*-L2, pEN-L1-*ESMD1*-L2, and pEN-R2-*KOR1*-L3. For transcriptional reporters, pEN-L4-*JAZ1op*-R1 and pEN-L4-*ESMD1*-R1 were recombined with pEN-L1-*NLS-3xVEN*-L2 into pEDO097, as described (Gasperini et al., 2015). All oligonucleotide sequences used for cloning are listed in Table S4. pEN-L4-*KOR1p*-R1 was also recombined with pEN-L1-*KOR1*-L2 into pEDO097 for complementation analysis. For translational reporters, pEN-L4-*KOR1p*-R1 or cell-type specific promoters were recombined with pEN-L1-*CIT*-L2 and pEN-R2-*KOR1*-L3 into a modified pH7m34gw vector named pFR7m34gw, which harbours seed Red Fluorescent Protein (RFP) expression (*OLE1p:RFP*) instead of hygromycin (Hg) resistance for in planta selection, to generate *Promoter:CIT-KOR1* constructs. Similarly, to obtain *ESMD1p:ESMD1-mT* and *ESMD1p:ESMD1-CIT*, I recombined pEN-L4-*ESMD1p*-R1, pEN-L1-*ESMD1*-L2, and pEN-R2-*mT*-L3, or pEN-R2-*CIT*-L3 into pFR7m34gw (in both cases, fluorescence signals were undetectable, although the constructs were functionally complementing the mutant phenotype). All constructs were verified by Sanger sequencing and analysis with the DNASTAR Lasergene software SeqBuilder and SeqMan Ultra. Transgenic plants were generated by floral dip with *Agrobacterium tumefaciens* strain GV3101. Transformed seeds expressing RFP in T<sub>1</sub>, T<sub>2</sub>, and T<sub>3</sub> generations were selected by fluorescence microscopy, and segregation analysis was performed in >12 independent T<sub>2</sub> lines. A minimum of two independent T<sub>3</sub> transgenic lines were used for each construct to perform experiments and verify reproducibility.



## Confocal microscopy

Confocal laser scanning microscopy was performed on Zeiss LSM 700 or LSM 880 instruments. For live imaging, 5-do vertically-grown seedling roots were mounted in 0.5x MS with 30 µg/ml PI. As *kor1* roots are thick and recalcitrant to PI penetration, *kor1* genotypes were fixed in 4% paraformaldehyde, cleared with ClearSee (10% Xylitol [w/v]; 15% Sodium deoxycholate [w/v] and 25% Urea w/v] in water), and stained with Direct Red 23 as described (Ursache et al., 2018). Excitation / detection ranges were set as follows: VEN and CIT: 514/ 515-545 nm; mT: 458/ 460-510 nm; Direct Red 23: 514/ 580-615 nm; PI: 561/ 600-700 nm. All images shown within one experiment were taken with identical settings, and by analyzing at least 10 individuals. Image processing was performed in Fiji. Z-Stacks were displayed as texture-based volume renderings using the 3DViewer plugin in Fiji.

## Suppressor screen and mapping by NGS sequencing

Approximately 5 000 seeds (0.1 g) of *kor1-4 JGP* were mutagenized with EMS as described (Acosta et al., 2013). Resulting M<sub>1</sub> plants were either harvested individually (n = 1 243) or in pools of 12 (n = 230). 20 M<sub>2</sub> seedlings were screened from individually harvested plants, and 480 M<sub>2</sub>s were screened from each pool to enlarge both the screening breadth and depth. A total of 135 260 M<sub>2</sub> seedlings, from 4 003 M<sub>1</sub> plants, were assayed for lack of *JGP* activity in 5-do *kor1-4* seedlings by live GUS staining as described (Acosta et al., 2013). To increase the screen stringency and avoid the recovery of false positives, M<sub>2</sub> seedlings were shifted from 21°C to 26°C 24 h prior GUS staining as *kor1* mutants are known exacerbate their phenotypes at higher temperatures (Lane et al., 2001). Putative M<sub>2</sub> suppressors were transferred to soil and crossed to JA-deficient (*aos*, *opr3-2*, *jar1-1*) and JA-insensitive (*coi1-34*) mutants to avoid the recovery of expected genes, and back crossed to *kor1-4 JGP* for segregation analysis, phenotype confirmation, and mapping population development. *esmd1-3* was identified as a *JGP* suppressor of *kor1-4* by pooling 120 individuals lacking *JGP* reporter activity from an BC<sub>1</sub>F<sub>2</sub> population and sequencing the bulk segregants by whole genome sequencing. Phenol/chloroform genomic DNA extraction was as in (Acosta et al., 2013). Library preparation (Illumina Shotgun TruSeq DNA PCR-free) and Illumina sequencing on a HiSeq X platform with a 150 bp paired-end (PE) read length was performed by Macrogen (www.macrogen.com). Sequencing output of 15 Gb resulted in an average of 118 sequencing depth for each base across the genome. EMS-generated SNPs were identified as described (Acosta et al., 2013), with updated software tools. Sequence analysis was performed in R by René Dreos (University of Lausanne, Switzerland). Reads were mapped to the TAIR10 Arabidopsis thaliana genome with bowtie2 aligner (v. 2.3.1, parameter-end-to-end). Alignment files were converted to BAM with SAMtools (v 1.8), and SNPs calling was performed with GATK tool (v.4.1.0.0). Common SNPs with the *kor1-4 JGP* parental line were filtered out with the intersectBed tool from BEDTools utilities (v.2.22.1). The SNPEff tool (v.2.0.4 RC1) was

used to predict the effect of the SNPs in coding regions. SNP frequencies (the number of reads supporting a given SNP over the total number of reads covering the SNP location) were extracted using the Unix command `awk` and plotted with R. Candidate SNPs were identified in genomic regions with high SNP frequencies (0.5-1) linked to the causal SNP, which had the expected frequency of 1. Validation of the candidate SNP was done by allelism test and by complementation by transformation.

### **Cell wall composition analysis**

Following material collection, the extraction, purification and analysis was performed by Cătălin Voiniciuc (Leibniz Institute of Plant Biochemistry, Halle, Germany).

Alcohol-insoluble residue (AIR) was extracted from shoots and roots of 12-do seedlings as previously described (Voiniciuc et al., 2015). Each biological replicate consisted of ~100 shoots (~150 mg FW) or ~300 roots (~80 mg FW). A slurry solution of AIR (1 mg/mL water) was prepared for each sample and homogenized using a ball mill followed by sonication. Matrix polysaccharide composition of 300 µg of AIR after 2 M trifluoroacetic acid hydrolysis was analyzed via high-performance anion-exchange chromatography with pulsed amperometric detection (HPAEC-PAD), similar to (Voiniciuc et al., 2015), but on a 940 Professional IC Vario ONE/ChS/PP/LPG instrument (Metrohm) equipped with Metrosep Carb2 250/4.0 analytical and guard columns. Each run consisted of neutral sugar separation (22 min; 2 mM sodium hydroxide and 3.4 mM sodium acetate isocratic gradient), followed by uronic acid separation (23 min; 100 mM sodium hydroxide and 170 mM sodium acetate), and a 14 min re-equilibration (starting eluents) steps.

Cellulose was quantified based on the two-step sulfuric acid hydrolysis method described by (Yeats et al., 2016), with some modifications. Aliquots of AIR (200 µg each) were first pre-treated with concentrated sulfuric acid (to swell cellulose) or were directly used for Seaman hydrolysis (to measure non-crystalline glucose), using ribose as an internal standard. Hydrolyzed glucose was quantified using the HPAEC-PAD system described above but with a shorter run: 2 mM sodium hydroxide and 3.4 mM sodium acetate isocratic gradient (22 min), followed by a 3 min rinse with 80 mM sodium hydroxide and 136 mM sodium acetate, and a 4 min re-equilibration with starting eluent.

### **Sectioning, segmentation and cell analysis**

Roots from vertically-grown 5-do seedlings were vacuum infiltrated and fixed in glutaraldehyde: formaldehyde: 50mM sodium phosphate buffer (pH7.2) (2:5:43, v/v/v) for 1 h, dehydrated through an EtOH series, and embedded in Technovit 7100 resin as described (Gasperini et al., 2015). Samples were sectioned on a Microm HM355S microtome with a carbide knife (Histoserve) into 5 µm sections,

mounted in 10% glycerol, and cell walls were visualized under dark-field of a Zeiss AxioImager microscope fitted with an AxioCam MRm camera. Tagged Image Files (TIF) images were segmented with PlantSeg (Wolny et al., 2020) using preset parameters of the prediction model "lightsheet\_unet\_bce\_dice\_ds1x", which empirically segmented our images most accurately. Cellular area was measured in Fiji. For display purposes only, dark field images were inverted and segmented images re-coloured in Photoshop to visualize different cell types more easily.

### **Root growth, phenotypic measurements and tropism assays**

Primary root length was evaluated in 7-do seedlings as described (Acosta et al., 2013) and root growth rate was determined by measuring primary root length in 4-do seedlings for 6 consecutive days, every 24 h. Root diameter was assessed in 7-do seedlings by imaging vertically grown seedlings on a Leica M165 FC stereomicroscope fitted with a Leica MC170 HD camera, measuring the root thickness in the early differentiation zone (marked by the appearance of root hairs).

For root meristem cellular measurements, 5-day-old vertically grown seedlings were mounted in a chloral hydrate:glycerol:water (8:3:1) solution and observed with DIC optics using a with a Leica DM6B microscope fitted with a Leica DMC6200 camera. The number of cells in the meristematic division zone was counted in the cortex cell file between the quiescent centre and the first elongating cell (Acosta et al., 2013). The distance between these cells was measured for meristem division zone length using Fiji, and delineates meristem length (Perilli and Sabatini, 2010). Cortex cell length was measured in 5-day-old vertically grown seedlings counterstained with PI, starting at the beginning of the differentiation zone shootwards, using the ruler function of the ZEN Software (Zeiss) at a confocal microscope LSM700.

Root gravitropism assays were performed on vertically-grown 5-do seedlings by rotating the plates by 90° and evaluating root bending angles 24 h after the rotation on scanned images with Fiji. For root hydrotropism assays, 5-do seedlings were transferred to split-agar plates containing either mock (MS/MS) or 400 mM mannitol (MS/mannitol) by aligning root tips 3 mm from the split-media boundary as in (Antoni et al., 2016). Root bending angles were evaluated 24 h after transfer to split-agar plates, by analysing scanned images with Fiji as described (Antoni et al., 2016).

### **Micrografting**

Grafting was performed as described by (Melnyk et al., 2015; Schulze et al., 2019) Graft formation was evaluated at 8 days by the attachment of scion to rootstock without the development of adventitious roots. Successful grafts were transferred to vertical MS plates and grown further for 6 days until they were transferred to soil for further assays.

### **Leaf area measurement**

True leaves from 5-weeks-old ungrafted plants or 7-weeks-old grafted plants grown in soil under short days were excised near the shoot apical meristem and taped on a double adhesive film placed on a black paper sheet from youngest to oldest, similar to (Vanhaeren et al., 2015). Curled leaves were cut to unfold the lamina and permit area measurements by photographing leaves series from each plant (n = 10). Total leaf area was measured by using the "Measure Rosette Area" tool in Fiji. Experiments were repeated at least two times with similar results.

### **Herbivory bioassays**

Herbivory bioassays were performed as described in (Mielke and Gasperini, 2020). Plant growth was synchronized so that all genotypes had a similar total leaf number at the beginning of the bioassay (WT and *aos* were 5 weeks old, while *kor1-4* and *kor1-aos* plants were 6 weeks old). For grafted plants, WT and *aos* grafts were 6 weeks old, while *kor1-4* and *kor1-4 aos* grafts were 7 weeks old. 12 plants per genotype planted in individual pots were transferred into 20 x 30 x 20 cm plexiglas boxes and three newly hatched *Spodoptera littoralis* larvae were placed on each plant. Boxes were brought back to the growth chamber and larvae were allowed to feed until the first genotype was eaten down to the meristem (9-10 days). Surviving larvae were collected and individually weighed. Experiments were repeated at least three times with similar results.

### **Statistical analysis**

Box plots, multiple comparisons [analysis of variance (ANOVA) followed by Tukey's honest significant difference (HSD) test], and circular histograms were performed in R.

## References

- Abe, H., Onnishi, J., Narusaka, M., Seo, S., Narusaka, Y., Tsuda, S., and Kobayashi, M. (2008). Arabidopsis-thrips system for analysis of plant response to insect feeding. *Plant Signal Behav* **3**, 446-447.
- Acosta, I.F., Gasperini, D., Chetelat, A., Stolz, S., Santuari, L., and Farmer, E.E. (2013). Role of NINJA in root jasmonate signaling. *Proc Natl Acad Sci U S A* **110**, 15473-15478.
- Alassimone, J., Fujita, S., Doblaz, V.G., van Dop, M., Barberon, M., Kalmbach, L., Vermeer, J.E.M., Rojas-Murcia, N., Santuari, L., Hardtke, C.S., and Geldner, N. (2016). Polarly localized kinase SGN1 is required for Casparian strip integrity and positioning. *Nat Plants* **2**.
- Alonso, J.M., Hirayama, T., Roman, G., Nourizadeh, S., and Ecker, J.R. (1999). EIN2, a bifunctional transducer of ethylene and stress responses in Arabidopsis. *Science* **284**, 2148-2152.
- Anders, S., Pyl, P.T., and Huber, W. (2015). HTSeq--a Python framework to work with high-throughput sequencing data. *Bioinformatics* **31**, 166-169.
- Andersen, T.G., Nour-Eldin, H.H., Fuller, V.L., Olsen, C.E., Burow, M., and Halkier, B.A. (2013). Integration of biosynthesis and long-distance transport establish organ-specific glucosinolate profiles in vegetative Arabidopsis. *Plant Cell* **25**, 3133-3145.
- Anderson, C.T. (2016). We be jammin': an update on pectin biosynthesis, trafficking and dynamics. *J Exp Bot* **67**, 495-502.
- Anderson, C.T., and Kieber, J.J. (2020). Dynamic Construction, Perception, and Remodeling of Plant Cell Walls. *Ann Rev Plant Biol* **71**, 39-69.
- Antoni, R., Dietrich, D., Bennett, M.J., and Rodriguez, P.L. (2016). Hydrotropism: Analysis of the Root Response to a Moisture Gradient. *Methods Mol Biol* **1398**, 3-9.
- Atmodjo, M.A., Hao, Z., and Mohnen, D. (2013). Evolving views of pectin biosynthesis. *Annu Rev Plant Biol* **64**, 747-779.
- Bacete, L., and Hamann, T. (2020). The Role of Mechanoperception in Plant Cell Wall Integrity Maintenance. *Plants* **9**.
- Bacete, L., Melida, H., Miedes, E., and Molina, A. (2018). Plant cell wall-mediated immunity: cell wall changes trigger disease resistance responses. *Plant J* **93**, 614-636.
- Bachmann, A., Hause, B., Maucher, H., Garbe, E., Voros, K., Weichert, H., Wasternack, C., and Feussner, I. (2002). Jasmonate-induced lipid peroxidation in barley leaves initiated by distinct 13-LOX forms of chloroplasts. *Biol Chem* **383**, 1645-1657.
- Bai, L., Ma, X.N., Zhang, G.Z., Song, S.F., Zhou, Y., Gao, L.J., Miao, Y.C., and Song, C.P. (2014). A Receptor-Like Kinase Mediates Ammonium Homeostasis and Is Important for the Polar Growth of Root Hairs in Arabidopsis. *Plant Cell* **26**, 1497-1511.
- Baldwin, I.T. (1998). Jasmonate-induced responses are costly but benefit plants under attack in native populations. *P Natl Acad Sci USA* **95**, 8113-8118.
- Bannenber, G., Martinez, M., Hamberg, M., and Castresana, C. (2009). Diversity of the enzymatic activity in the lipoxygenase gene family of Arabidopsis thaliana. *Lipids* **44**, 85-95.
- Baskin, T.I., Betzner, A.S., Hoggart, R., Cork, A., and Williamson, R.E. (1992). Root Morphology Mutants in Arabidopsis-Thaliana. *Aust J Plant Physiol* **19**, 427-437.
- Basu, D., and Haswell, E.S. (2020). The Mechanosensitive Ion Channel MSL10 Potentiates Responses to Cell Swelling in Arabidopsis Seedlings. *Curr Biol* **30**, 2716-2728.
- Beauzamy, L., Nakayama, N., and Boudaoud, A. (2014). Flowers under pressure: ins and outs of turgor regulation in development. *Ann Bot* **114**, 1517-1533.
- Beltran, J., Wamboldt, Y., Sanchez, R., LaBrant, E.W., Kundariya, H., Viridi, K.S., Elowsky, C., and Mackenzie, S.A. (2018). Specialized Plastids Trigger Tissue-Specific Signaling for Systemic Stress Response in Plants. *Plant Physiol* **178**, 672-683.
- Benjamins, R., Ampudia, C.S., Hooykaas, P.J., and Offringa, R. (2003). PINOID-mediated signaling involves calcium-binding proteins. *Plant Physiol* **132**, 1623-1630.

- Benny, J., Pisciotta, A., Caruso, T., and Martinelli, F.** (2019). Identification of key genes and its chromosome regions linked to drought responses in leaves across different crops through meta-analysis of RNA-Seq data. *BMC Plant Biology* **19**.
- Berkowitz, O., Xu, Y., Wang, Y., Liew, L.C., Zhu, Y., Lewsey, M.G., and Whelan, J.** (2020). RNA-seq analysis of laser micro-dissected *Arabidopsis thaliana* leaf epidermis, mesophyll and vasculature defines tissue-specific transcriptional responses to multiple stress treatments bioRxiv doi: <https://doi.org/10.1101/2020.11.01.364257>
- Bhalerao, R.P., Salchert, K., Bako, L., Okresz, L., Szabados, L., Muranaka, T., Machida, Y., Schell, J., and Koncz, C.** (1999). Regulatory interaction of PRL1 WD protein with *Arabidopsis* SNF1-like protein kinases. *Proc Natl Acad Sci U S A* **96**, 5322-5327.
- Blazquez, M.A., Nelson, D.C., and Weijers, D.** (2020). Evolution of Plant Hormone Response Pathways. *Ann Rev Plant Biol* **71**, 327-353.
- Boari, F., and Malone, M.** (1993). Wound-Induced Hydraulic Signals - Survey of Occurrence in a Range of Species. *J Exp Bot* **44**, 741-746.
- Bohlmann, H., and Wieczorek, K.** (2015). Infection Assay of Cyst Nematodes on *Arabidopsis* Roots. *Bio Protoc* **5**.
- Boisson-Dernier, A., Franck, C.M., Lituiev, D.S., and Grossniklaus, U.** (2015). Receptor-like cytoplasmic kinase MARIS functions downstream of CrRLK1L-dependent signaling during tip growth. *P Natl Acad Sci USA* **112**, 12211-12216.
- Bonaventure, G., Gfeller, A., Rodriguez, V.M., Armand, F., and Farmer, E.E.** (2007a). The four gain-of-function allele and the wild-type allele of Two Pore Channel 1 contribute to different extents or by different mechanisms to defense gene expression in *Arabidopsis*. *Plant Cell Physiol* **48**, 1775-1789.
- Bonaventure, G., Gfeller, A., Proebsting, W.M., Hortensteiner, S., Chetelat, A., Martinoia, E., and Farmer, E.E.** (2007b). A gain-of-function allele of TPC1 activates oxylipin biogenesis after leaf wounding in *Arabidopsis*. *Plant J* **49**, 889-898.
- Bouton, S., Leboeuf, E., Mouille, G., Leydecker, M.T., Talbotec, J., Granier, F., Lahaye, M., Hofte, H., and Truong, H.N.** (2002). QUASIMODO1 encodes a putative membrane-bound glycosyltransferase required for normal pectin synthesis and cell adhesion in *Arabidopsis*. *Plant Cell* **14**, 2577-2590.
- Bouzid, M., He, F., Schmitz, G., Hausler, R.E., Weber, A.P.M., Mettler-Altmann, T., and de Meaux, J.** (2019). *Arabidopsis* species deploy distinct strategies to cope with drought stress. *Ann Bot* **124**, 27-40.
- Braam, J., and Davis, R.W.** (1990). Rain-Induced, Wind-Induced, and Touch-Induced Expression of Calmodulin and Calmodulin-Related Genes in *Arabidopsis*. *Cell* **60**, 357-364.
- Breithaupt, C., Kurzbauer, R., Lilie, H., Schaller, A., Strassner, J., Huber, R., Macheroux, P., and Clausen, T.** (2006). Crystal structure of 12-oxophytodienoate reductase 3 from tomato: self-inhibition by dimerization. *Proc Natl Acad Sci U S A* **103**, 14337-14342.
- Brocard-Gifford, I., Lynch, T.J., Garcia, M.E., Malhotra, B., and Finkelstein, R.R.** (2004). The *Arabidopsis thaliana* ABSCISIC ACID-INSENSITIVE8 encodes a novel protein mediating abscisic acid and sugar responses essential for growth. *Plant Cell* **16**, 406-421.
- Browse, J., and Wallis, J.G.** (2019). *Arabidopsis* Flowers Unlocked the Mechanism of Jasmonate Signaling. *Plants* **8**.
- Brutus, A., Sicilia, F., Macone, A., Cervone, F., and De Lorenzo, G.** (2010). A domain swap approach reveals a role of the plant wall-associated kinase 1 (WAK1) as a receptor of oligogalacturonides. *Proc Natl Acad Sci U S A* **107**, 9452-9457.
- Burn, J.E., Hocart, C.H., Birch, R.J., Cork, A.C., and Williamson, R.E.** (2002). Functional analysis of the cellulose synthase genes *CesA1*, *CesA2*, and *CesA3* in *Arabidopsis*. *Plant Physiol* **129**, 797-807.
- Caarls, L., Elberse, J., Awwanah, M., Ludwig, N.R., de Vries, M., Zeilmaker, T., Van Wees, S.C.M., Schuurink, R.C., and Van den Ackerveken, G.** (2017). *Arabidopsis* JASMONATE-INDUCED OXYGENASES down-regulate plant immunity by hydroxylation and inactivation of the hormone jasmonic acid. *P Natl Acad Sci USA* **114**, 6388-6393.

- Caldelari, D., Wang, G., Farmer, E.E., and Dong, X.** (2011). *Arabidopsis lox3 lox4* double mutants are male sterile and defective in global proliferative arrest. *Plant Mol Biol* **75**, 25-33.
- Campos, M.L., Kang, J.H., and Howe, G.A.** (2014). Jasmonate-triggered plant immunity. *J Chem Ecol* **40**, 657-675.
- Campos, M.L., Yoshida, Y., Major, I.T., de Oliveira Ferreira, D., Weraduwage, S.M., Froehlich, J.E., Johnson, B.F., Kramer, D.M., Jander, G., Sharkey, T.D., and Howe, G.A.** (2016). Rewiring of jasmonate and phytochrome B signalling uncouples plant growth-defense tradeoffs. *Nat Commun* **7**, 12570.
- Cano-Delgado, A., Penfield, S., Smith, C., Catley, M., and Bevan, M.** (2003). Reduced cellulose synthesis invokes lignification and defense responses in *Arabidopsis thaliana*. *Plant J* **34**, 351-362.
- Cano-Delgado, A.I., Metzlauff, K., and Bevan, M.W.** (2000). The *eli1* mutation reveals a link between cell expansion and secondary cell wall formation in *Arabidopsis thaliana*. *Development* **127**, 3395-3405.
- Carpita, N.C.** (2011). Update on mechanisms of plant cell wall biosynthesis: how plants make cellulose and other (1->4)-beta-D-glycans. *Plant Physiol* **155**, 171-184.
- Cevik, V., Kidd, B.N., Zhang, P., Hill, C., Kiddle, S., Denby, K.J., Holub, E.B., Cahill, D.M., Manners, J.M., Schenk, P.M., Beynon, J., and Kazan, K.** (2012). MEDIATOR25 acts as an integrative hub for the regulation of jasmonate-responsive gene expression in *Arabidopsis*. *Plant Physiol* **160**, 541-555.
- Chaumont, F., and Tyerman, S.D.** (2014). Aquaporins: Highly Regulated Channels Controlling Plant Water Relations. *Plant Physiol* **164**, 1600-1618.
- Chauvin, A., Caldeleri, D., Wolfender, J.L., and Farmer, E.E.** (2013). Four 13-lipoxygenases contribute to rapid jasmonate synthesis in wounded *Arabidopsis thaliana* leaves: a role for lipoxygenase 6 in responses to long-distance wound signals. *New Phytol* **197**, 566-575.
- Chen, H., Wang, B., Geng, S., Arellano, C., Chen, S., and Qu, R.** (2018). Effects of overexpression of jasmonic acid biosynthesis genes on nicotine accumulation in tobacco. *Plant Direct* **2**, e00036.
- Chen, Q., Sun, J., Zhai, Q., Zhou, W., Qi, L., Xu, L., Wang, B., Chen, R., Jiang, H., Qi, J., Li, X., Palme, K., and Li, C.** (2011). The basic helix-loop-helix transcription factor MYC2 directly represses PLETHORA expression during jasmonate-mediated modulation of the root stem cell niche in *Arabidopsis*. *Plant Cell* **23**, 3335-3352.
- Chhajed, S., Mostafa, I., He, Y., Abou-Hashem, M., El-Domiaty, M., and Chen, S.X.** (2020). Glucosinolate Biosynthesis and the Glucosinolate-Myrosinase System in Plant Defense. *Agronomy* **10**.
- Chini, A., Fonseca, S., Fernandez, G., Adie, B., Chico, J.M., Lorenzo, O., Garcia-Casado, G., Lopez-Vidriero, I., Lozano, F.M., Ponce, M.R., Micol, J.L., and Solano, R.** (2007). The JAZ family of repressors is the missing link in jasmonate signalling. *Nature* **448**, 666-671.
- Chini, A., Monte, I., Zamarreno, A.M., Hamberg, M., Lassueur, S., Reymond, P., Weiss, S., Stintzi, A., Schaller, A., Porzel, A., Garcia-Mina, J.M., and Solano, R.** (2018). An OPR3-independent pathway uses 4,5-didehydrojasmonate for jasmonate synthesis. *Nat Chem Biol* **14**, 171-178.
- Chung, H.S., Koo, A.J., Gao, X., Jayanty, S., Thines, B., Jones, A.D., and Howe, G.A.** (2008). Regulation and function of *Arabidopsis* JASMONATE ZIM-domain genes in response to wounding and herbivory. *Plant Physiol* **146**, 952-964.
- Colin, L., Chevallier, A., Tsugawa, S., Gacon, F., Godin, C., Viasnoff, V., Saunders, T.E., and Hamant, O.** (2020). Cortical tension overrides geometrical cues to orient microtubules in confined protoplasts. *P Natl Acad Sci USA* **117**, 32731-32738.
- Cosgrove, D.J.** (2016a). Plant cell wall extensibility: connecting plant cell growth with cell wall structure, mechanics, and the action of wall-modifying enzymes. *J Exp Bot* **67**, 463-476.
- Cosgrove, D.J.** (2016b). Catalysts of plant cell wall loosening. *F1000Res* **5**.
- Cosgrove, D.J.** (2018). Diffuse Growth of Plant Cell Walls. *Plant Physiol* **176**, 16-27.

- Cosgrove, D.J., and Jarvis, M.C.** (2012). Comparative structure and biomechanics of plant primary and secondary cell walls. *Front Plant Sci* **3**, 204.
- Dave, A., and Graham, I.A.** (2012). Oxylipin signaling: a distinct role for the jasmonic acid precursor cis-(+)-12-oxo-phytodienoic acid (cis-OPDA). *Front Plant Sci* **3**, 42.
- De Vriese, K., Costa, A., Beeckman, T., and Vanneste, S.** (2018). Pharmacological Strategies for Manipulating Plant Ca<sup>2+</sup> Signalling. *Int J Mol Sci* **19**, 1506.
- Decreux, A., Thomas, A., Spies, B., Brasseur, R., Van Cutsem, P., and Messiaen, J.** (2006). In vitro characterization of the homogalacturonan-binding domain of the wall-associated kinase WAK1 using site-directed mutagenesis. *Phytochemistry* **67**, 1068-1079.
- Delker, C., Zolman, B.K., Miersch, O., and Wasternack, C.** (2007). Jasmonate biosynthesis in *Arabidopsis thaliana* requires peroxisomal beta-oxidation enzymes--additional proof by properties of pex6 and aim1. *Phytochemistry* **68**, 1642-1650.
- Denness, L., McKenna, J.F., Segonzac, C., Wormit, A., Madhou, P., Bennett, M., Mansfield, J., Zipfel, C., and Hamann, T.** (2011). Cell wall damage-induced lignin biosynthesis is regulated by a reactive oxygen species- and jasmonic acid-dependent process in *Arabidopsis*. *Plant Physiol* **156**, 1364-1374.
- Dennis, E.A., and Norris, P.C.** (2015). Eicosanoid storm in infection and inflammation. *Nat Rev Immunol* **15**, 511-523.
- Dietrich, D., Pang, L., Kobayashi, A., Fozard, J.A., Boudolf, V., Bhosale, R., Antoni, R., Nguyen, T., Hiratsuka, S., Fujii, N., Miyazawa, Y., Bae, T.W., Wells, D.M., Owen, M.R., Band, L.R., Dyson, R.J., Jensen, O.E., King, J.R., Tracy, S.R., Sturrock, C.J., Mooney, S.J., Roberts, J.A., Bhalerao, R.P., Dinneny, J.R., Rodriguez, P.L., Nagatani, A., Hosokawa, Y., Baskin, T.I., Pridmore, T.P., De Veylder, L., Takahashi, H., and Bennett, M.J.** (2017). Root hydrotropism is controlled via a cortex-specific growth mechanism. *Nat Plants* **3**, 17057.
- Ding, S.Y., and Himmel, M.E.** (2006). The maize primary cell wall microfibril: A new model derived from direct visualization. *J Agr Food Chem* **54**, 597-606.
- Doares, S.H., Syrovets, T., Weiler, E.W., and Ryan, C.A.** (1995). Oligogalacturonides and chitosan activate plant defensive genes through the octadecanoid pathway. *Proc Natl Acad Sci U S A* **92**, 4095-4098.
- Dobritzsch, S., Weyhe, M., Schubert, R., Dindas, J., Hause, G., Kopka, J., and Hause, B.** (2015). Dissection of jasmonate functions in tomato stamen development by transcriptome and metabolome analyses. *BMC Biol* **13**, 28.
- Duan, Q., Bonn, B., and Kreuzwieser, J.** (2020). Terpenoids are transported in the xylem sap of Norway spruce. *Plant Cell Environ* **43**, 1766-1778.
- Dubois, M., Van den Broeck, L., and Inze, D.** (2018). The Pivotal Role of Ethylene in Plant Growth. *Trends Plant Sci* **23**, 311-323.
- Dunser, K., Gupta, S., Herger, A., Feraru, M.I., Ringli, C., and Kleine-Vehn, J.** (2019). Extracellular matrix sensing by FERONIA and Leucine-Rich Repeat Extensins controls vacuolar expansion during cellular elongation in *Arabidopsis thaliana*. *EMBO J* **38**, e100353.
- Ellinger, D., Stingl, N., Kubigsteltig, I.I., Bals, T., Juenger, M., Pollmann, S., Berger, S., Schuenemann, D., and Mueller, M.J.** (2010). DONGLE and DEFECTIVE IN ANTHOR DEHISCENCE1 Lipases Are Not Essential for Wound- and Pathogen-Induced Jasmonate Biosynthesis: Redundant Lipases Contribute to Jasmonate Formation. *Plant Physiol* **153**, 114-127.
- Ellis, C., and Turner, J.G.** (2001). The *Arabidopsis* mutant *cev1* has constitutively active jasmonate and ethylene signal pathways and enhanced resistance to pathogens. *Plant Cell* **13**, 1025-1033.
- Ellis, C., Karafyllidis, I., Wasternack, C., and Turner, J.G.** (2002). The *Arabidopsis* mutant *cev1* links cell wall signaling to jasmonate and ethylene responses. *Plant Cell* **14**, 1557-1566.
- Engelsdorf, T., Gigli-Bisceglia, N., Veerabagu, M., McKenna, J.F., Vaahtera, L., Augstein, F., Van der Does, D., Zipfel, C., and Hamann, T.** (2018). The plant cell wall integrity maintenance and immune signaling systems cooperate to control stress responses in *Arabidopsis thaliana*. *Sci Signal* **11**, eaa03070.



- Evans, M.J., and Morris, R.J.** (2017). Chemical agents transported by xylem mass flow propagate variation potentials. *Plant J* **91**, 1029-1037.
- Farmer, E.E., and Dubugnon, L.** (2009). Detritivorous crustaceans become herbivores on jasmonate-deficient plants. *Proc Natl Acad Sci U S A* **106**, 935-940.
- Farmer, E.E., Gasperini, D., and Acosta, I.F.** (2014). The squeeze cell hypothesis for the activation of jasmonate synthesis in response to wounding. *New Phytol* **204**, 282-288.
- Farmer, E.E., Gao, Y.Q., Lenzone, G., Wolfender, J.L., and Wu, Q.** (2020). Wound- and mechanostimulated electrical signals control hormone responses. *New Phytol* **227**, 1037-1050.
- Feng, W., Kita, D., Peaucelle, A., Cartwright, H.N., Doan, V., Duan, Q., Liu, M.C., Maman, J., Steinhorst, L., Schmitz-Thom, I., Yvon, R., Kudla, J., Wu, H.M., Cheung, A.Y., and Dinneny, J.R.** (2018). The FERONIA Receptor Kinase Maintains Cell-Wall Integrity during Salt Stress through Ca<sup>2+</sup> Signaling. *Curr Biol* **28**, 666-675.
- Fernandez-Calvo, P., Chini, A., Fernandez-Barbero, G., Chico, J.M., Gimenez-Ibanez, S., Geerinck, J., Eeckhout, D., Schweizer, F., Godoy, M., Franco-Zorrilla, J.M., Pauwels, L., Witters, E., Puga, M.I., Paz-Ares, J., Goossens, A., Reymond, P., De Jaeger, G., and Solano, R.** (2011). The Arabidopsis bHLH transcription factors MYC<sub>3</sub> and MYC<sub>4</sub> are targets of JAZ repressors and act additively with MYC<sub>2</sub> in the activation of jasmonate responses. *Plant Cell* **23**, 701-715.
- Fernandez-Perez, F., Pomar, F., Pedreno, M.A., and Novo-Uzal, E.** (2015). The suppression of AtPrx52 affects fibers but not xylem lignification in Arabidopsis by altering the proportion of syringyl units. *Physiol Plant* **154**, 395-406.
- Fernandez-Sanchez, M.E., Barbier, S., Whitehead, J., Bealle, G., Michel, A., Latorre-Ossa, H., Rey, C., Fouassier, L., Claperon, A., Brulle, L., Girard, E., Servant, N., Rio-Frio, T., Marie, H., Lesieur, S., Housset, C., Gennisson, J.L., Tanter, M., Menager, C., Fre, S., Robine, S., and Farge, E.** (2015). Mechanical induction of the tumorigenic beta-catenin pathway by tumour growth pressure. *Nature* **523**, 92-95.
- Feussner, I., Kuhn, H., and Wasternack, C.** (2001). Lipooxygenase-dependent degradation of storage lipids. *Trends Plant Sci* **6**, 268-273.
- Feys, B., Benedetti, C.E., Penfold, C.N., and Turner, J.G.** (1994). Arabidopsis Mutants Selected for Resistance to the Phytotoxin Coronatine Are Male Sterile, Insensitive to Methyl Jasmonate, and Resistant to a Bacterial Pathogen. *Plant Cell* **6**, 751-759.
- Finiti, I., Leyva, M.O., Lopez-Cruz, J., Calderan Rodrigues, B., Vicedo, B., Angulo, C., Bennett, A.B., Grant, M., Garcia-Agustin, P., and Gonzalez-Bosch, C.** (2013). Functional analysis of endo-1,4-beta-glucanases in response to Botrytis cinerea and Pseudomonas syringae reveals their involvement in plant-pathogen interactions. *Plant Biol* **15**, 819-831.
- Fonseca, S., Chini, A., Hamberg, M., Adie, B., Porzel, A., Kramell, R., Miersch, O., Wasternack, C., and Solano, R.** (2009). (+)-7-iso-Jasmonoyl-L-isoleucine is the endogenous bioactive jasmonate. *Nat Chem Biol* **5**, 344-350.
- Forieri, I., Sticht, C., Reichelt, M., Gretz, N., Hawkesford, M.J., Malagoli, M., Wirtz, M., and Hell, R.** (2017). System analysis of metabolism and the transcriptome in Arabidopsis thaliana roots reveals differential co-regulation upon iron, sulfur and potassium deficiency. *Plant Cell Environ* **40**, 95-107.
- Fragoso, V., Rothe, E., Baldwin, I.T., and Kim, S.G.** (2014). Root jasmonic acid synthesis and perception regulate folivore-induced shoot metabolites and increase Nicotiana attenuata resistance. *New Phytol* **202**, 1335-1345.
- Frank, M., Guivarc'h, A., Krupkova, E., Lorenz-Meyer, I., Chriqui, D., and Schmulling, T.** (2002). Tumorous shoot development (TSD) genes are required for co-ordinated plant shoot development. *Plant J* **29**, 73-85.

- Frei dit Frey, N., Mbengue, M., Kwaaitaal, M., Nitsch, L., Altenbach, D., Haweker, H., Lozano-Duran, R., Njo, M.F., Beeckman, T., Huettel, B., Borst, J.W., Panstruga, R., and Robatzek, S. (2012). Plasma membrane calcium ATPases are important components of receptor-mediated signaling in plant immune responses and development. *Plant Physiol* **159**, 798-809.
- Fujita, M., Himmelspach, R., Ward, J., Whittington, A., Hasenbein, N., Liu, C., Truong, T.T., Galway, M.E., Mansfield, S.D., Hocart, C.H., and Wasteneys, G.O. (2013). The anisotropy1 D604N mutation in the Arabidopsis cellulose synthase1 catalytic domain reduces cell wall crystallinity and the velocity of cellulose synthase complexes. *Plant Physiol* **162**, 74-85.
- Funakawa, H., and Miwa, K. (2015). Synthesis of borate cross-linked rhamnogalacturonan II. *Front Plant Sci* **6**, 223.
- Gasperini, D., Chetelat, A., Acosta, I.F., Goossens, J., Pauwels, L., Goossens, A., Dreos, R., Alfonso, E., and Farmer, E.E. (2015). Multilayered Organization of Jasmonate Signalling in the Regulation of Root Growth. *PLoS Genetics* **11**, e1005300.
- Ge, Z.X., Bergonci, T., Zhao, Y.L., Zou, Y.J., Du, S., Liu, M.C., Luo, X.J., Ruan, H., Garcia-Valencia, L.E., Zhong, S., Hou, S.Y., Huang, Q.P., Lai, L.H., Moura, D.S., Gu, H.Y., Dong, J., Wu, H.M., Dresselhaus, T., Xiao, J.Y., Cheung, A.Y., and Qu, L.J. (2017). Arabidopsis pollen tube integrity and sperm release are regulated by RALF-mediated signaling. *Science* **358**, 1596-1599.
- Genva, M., Akong, F.O., Andersson, M.X., Deleu, M., Lins, L., and Fauconnier, M.L. (2019). New insights into the biosynthesis of esterified oxylipins and their involvement in plant defense and developmental mechanisms. *Phytochem Rev* **18**, 343-358.
- Gidda, S.K., Miersch, O., Levitin, A., Schmidt, J., Wasternack, C., and Varin, L. (2003). Biochemical and molecular characterization of a hydroxyjasmonate sulfotransferase from Arabidopsis thaliana. *J Biol Chem* **278**, 17895-17900.
- Gillmor, C.S., Poindexter, P., Lorieau, J., Palcic, M.M., and Somerville, C. (2002). Alpha-glucosidase I is required for cellulose biosynthesis and morphogenesis in Arabidopsis. *J Cell Biol* **156**, 1003-1013.
- Glauser, G., Grata, E., Dubugnon, L., Rudaz, S., Farmer, E.E., and Wolfender, J.L. (2008). Spatial and temporal dynamics of jasmonate synthesis and accumulation in Arabidopsis in response to wounding. *J Biol Chem* **283**, 16400-16407.
- Glauser, G., Dubugnon, L., Mousavi, S.A., Rudaz, S., Wolfender, J.L., and Farmer, E.E. (2009). Velocity estimates for signal propagation leading to systemic jasmonic acid accumulation in wounded Arabidopsis. *J Biol Chem* **284**, 34506-34513.
- Goossens, J., Mertens, J., and Goossens, A. (2017). Role and functioning of bHLH transcription factors in jasmonate signalling. *J Exp Bot* **68**, 1333-1347.
- Govindarajan, M., Vaseeharan, B., Alharbi, N.S., Kadaikunnan, S., Khaled, J.M., Al-Anbr, M.N., Alyahya, S.A., Maggi, F., and Benelli, G. (2018). High efficacy of (Z)-gamma-bisabolene from the essential oil of Galinsoga parviflora (Asteraceae) as larvicide and oviposition deterrent against six mosquito vectors. *Environ Sci Pollut R* **25**, 10555-10566.
- Grebner, W., Stingl, N.E., Oenel, A., Mueller, M.J., and Berger, S. (2013). Lipooxygenase6-dependent oxylipin synthesis in roots is required for abiotic and biotic stress resistance of Arabidopsis. *Plant Physiol* **161**, 2159-2170.
- Gruber, B.D., Giehl, R.F.H., Friedel, S., and von Wiren, N. (2013). Plasticity of the Arabidopsis Root System under Nutrient Deficiencies. *Plant Physiol* **163**, 161-179.
- Guan, L., Denkert, N., Eisa, A., Lehmann, M., Sjuts, I., Weiberg, A., Soll, J., Meinecke, M., and Schwenkert, S. (2019). JASSY, a chloroplast outer membrane protein required for jasmonate biosynthesis. *Proc Natl Acad Sci U S A* **116**, 10568-10575.
- Guerriero, G., Hausman, J.F., and Cai, G. (2014). No Stress! Relax! Mechanisms Governing Growth and Shape in Plant Cells. *Int J Mol Sci* **15**, 5094-5114.
- Guo, H., Nolan, T.M., Song, G., Liu, S., Xie, Z., Chen, J., Schnable, P.S., Walley, J.W., and Yin, Y. (2018a). FERONIA Receptor Kinase Contributes to Plant Immunity by Suppressing Jasmonic Acid Signaling in Arabidopsis thaliana. *Curr Biol* **28**, 3316-3324.

- Guo, H.Q., Li, L., Ye, H.X., Yu, X.F., Algreen, A., and Yin, Y.H. (2009). Three related receptor-like kinases are required for optimal cell elongation in *Arabidopsis thaliana*. *Proc Natl Acad Sci USA* **106**, 7648-7653.
- Guo, Q., Yoshida, Y., Major, I.T., Wang, K., Sugimoto, K., Kapali, G., Havko, N.E., Benning, C., and Howe, G.A. (2018b). JAZ repressors of metabolic defense promote growth and reproductive fitness in *Arabidopsis*. *Proc Natl Acad Sci U S A* **115**, E10768-E10777.
- Hamant, O., and Traas, J. (2010). The mechanics behind plant development. *New Phytol* **185**, 369-385.
- Hamant, O., and Haswell, E.S. (2017). Life behind the wall: sensing mechanical cues in plants. *BMC Biol* **15**, 59.
- Hammarberg, T., Provost, P., Persson, B., and Radmark, O. (2000). The N-terminal domain of 5-lipoxygenase binds calcium and mediates calcium stimulation of enzyme activity. *J Biol Chem* **275**, 38787-38793.
- Hansen, S.F., Bettler, E., Wimmerova, M., Imberty, A., Lerouxel, O., and Breton, C. (2009). Combination of Several Bioinformatics Approaches for the Identification of New Putative Glycosyltransferases in *Arabidopsis*. *J Proteome Res* **8**, 743-753.
- Haruta, M., Sabat, G., Stecker, K., Minkoff, B.B., and Sussman, M.R. (2014). A peptide hormone and its receptor protein kinase regulate plant cell expansion. *Science* **343**, 408-411.
- Haswell, E.S., and Meyerowitz, E.M. (2006). MscS-like proteins control plastid size and shape in *Arabidopsis thaliana*. *Curr Biol* **16**, 1-11.
- Haswell, E.S., Peyronnet, R., Barbier-Brygoo, H., Meyerowitz, E.M., and Frachisse, J.M. (2008). Two MscS homologs provide mechanosensitive channel activities in the *Arabidopsis* root. *Curr Biol* **18**, 730-734.
- Hause, B., Hause, G., Kutter, C., Miersch, O., and Wasternack, C. (2003). Enzymes of jasmonate biosynthesis occur in tomato sieve elements. *Plant Cell Physiol* **44**, 643-648.
- Havko, N.E., Major, I.T., Jewell, J.B., Attaran, E., Browse, J., and Howe, G.A. (2016). Control of Carbon Assimilation and Partitioning by Jasmonate: An Accounting of Growth-Defense Tradeoffs. *Plants* **5**, 7.
- Heinisch, J.J., Lorberg, A., Schmitz, H.P., and Jacoby, J.J. (1999). The protein kinase C-mediated MAP kinase pathway involved in the maintenance of cellular integrity in *Saccharomyces cerevisiae*. *Mol Microbiol* **32**, 671-680.
- Heitz, T., Smirnova, E., Marquis, V., and Poirier, L. (2019). Metabolic Control within the Jasmonate Biochemical Pathway. *Plant Cell Physiol* **60**, 2621-2628.
- Heitz, T., Widemann, E., Lugan, R., Miesch, L., Ullmann, P., Desaubry, L., Holder, E., Grausem, B., Kandel, S., Miesch, M., Werck-Reichhart, D., and Pinot, F. (2012). Cytochromes P450 CYP94C1 and CYP94B3 Catalyze Two Successive Oxidation Steps of Plant Hormone Jasmonoyl-isoleucine for Catabolic Turnover. *J Biol Chem* **287**, 6296-6306.
- Hematy, K., Sado, P.E., Van Tuinen, A., Rochange, S., Desnos, T., Balzergue, S., Pelletier, S., Renou, J.P., and Hofte, H. (2007). A receptor-like kinase mediates the response of *Arabidopsis* cells to the inhibition of cellulose synthesis. *Curr Biol* **17**, 922-931.
- Hernandez-Blanco, C., Feng, D.X., Hu, J., Sanchez-Vallet, A., Deslandes, L., Llorente, F., Berrocal-Lobo, M., Keller, H., Barlet, X., Sanchez-Rodriguez, C., Anderson, L.K., Somerville, S., Marco, Y., and Molina, A. (2007). Impairment of cellulose synthases required for *Arabidopsis* secondary cell wall formation enhances disease resistance. *Plant Cell* **19**, 890-903.
- Hickman, R., Van Verk, M.C., Van Dijken, A.J.H., Mendes, M.P., Vroegop-Vos, I.A., Caarls, L., Steenbergen, M., Van der Nagel, I., Wesselink, G.J., Jironkin, A., Talbot, A., Rhodes, J., De Vries, M., Schuurink, R.C., Denby, K., Pieterse, C.M.J., and Van Wees, S.C.M. (2017). Architecture and Dynamics of the Jasmonic Acid Gene Regulatory Network. *Plant Cell* **29**, 2086-2105.
- His, I., Driouich, A., Nicol, F., Jauneau, A., and Hofte, H. (2001). Altered pectin composition in primary cell walls of korrigan, a dwarf mutant of *Arabidopsis* deficient in a membrane-bound endo-1,4-beta-glucanase. *Planta* **212**, 348-358.

- Hoffmann, N., Benske, A., Betz, H., Schuetz, M., and Samuels, A.L. (2020). Laccases and Peroxidases Co-Localize in Lignified Secondary Cell Walls throughout Stem Development. *Plant Physiol* **184**, 806-822.
- Hou, S.G., Liu, Z.Y., Shen, H.X., and Wu, D.J. (2019). Damage-Associated Molecular Pattern-Triggered Immunity in Plants. *Front Plant Sci* **10**, 646
- Hu, H.Z., Zhang, R., Tao, Z.S., Li, X.K., Li, Y.Y., Huang, J.F., Li, X.X., Han, X., Feng, S.Q., Zhang, G.M., and Pen, L.C. (2018). Cellulose Synthase Mutants Distinctively Affect Cell Growth and Cell Wall Integrity for Plant Biomass Production in Arabidopsis. *Plant Cell Physiol* **59**, 1144-1157.
- Huang, H., Liu, B., Liu, L., and Song, S. (2017). Jasmonate action in plant growth and development. *J Exp Bot* **68**, 1349-1359.
- Huang, H.L., Ullah, F., Zhou, D.X., Yi, M., and Zhao, Y. (2019). Mechanisms of ROS Regulation of Plant Development and Stress Responses. *Front Plant Sci* **10**, 800.
- Huber, A.E., and Bauerle, T.L. (2016). Long-distance plant signaling pathways in response to multiple stressors: the gap in knowledge. *J Exp Bot* **67**, 2063-2079.
- Huffaker, A., Pearce, G., Veyrat, N., Erb, M., Turlings, T.C.J., Sartor, R., Shen, Z.X., Briggs, S.P., Vaughan, M.M., Alborn, H.T., Teal, P.E.A., and Schmelz, E.A. (2013). Plant elicitor peptides are conserved signals regulating direct and indirect antiherbivore defense. *P Natl Acad Sci USA* **110**, 5707-5712.
- Huttner, S., Veit, C., Schoberer, J., Grass, J., and Strasser, R. (2012). Unraveling the function of Arabidopsis thaliana OS9 in the endoplasmic reticulum-associated degradation of glycoproteins. *Plant Mol Biol* **79**, 21-33.
- Ishiguro, S., Kawai-Oda, A., Ueda, J., Nishida, I., and Okada, K. (2001). The DEFECTIVE IN ANTHER DEHISCENCE gene encodes a novel phospholipase A1 catalyzing the initial step of jasmonic acid biosynthesis, which synchronizes pollen maturation, anther dehiscence, and flower opening in Arabidopsis. *Plant Cell* **13**, 2191-2209.
- Iwano, M., Igarashi, M., Tarutani, Y., Kaothien-Nakayama, P., Nakayama, H., Moriyama, H., Yakabe, R., Entani, T., Shimosato-Asano, H., Ueki, M., Tamiya, G., and Takayama, S. (2014). A pollen coat-inducible autoinhibited Ca<sup>2+</sup>-ATPase expressed in stigmatic papilla cells is required for compatible pollination in the Brassicaceae. *Plant Cell* **26**, 636-649.
- Ji, H., Wang, S., Li, K., Szakonyi, D., Koncz, C., and Li, X. (2015). PRL1 modulates root stem cell niche activity and meristem size through WOX5 and PLTs in Arabidopsis. *Plant J* **81**, 399-412.
- Jimenez-Aleman, G.H., Almeida-Trapp, M., Fernandez-Barbero, G., Gimenez-Ibanez, S., Reichelt, M., Vadassery, J., Mithofer, A., Caballero, J., Boland, W., and Solano, R. (2019). Omega hydroxylated JA-Ile is an endogenous bioactive jasmonate that signals through the canonical jasmonate signaling pathway. *Bba-Mol Cell Biol L* **1864**.
- Kallenbach, M., Bonaventure, G., Gilardoni, P.A., Wissgott, A., and Baldwin, I.T. (2012). Empoasca leafhoppers attack wild tobacco plants in a jasmonate-dependent manner and identify jasmonate mutants in natural populations. *P Natl Acad Sci USA* **109**, E1548-E1557.
- Kang, J.S., Frank, J., Kang, C.H., Kajiura, H., Vikram, M., Ueda, A., Kim, S., Bahk, J.D., Triplett, B., Fujiyama, K., Lee, S.Y., von Schaewen, A., and Koiwa, H. (2008). Salt tolerance of Arabidopsis thaliana requires maturation of N-glycosylated proteins in the Golgi apparatus. *Proc Natl Acad Sci U S A* **105**, 5933-5938.
- Kesten, C., Gamez-Arjona, F.M., Menna, A., Scholl, S., Dora, S., Huerta, A.I., Huang, H.Y., Tintor, N., Kinoshita, T., Rep, M., Krebs, M., Schumacher, K., and Sanchez-Rodriguez, C. (2019). Pathogen-induced pH changes regulate the growth-defense balance in plants. *EMBO J* **38**, e101822.
- Kienow, L., Schneider, K., Bartsch, M., Stuible, H.P., Weng, H., Miersch, O., Wasternack, C., and Kombrink, E. (2008). Jasmonates meet fatty acids: functional analysis of a new acyl-coenzyme A synthetase family from Arabidopsis thaliana. *J Exp Bot* **59**, 403-419.

- Kilian, J., Whitehead, D., Horak, J., Wanke, D., Weinl, S., Batistic, O., D'Angelo, C., Bornberg-Bauer, E., Kudla, J., and Harter, K. (2007). The AtGenExpress global stress expression data set: protocols, evaluation and model data analysis of UV-B light, drought and cold stress responses. *Plant J* **50**, 347-363.
- Kim, J.M., To, T.K., Matsui, A., Tanoi, K., Kobayashi, N.I., Matsuda, F., Habu, Y., Ogawa, D., Sakamoto, T., Matsunaga, S., Bashir, K., Rasheed, S., Ando, M., Takeda, H., Kawaura, K., Kusano, M., Fukushima, A., Endo, T.A., Kuromori, T., Ishida, J., Morosawa, T., Tanaka, M., Torii, C., Takebayashi, Y., Sakakibara, H., Ogihara, Y., Saito, K., Shinozaki, K., Devoto, A., and Seki, M. (2017). Acetate-mediated novel survival strategy against drought in plants. *Nat Plants* **3**, 17097.
- Kim, Y., Tsuda, K., Igarashi, D., Hillmer, R.A., Sakakibara, H., Myers, C.L., and Katagiri, F. (2014). Mechanisms Underlying Robustness and Tunability in a Plant Immune Signaling Network. *Cell Host & Microbe* **15**, 84-94.
- Kimura, S., Laosinchai, W., Itoh, T., Cui, X., Linder, C.R., and Brown, R.M., Jr. (1999). Immunogold labeling of rosette terminal cellulose-synthesizing complexes in the vascular plant *Vigna angularis*. *Plant Cell* **11**, 2075-2086.
- Kitaoka, N., Matsubara, T., Sato, M., Takahashi, K., Wakuta, S., Kawaide, H., Matsui, H., Nabeta, K., and Matsuura, H. (2011). Arabidopsis CYP94B3 Encodes Jasmonyl-L-Isoleucine 12-Hydroxylase, a Key Enzyme in the Oxidative Catabolism of Jasmonate. *Plant Cell Physiol* **52**, 1757-1765.
- Ko, D., Kang, J., Kiba, T., Park, J., Kojima, M., Do, J., Kim, K.Y., Kwon, M., Endler, A., Song, W.Y., Martinoia, E., Sakakibara, H., and Lee, Y. (2014). Arabidopsis ABCG14 is essential for the root-to-shoot translocation of cytokinin. *P Natl Acad Sci USA* **111**, 7150-7155.
- Ko, J.H., Kim, J.H., Jayanty, S.S., Howe, G.A., and Han, K.H. (2006). Loss of function of COBRA, a determinant of oriented cell expansion, invokes cellular defence responses in *Arabidopsis thaliana*. *J Exp Bot* **57**, 2923-2936.
- Kohlen, W., Charnikhova, T., Liu, Q., Bours, R., Domagalska, M.A., Beguerie, S., Verstappen, F., Leyser, O., Bouwmeester, H., and Ruyter-Spira, C. (2011). Strigolactones Are Transported through the Xylem and Play a Key Role in Shoot Architectural Response to Phosphate Deficiency in Nonarbuscular Mycorrhizal Host *Arabidopsis*. *Plant Physiol* **155**, 974-987.
- Kohorn, B.D., Johansen, S., Shishido, A., Todorova, T., Martinez, R., Defeo, E., and Obregon, P. (2009). Pectin activation of MAP kinase and gene expression is WAK2 dependent. *Plant J* **60**, 974-982.
- Konishi, N., Ishiyama, K., Beier, M.P., Inoue, E., Kanno, K., Yamaya, T., Takahashi, H., and Kojima, S. (2017). Contributions of two cytosolic glutamine synthetase isozymes to ammonium assimilation in *Arabidopsis* roots. *J Exp Bot* **68**, 610-625.
- Koo, A.J. (2018). Metabolism of the plant hormone jasmonate: a sentinel for tissue damage and master regulator of stress response. *Phytochem Rev* **17**, 51-80.
- Koo, A.J., and Howe, G.A. (2009). The wound hormone jasmonate. *Phytochemistry* **70**, 1571-1580.
- Koo, A.J., Gao, X., Jones, A.D., and Howe, G.A. (2009). A rapid wound signal activates the systemic synthesis of bioactive jasmonates in *Arabidopsis*. *Plant J* **59**, 974-986.
- Koo, A.J.K., Cooke, T.F., and Howe, G.A. (2011). Cytochrome P450 CYP94B3 mediates catabolism and inactivation of the plant hormone jasmonoyl-L-isoleucine. *P Natl Acad Sci USA* **108**, 9298-9303.
- Korasick, D.A., Enders, T.A., and Strader, L.C. (2013). Auxin biosynthesis and storage forms. *J Exp Bot* **64**, 2541-2555.
- Krupkova, E., Immerzeel, P., Pauly, M., and Schmulling, T. (2007). The TUMOROUS SHOOT DEVELOPMENT2 gene of *Arabidopsis* encoding a putative methyltransferase is required for cell adhesion and co-ordinated plant development. *Plant J* **50**, 735-750.
- Kulkarni, S., Das, S., Funk, C.D., Murray, D., and Cho, W. (2002). Molecular basis of the specific subcellular localization of the C2-like domain of 5-lipoxygenase. *J Biol Chem* **277**, 13167-13174.

- Lampugnani, E.R., Khan, G.A., Somssich, M., and Persson, S. (2018). Building a plant cell wall at a glance. *J Cell Sci* **131**.
- Lane, D.R., Wiedemeier, A., Peng, L., Hofte, H., Vernhettes, S., Desprez, T., Hocart, C.H., Birch, R.J., Baskin, T.I., Burn, J.E., Arioli, T., Betzner, A.S., and Williamson, R.E. (2001). Temperature-sensitive alleles of RSW2 link the KORRIGAN endo-1,4-beta-glucanase to cellulose synthesis and cytokinesis in Arabidopsis. *Plant Physiol* **126**, 278-288.
- Larrieu, A., Champion, A., Legrand, J., Lavenus, J., Mast, D., Brunoud, G., Oh, J., Guyomarc'h, S., Pizot, M., Farmer, E.E., Turnbull, C., Vernoux, T., Bennett, M.J., and Laplace, L. (2015). A fluorescent hormone biosensor reveals the dynamics of jasmonate signalling in plants. *Nat Commun* **6**, 6043.
- Laudert, D., Pfannschmidt, U., Lottspeich, F., Hollander-Czytko, H., and Weiler, E.W. (1996). Cloning, molecular and functional characterization of Arabidopsis thaliana allene oxide synthase (CYP 74), the first enzyme of the octadecanoid pathway to jasmonates. *Plant Mol Biol* **31**, 323-335.
- Lee, D., Polisensky, D.H., and Braam, J. (2005). Genome-wide identification of touch- and darkness-regulated Arabidopsis genes: a focus on calmodulin-like and XTH genes. *New Phytol* **165**, 429-444.
- Lei, L., Zhang, T., Strasser, R., Lee, C.M., Gonneau, M., Mach, L., Vernhettes, S., Kim, S.H., D, J.C., Li, S., and Gu, Y. (2014). The jiaoyao1 Mutant Is an Allele of korrigan1 That Abolishes Endoglucanase Activity and Affects the Organization of Both Cellulose Microfibrils and Microtubules in Arabidopsis. *Plant Cell* **26**, 2601-2616.
- Lenglet, A., Jaslan, D., Toyota, M., Mueller, M., Muller, T., Schonknecht, G., Marten, I., Gilroy, S., Hedrich, R., and Farmer, E.E. (2017). Control of basal jasmonate signalling and defence through modulation of intracellular cation flux capacity. *New Phytol* **216**, 1161-1169.
- Lenka, S.K., Nims, N.E., Vongpaseuth, K., Boshar, R.A., Roberts, S.C., and Walker, E.L. (2015). Jasmonate-responsive expression of paclitaxel biosynthesis genes in Taxus cuspidata cultured cells is negatively regulated by the bHLH transcription factors TcJAMYC1, TcJAMYC2, and TcJAMYC4. *Front Plant Sci* **6**, 115.
- Li, C., Schillmiller, A.L., Liu, G., Lee, G.I., Jayanty, S., Sageman, C., Vrebalov, J., Giovannoni, J.J., Yagi, K., Kobayashi, Y., and Howe, G.A. (2005). Role of beta-oxidation in jasmonate biosynthesis and systemic wound signaling in tomato. *Plant Cell* **17**, 971-986.
- Li, H.M., and Yu, C.W. (2018). Chloroplast Galactolipids: The Link Between Photosynthesis, Chloroplast Shape, Jasmonates, Phosphate Starvation and Freezing Tolerance. *Plant and Cell Physiology* **59**, 1128-1134.
- Li, J.Y., Fu, Y.L., Pike, S.M., Bao, J., Tian, W., Zhang, Y., Chen, C.Z., Zhang, Y., Li, H.M., Huang, J., Li, L.G., Schroeder, J.I., Gassmann, W., and Gong, J.M. (2010). The Arabidopsis nitrate transporter NRT1.8 functions in nitrate removal from the xylem sap and mediates cadmium tolerance. *Plant Cell* **22**, 1633-1646.
- Li, L., Zhao, Y., McCaig, B.C., Wingerd, B.A., Wang, J., Whalon, M.E., Pichersky, E., and Howe, G.A. (2004). The tomato homolog of CORONATINE-INSENSITIVE1 is required for the maternal control of seed maturation, jasmonate-signaled defense responses, and glandular trichome development. *Plant Cell* **16**, 126-143.
- Li, M., Wang, F., Li, S., Yu, G., Wang, L., Li, Q., Zhu, X., Li, Z., Yuan, L., and Liu, P. (2020a). Importers drive leaf-to-leaf transmission of jasmonic acid in wound induced systemic immunity. *Mol Plant* **13**, 1485-1498.
- Li, Q., Wang, C.G., and Mou, Z.L. (2020b). Perception of Damaged Self in Plants. *Plant Physiol* **182**, 1545-1565.
- Liebinger, E., Huttner, S., Vavra, U., Fischl, R., Schoberer, J., Grass, J., Blaukopf, C., Seifert, G.J., Altmann, F., Mach, L., and Strasser, R. (2009). Class I alpha-Mannosidases Are Required for N-Glycan Processing and Root Development in Arabidopsis thaliana. *Plant Cell* **21**, 3850-3867.

- Lin, S.H., Kuo, H.F., Canivenc, G., Lin, C.S., Lepetit, M., Hsu, P.K., Tillard, P., Lin, H.L., Wang, Y.Y., Tsai, C.B., Gojon, A., and Tsay, Y.F. (2008). Mutation of the Arabidopsis NRT1.5 nitrate transporter causes defective root-to-shoot nitrate transport. *Plant Cell* **20**, 2514-2528.
- Liu, Y.L., Ahn, J.E., Datta, S., Salzman, R.A., Moon, J., Huyghues-Despointes, B., Pittendrigh, B., Murdock, L.L., Koiwa, H., and Zhu-Salzman, K. (2005). Arabidopsis vegetative storage protein is an anti-insect acid phosphatase. *Plant Physiol* **139**, 1545-1556.
- Lopez-Cruz, J., Finiti, I., Fernandez-Crespo, E., Crespo-Salvador, O., Garcia-Agustin, P., and Gonzalez-Bosch, C. (2014). Absence of endo-1,4-beta-glucanase KOR1 alters the jasmonate-dependent defence response to *Pseudomonas syringae* in Arabidopsis. *J Plant Physiol* **171**, 1524-1532.
- Lopez, R., Badel, E., Peraudeau, S., Leblanc-Fournier, N., Beaujard, F., Julien, J.L., Cochard, H., and Moulia, B. (2014). Tree shoot bending generates hydraulic pressure pulses: a new long-distance signal? *J Exp Bot* **65**, 1997-2008.
- Lorenzo, O., Chico, J.M., Sanchez-Serrano, J.J., and Solano, R. (2004). JASMONATE-INSENSITIVE1 encodes a MYC transcription factor essential to discriminate between different jasmonate-regulated defense responses in Arabidopsis. *Plant Cell* **16**, 1938-1950.
- Louveaux, M., Julien, J.D., Mirabet, V., Boudaoud, A., and Hamant, O. (2016). Cell division plane orientation based on tensile stress in Arabidopsis thaliana. *Proc Natl Acad Sci U S A* **113**, 4294-4303.
- Love, M.I., Huber, W., and Anders, S. (2014). Moderated estimation of fold change and dispersion for RNA-seq data with DESeq2. *Genome Biol* **15**, 550.
- Luesse, D.R., Wilson, M.E., and Haswell, E.S. (2015). RNA Sequencing Analysis of the *msl2msl3*, *crl*, and *ggps1* Mutants Indicates that Diverse Sources of Plastid Dysfunction Do Not Alter Leaf Morphology Through a Common Signaling Pathway. *Front Plant Sci* **6**, 1148.
- Machado, R.A.R., McClure, M., Herve, M.R., Baldwin, I.T., and Erb, M. (2016). Benefits of jasmonate-dependent defenses against vertebrate herbivores in nature. *Elife* **5**, e13720.
- Madsen, S.R., Olsen, C.E., Nour-Eldin, H.H., and Halkier, B.A. (2014). Elucidating the role of transport processes in leaf glucosinolate distribution. *Plant Physiol* **166**, 1450-1462.
- Mafli, A., Goudet, J., and Farmer, E.E. (2012). Plants and tortoises: mutations in the Arabidopsis jasmonate pathway increase feeding in a vertebrate herbivore. *Mol Ecol* **21**, 2534-2541.
- Major, I.T., Guo, Q., Zhai, J., Kapali, G., Kramer, D.M., and Howe, G.A. (2020). A Phytochrome B-Independent Pathway Restricts Growth at High Levels of Jasmonate Defense. *Plant Physiol* **183**, 733-749.
- Major, I.T., Yoshida, Y., Campos, M.L., Kapali, G., Xin, X.F., Sugimoto, K., de Oliveira Ferreira, D., He, S.Y., and Howe, G.A. (2017). Regulation of growth-defense balance by the JASMONATE ZIM-DOMAIN (JAZ)-MYC transcriptional module. *New Phytol* **215**, 1533-1547.
- Malone, M., and Stanković, B. (1991). Surface potentials and hydraulic signals in wheat leaves following localized wounding by heat. *Plant Cell Environ* **14**, 431-436.
- Maloney, V.J., and Mansfield, S.D. (2010). Characterization and varied expression of a membrane-bound endo-beta-1,4-glucanase in hybrid poplar. *Plant Biotechnol J* **8**, 294-307.
- Maloney, V.J., Samuels, A.L., and Mansfield, S.D. (2012). The endo-1,4-beta-glucanase Korrigan exhibits functional conservation between gymnosperms and angiosperms and is required for proper cell wall formation in gymnosperms. *New Phytol* **193**, 1076-1087.
- Manfield, I.W., Orfila, C., McCartney, L., Harholt, J., Bernal, A.J., Scheller, H.V., Gilmartin, P.M., Mikkelsen, J.D., Paul Knox, J., and Willats, W.G. (2004). Novel cell wall architecture of isoxaben-habituated Arabidopsis suspension-cultured cells: global transcript profiling and cellular analysis. *Plant J* **40**, 260-275.
- Mansoori, N., Timmers, J., Desprez, T., Alvim-Kamei, C.L., Dees, D.C., Vincken, J.P., Visser, R.G., Hofte, H., Vernhettes, S., and Trindade, L.M. (2014). KORRIGAN1 interacts specifically with integral components of the cellulose synthase machinery. *PLoS One* **9**, e112387.
- Marhavy, P., Kurenda, A., Siddique, S., Denervaud Tendon, V., Zhou, F., Holbein, J., Hasan, M.S., Grundler, F.M., Farmer, E.E., and Geldner, N. (2019). Single-cell damage elicits regional, nematode-restricting ethylene responses in roots. *EMBO J* **38**, e100972.

- Marques-Bueno, M.M., Morao, A.K., Cayrel, A., Platre, M.P., Barberon, M., Caillieux, E., Colot, V., Jaillais, Y., Roudier, F., and Vert, G.** (2016). A versatile Multisite Gateway-compatible promoter and transgenic line collection for cell type-specific functional genomics in *Arabidopsis*. *Plant J* **85**, 320-333.
- Marquis, V., Smirnova, E., Poirier, L., Zumsteg, J., Schweizer, F., Reymond, P., and Heitz, T.** (2020). Stress- and pathway-specific impacts of impaired jasmonoyl-isoleucine (JA-Ile) catabolism on defense signalling and biotic stress resistance. *Plant Cell Environ* **43**, 1558-1570.
- Martin, D., Tholl, D., Gershenzon, J., and Bohlmann, J.** (2002). Methyl jasmonate induces traumatic resin ducts, terpenoid resin biosynthesis, and terpenoid accumulation in developing xylem of Norway spruce stems. *Plant Physiol* **129**, 1003-1018.
- Master, E.R., Rudsander, U.J., Zhou, W.L., Henriksson, H., Divne, C., Denman, S., Wilson, D.B., and Teeri, T.T.** (2004). Recombinant expression and enzymatic characterization of PttCel9A, a KOR homologue from *Populus tremula* x *tremuloides*. *Biochemistry* **43**, 10080-10089.
- Matschi, S., Hake, K., Herde, M., Hause, B., and Romeis, T.** (2015). The calcium-dependent protein kinase CPK28 regulates development by inducing growth phase-specific, spatially restricted alterations in jasmonic acid levels independent of defense responses in *Arabidopsis*. *Plant Cell* **27**, 591-606.
- Melnyk, C.W., Schuster, C., Leyser, O., and Meyerowitz, E.M.** (2015). A Developmental Framework for Graft Formation and Vascular Reconnection in *Arabidopsis thaliana*. *Curr Biology* **25**, 1306-1318.
- Mewis, I., Tokuhisa, J.G., Schultz, J.C., Appel, H.M., Ulrichs, C., and Gershenzon, J.** (2006). Gene expression and glucosinolate accumulation in *Arabidopsis thaliana* in response to generalist and specialist herbivores of different feeding guilds and the role of defense signaling pathways. *Phytochemistry* **67**, 2450-2462.
- Michels, L., Gorelova, V., Harnvanichvech, Y., Borst, J.W., Albada, B., Weijers, D., and Sprakel, J.** (2020). Complete microviscosity maps of living plant cells and tissues with a toolbox of targeting mechanoprobes. *Proc Natl Acad Sci U S A* **117**, 18110-18118.
- Mielke, S., and Gasperini, D.** (2019). Interplay between Plant Cell Walls and Jasmonate Production. *Plant Cell Physiol* **60**, 2629-2637.
- Mielke, S., and Gasperini, D.** (2020). Plant-Insect Bioassay for Testing *Arabidopsis* Resistance to the Generalist Herbivore *Spodoptera littoralis*. *Methods Mol Biol* **2085**, 69-78.
- Mielke, S., Zimmer, M., Meena, M.K., Dreos, R., Stellmach, H., Hause, B., Voiniciuc, C., and Gasperini, D.** (2021). Jasmonate biosynthesis arising from altered cell walls is prompted by turgor-driven mechanical compression. *Sci Adv* **7**, eabf0356.
- Monte, I., Ishida, S., Zamarreno, A.M., Hamberg, M., Franco-Zorrilla, J.M., Garcia-Casado, G., Gouhier-Darimont, C., Reymond, P., Takahashi, K., Garcia-Mina, J.M., Nishihama, R., Kohchi, T., and Solano, R.** (2018). Ligand-receptor co-evolution shaped the jasmonate pathway in land plants. *Nat Chem Biol* **14**, 480-488.
- Morikawa-Ichinose, T., Miura, D., Zhang, L., Kim, S.J., and Maruyama-Nakashita, A.** (2020). Involvement of BGLU30 in Glucosinolate Catabolism in the *Arabidopsis* Leaf under Dark Conditions. *Plant Cell Physiol* **61**, 1095-1106.
- Moscatiello, R., Mariani, P., Sanders, D., and Maathuis, F.J.** (2006). Transcriptional analysis of calcium-dependent and calcium-independent signalling pathways induced by oligogalacturonides. *J Exp Bot* **57**, 2847-2865.
- Moschopoulos, A., Derbyshire, P., and Byrne, M.E.** (2012). The *Arabidopsis* organelle-localized glycyl-tRNA synthetase encoded by EMBRYO DEFECTIVE DEVELOPMENT1 is required for organ patterning. *J Exp Bot* **63**, 5233-5243.
- Mouille, G., Ralet, M.C., Cavalier, C., Eland, C., Effroy, D., Hematy, K., McCartney, L., Truong, H.N., Gaudon, V., Thibault, J.F., Marchant, A., and Hofte, H.** (2007). Homogalacturonan synthesis in *Arabidopsis thaliana* requires a Golgi-localized protein with a putative methyltransferase domain. *Plant J* **50**, 605-614.
- Mousavi, S.A., Chauvin, A., Pascaud, F., Kellenberger, S., and Farmer, E.E.** (2013). GLUTAMATE RECEPTOR-LIKE genes mediate leaf-to-leaf wound signalling. *Nature* **500**, 422-426.



- Muller, M., and Munne-Bosch, S.** (2015). Ethylene Response Factors: A Key Regulatory Hub in Hormone and Stress Signaling. *Plant Physiol* **169**, 32-41.
- Nagashima, Y., Ma, Z.Y., Zhang, X.R., von Schaewen, A., and Koiwa, H.** (2020a). Lack of endoplasmic reticulum quality control (ERQC) promotes tonoplast (TP) targeting of KORRIGAN1 (KOR1). *Plant Signal Behav* **15**, 1744348.
- Nagashima, Y., Ma, Z.Y., Liu, X.T., Qian, X.N., Zhang, X.R., von Schaewen, A., and Koiwa, H.** (2020b). Multiple Quality Control Mechanisms in the ER and TGN Determine Subcellular Dynamics and Salt-Stress Tolerance Function of KORRIGAN1. *Plant Cell* **32**, 470-485.
- Nakagawa, Y., Katagiri, T., Shinozaki, K., Qi, Z., Tatsumi, H., Furuichi, T., Kishigami, A., Sokabe, M., Kojima, I., Sato, S., Kato, T., Tabata, S., Iida, K., Terashima, A., Nakano, M., Ikeda, M., Yamanaka, T., and Iida, H.** (2007). Arabidopsis plasma membrane protein crucial for Ca<sup>2+</sup> influx and touch sensing in roots. *P Natl Acad Sci USA* **104**, 3639-3644.
- Nalam, V.J., Keeretaweep, J., Sarowar, S., and Shah, J.** (2012). Root-derived oxylipins promote green peach aphid performance on Arabidopsis foliage. *Plant Cell* **24**, 1643-1653.
- Naseer, S., Lee, Y., Lapierre, C., Franke, R., Nawrath, C., and Geldner, N.** (2012). Casparian strip diffusion barrier in Arabidopsis is made of a lignin polymer without suberin. *P Natl Acad Sci USA* **109**, 10101-10106.
- Nemeth, K., Salchert, K., Putnoky, P., Bhalerao, R., Koncz-Kalman, Z., Stankovic-Stangeland, B., Bako, L., Mathur, J., Okresz, L., Stabel, S., Geigenberger, P., Stitt, M., Redei, G.P., Schell, J., and Koncz, C.** (1998). Pleiotropic control of glucose and hormone responses by PRL1, a nuclear WD protein, in Arabidopsis. *Genes Dev* **12**, 3059-3073.
- Nguyen, C.T., Kurenda, A., Stolz, S., Chetelat, A., and Farmer, E.E.** (2018). Identification of cell populations necessary for leaf-to-leaf electrical signaling in a wounded plant. *Proc Natl Acad Sci U S A* **115**, 10178-10183.
- Nicol, F., His, I., Jauneau, A., Vernhettes, S., Canut, H., and Hofte, H.** (1998). A plasma membrane-bound putative endo-1,4-beta-D-glucanase is required for normal wall assembly and cell elongation in Arabidopsis. *EMBO J* **17**, 5563-5576.
- Noir, S., Bomer, M., Takahashi, N., Ishida, T., Tsui, T.L., Balbi, V., Shanahan, H., Sugimoto, K., and Devoto, A.** (2013). Jasmonate controls leaf growth by repressing cell proliferation and the onset of endoreduplication while maintaining a potential stand-by mode. *Plant Physiol* **161**, 1930-1951.
- Paredes, A.R., Somerville, C.R., and Ehrhardt, D.W.** (2006). Visualization of cellulose synthase demonstrates functional association with microtubules. *Science* **312**, 1491-1495.
- Paredes, A.R., Persson, S., Ehrhardt, D.W., and Somerville, C.R.** (2008). Genetic evidence that cellulose synthase activity influences microtubule cortical array organization. *Plant Physiol* **147**, 1723-1734.
- Park, J.H., Halitschke, R., Kim, H.B., Baldwin, I.T., Feldmann, K.A., and Feyereisen, R.** (2002). A knock-out mutation in allene oxide synthase results in male sterility and defective wound signal transduction in Arabidopsis due to a block in jasmonic acid biosynthesis. *Plant J* **31**, 1-12.
- Park, Y.B., and Cosgrove, D.J.** (2015). Xyloglucan and its interactions with other components of the growing cell wall. *Plant Cell Physiol* **56**, 180-194.
- Paschold, A., Halitschke, R., and Baldwin, I.T.** (2007). Co(i)-ordinating defenses: NaCOL1 mediates herbivore-induced resistance in *Nicotiana attenuata* and reveals the role of herbivore movement in avoiding defenses. *Plant J* **51**, 79-91.
- Pauly, M., and Keegstra, K.** (2016). Biosynthesis of the Plant Cell Wall Matrix Polysaccharide Xyloglucan. *Annu Rev Plant Biol* **67**, 235-259.
- Pauly, M., Gille, S., Liu, L., Mansoori, N., de Souza, A., Schultink, A., and Xiong, G.** (2013). Hemicellulose biosynthesis. *Planta* **238**, 627-642.
- Pauwels, L., Barbero, G.F., Geerinck, J., Tilleman, S., Grunewald, W., Perez, A.C., Chico, J.M., Bossche, R.V., Sewell, J., Gil, E., Garcia-Casado, G., Witters, E., Inze, D., Long, J.A., De Jaeger, G., Solano, R., and Goossens, A.** (2010). NINJA connects the co-repressor TOPLESS to jasmonate signalling. *Nature* **464**, 788-791.

- Peaucelle, A.** (2014). AFM-based Mapping of the Elastic Properties of Cell Walls: at Tissue, Cellular, and Subcellular Resolutions. *J Vis Exp* **89**, 51317.
- Peng, L., Hocart, C.H., Redmond, J.W., and Williamson, R.E.** (2000). Fractionation of carbohydrates in Arabidopsis root cell walls shows that three radial swelling loci are specifically involved in cellulose production. *Planta* **211**, 406-414.
- Peng, L.C., Kawagoe, Y., Hogan, P., and Delmer, D.** (2002). Sitosterol-beta-glucoside as primer for cellulose synthesis in plants. *Science* **295**, 147-150.
- Penninckx, I.A., Thomma, B.P., Buchala, A., Metraux, J.P., and Broekaert, W.F.** (1998). Concomitant activation of jasmonate and ethylene response pathways is required for induction of a plant defensin gene in Arabidopsis. *Plant Cell* **10**, 2103-2113.
- Perilli, S., and Sabatini, S.** (2010). Analysis of root meristem size development. *Methods Mol Biol* **655**, 177-187.
- Perrella, G., Carr, C., Asensi-Fabado, M.A., Donald, N.A., Paldi, K., Hannah, M.A., and Amtmann, A.** (2016). The Histone Deacetylase Complex 1 Protein of Arabidopsis Has the Capacity to Interact with Multiple Proteins Including Histone 3-Binding Proteins and Histone 1 Variants. *Plant Physiol* **171**, 62-70.
- Perrella, G., Lopez-Vernaza, M.A., Carr, C., Sani, E., Gossele, V., Verduyn, C., Kellermeier, F., Hannah, M.A., and Amtmann, A.** (2013). Histone deacetylase complex1 expression level titrates plant growth and abscisic acid sensitivity in Arabidopsis. *Plant Cell* **25**, 3491-3505.
- Persson, S., Wei, H., Milne, J., Page, G.P., and Somerville, C.R.** (2005). Identification of genes required for cellulose synthesis by regression analysis of public microarray data sets. *Proc Natl Acad Sci U S A* **102**, 8633-8638.
- Pettolino, F.A., Walsh, C., Fincher, G.B., and Bacic, A.** (2012). Determining the polysaccharide composition of plant cell walls. *Nat Protoc* **7**, 1590-1607.
- Pfalz, M., Vogel, H., and Kroymann, J.** (2009). The Gene Controlling the Indole Glucosinolate Modifier1 Quantitative Trait Locus Alters Indole Glucosinolate Structures and Aphid Resistance in Arabidopsis. *Plant Cell* **21**, 985-999.
- Polko, J.K., and Kieber, J.J.** (2019). The Regulation of Cellulose Biosynthesis in Plants. *Plant Cell* **31**, 282-296.
- Poudel, A.N., Holtsclaw, R.E., Kimberlin, A., Sen, S., Zeng, S., Joshi, T., Lei, Z.T., Sumner, L.W., Singh, K., Matsuura, H., and Koo, A.J.** (2019). 12-Hydroxy-Jasmonoyl-l-Isoleucine Is an Active Jasmonate That Signals through CORONATINE INSENSITIVE 1 and Contributes to the Wound Response in Arabidopsis. *Plant Cell Physiol* **60**, 2152-2166.
- Pourcel, L., Irani, N.G., Koo, A.J.K., Bohorquez-Restrepo, A., Howe, G.A., and Grotewold, E.** (2013). A chemical complementation approach reveals genes and interactions of flavonoids with other pathways. *Plant J* **74**, 383-397.
- Ramakrishna, P., and Barberon, M.** (2019). Polarized transport across root epithelia. *Curr Opin Plant Biol* **52**, 23-29.
- Reymond, P., Weber, H., Damond, M., and Farmer, E.E.** (2000). Differential gene expression in response to mechanical wounding and insect feeding in Arabidopsis. *Plant Cell* **12**, 707-720.
- Reymond, P., Bodenhausen, N., Van Poecke, R.M., Krishnamurthy, V., Dicke, M., and Farmer, E.E.** (2004). A conserved transcript pattern in response to a specialist and a generalist herbivore. *Plant Cell* **16**, 3132-3147.
- Rips, S., Bentley, N., Jeong, I.S., Welch, J.L., von Schaewen, A., and Koiwa, H.** (2014). Multiple N-glycans cooperate in the subcellular targeting and functioning of Arabidopsis KORRIGAN1. *Plant Cell* **26**, 3792-3808.
- Ro, D.K., Ehltng, J., Keeling, C.I., Lin, R., Mattheus, N., and Bohlmann, J.** (2006). Microarray expression profiling and functional characterization of AtTPS genes: duplicated Arabidopsis thaliana sesquiterpene synthase genes At4g13280 and At4g13300 encode root-specific and wound-inducible (Z)-gamma-bisabolene synthases. *Arch Biochem Biophys* **448**, 104-116.

- Robert, S., Bichet, A., Grandjean, O., Kierzkowski, D., Satiat-Jeunemaitre, B., Pelletier, S., Hauser, M.T., Hofte, H., and Vernhettes, S. (2005). An Arabidopsis endo-1,4-beta-D-glucanase involved in cellulose synthesis undergoes regulated intracellular cycling. *Plant Cell* **17**, 3378-3389.
- Roeder, A.H., Cunha, A., Ohno, C.K., and Meyerowitz, E.M. (2012). Cell cycle regulates cell type in the Arabidopsis sepal. *Development* **139**, 4416-4427.
- Routier-Kierzkowska, A.L., Weber, A., Kochova, P., Felekis, D., Nelson, B.J., Kuhlemeier, C., and Smith, R.S. (2012). Cellular force microscopy for in vivo measurements of plant tissue mechanics. *Plant Physiol* **158**, 1514-1522.
- Ruan, J., Zhou, Y., Zhou, M., Yan, J., Khurshid, M., Weng, W., Cheng, J., and Zhang, K. (2019). Jasmonic Acid Signaling Pathway in Plants. *Int J Mol Sci* **20**.
- Rui, Y., and Dinneny, J.R. (2020). A wall with integrity: surveillance and maintenance of the plant cell wall under stress. *New Phytol* **225**, 1428-1439.
- Sager, R.E., and Lee, J.Y. (2018). Plasmodesmata at a glance. *J Cell Sci* **131**.
- Sakai, K., Tacconat, L., Borrega, N., Yansouni, J., Brunaud, V., Paysant-Le Roux, C., Delannoy, E., Martin Magniette, M.L., Lepiniec, L., Faure, J.D., Balzergue, S., and Dubreucq, B. (2018). Combining laser-assisted microdissection (LAM) and RNA-seq allows to perform a comprehensive transcriptomic analysis of epidermal cells of Arabidopsis embryo. *Plant Methods* **14**, 10.
- Sampathkumar, A., Yan, A., Krupinski, P., and Meyerowitz, E.M. (2014). Physical forces regulate plant development and morphogenesis. *Curr Biol* **24**, R475-483.
- Sanchez-Rodriguez, C., Rubio-Somoza, I., Sibout, R., and Persson, S. (2010). Phytohormones and the cell wall in Arabidopsis during seedling growth. *Trends Plant Sci* **15**, 291-301.
- Sasaki-Sekimoto, Y., Taki, N., Obayashi, T., Aono, M., Matsumoto, F., Sakurai, N., Suzuki, H., Hirai, M.Y., Noji, M., Saito, K., Masuda, T., Takamiya, K., Shibata, D., and Ohta, H. (2005). Coordinated activation of metabolic pathways for antioxidants and defence compounds by jasmonates and their roles in stress tolerance in Arabidopsis. *Plant J* **44**, 653-668.
- Sato, S., Kato, T., Kakegawa, K., Ishii, T., Liu, Y.G., Awano, T., Takabe, K., Nishiyama, Y., Kuga, S., Sato, S., Nakamura, Y., Tabata, S., and Shibata, D. (2001). Role of the putative membrane-bound endo-1,4-beta-glucanase KORRIGAN in cell elongation and cellulose synthesis in Arabidopsis thaliana. *Plant Cell Physiol* **42**, 251-263.
- Schaller, G.E., and Binder, B.M. (2017). Inhibitors of Ethylene Biosynthesis and Signaling. *Methods Mol Biol* **1573**, 223-235.
- Schmelz, E.A., Engelberth, J., Alborn, H.T., Tumlinson, J.H., and Teal, P.E.A. (2009). Phytohormone-based activity mapping of insect herbivore-produced elicitors. *P Natl Acad Sci USA* **106**, 653-657.
- Schmieder, R., and Edwards, R. (2011). Quality control and preprocessing of metagenomic datasets. *Bioinformatics* **27**, 863-864.
- Scholz, S.S., Vadassery, J., Heyer, M., Reichelt, M., Bender, K.W., Snedden, W.A., Boland, W., and Mithofer, A. (2014). Mutation of the Arabidopsis calmodulin-like protein CML37 deregulates the jasmonate pathway and enhances susceptibility to herbivory. *Mol Plant* **7**, 1712-1726.
- Schubert, R., Grunewald, S., von Sivers, L., and Hause, B. (2019a). Effects of Jasmonate on Ethylene Function during the Development of Tomato Stamens. *Plants* **8**, 277.
- Schubert, R., Dobritsch, S., Gruber, C., Hause, G., Athmer, B., Schreiber, T., Marillonnet, S., Okabe, Y., Ezura, H., Acosta, I.F., Tarkowska, D., and Hause, B. (2019b). Tomato MYB21 Acts in Ovules to Mediate Jasmonate-Regulated Fertility. *Plant Cell* **31**, 1043-1062.
- Schulze, A., Zimmer, M., Mielke, S., Stellmach, H., Melnyk, C.W., Hause, B., and Gasperini, D. (2019). Wound-induced shoot-to-root relocation of JA-Ile precursors coordinates Arabidopsis growth. *Mol Plant* **12**, 1383-1394.
- Seiwert, D., Witt, H., Janshoff, A., and Paulsen, H. (2017). The non-bilayer lipid MGDG stabilizes the major light-harvesting complex (LHCII) against unfolding. *Sci Rep* **7**, 5158.

- Senechal, F., Wattier, C., Rusterucci, C., and Pelloux, J.** (2014). Homogalacturonan-modifying enzymes: structure, expression, and roles in plants. *J Exp Bot* **65**, 5125-5160.
- Seo, H.S., Song, J.T., Cheong, J.J., Lee, Y.H., Lee, Y.W., Hwang, I., Lee, J.S., and Choi, Y.D.** (2001). Jasmonic acid carboxyl methyltransferase: A key enzyme for jasmonate-regulated plant responses. *P Natl Acad Sci USA* **98**, 4788-4793.
- Sharma, V.K., Monostori, T., Gobel, C., Hansch, R., Bittner, F., Wasternack, C., Feussner, I., Mendel, R.R., Hause, B., and Schulze, J.** (2006). Transgenic barley plants overexpressing a 13-lipoxygenase to modify oxylipin signature. *Phytochemistry* **67**, 264-276.
- Shaw, R., Tian, X., and Xu, J.** (2021). Single-Cell Transcriptome Analysis in Plants: Advances and Challenges. *Mol Plant* **14**, 115-126.
- Sheard, L.B., Tan, X., Mao, H., Withers, J., Ben-Nissan, G., Hinds, T.R., Kobayashi, Y., Hsu, F.F., Sharon, M., Browse, J., He, S.Y., Rizo, J., Howe, G.A., and Zheng, N.** (2010). Jasmonate perception by inositol-phosphate-potentiated COI1-JAZ co-receptor. *Nature* **468**, 400-405.
- Shimmen, T.** (2001). Electrical perception of "death message" in Chara: Involvement of turgor pressure. *Plant Cell Physiol* **42**, 366-373.
- Shin, J., Heidrich, K., Sanchez-Villarreal, A., Parker, J.E., and Davis, S.J.** (2012). TIME FOR COFFEE represses accumulation of the MYC2 transcription factor to provide time-of-day regulation of jasmonate signaling in Arabidopsis. *Plant Cell* **24**, 2470-2482.
- Shin, Y.J., Vavra, U., Veit, C., and Strasser, R.** (2018). The glycan-dependent ERAD machinery degrades topologically diverse misfolded proteins. *Plant J* **94**, 246-259.
- Shoji, T., Ogawa, T., and Hashimoto, T.** (2008). Jasmonate-induced nicotine formation in tobacco is mediated by tobacco COI1 and JAZ genes. *Plant Cell Physiol* **49**, 1003-1012.
- Shyu, C., Figueroa, P., Depew, C.L., Cooke, T.F., Sheard, L.B., Moreno, J.E., Katsir, L., Zheng, N., Browse, J., and Howe, G.A.** (2012). JAZ8 lacks a canonical degron and has an EAR motif that mediates transcriptional repression of jasmonate responses in Arabidopsis. *Plant Cell* **24**, 536-550.
- Smirnova, E., Marquis, V., Poirier, L., Aubert, Y., Zumsteg, J., Menard, R., Miesch, L., and Heitz, T.** (2017). Jasmonic Acid Oxidase 2 Hydroxylates Jasmonic Acid and Represses Basal Defense and Resistance Responses against Botrytis cinerea Infection. *Mol Plant* **10**, 1159-1173.
- Sohrabi, R., Huh, J.H., Badiyan, S., Rakotondraibe, L.H., Kliebenstein, D.J., Sobrado, P., and Tholl, D.** (2015). In planta variation of volatile biosynthesis: an alternative biosynthetic route to the formation of the pathogen-induced volatile homoterpene DMNT via triterpene degradation in Arabidopsis roots. *Plant Cell* **27**, 874-890.
- Somerville, C., Bauer, S., Brininstool, G., Facette, M., Hamann, T., Milne, J., Osborne, E., Paredez, A., Persson, S., Raab, T., Vorwerk, S., and Youngs, H.** (2004). Toward a systems approach to understanding plant cell walls. *Science* **306**, 2206-2211.
- Song, S.S., Huang, H., Gao, H., Wang, J.J., Wu, D.W., Liu, X.L., Yang, S.H., Zhai, Q.Z., Li, C.Y., Qi, T.C., and Xie, D.X.** (2014). Interaction between MYC2 and ETHYLENE INSENSITIVE3 Modulates Antagonism between Jasmonate and Ethylene Signaling in Arabidopsis. *Plant Cell* **26**, 263-279.
- Souza, C.A., Li, S., Lin, A.Z., Boutrot, F., Grossmann, G., Zipfel, C., and Somerville, S.C.** (2017). Cellulose-Derived Oligomers Act as Damage-Associated Molecular Patterns and Trigger Defense-Like Responses. *Plant Physiol* **173**, 2383-2398.
- Stahlberg, R., and Cosgrove, D.J.** (1992). Rapid alterations in growth rate and electrical potentials upon stem excision in pea seedlings. *Planta* **187**, 523-531.
- Stahlberg, R., and Cosgrove, D.J.** (1997). The Propagation of Slow Wave Potentials in Pea Epicotyls. *Plant Physiol* **113**, 209-217.
- Staswick, P.E., and Tiryaki, I.** (2004). The oxylipin signal jasmonic acid is activated by an enzyme that conjugates it to isoleucine in Arabidopsis. *Plant Cell* **16**, 2117-2127.
- Staswick, P.E., Su, W., and Howell, S.H.** (1992). Methyl jasmonate inhibition of root growth and induction of a leaf protein are decreased in an Arabidopsis thaliana mutant. *Proc Natl Acad Sci U S A* **89**, 6837-6840.

- Staswick, P.E., Yuen, G.Y., and Lehman, C.C. (1998). Jasmonate signaling mutants of Arabidopsis are susceptible to the soil fungus *Pythium irregulare*. *Plant J* **15**, 747-754.
- Stegmann, M., Monaghan, J., Smakowska-Luzan, E., Rovenich, H., Lehner, A., Holton, N., Belkhadir, Y., and Zipfel, C. (2017). The receptor kinase FER is a RALF-regulated scaffold controlling plant immune signaling. *Science* **355**, 287-289.
- Steinbrenner, A.D., Munoz-Amatriain, M., Chaparro, A.F., Aguilar-Venegas, J.M., Lo, S., Okuda, S., Glauser, G., Dongiovanni, J., Shi, D., Hall, M., Crubagh, D., Holton, N., Zipfel, C., Abagyan, R., Turlings, T.C.J., Close, T.J., Huffaker, A., and Schmelz, E.A. (2020). A receptor-like protein mediates plant immune responses to herbivore-associated molecular patterns. *P Natl Acad Sci USA* **117**, 31510-31518.
- Stelmach, B.A., Muller, A., Hennig, P., Gebhardt, S., Schubert-Zsilavec, M., and Weiler, E.W. (2001). A novel class of oxylipins, sn1-O-(12-oxophytodienoyl)-sn2-O-(hexadecatrienoyl)-monogalactosyl diglyceride, from Arabidopsis thaliana. *J Biol Chem* **276**, 12832-12838.
- Stenzel, I., Hause, B., Maucher, H., Pitzschke, A., Miersch, O., Ziegler, J., Ryan, C.A., and Wasternack, C. (2003). Allene oxide cyclase dependence of the wound response and vascular bundle-specific generation of jasmonates in tomato - amplification in wound signalling. *Plant J* **33**, 577-589.
- Steppuhn, A., Gase, K., Krock, B., Halitschke, R., and Baldwin, I.T. (2004). Nicotine's defensive function in nature. *Plos Biol* **2**, E217.
- Strassner, J., Schaller, F., Frick, U.B., Howe, G.A., Weiler, E.W., Amrhein, N., Macheroux, P., and Schaller, A. (2002). Characterization and cDNA-microarray expression analysis of 12-oxophytodienoate reductases reveals differential roles for octadecanoid biosynthesis in the local versus the systemic wound response. *Plant J* **32**, 585-601.
- Su, S.H., Gibbs, N.M., Jancewicz, A.L., and Masson, P.H. (2017). Molecular Mechanisms of Root Gravitropism. *Curr Biol* **27**, 964-972.
- Su, W., Liu, Y.D., Xia, Y., Hong, Z., and Li, J.M. (2012). The Arabidopsis Homolog of the Mammalian OS-9 Protein Plays a Key Role in the Endoplasmic Reticulum-Associated Degradation of Misfolded Receptor-Like Kinases Degradation. *Mol Plant* **5**, 929-940.
- Swain, S., Jiang, H.W., and Hsieh, H.L. (2017). FAR-RED INSENSITIVE 219/JAR1 Contributes to Shade Avoidance Responses of Arabidopsis Seedlings by Modulating Key Shade Signaling Components. *Front Plant Sci* **8**, 1901.
- Szyjanowicz, P.M., McKinnon, I., Taylor, N.G., Gardiner, J., Jarvis, M.C., and Turner, S.R. (2004). The irregular xylem 2 mutant is an allele of korrikan that affects the secondary cell wall of Arabidopsis thaliana. *Plant J* **37**, 730-740.
- Takahashi, J., Rudsander, U.J., Hedenstrom, M., Banasiak, A., Harholt, J., Amelot, N., Immerzeel, P., Ryden, P., Endo, S., Ibatullin, F.M., Brumer, H., del Campillo, E., Master, E.R., Scheller, H.V., Sundberg, B., Teeri, T.T., and Mellerowicz, E.J. (2009). KORRIGAN1 and its Aspen Homolog PttCelgA1 Decrease Cellulose Crystallinity in Arabidopsis Stems. *Plant Cell Physiol* **50**, 1099-1115.
- Takahashi, N., Goto, N., Okada, K., and Takahashi, H. (2002). Hydrotropism in abscisic acid, wavy, and gravitropic mutants of Arabidopsis thaliana. *Planta* **216**, 203-211.
- Takenaka, Y., Kato, K., Ogawa-Ohnishi, M., Tsuruhama, K., Kajiura, H., Yagyu, K., Takeda, A., Takeda, Y., Kunieda, T., Hara-Nishimura, I., Kuroha, T., Nishitani, K., Matsubayashi, Y., and Ishimizu, T. (2018). Pectin RG-I rhamnosyltransferases represent a novel plant-specific glycosyltransferase family. *Nat Plants* **4**, 669-676.
- Thaler, J.S., Owen, B., and Higgins, V.J. (2004). The role of the jasmonate response in plant susceptibility to diverse pathogens with a range of lifestyles. *Plant Physiol* **135**, 530-538.
- Thatcher, L.F., Cevik, V., Grant, M., Zhai, B., Jones, J.D., Manners, J.M., and Kazan, K. (2016). Characterization of a JAZ7 activation-tagged Arabidopsis mutant with increased susceptibility to the fungal pathogen *Fusarium oxysporum*. *J Exp Bot* **67**, 2367-2386.

- Theodoulou, F.L., Job, K., Slocombe, S.P., Footitt, S., Holdsworth, M., Baker, A., Larson, T.R., and Graham, I.A. (2005). Jasmonic acid levels are reduced in COMATOSE ATP-binding cassette transporter mutants. Implications for transport of jasmonate precursors into peroxisomes. *Plant Physiol* **137**, 835-840.
- Thieme, C.J., Rojas-Triana, M., Stecyk, E., Schudoma, C., Zhang, W., Yang, L., Minambres, M., Walther, D., Schulze, W.X., Paz-Ares, J., Scheible, W.R., and Kragler, F. (2015). Endogenous Arabidopsis messenger RNAs transported to distant tissues. *Nat Plants* **1**, 15025.
- Thines, B., Katsir, L., Melotto, M., Niu, Y., Mandaokar, A., Liu, G., Nomura, K., He, S.Y., Howe, G.A., and Browse, J. (2007). JAZ repressor proteins are targets of the SCF(CO1) complex during jasmonate signalling. *Nature* **448**, 661-665.
- Thireault, C., Shyu, C., Yoshida, Y., St Aubin, B., Campos, M.L., and Howe, G.A. (2015). Repression of jasmonate signaling by a non-TIFY JAZ protein in Arabidopsis. *Plant J* **82**, 669-679.
- Thomma, B.P.H.J., Eggermont, K., Penninckx, I.A.M.A., Mauch-Mani, B., Vogelsang, R., Cammue, B.P.A., and Broekaert, W.F. (1998). Separate jasmonate-dependent and salicylate-dependent defense-response pathways in Arabidopsis are essential for resistance to distinct microbial pathogens. *Proc Natl Acad Sci USA* **95**, 15107-15111.
- Tong, H., Leasure, C.D., Hou, X., Yuen, G., Briggs, W., and He, Z.H. (2008). Role of root UV-B sensing in Arabidopsis early seedling development. *Proc Natl Acad Sci U S A* **105**, 21039-21044.
- Toyooka, K., Goto, Y., Asatsuma, S., Koizumi, M., Mitsui, T., and Matsuoka, K. (2009). A mobile secretory vesicle cluster involved in mass transport from the Golgi to the plant cell exterior. *Plant Cell* **21**, 1212-1229.
- Toyota, M., Spencer, D., Sawai-Toyota, S., Jiaqi, W., Zhang, T., Koo, A.J., Howe, G.A., and Gilroy, S. (2018). Glutamate triggers long-distance, calcium-based plant defense signaling. *Science* **361**, 1112-1115.
- Trapnell, C., Pachter, L., and Salzberg, S.L. (2009). TopHat: discovering splice junctions with RNA-Seq. *Bioinformatics* **25**, 1105-1111.
- Tsang, S.S.K., Law, S.T.S., Li, C.D., Qu, Z., Bendena, W.G., Tobe, S.S., and Hui, J.H.L. (2020). Diversity of Insect Sesquiterpenoid Regulation. *Front Genet* **11**.
- Urbanowicz, B.R., Bennett, A.B., del Campillo, E., Catala, C., Hayashi, T., Henrissat, B., Hofte, H., McQueen-Mason, S.J., Patterson, S.E., Shoseyov, O., Teeri, T.T., and Rose, J.K.C. (2007). Structural organization and a standardized nomenclature for plant endo-1,4-beta-glucanases (Cellulases) of glycosyl hydrolase family 9. *Plant Physiol* **144**, 1693-1696.
- Ursache, R., Andersen, T.G., Marhavy, P., and Geldner, N. (2018). A protocol for combining fluorescent proteins with histological stains for diverse cell wall components. *Plant J* **93**, 399-412.
- Uwer, U., Willmitzer, T., and Altmann, T. (1998). Inactivation of a glycyl-tRNA synthetase leads to an arrest in plant embryo development. *Plant Cell* **10**, 1277-1294.
- Vaddepalli, P., Fulton, L., Batoux, M., Yadav, R.K., and Schneitz, K. (2011). Structure-function analysis of STRUBBELIG, an Arabidopsis atypical receptor-like kinase involved in tissue morphogenesis. *PLoS One* **6**, e19730.
- Vain, T., Crowell, E.F., Timpano, H., Biot, E., Desprez, T., Mansoori, N., Trindade, L.M., Pagant, S., Robert, S., Hofte, H., Gonneau, M., and Vernhettes, S. (2014). The Cellulase KORRIGAN Is Part of the Cellulose Synthase Complex. *Plant Physiol* **165**, 1521-1532.
- Vanhaeren, H., Gonzalez, N., and Inze, D. (2015). A Journey Through a Leaf: Phenomics Analysis of Leaf Growth in Arabidopsis thaliana. *Arabidopsis Book* **13**, e0181.
- Velasquez, S.M., Ricardi, M.M., Dorosz, J.G., Fernandez, P.V., Nadra, A.D., Pol-Fachin, L., Egelund, J., Gille, S., Harholt, J., Ciancia, M., Verli, H., Pauly, M., Bacic, A., Olsen, C.E., Ulvskov, P., Petersen, B.L., Somerville, C., Iusem, N.D., and Estevez, J.M. (2011). O-glycosylated cell wall proteins are essential in root hair growth. *Science* **332**, 1401-1403.
- Veley, K.M., Marshburn, S., Clure, C.E., and Haswell, E.S. (2012). Mechanosensitive Channels Protect Plastids from Hypoosmotic Stress During Normal Plant Growth. *Curr Biol* **22**, 408-413.

- Vembar, S.S., and Brodsky, J.L.** (2008). One step at a time: endoplasmic reticulum-associated degradation. *Nat Rev Mol Cell Bio* **9**, 944-U930.
- Verger, S., Chabout, S., Gineau, E., and Mouille, G.** (2016). Cell adhesion in plants is under the control of putative O-fucosyltransferases. *Development* **143**, 2536-2540.
- Verherbruggen, Y., Marcus, S.E., Haeger, A., Ordaz-Ortiz, J.J., and Knox, J.P.** (2009). An extended set of monoclonal antibodies to pectic homogalacturonan. *Carbohydr Res* **344**, 1858-1862.
- Vijayan, P., Shockey, J., Levesque, C.A., Cook, R.J., and Browse, J.** (1998). A role for jasmonate in pathogen defense of Arabidopsis. *Proc Natl Acad Sci U S A* **95**, 7209-7214.
- Viridi, K.S., Wamboldt, Y., Kundariya, H., Laurie, J.D., Keren, I., Kumar, K.R.S., Block, A., Basset, G., Luebker, S., Elowsky, C., Day, P.M., Roose, J.L., Bricker, T.M., Elthon, T., and Mackenzie, S.A.** (2016). MSH1 Is a Plant Organellar DNA Binding and Thylakoid Protein under Precise Spatial Regulation to Alter Development. *Mol Plant* **9**, 245-260.
- Voiniciuc, C., Schmidt, M.H.W., Berger, A., Yang, B., Ebert, B., Scheller, H.V., North, H.M., Usadel, B., and Gunl, M.** (2015). MUCILAGE-RELATED10 Produces Galactoglucomannan That Maintains Pectin and Cellulose Architecture in Arabidopsis Seed Mucilage. *Plant Physiol* **169**, 403-420.
- Voxeur, A., and Hofte, H.** (2016). Cell wall integrity signaling in plants: "To grow or not to grow that's the question". *Glycobiology* **26**, 950-960.
- Wachananawat, B., Kuroha, T., Takenaka, Y., Kajiura, H., Naramoto, S., Yokoyama, R., Ishizaki, K., Nishitani, K., and Ishimizu, T.** (2020). Diversity of Pectin Rhamnogalacturonan I Rhamnosyltransferases in Glycosyltransferase Family 106. *Front Plant Sci* **11**, 997.
- Wang, G., Ellendorff, U., Kemp, B., Mansfield, J.W., Forsyth, A., Mitchell, K., Bastas, K., Liu, C.M., Woods-Tor, A., Zipfel, C., de Wit, P.J., Jones, J.D., Tor, M., and Thomma, B.P.** (2008). A genome-wide functional investigation into the roles of receptor-like proteins in Arabidopsis. *Plant Physiol* **147**, 503-517.
- Wang, P., Calvo-Polanco, M., Reyt, G., Barberon, M., Champeyroux, C., Santoni, V., Maurel, C., Franke, R.B., Ljung, K., Novak, O., Geldner, N., Boursiac, Y., and Salt, D.E.** (2019). Surveillance of cell wall diffusion barrier integrity modulates water and solute transport in plants. *Sci Rep* **9**, 4227.
- Wang, T., Park, Y.B., Cosgrove, D.J., and Hong, M.** (2015). Cellulose-Pectin Spatial Contacts Are Inherent to Never-Dried Arabidopsis Primary Cell Walls: Evidence from Solid-State Nuclear Magnetic Resonance. *Plant Physiol* **168**, 871-884.
- Wang, T., Liang, L., Xue, Y., Jia, P.F., Chen, W., Zhang, M.X., Wang, Y.C., Li, H.J., and Yang, W.C.** (2016). A receptor heteromer mediates the male perception of female attractants in plants. *Nature* **531**, 241-244.
- Wang, Y.C., Wang, B.C., Gilroy, S., Chehab, E.W., and Braam, J.** (2011). CML24 is Involved in Root Mechanoresponses and Cortical Microtubule Orientation in Arabidopsis. *J Plant Growth Regul* **30**, 467-479.
- Wasternack, C., and Hause, B.** (2013). Jasmonates: biosynthesis, perception, signal transduction and action in plant stress response, growth and development. An update to the 2007 review in *Annals of Botany*. *Ann Bot* **111**, 1021-1058.
- Wasternack, C., and Strnad, M.** (2018). Jasmonates: News on Occurrence, Biosynthesis, Metabolism and Action of an Ancient Group of Signaling Compounds. *Int J Mol Sci* **19**.
- Wasternack, C., and Feussner, I.** (2018). The Oxylin Pathways: Biochemistry and Function. *Annu Rev Plant Biol* **69**, 363-386.
- Westfall, C.S., Zubieta, C., Herrmann, J., Kapp, U., Nanao, M.H., and Jez, J.M.** (2012). Structural basis for prereceptor modulation of plant hormones by GH3 proteins. *Science* **336**, 1708-1711.
- Widemann, E., Miesch, L., Lugan, R., Holder, E., Heinrich, C., Aubert, Y., Miesch, M., Pinot, F., and Heitz, T.** (2013). The amidohydrolases IAR3 and ILL6 contribute to jasmonoyl-isoleucine hormone turnover and generate 12-hydroxyjasmonic acid upon wounding in Arabidopsis leaves. *J Biol Chem* **288**, 31701-31714.

- Williamson, R.E., Burn, J.E., Birch, R., Baskin, T.I., Arioli, T., Betzner, A.S., and Cork, A.** (2001). Morphology of *rsw1*, a cellulose-deficient mutant of *Arabidopsis thaliana*. *Protoplasma* **215**, 116-127.
- Wilson, M.E., Basu, M.R., Bhaskara, G.B., Verslues, P.E., and Haswell, E.S.** (2014). Plastid Osmotic Stress Activates Cellular Stress Responses in *Arabidopsis*. *Plant Physiol* **165**, 119-128.
- Wolf, S.** (2017). Plant cell wall signalling and receptor-like kinases. *Biochem J* **474**, 471-492.
- Wolf, S., van der Does, D., Ladwig, F., Sticht, C., Kolbeck, A., Schurholz, A.K., Augustin, S., Keinath, N., Rausch, T., Greiner, S., Schumacher, K., Harter, K., Zipfel, C., and Hofte, H.** (2014). A receptor-like protein mediates the response to pectin modification by activating brassinosteroid signaling. *Proc Natl Acad Sci U S A* **111**, 15261-15266.
- Wolny, A., Cerrone, L., Vijayan, A., Tofanelli, R., Barro, A.V., Louveaux, M., Wenzl, C., Strauss, S., Wilson-Sanchez, D., Lymbouridou, R., Steigleder, S.S., Pape, C., Bailoni, A., Duran-Nebreda, S., Bassel, G.W., Lohmann, J.U., Tsiantis, M., Hamprecht, F.A., Schneitz, K., Maizel, A., and Kreshuk, A.** (2020). Accurate and versatile 3D segmentation of plant tissues at cellular resolution. *Elife* **9**, e57613.
- Xie, D.X., Feys, B.F., James, S., Nieto-Rostro, M., and Turner, J.G.** (1998). *COL1*: an *Arabidopsis* gene required for jasmonate-regulated defense and fertility. *Science* **280**, 1091-1094.
- Yan, C., and Xie, D.** (2015). Jasmonate in plant defence: sentinel or double agent? *Plant Biotechnol J* **13**, 1233-1240.
- Yan, J.B., Li, S.H., Gu, M., Yao, R., Li, Y.W., Chen, J., Yang, M., Tong, J.H., Xiao, L.T., Nan, F.J., and Xie, D.X.** (2016). Endogenous Bioactive Jasmonate Is Composed of a Set of (+)-7-iso-JA-Amino Acid Conjugates. *Plant Physiol* **172**, 2154-2164.
- Yan, Y., Stolz, S., Chetelat, A., Reymond, P., Pagni, M., Dubugnon, L., and Farmer, E.E.** (2007). A downstream mediator in the growth repression limb of the jasmonate pathway. *Plant Cell* **19**, 2470-2483.
- Yang, D.L., Yao, J., Mei, C.S., Tong, X.H., Zeng, L.J., Li, Q., Xiao, L.T., Sun, T.P., Li, J., Deng, X.W., Lee, C.M., Thomashow, M.F., Yang, Y., He, Z., and He, S.Y.** (2012). Plant hormone jasmonate prioritizes defense over growth by interfering with gibberellin signaling cascade. *Proc Natl Acad Sci U S A* **109**, 1192-1200.
- Yang, Y., Yuan, J.S., Ross, J., Noel, J.P., Pichersky, E., and Chen, F.** (2006). An *Arabidopsis thaliana* methyltransferase capable of methylating farnesoic acid. *Arch Biochem Biophys* **448**, 123-132.
- Ye, Z.W., Lung, S.C., Hu, T.A., Chen, Q.F., Suen, Y.L., Wang, M.F., Hoffmann-Benning, S., Yeung, E., and Chye, M.L.** (2016). *Arabidopsis* acyl-CoA-binding protein ACBP6 localizes in the phloem and affects jasmonate composition. *Plant Mol Biol* **92**, 717-730.
- Yeats, T., Vellosillo, T., Sorek, N., Ibáñez, A., and Bauer, S.** (2016). Rapid Determination of Cellulose, Neutral Sugars, and Uronic Acids from Plant Cell Walls by One-step Two-step Hydrolysis and HPAEC-PAD. *Bio-Protocol* **6**.
- Yu, C.W., Lin, Y.T., and Li, H.M.** (2020). Increased ratio of galactolipid MGDG : DGDG induces jasmonic acid overproduction and changes chloroplast shape. *New Phytol* **228**, 1327-1335.
- Yu, G., and He, Q.Y.** (2016). ReactomePA: an R/Bioconductor package for reactome pathway analysis and visualization. *Mol Biosyst* **12**, 477-479.
- Yuan, F., Yang, H., Xue, Y., Kong, D., Ye, R., Li, C., Zhang, J., Theprungsirikul, L., Shrift, T., Krichilsky, B., Johnson, D.M., Swift, G.B., He, Y., Siedow, J.N., and Pei, Z.M.** (2014). *OSCA1* mediates osmotic-stress-evoked  $Ca^{2+}$  increases vital for osmosensing in *Arabidopsis*. *Nature* **514**, 367-371.
- Yukimune, Y., Tabata, H., Higashi, Y., and Hara, Y.** (1996). Methyl jasmonate-induced overproduction of paclitaxel and baccatin III in *Taxus* cell suspension cultures. *Nat Biotechnol* **14**, 1129-1132.
- Zarattini, M., Launay, A., Farjad, M., Wenes, E., Taconnat, L., Boutet, S., Bernacchia, G., and Fagard, M.** (2017). The bile acid deoxycholate elicits defences in *Arabidopsis* and reduces bacterial infection. *Mol Plant Pathol* **18**, 540-554.



- Zeng, H., Xu, L., Singh, A., Wang, H., Du, L., and Poovaiah, B.W. (2015). Involvement of calmodulin and calmodulin-like proteins in plant responses to abiotic stresses. *Front Plant Sci* **6**, 600.
- Zhang, C., Lei, Y., Lu, C., Wang, L., and Wu, J. (2020). MYC2, MYC3, and MYC4 function additively in wounding-induced jasmonic acid biosynthesis and catabolism. *J Integr Plant Biol* **62**, 1159-1175.
- Zhang, F., Yao, J., Ke, J., Zhang, L., Lam, V.Q., Xin, X.F., Zhou, X.E., Chen, J., Brunzelle, J., Griffin, P.R., Zhou, M., Xu, H.E., Melcher, K., and He, S.Y. (2015a). Structural basis of JAZ repression of MYC transcription factors in jasmonate signalling. *Nature* **525**, 269-273.
- Zhang, G.B., Yi, H.Y., and Gong, J.M. (2014a). The Arabidopsis Ethylene/Jasmonic Acid-NRT Signaling Module Coordinates Nitrate Reallocation and the Trade-Off between Growth and Environmental Adaptation. *Plant Cell* **26**, 3984-3998.
- Zhang, L., Zhang, F., Melotto, M., Yao, J., and He, S.Y. (2017). Jasmonate signaling and manipulation by pathogens and insects. *J Exp Bot* **68**, 1371-1385.
- Zhang, L., Yao, J., Withers, J., Xin, X.F., Banerjee, R., Fariduddin, Q., Nakamura, Y., Nomura, K., Howe, G.A., Boland, W., Yan, H.G., and He, S.Y. (2015b). Host target modification as a strategy to counter pathogen hijacking of the jasmonate hormone receptor. *P Natl Acad Sci USA* **112**, 14354-14359.
- Zhang, S., Liu, Y., and Yu, B. (2014b). PRL1, an RNA-binding protein, positively regulates the accumulation of miRNAs and siRNAs in Arabidopsis. *PLoS Genet* **10**, e1004841.
- Zhang, X.W., Zhou, L.Y., Qin, Y.K., Chen, Y.W., Liu, X.L., Wang, M.Y., Mao, J., Zhang, J.J., He, Z.H., Liu, L.C., and Li, J.M. (2018). A Temperature-Sensitive Misfolded bri1-301 Receptor Requires Its Kinase Activity to Promote Growth. *Plant Physiol* **178**, 1704-1719.
- Zhang, Y., and Turner, J.G. (2008). Wound-induced endogenous jasmonates stunt plant growth by inhibiting mitosis. *PLoS One* **3**, e3699.
- Zhong, R., Burk, D.H., Morrison, W.H., 3rd, and Ye, Z.H. (2002a). A kinesin-like protein is essential for oriented deposition of cellulose microfibrils and cell wall strength. *Plant Cell* **14**, 3101-3117.
- Zhong, R.Q., Kays, S.J., Schroeder, B.P., and Ye, Z.H. (2002b). Mutation of a chitinase-like gene causes ectopic deposition of lignin, aberrant cell shapes, and overproduction of ethylene. *Plant Cell* **14**, 165-179.
- Zhu, Z., and Lee, B. (2015). Friends or foes: new insights in jasmonate and ethylene co-actions. *Plant Cell Physiol* **56**, 414-420.
- Zhu, Z., An, F., Feng, Y., Li, P., Xue, L., A, M., Jiang, Z., Kim, J.M., To, T.K., Li, W., Zhang, X., Yu, Q., Dong, Z., Chen, W.Q., Seki, M., Zhou, J.M., and Guo, H. (2011). Derepression of ethylene-stabilized transcription factors (EIN3/EIL1) mediates jasmonate and ethylene signaling synergy in Arabidopsis. *Proc Natl Acad Sci U S A* **108**, 12539-12544.
- Zhurov, V., Navarro, M., Bruinsma, K.A., Arbona, V., Santamaria, M.E., Cazaux, M., Wybouw, N., Osborne, E.J., Ens, C., Rioja, C., Vermeirssen, V., Rubio-Somoza, I., Krishna, P., Diaz, I., Schmid, M., Gomez-Cadenas, A., Van de Peer, Y., Grbic, M., Clark, R.M., Van Leeuwen, T., and Grbic, V. (2014). Reciprocal responses in the interaction between Arabidopsis and the cell-content-feeding chelicerate herbivore spider mite. *Plant Physiol* **164**, 384-399.
- Zou, W., Liu, K., Gao, X., Yu, C., Wang, X., Shi, J., Chao, Y., Yu, Q., Zhou, G., and Ge, L. (2021). Arabidopsis WXR1/3 regulate transitory starch metabolism in young seedlings corresponding to circadian rhythm. *J Exp Bot* **72**, 3074-3090.
- Zou, Y., Chintamanani, S., He, P., Fukushige, H., Yu, L., Shao, M., Zhu, L., Hildebrand, D.F., Tang, X., and Zhou, J.M. (2016). A gain-of-function mutation in Msl10 triggers cell death and wound-induced hyperaccumulation of jasmonic acid in Arabidopsis. *J Integr Plant Biol* **58**, 600-609.
- Zuo, J., Niu, Q.W., Nishizawa, N., Wu, Y., Kost, B., and Chua, N.H. (2000). KORRIGAN, an Arabidopsis endo-1,4-beta-glucanase, localizes to the cell plate by polarized targeting and is essential for cytokinesis. *Plant Cell* **12**, 1137-1152.

## Appendix

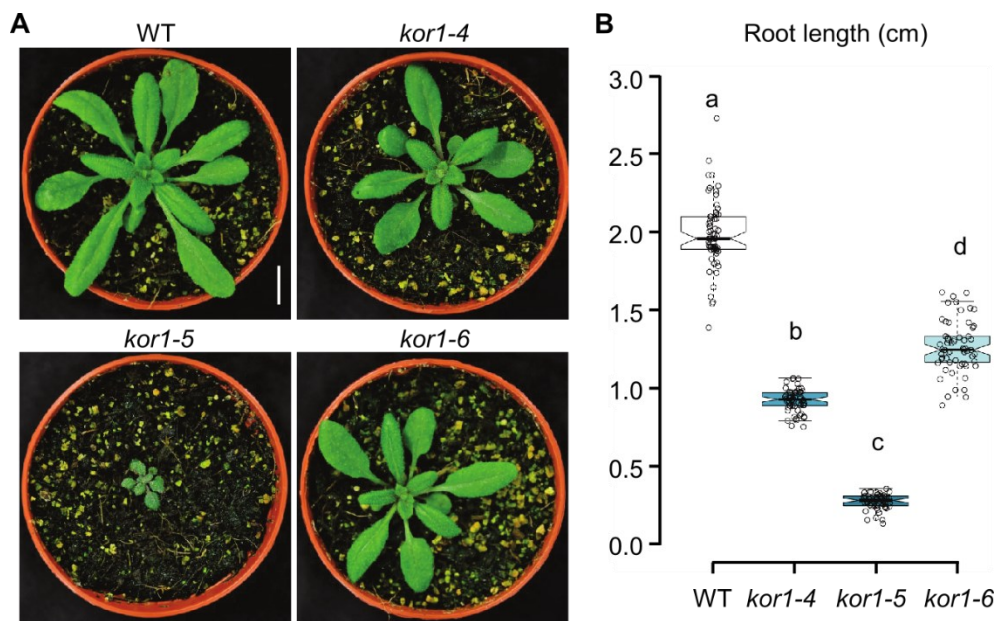


**Figure S1: *kor1* mutants show stunted growth.** (A) Representative 4-week-old rosettes of WT and *kor1* mutants grown in constant light. (B) Box plot summary of primary root length from 7-day seedlings in indicated genotypes. Medians are represented inside the boxes by solid lines, circles depict individual measurements ( $n = 51-61$ ). Letters denote statistically significant differences among samples as determined by ANOVA followed by Tukey's HSD test ( $P < 0.05$ ). Scale bars (A) = 1cm.

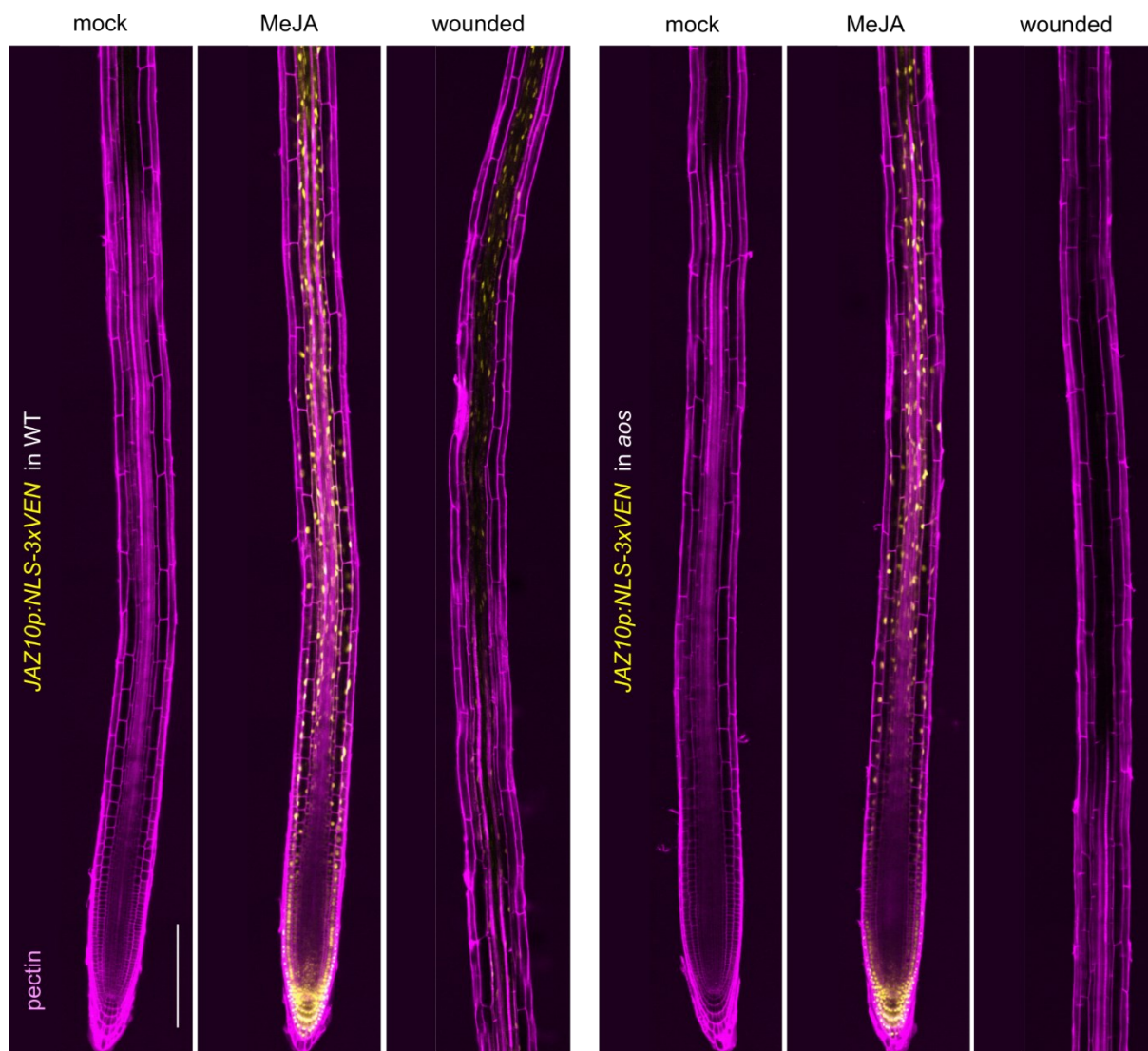


**Figure S2: Basal and induced *JAZ10p:NLS-3xVEN* reporter induction in WT and JA-deficient *aos* seedlings.** *JAZ10p:NLS-3xVEN* reporter expression in 5-d-old WT and *aos* roots at mock (basal) conditions, 2 h after 10  $\mu$ M MeJA treatment and 3 h after cotyledon wounding (n = 10). Cell wall pectins were counterstained with propidium iodide. Note that the reporter is activated broadly in WT and *aos* after MeJA treatment while after wounding activation is constrained to vascular tissues in the late differentiation zone in WT only. Scale bar = 200  $\mu$ m.

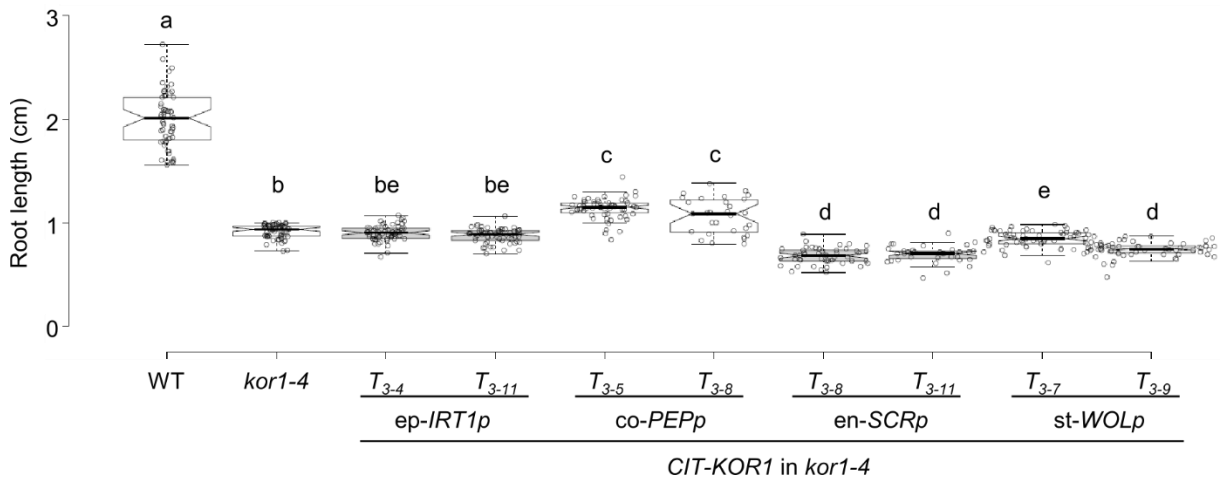


**Figure S3: Cortex-specific KOR1 expression partially complements the reduced root length of *kor1-4*.** Box plot summary of primary root length of 7-day seedlings in indicated genotypes. Medians are represented inside the boxes by solid lines, circles depict individual measurements (n = 30-60), and letters denote statistically significant differences among samples as determined by ANOVA followed by Tukey's HSD test (P < 0.05). Note that WT and *kor1-4* samples are in common with the data set presented in Fig. 7C.

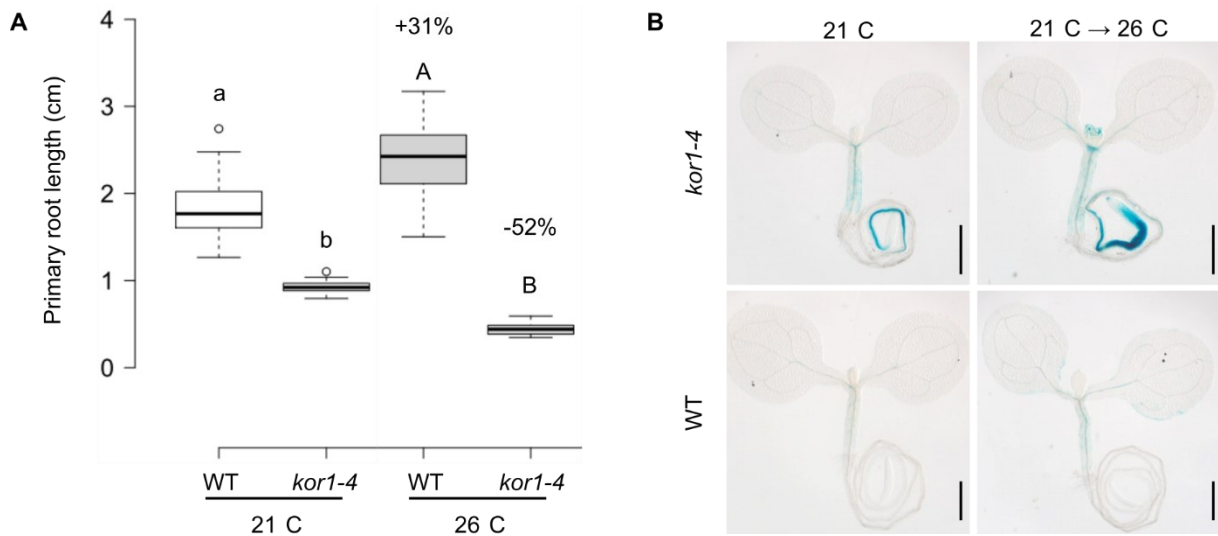


**Figure S4: Elevated temperature intensifies growth and JA-Ile signalling phenotypes in *kor1-4*.** (A) Box plot summary of primary root length of 7-day-old WT and *kor1-4* plants grown continuously at either 21°C or 26°C. Medians are represented inside the boxes by solid lines (n = 39-51), and letters denote statistically significant differences among samples as determined by ANOVA followed by Tukey's HSD test (P < 0.05) for each treatment individually. Differences in root length caused by temperature were calculated for each genotype and are displayed as percentage. (B) Representative images of *JGP* reporter expression in 5-day-old seedlings of WT and *kor1-4* at different temperatures revealed by GUS staining. Plants were grown either continuously at 21°C or shifted 24h prior staining from 21°C to 26°C. Scale bars = 0.5 mm.

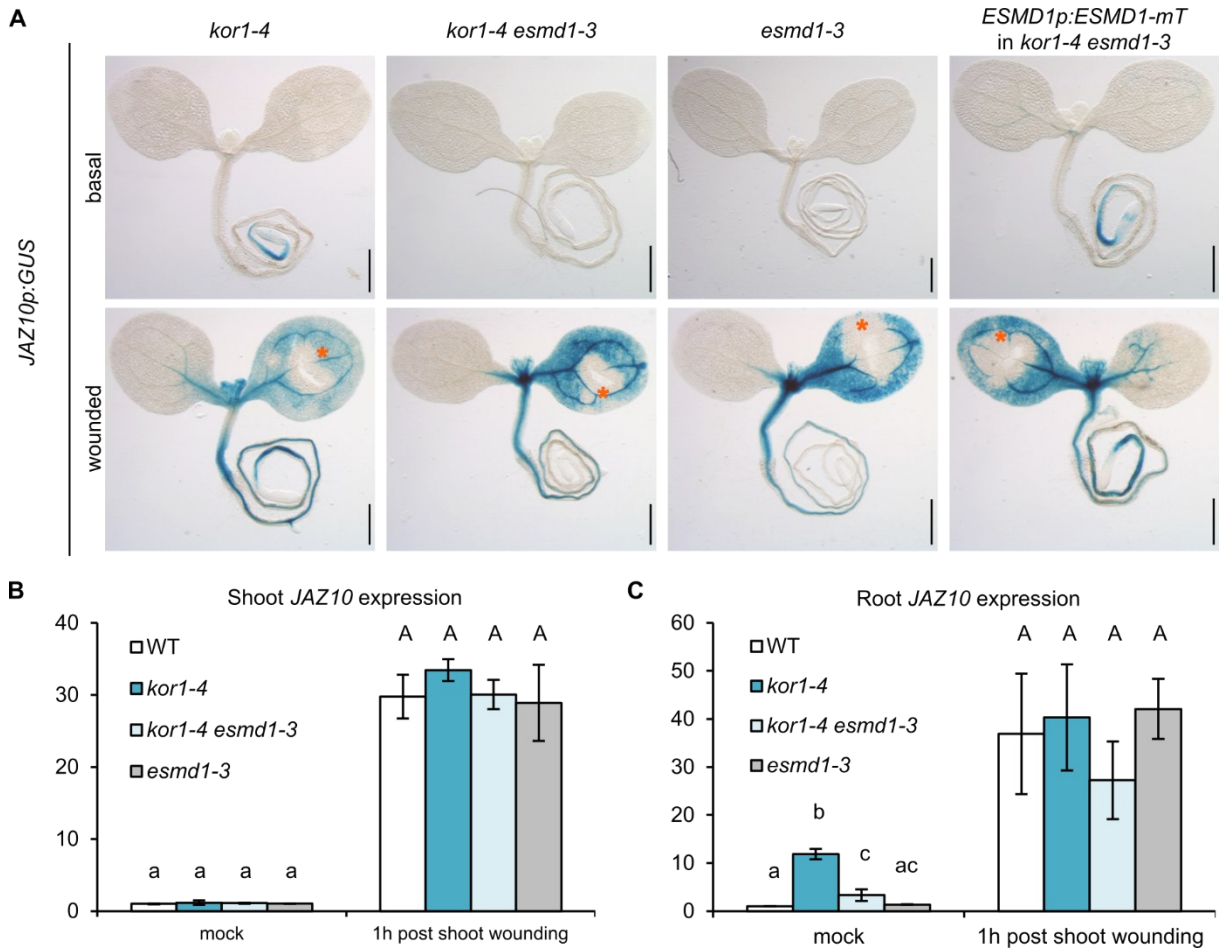


**Figure S5: ESMD1 does not regulate JA-Ile signalling upon wounding.** (A) *JAZ10p:GUS* expression in *kor1-4*, *kor1-4 esmd1-3*, *esmd1-3*, and *kor1-4 esmd1-3* complemented with *ESMD1p:ESMD1-mT* at basal conditions and 2 h after cotyledon wounding (orange asterisks). Scale bars = 0.5 mm. (B and C) qRT-PCR of *JAZ10* expression in (B) shoots and (C) roots of indicated genotypes basally and 1 h post cotyledon wounding. *JAZ10* transcript levels were normalized to those of *UBC21*. Bars represent the means of 3 biological replicates ( $\pm$ SD), each containing a pool of ~60 organs from 5-day seedlings. Letters in (B, C) denote statistically significant differences among samples as determined by ANOVA followed by Tukey's HSD test ( $P < 0.05$ ).

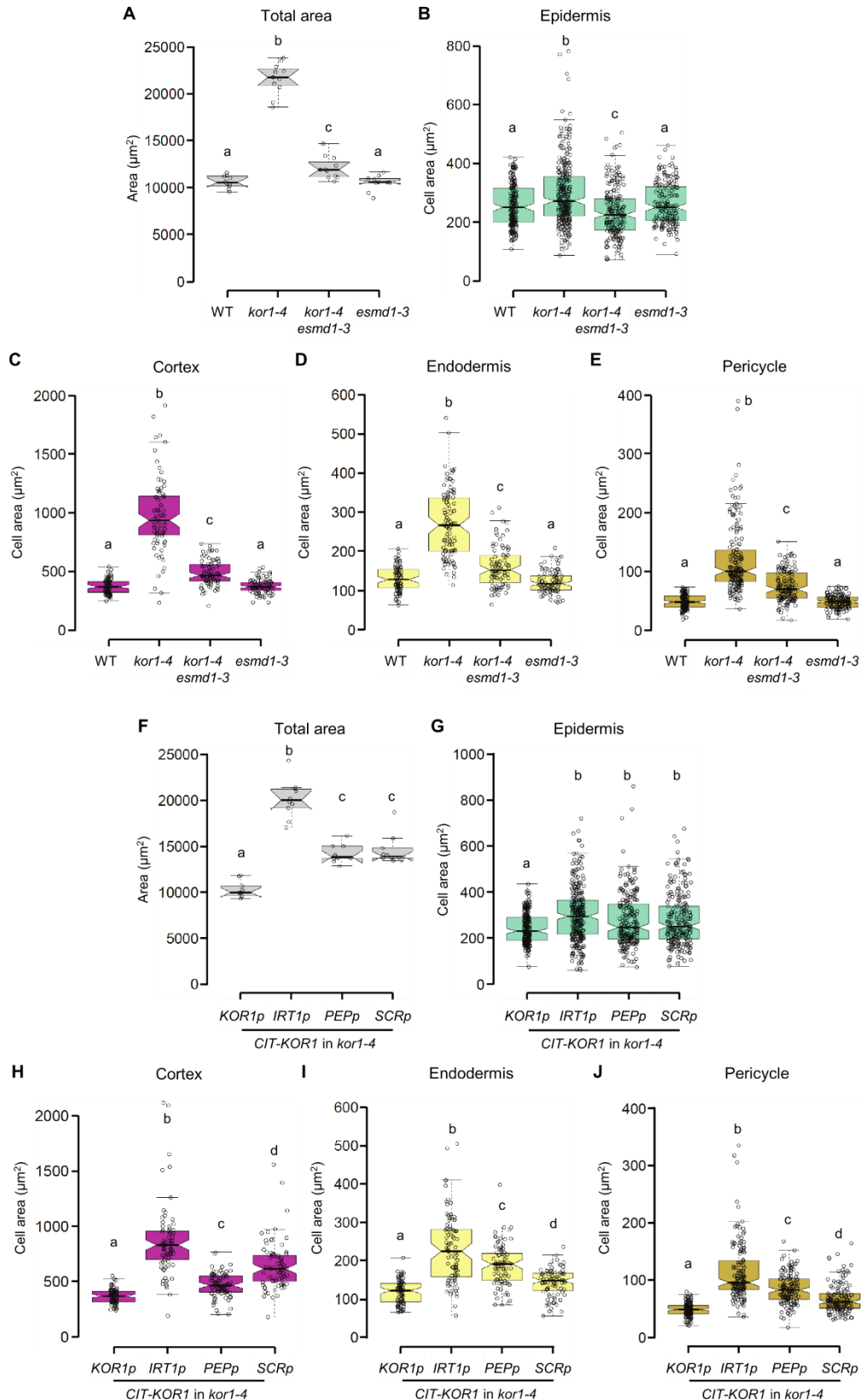


**Figure S6: Cellular measurements in transverse root sections of *kor1*, its suppressor *kor1 esmd1*, and cell-type-specific CIT-KOR1 expression lines. (A to J)** Box plot summary of (A and F) primary root total area, and cell-type specific areas in (B and G) epidermis, (C and H) cortex, (D and I) endodermis, and (E and J) pericycle cells from transverse sections of the early differentiation zone in indicated genotypes of 5-day seedlings. Medians are represented inside the boxes by solid lines, circles depict individual cell measurements from 10-11 roots. Letters denote statistically significant differences among samples as determined by ANOVA followed by Tukey's HSD test ( $P < 0.05$ ).

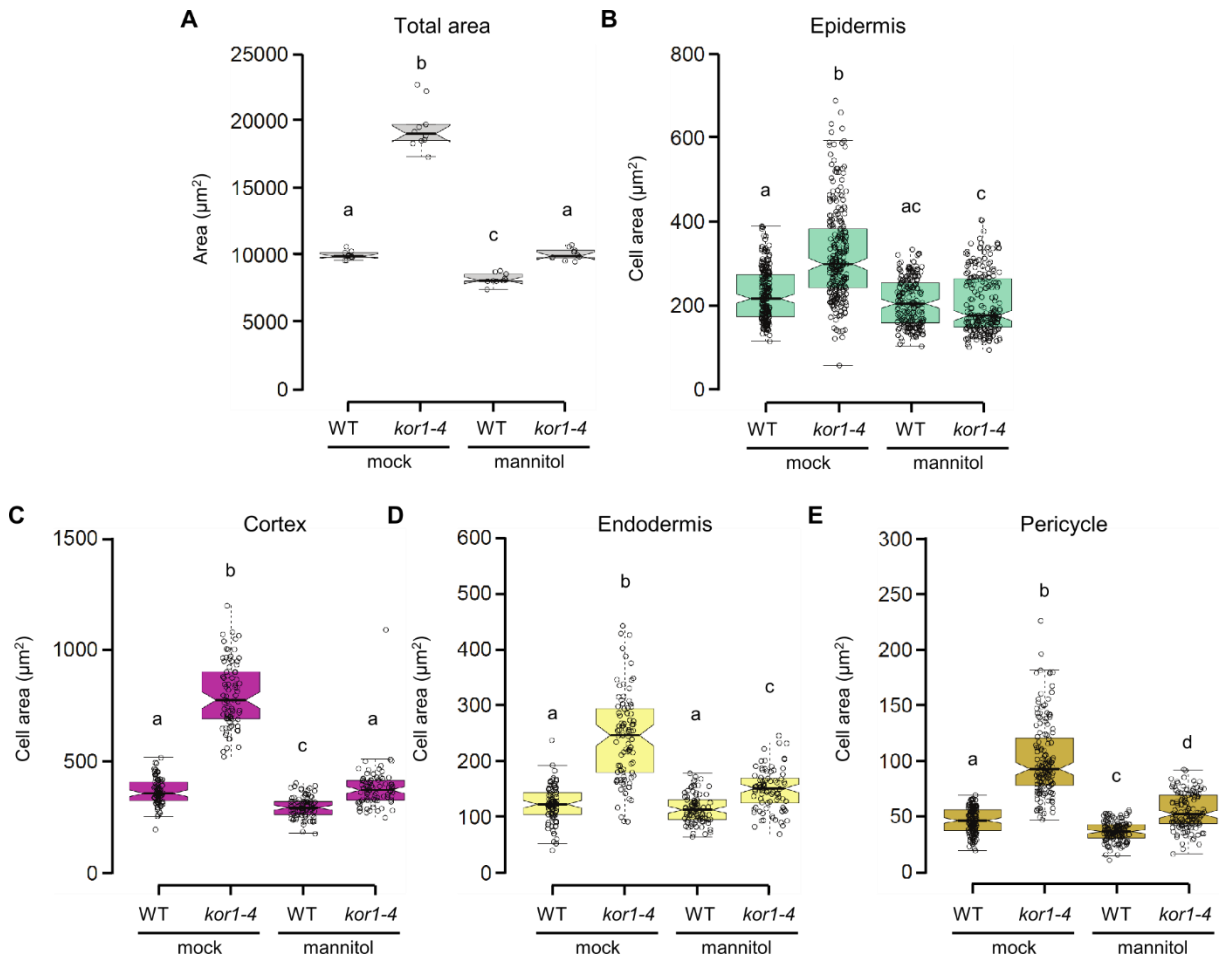


**Figure S7: Cellular measurements in transverse root sections of *kor1* grown at basal or hyperosmotic conditions.** (A to E) Box plot summary of (A) primary root total area, and cell-type specific areas of (B) epidermis, (C) cortex, (D) endodermis, and (E) pericycle cells from transversal cross sections of the early differentiation zone in WT and *kor1-4* 5-do seedlings, grown in the absence or presence of 3% mannitol. Medians are represented inside the boxes by solid lines, circles depict individual cell measurements from 10 roots. Letters denote statistically significant differences among samples as determined by ANOVA followed by Tukey's HSD test (P < 0.05). Measurements were performed by Dr. Mukesh K. Meena under my supervision.



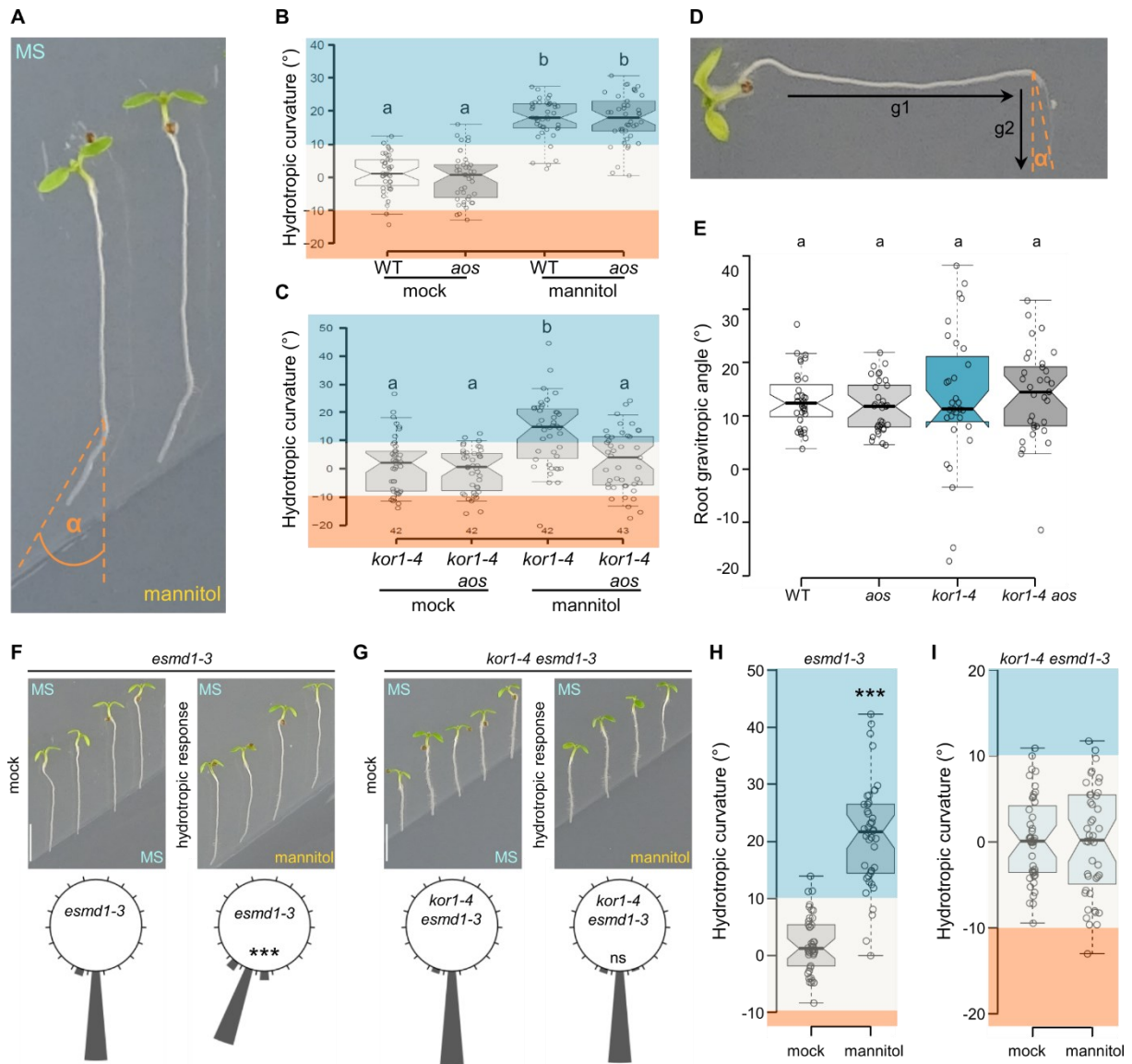


**Figure S8: Measurements of *kor1* root hydrotropic and gravitropic responses.** (A to C) Root hydrotropic responses in indicated genotypes. (A) Representative image of a WT seedling 24 h after transfer to a split-agar plate under hydrotropism-inducing conditions (MS/400 mM mannitol) depicting the measurement of its hydrotropic root curvature angle ( $\alpha$ ). Box plot summary of root hydrotropic curvatures in (B) WT and *aos*, and (C) *kor1-4* and *kor1-4 aos* seedlings 24 h after transfer to split-agar (MS/MS, mock) or hydrotropism-inducing (MS/400 mM mannitol) plates. Medians are represented inside the boxes by solid lines, circles depict individual measurements ( $n = 42$ ). Hydrotropic responses were highlighted as positive (blue, towards greater water availability), neutral (light grey, straight growth) and negative (orange, towards lower water availability) along the y-axis. (D and E) Root gravitropic responses in indicated genotypes. (D) Representative image depicting a WT seedling grown vertically for 5-d in the 1<sup>st</sup> gravity direction ( $g_1$ ), turned by 90° and grown for additional 24 h in the 2<sup>nd</sup> gravity vector ( $g_2$ ) before measuring the gravitropic root curvature angle ( $\alpha$ ). (E) Box plot summary of the root gravitropic angle of WT, *aos*, *kor1-4*, and *kor1-4 aos* seedlings. Medians are represented inside the boxes by solid lines, circles depict individual measurements ( $n = 31-35$ ). (F to I) Root hydrotropic response of (F) *esmd1-3* and (G) *kor1-4 esmd1-3* seedlings. Representative images and circular histograms summarizing root curvatures of indicated genotypes 24 h after transfer to split-agar MS plates under mock (MS/MS) or hydrotropism-inducing (MS/400 mM mannitol) conditions. Bars indicate the percentage of seedlings exhibiting a root bending angle assigned to one of the 18 20° sectors on the circular diagram,  $n = 42-43$ . Scale bars = 5 mm. (H and I) Box plot summary of individual measurements from (F and G). No statistically significant (ns) difference between treatments was found for *kor1-4 esmd1-3* by Student's t-test (G and I). Letters and asterisks indicate statistically significant differences as determined by Two-Way-ANOVA followed by Tukey's HSD test ( $P < 0.05$ ) in (B, C and E) and by Student's t-test ( $P < 0.001$ ) in (F and H).

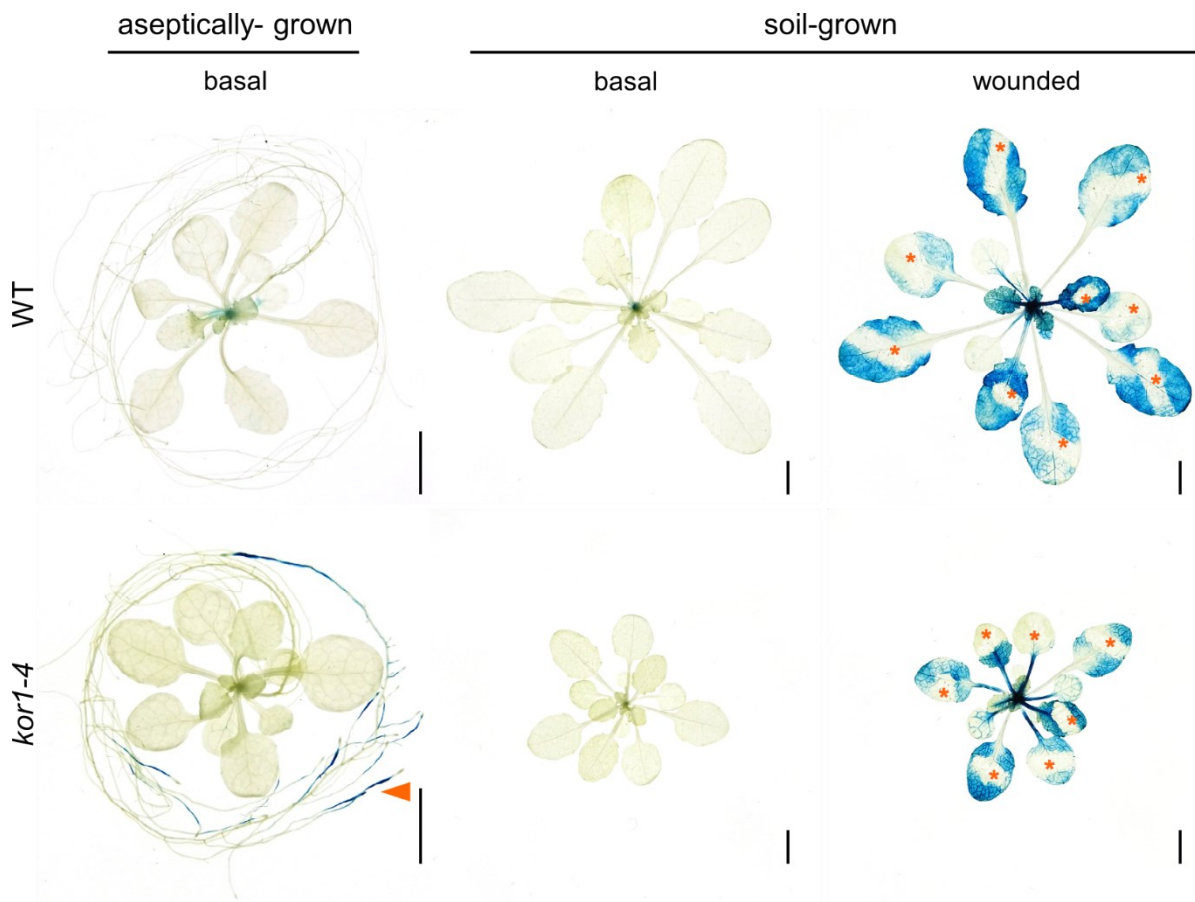


**Figure S9: Adult *kor1* rosettes do not exhibit ectopic JA-Ile signalling.** *JAZ1op:GUS* expression in 4-weeks-old aseptically grown plants or 5-weeks-old soil-grown rosettes of WT and *kor1-4* at basal conditions and 2 h after cotyledon wounding (orange asterisks). Note the presence of ectopic reporter activity in *kor1-4* roots (orange arrowhead) and reporter activation in wounded leaves (orange asterisks) while the signal is absent in aerial organs. Scale bars = 0.5 cm.

**Table S1: Overview on different mutant alleles of *KORz* in Arabidopsis**

Allele	Mutation	Identification	KO or KD?	Phenotype	Reference(s)
<i>kor1-1</i> ( <i>korrigan 1-1</i> )	T-DNA insertion in promoter	Combined T-DNA- and EMS-mutagenesis screen for mutants with short etiolated hypocotyls	KD	decreased etiolated hypocotyl length; short roots; reduced size of stems, rosette leaves, flowers and siliques; cells collapse or fail to expand; increased radial expansion of hypocotyl cells	(Nicol et al., 1998)
<i>kor1-2</i> ( <i>korrigan 1-2</i> )	T-DNA insertion in promoter	T-DNA-mutagenesis screen for mutants with defects in shoot organogenesis (callus formation)	KD	impaired cell division and cell elongation; cells are randomly divided and misshapen; aberrant cell plates; incomplete cell walls and multinucleated cells; shoot apical meristem forms calli instead of leaves; sterile	(Zuo et al., 2000)
<i>rsw2-1</i> ( <i>radial swelling 2-1</i> )	Gly429Arg	EMS-mutagenesis screen for mutants that show temperature-sensitive radial swelling of primary roots	n.d.	temperature-sensitive allele (phenotype stronger at 31°C than 21°C); radial swelling of root and hypocotyl; short bolts; smaller sepals and petals; distorted pistils; short stamen filaments; rare self-pollination; reduced cellulose content in roots and shoots; salt-sensitive	(Lane et al., 2001) (Kang et al., 2008)
<i>rsw2-3</i> ( <i>radial swelling 2-3</i> )	Ser183Asn	EMS-mutagenesis screen for mutants that show temperature-sensitive radial swelling of primary roots	n.d.	similar to <i>rsw2-1</i>	(Lane et al., 2001)
<i>rsw2-4</i> ( <i>radial swelling 2-4</i> )	Gly344Arg	EMS-mutagenesis screen for mutants that show temperature-sensitive radial swelling of primary roots	n.d.	similar to <i>rsw2-1</i>	(Lane et al., 2001)
<i>acw1</i> ( <i>altered cell wall 1</i> )	Gly429Arg	EMS-mutagenesis screen for mutants with altered cell wall composition by exhibiting swollen roots	n.d.	similar to <i>rsw2-1</i> (same mutation)	(Sato et al., 2001)
<i>irx2-1</i> ( <i>irregular xylem 2-1</i> )	Pro250Leu	EMS-mutagenesis screen for mutants with collapsed xylems by staining seedling stem sections with toluidine blue	KD	slight dwarf phenotype; decreased etiolated hypocotyl length; collapsed xylem cells; decreased cellulose content in secondary cell wall	(Szyjanowicz et al., 2004)

**Table S1 (continued)**

Allele	Mutation	Identification	KO or KD?	Phenotype	Reference(s)
<i>irx2-2</i> ( <i>irregular xylem 2-2</i> )	Pro553Leu	EMS-mutagenesis screen for mutants with collapsed xylems by staining seedling stem sections with toluidine blue	KD	similar to <i>irx2-1</i>	(Szyjanowicz et al., 2004)
<i>tsd1</i> ( <i>tumorous shoot development 1</i> )	Gly126Glu	EMS-mutagenesis screen for mutants that grow calli	n.d.	decreased etiolated hypocotyl length; swollen hypocotyl; early growth arrest of roots and cotyledons; shoot apical meristem forms calli instead of leaves; seedlings form no apical hook; sterile; altered auxin and cytokinin response	(Frank et al., 2002) (Krupkova et al., 2007)
<i>kor1-3</i> ( <i>korrigan 1-3</i> )	Thr343Ile	EMS-mutagenesis screen to identify factors that affect microtubule organization; seedlings were screened for root swelling after treatment with microtubule-destabilizing drug oryzalin	n.d.	short swollen roots; decreased etiolated hypocotyl length; altered microtubule organization; phenotype temperature-sensitive (abolished over 29°C)	(Paredes et al., 2008)
<i>jia1</i> ( <i>jiaoyao 1</i> )	Ala577Val	EMS-mutagenesis screen for mutants that show a root-swelling phenotype	KD	decreased etiolated hypocotyl length; short and radially swollen root; small siliques; cellulose deficient; altered microtubule organization	(Lei et al., 2014)

Abbreviations: KO = knockout; KD = knockdown; n.d. = not determined

**Table S2: Differentially expressed JA-dependent genes in *kor1-4* roots**

AGI code <sup>A</sup>	<i>aos</i>	logFC <sup>B</sup>		<i>aos</i>	p-value <sup>C</sup>		Description
		<i>kor1-4</i>	<i>kor1-4 aos</i>		<i>kor1-4</i>	<i>kor1-4 aos</i>	
<b>JA pathway</b>							
AT1G17420	0.35	5.01	1.64	6.6E-02	1.9E-08	6.0E-03	lipoxigenase 3 (LOX3)
AT5G13220	-0.07	3.43	0.27	8.1E-01	1.3E-35	2.1E-01	jasmonate-zim-domain protein 10 (JAZ10)
AT3G55970	0.03	2.18	0.08	9.1E-01	8.6E-05	7.1E-01	jasmonate oxygenase 3 (JOX3)
AT5G07010	0.26	1.34	0.23	1.6E-01	1.8E-15	1.8E-01	sulfotransferase 2A (SOT15)
<b>Secondary metabolism</b>							
AT3G44860	-0.01	8.27	-0.02	9.1E-01	1.2E-09	9.1E-01	farnesoic acid carboxyl-O-methyltransferase (FAMT)
AT3G44870	-0.22	4.70	-0.13	9.0E-02	5.9E-15	5.1E-01	farnesoic acid methyl transferase-like (FAMT-L)
AT4G13300	0.51	3.37	0.12	4.2E-02	2.3E-10	5.7E-01	terpenoid synthase 13 (TPS13)
AT5G42600	-0.02	2.66	0.18	9.4E-01	2.5E-08	4.1E-01	marneral synthase (MRN1)
AT5G24140	-0.05	2.03	0.60	8.3E-01	1.8E-20	4.8E-03	squalene monooxygenase 2 (SQP2)
AT3G29110	0.09	1.55	0.49	-	4.8E-03	7.2E-02	Terpenoid cyclases/Protein prenyltransferases superfamily protein (TPS16)
AT5G24160	0.82	1.54	0.74	4.4E-03	3.7E-05	2.0E-02	squalene monooxygenase 6 (SQE6)
AT3G60140	1.01	1.48	0.61	1.8E-04	8.9E-08	1.6E-02	Glycosyl hydrolase superfamily protein (BGLU30)
AT5G48110	0.36	1.38	0.36	8.3E-03	2.2E-34	3.8E-03	Terpenoid cyclases/Protein prenyltransferases superfamily protein
AT1G21100	0.35	1.38	0.40	1.4E-01	2.5E-07	8.0E-02	O-methyltransferase family protein (IGMT1)
AT2G32860	0.02	-1.34	-0.13	-	7.0E-03	5.2E-01	beta glucosidase 33 (BGLU33)
AT5G26000	-0.04	-1.35	0.01	7.8E-01	6.2E-03	9.5E-01	thioglucoside glucohydrolase 1 (TGG1)
AT5G54060	-0.44	-1.51	-0.19	2.4E-02	4.3E-03	3.5E-01	UDP-glucose:flavonoid 3-o-glucosyltransferase (A3G2XYLT)
AT5G17220	-0.21	-1.58	-0.65	4.0E-01	5.8E-04	4.3E-02	glutathione S-transferase phi 12 (GSTF12)
AT5G17050	-0.64	-1.60	-0.68	7.2E-03	1.5E-10	4.0E-03	UDP-glucosyl transferase 78D2 (UGT78G2)
AT2G47460	-0.90	-1.77	-0.41	2.2E-05	1.2E-17	3.2E-02	myb domain protein 12 (MYB12)
AT3G21560	-0.42	-1.80	-0.59	6.1E-02	1.6E-13	8.7E-03	UDP-Glycosyltransferase superfamily protein (UGT84A2)
AT3G25820	-0.22	-2.24	-0.20	1.1E-01	1.8E-03	2.7E-01	terpene synthase-like sequence-1.8-cineole (TPS27)
<b>Amino acid metabolism</b>							
AT2G24850	0.33	7.78	1.20	1.1E-01	9.2E-26	1.1E-02	tyrosine aminotransferase 3 (TAT3)
AT3G47340	1.08	3.57	1.32	2.2E-04	4.0E-26	5.5E-05	glutamine-dependent asparagine synthase 1 (ASN1)
AT5G38710	0.74	2.43	1.01	1.1E-03	9.3E-30	6.1E-06	Methylenetetrahydrofolate reductase family protein (POX2)
AT1G03090	0.64	1.63	0.45	8.0E-03	2.4E-10	4.3E-02	methylcrotonyl-CoA carboxylase alpha chain, mitochondrial / 3-methylcrotonyl-CoA carboxylase 1 (MCCA)
AT1G64660	0.42	1.38	0.49	7.3E-02	8.8E-08	3.4E-02	methionine gamma-lyase (MGA)
<b>Response to stress</b>							
AT5G17960	0.75	3.46	1.30	7.2E-03	9.7E-10	3.9E-03	Cysteine/Histidine-rich C1 domain family protein
AT5G56550	2.50	3.22	0.62	1.1E-15	6.5E-27	1.9E-02	oxidative stress 3 (OXS3)
AT1G23870	1.63	2.99	1.49	2.8E-08	2.6E-22	9.2E-07	trehalose-phosphatase/synthase 9 (TPS9)
AT1G70290	1.74	2.90	1.26	7.9E-21	5.9E-56	3.0E-11	trehalose-6-phosphatase synthase S8 (TPS8)
AT4G38470	1.29	2.81	1.21	4.1E-10	4.9E-40	2.1E-08	ACT-like protein tyrosine kinase family protein (STY46)
AT4G22214	-0.22	2.71	0.34	3.9E-01	5.8E-16	1.5E-01	Defensin-like (DEFL) family protein
AT4G35770	0.77	1.67	0.29	5.0E-03	3.9E-07	2.0E-01	Rhodanese/Cell cycle control phosphatase protein (STR15)
AT5G02020	0.36	1.58	0.61	1.5E-01	1.9E-07	2.3E-02	Salt induced serine rich (SIS)
AT2G33830	0.25	1.46	-0.10	2.7E-01	6.4E-10	6.4E-01	Dormancy/auxin associated family protein (DRMH1)

AT4G39770	0.33	1.39	0.31	1.9E-01	9.1E-06	1.8E-01	Haloacid dehalogenase-like hydrolase (HAD) protein (TPPH)
AT5G59720	-0.55	-1.33	-0.56	3.5E-02	6.4E-04	5.7E-02	heat shock protein 18.2 (HSP18.2)
AT5G49480	-0.69	-1.33	-0.51	1.9E-03	2.4E-10	1.1E-02	Ca <sup>2+</sup> -binding protein 1 (ATCP1)
AT4G25380	-0.41	-1.41	-0.58	1.0E-01	4.2E-04	5.1E-02	stress-associated protein 10 (SAP10)
AT3G15353	-1.03	-1.42	-0.66	6.74E-05	6.44E-08	7.31E-03	metallothionein 3 (MT3)
AT2G42540	-0.17	-1.52	-0.08	-	4.6E-03	6.4E-01	cold-regulated 15a (COR15A)
AT4G17670	-0.66	-1.54	-0.76	6.9E-03	1.0E-08	2.9E-03	Protein of unknown function (DUF581)
AT5G24655	-0.64	-1.90	-0.39	1.5E-02	1.5E-04	1.3E-01	response to low sulfur 4 (LSU4)
AT1G53130	-0.76	-2.06	-0.37	2.3E-04	1.8E-22	4.4E-02	Stigma-specific Stig1 family protein (GRI)
AT3G50610	-0.65	-2.75	-0.60	1.2E-02	2.6E-13	2.6E-02	C-terminally encoded peptide 9 (CEP9)

#### Other metabolic processes

AT1G15330	1.18	5.93	2.29	1.5E-03	2.3E-14	9.0E-04	Cystathionine beta-synthase (CBS) protein (PV42A)
AT1G32970	-0.17	4.56	-0.17	3.9E-01	3.0E-12	4.0E-01	Subtilisin-like serine endopeptidase family protein (SBT3.2)
AT5G20250	2.46	3.78	1.58	1.7E-17	1.9E-41	1.5E-08	Raffinose synthase family protein (DIN10)
AT5G19110	0.23	3.03	0.70	2.8E-01	5.6E-43	1.2E-03	Eukaryotic aspartyl protease family protein
AT5G65690	0.86	2.76	1.26	2.8E-05	8.5E-45	2.9E-10	phosphoenolpyruvate carboxykinase 2 (PCK2)
AT1G30820	1.15	2.75	1.37	1.6E-08	2.6E-40	4.9E-11	CTP synthase family protein
AT5G18670	1.86	2.70	1.00	3.4E-22	3.8E-46	3.2E-07	beta-amylase 3 (BAM9)
AT5G24490	0.85	2.61	0.66	5.8E-04	2.5E-26	5.1E-03	30S ribosomal protein. putative
AT5G24200	-0.05	2.51	0.47	8.2E-01	1.4E-04	9.1E-02	alpha/beta-Hydrolases superfamily protein
AT1G80380	0.72	2.12	0.61	3.1E-03	4.6E-17	9.0E-03	P-loop containing nucleoside triphosphate hydrolases superfamily protein (GLYK)
AT3G57520	0.92	2.09	0.93	4.1E-04	4.1E-14	5.3E-04	seed imbibition 2 (RFS2)
AT4G39650	-0.20	1.69	0.33	4.2E-01	4.8E-05	1.7E-01	gamma-glutamyl transpeptidase 2 (GGT2)
AT3G21720	0.55	1.56	0.58	1.3E-02	2.8E-12	6.8E-03	isocitrate lyase (ICL)
AT3G14050	0.93	1.51	0.71	3.5E-05	6.3E-12	1.1E-03	RELA/SPOT homolog 2 (RSH2)
AT3G23080	0.31	1.45	0.46	1.7E-01	8.7E-10	3.8E-02	Polyketide cyclase/dehydrase and lipid transport superfamily protein
AT3G51450	0.16	1.38	0.58	4.4E-01	6.1E-15	1.4E-03	Calcium-dependent phosphotriesterase superfamily protein (SSL7)
AT4G36880	0.22	-1.36	-0.44	2.7E-01	6.7E-12	2.2E-02	cysteine proteinase1 (CP1)
AT3G04330	-0.49	-1.46	-0.23	3.4E-02	4.6E-08	2.6E-01	Kunitz family trypsin and protease inhibitor protein
AT2G46390	-1.19	-1.51	-0.55	2.74E-04	3.38E-05	4.97E-02	Succinate dehydrogenase 8 (SDH8)
AT2G27420	-0.18	-1.74	-0.24	4.3E-01	1.1E-03	2.8E-01	Cysteine proteinases superfamily protein
AT1G61130	-0.12	-2.05	-0.53	6.5E-01	6.0E-04	7.5E-02	serine carboxypeptidase-like 32 (SCPL32)

#### Other cellular processes

AT2G26380	-0.13	5.05	2.28	5.0E-01	1.1E-14	2.6E-04	Leucine-rich repeat (LRR) family protein
AT2G02710	1.49	2.45	1.35	4.9E-14	1.8E-34	3.1E-11	PAS/LOV protein B (TLP1)
AT1G28330	1.08	2.42	0.42	1.4E-07	3.0E-32	3.3E-02	dormancy-associated protein-like 1 (DRM1)
AT3G07250	0.45	2.01	0.82	7.4E-02	1.1E-05	2.0E-02	nuclear transport factor 2 (NTF2) family protein / RNA recognition motif (RRM)-containing protein
AT5G05490	0.30	1.76	0.33	2.3E-01	4.8E-06	1.7E-01	Rad21/Rec8-like family protein (SYN1)
AT1G14640	0.73	1.70	0.71	8.6E-03	2.6E-05	2.7E-02	SWAP (Suppressor-of-White-APricot)/surp domain-containing protein
AT4G28703	0.27	1.58	0.14	3.0E-01	5.3E-06	5.2E-01	RmlC-like cupins superfamily protein
AT1G80920	0.49	1.44	0.36	3.9E-02	5.7E-08	9.9E-02	DnaJ-domain superfamily protein (ATJ8)
AT4G24230	0.42	1.38	0.20	5.4E-02	1.0E-09	3.0E-01	acyl-CoA-binding domain 3 (ACBP3)
AT3G45930	-0.86	-1.39	-0.64	3.3E-03	8.7E-05	3.2E-02	Histone superfamily protein
AT3G11120	-0.80	-1.45	-0.59	5.3E-03	1.5E-03	5.8E-02	Ribosomal protein L41 family (RPL41G)

AT5G02120	-0.46	-1.49	-0.44	6.5E-02	1.2E-05	8.1E-02	one helix protein (OHP1)
AT4G01150	-0.43	-1.50	-0.41	6.7E-02	6.1E-08	7.3E-02	NA
AT1G66725	-1.11	-1.73	-0.76	8.0E-05	1.5E-08	6.2E-03	MIR163; miRNA
AT4G28660	-0.82	-1.78	-0.71	9.9E-04	3.2E-12	3.0E-03	photosystem II reaction center PSB28 protein (PSB28)
AT5G65340	-0.14	-2.39	-1.05	6.0E-01	1.9E-08	2.5E-03	MIZU-KUSSEI-like protein
AT3G22840	-0.98	-2.81	-1.17	4.1E-04	3.1E-19	1.0E-04	Chlorophyll A-B binding family protein (ELIP1)
AT3G44450	-1.33	-2.87	-0.55	2.1E-04	2.0E-09	5.6E-02	Blue light inhibitor of cryptochromes 2 (BIC2)
AT3G25655	-0.81	-3.02	-1.29	3.3E-03	5.3E-13	1.0E-04	inflorescence deficient in abscission (IDA)-like 1 (IDL1)

#### Regulation of transcription

AT2G25900	2.70	3.82	1.37	1.5E-23	1.0E-48	2.5E-07	Zinc finger C-x8-C-x5-C-x3-H type family protein (ATCTH)
AT3G48390	0.62	2.55	0.17	1.9E-02	3.8E-11	4.4E-01	MA3 domain-containing protein
AT2G15890	1.38	2.32	0.44	4.6E-08	2.7E-18	5.0E-02	maternal effect embryo arrest 14 (MEE14)
AT1G13260	1.23	2.27	0.96	4.9E-12	2.4E-37	1.6E-07	related to ABI3/VP1 1 (RAV1)
AT5G28770	1.08	2.27	0.94	2.3E-06	2.0E-22	6.8E-05	bZIP transcription factor family protein (BZIP63)
AT5G44260	1.01	1.94	0.85	3.7E-04	3.8E-10	3.6E-03	Zinc finger C-x8-C-x5-C-x3-H type family protein (TZF5)
AT5G43650	-0.01	1.49	0.59	-	5.3E-03	5.5E-02	basic helix-loop-helix (bHLH) DNA-binding protein (BHLH92)
AT2G19810	0.96	1.43	-0.01	1.1E-04	5.8E-09	9.7E-01	CCCH-type zinc finger family protein
AT4G30180	-0.51	-1.37	-0.37	4.4E-02	8.4E-04	1.5E-01	sequence-specific DNA binding transcription factor (BHLH146)
AT3G47710	-0.92	-1.38	-0.51	3.0E-03	7.5E-04	7.4E-02	BANQUO 3
AT5G48870	-1.02	-1.38	-0.66	1.1E-03	1.5E-04	3.0E-02	Small nuclear ribonucleoprotein family protein (LSM5)
AT3G02380	-0.18	-1.41	-0.06	4.8E-01	8.9E-04	7.8E-01	CONSTANS-like 2 (COL2)
AT3G58850	-0.72	-1.45	-0.33	3.1E-03	1.8E-08	1.1E-01	phy rapidly regulated 2 (PAR2)
AT2G28740	-1.03	-1.45	-0.61	7.9E-04	4.0E-05	3.4E-02	histone H4 (HIS4)
AT3G17609	-0.90	-1.49	-0.53	7.2E-04	9.2E-08	2.9E-02	HY5-homolog (HYH)
AT3G53730	-1.09	-1.55	-0.72	8.41E-04	7.57E-05	2.49E-02	Histone superfamily protein
AT4G01060	-0.53	-1.67	-0.41	2.9E-02	9.1E-04	1.2E-01	CAPRICE-like MYB3 (ETC3)
AT3G17185	-0.37	-1.68	-0.72	1.1E-01	6.5E-10	4.1E-03	TAS3/TASIR-ARF (TRANS-ACTING SIRNA3); other RNA
AT5G54470	-0.74	-1.79	-0.54	6.4E-03	2.3E-07	4.2E-02	B-box type zinc finger family protein
AT3G21890	-1.63	-2.49	-0.93	1.4E-05	4.2E-09	6.1E-03	B-box type zinc finger family protein (MIP1B)
AT4G15248	-1.02	-3.29	-0.84	2.0E-03	1.2E-07	2.2E-02	B-box type zinc finger family protein (MIP1A)

#### Cell wall organization & biogenesis

AT2G15880	2.75	3.47	1.32	1.4E-08	2.0E-13	1.3E-03	Leucine-rich repeat (LRR) family protein (PEX3)
AT4G31370	-0.10	2.20	0.95	6.7E-01	2.7E-05	1.6E-02	FASCICLIN-like arabinogalactan protein 5 precursor (FLA5)
AT2G27380	0.60	1.48	0.28	1.9E-02	1.2E-03	2.3E-01	extensin proline-rich 1 (EPR1)
AT4G18340	0.91	1.36	0.48	1.1E-09	2.5E-21	1.3E-03	Glycosyl hydrolase superfamily protein
AT5G49360	1.09	1.36	1.13	1.1E-06	1.2E-09	1.1E-06	beta-xylosidase 1 (BXL1)
AT5G36870	0.29	1.35	0.13	2.5E-01	5.1E-05	5.5E-01	glucan synthase-like 9 (CALS4)
AT1G10640	-0.01	-1.33	-0.29	9.8E-01	2.1E-03	2.2E-01	Pectin lyase-like superfamily protein
AT1G05650	-0.11	-1.38	-0.55	6.5E-01	7.3E-10	9.7E-03	Pectin lyase-like superfamily protein
AT4G16980	-0.10	-1.99	-0.28	7.3E-01	3.6E-06	2.3E-01	arabinogalactan-protein family
AT3G17130	-0.58	-3.18	-1.14	2.7E-02	1.1E-08	3.0E-03	Plant invertase/pectin methylesterase inhibitor superfamily protein

#### Oxidation-reduction process

AT3G59710	-0.03	3.45	0.81	9.1E-01	6.0E-84	3.0E-05	NAD(P)-binding Rossmann-fold superfamily protein
AT3G49620	-0.01	2.19	0.05	9.1E-01	1.9E-03	7.6E-01	2-oxoglutarate (2OG) and Fe(II)-dependent oxygenase superfamily protein (DIN11)

AT4G13310	0.49	1.48	-0.41	5.6E-02	4.9E-05	1.2E-01	cytochrome P450. family 71. subfamily A. polypeptide 20 (CYP71A20)
AT5G61440	1.19	1.39	0.37	5.9E-12	5.9E-16	3.2E-02	atypical CYS HIS rich thioredoxin 5 (ACHT5)
AT5G51480	-0.03	1.37	0.66	8.9E-01	3.3E-03	4.8E-02	SKU5 similar 2 (SKS2)
AT1G45145	-0.97	-1.43	-0.70	1.7E-03	1.7E-04	2.6E-02	thioredoxin H-type 5 (TRX5)
AT1G08500	-0.36	-1.47	-0.66	5.4E-02	3.1E-15	2.5E-04	early nodulin-like protein 18 (ENODL18)
AT4G30470	-0.48	-1.68	-0.81	4.6E-03	6.5E-28	1.6E-07	NAD(P)-binding Rossmann-fold superfamily protein

#### Hormone biosynthesis & signalling

AT3G48360	2.43	3.50	0.94	1.2E-18	1.4E-39	3.6E-04	BTB and TAZ domain protein 2 (BT2)
AT1G06160	-0.09	2.33	0.52	6.6E-01	1.9E-04	7.6E-02	octadecanoid-responsive Arabidopsis AP2/ERF 59 (ERF094)
AT3G23230	0.21	1.93	0.44	1.6E-01	2.3E-03	9.2E-02	Integrase-type DNA-binding superfamily protein (ERF098)
AT4G34410	0.06	1.82	0.33	-	3.2E-03	1.3E-01	redox responsive transcription factor 1 (ERF109)
AT1G74710	-0.01	1.74	0.75	9.8E-01	2.9E-13	1.4E-03	Isochorismate synthase 1 (ICS1)
AT4G37610	1.27	1.71	0.59	5.0E-12	2.2E-20	1.4E-03	BTB and TAZ domain protein 5 (BT5)
AT1G44090	0.04	1.69	0.62	-	3.8E-03	5.1E-02	gibberellin 20-oxidase 5 (GA20OX5)
AT5G61590	0.74	1.60	0.73	2.9E-03	1.0E-10	2.8E-03	Integrase-type DNA-binding superfamily protein (ERF107)
AT1G80340	-0.04	-1.32	-0.52	9.1E-01	3.3E-05	4.7E-02	gibberellin 3-oxidase 2 (GA3OX2)
AT5G45870	-0.28	-1.51	-0.43	2.3E-01	1.5E-03	1.1E-01	PYR1-like 12 (PYL12)
AT1G26210	-0.54	-1.57	-0.73	3.7E-02	6.0E-05	2.1E-02	SOB five-like 1 (SOFL1)
AT4G31320	-0.99	-1.76	-0.59	3.0E-05	2.4E-13	7.9E-03	SAUR-like auxin-responsive protein family
AT1G24020	-0.19	-2.02	-0.45	3.3E-01	1.2E-03	9.8E-02	MLP-like protein 423 (MLP423)

#### Transferases

AT1G15040	2.22	3.68	1.74	5.0E-21	1.0E-58	5.1E-14	Class I glutamine amidotransferase-like superfamily protein (GAT1_2.1)
AT5G22920	2.22	3.27	1.17	1.1E-15	3.0E-34	1.6E-05	CHY-type/CTCHY-type/RING-type Zinc finger protein (RZPF34)
AT3G06850	0.65	1.92	0.32	3.4E-03	4.6E-19	1.0E-01	2-oxoacid dehydrogenases acyltransferase family protein (BCE2)
AT2G30600	0.88	1.89	0.92	5.5E-04	6.0E-13	3.8E-04	BTB/POZ domain-containing protein
AT1G76410	0.02	1.83	0.43	9.5E-01	1.6E-08	8.1E-02	RING/U-box superfamily protein (ATL8)
AT3G53160	0.60	1.77	0.76	1.5E-02	1.5E-10	4.2E-03	UDP-glucosyl transferase 73C7 (UGT73C7)
AT1G35625	0.14	1.62	-0.09	2.8E-01	4.3E-03	5.5E-01	RING/U-box superfamily protein (RMR6)
AT5G16370	0.75	1.56	0.48	5.8E-04	3.8E-14	1.6E-02	acyl activating enzyme 5 (AAE5)
AT5G02502	-0.88	-1.47	-0.71	3.3E-03	2.2E-04	2.8E-02	Oligosaccharyltransferase (OST4B)
AT3G18710	-0.58	-1.50	-0.54	4.8E-03	6.9E-14	4.1E-03	plant U-box 29 (PUB29)
AT3G47180	-0.65	-1.60	-0.46	1.5E-02	2.1E-04	9.0E-02	RING/U-box superfamily protein
AT1G53680	-0.65	-1.63	-0.64	1.2E-02	1.4E-07	1.8E-02	glutathione S-transferase TAU 28 (GSTU28)
AT2G22590	-0.20	-1.72	-0.85	4.5E-01	1.4E-07	4.9E-03	UDP-Glycosyltransferase superfamily protein (UGT91A1)
AT4G15480	-0.26	-1.83	-0.91	2.9E-01	6.7E-10	1.3E-03	UDP-Glycosyltransferase superfamily protein (UGT84A1)

#### Transport

AT4G21680	0.61	2.95	1.45	1.1E-02	1.3E-27	1.2E-07	NITRATE TRANSPORTER 1.8 (NRT1.8)
AT3G45060	1.21	2.41	0.92	1.6E-08	9.8E-28	3.6E-05	high affinity nitrate transporter 2.6 (NRT2.6)
AT3G23550	0.08	2.15	0.48	7.8E-01	5.7E-13	5.2E-02	MATE efflux family protein (DTX18)
AT4G36670	0.84	1.69	0.07	2.5E-03	5.7E-08	7.8E-01	Major facilitator superfamily protein (PLT6)
AT5G49630	0.44	1.55	0.76	7.7E-02	7.4E-07	9.0E-03	amino acid permease 6 (AAP6)
AT1G72820	0.84	1.48	0.40	4.9E-06	4.5E-18	2.3E-02	Mitochondrial substrate carrier family protein
AT2G37280	0.58	1.43	0.67	2.4E-02	6.1E-06	1.7E-02	pleiotropic drug resistance 5 (PDR5)
AT5G10180	0.57	1.40	0.69	8.3E-03	4.1E-11	1.1E-03	sulfate transporter 2;1 (SULTR2;1)



AT1G68600	-0.23	-1.34	-0.20	-	6.7E-03	-	Aluminium activated malate transporter protein (ALMT5)
AT2G25680	-0.18	-1.40	-0.68	4.0E-01	7.6E-11	9.3E-04	molybdate transporter 1 (MOT1)
AT3G51600	-0.34	-1.41	-0.34	1.6E-01	2.0E-06	1.3E-01	lipid transfer protein 5 (LTP5)
AT5G35525	-0.44	-1.47	-0.34	8.1E-02	5.8E-05	1.5E-01	PLAC8 family protein (PCR3)
AT5G02270	-0.86	-1.51	-0.51	4.6E-04	4.5E-10	2.1E-02	non-intrinsic ABC protein 9
AT4G08570	-0.41	-1.52	-0.62	9.4E-02	5.9E-07	1.9E-02	Heavy metal transport/detoxification superfamily protein (NAP6)
AT5G23760	-0.76	-1.52	-0.73	7.1E-03	2.1E-04	2.6E-02	Copper transport protein family
AT5G23660	-0.19	-1.54	-0.29	4.2E-01	2.1E-03	2.2E-01	homolog of Medicago truncatula MTN3 (SWEET12)
AT5G09930	0.01	-1.78	-0.14	9.7E-01	9.2E-04	5.1E-01	ABC transporter family protein (ABCF2)
AT5G46610	-0.02	-2.07	-0.60	-	2.3E-03	5.6E-02	Aluminium activated malate transporter protein (ALMT14)
AT3G48740	0.02	-2.22	0.02	9.3E-01	1.0E-03	9.2E-01	Nodulin MtN3 family protein (SWEET11)

#### Other signalling processes

AT2G34180	1.67	2.49	0.87	1.1E-09	9.2E-19	1.3E-03	CBL-interacting protein kinase 13 (CIPK13)
AT2G22860	-0.26	2.45	0.36	3.0E-01	5.8E-18	1.1E-01	phytosulfokine 2 precursor (PKS2)
AT1G76640	-0.48	1.59	0.13	4.9E-02	8.6E-05	5.4E-01	Calcium-binding EF-hand family protein (CML39)
AT5G21940	0.91	1.57	0.10	9.1E-04	1.2E-07	6.6E-01	hybrid signal transduction histidine kinase M-like protein
AT2G17050	0.64	1.44	0.31	1.7E-02	7.6E-05	1.9E-01	disease resistance protein (TIR-NBS-LRR class). putative
AT1G55350	0.86	1.37	0.48	1.5E-03	1.4E-06	4.8E-02	calpain-type cysteine protease family (DEK1)
AT5G23730	-0.39	-1.33	-0.45	1.6E-02	1.5E-18	2.3E-03	Transducin/WD40 repeat-like superfamily protein (RUP2)
AT5G09990	-0.34	-1.47	-0.27	1.5E-01	1.8E-03	2.4E-01	elicitor peptide 5 precursor (PEP5)
AT3G52740	-0.96	-1.52	-0.44	3.1E-04	3.8E-08	5.6E-02	Blue light inhibitor of cryptochromes 1 (BIC1)
AT3G44735	-0.77	-1.79	-0.47	3.4E-03	2.6E-09	4.8E-02	Phytosulfokine 6 precursor (PSK6)
AT2G43290	-0.77	-1.85	-0.82	2.1E-03	1.3E-12	1.0E-03	Calcium-binding EF-hand family protein (CML5)

#### Unclassified or unknown

AT3G15450	2.20	3.78	1.47	7.0E-12	1.8E-33	2.1E-06	Aluminium induced protein with YGL and LRDR motifs
AT4G15990	-0.03	3.01	1.12	9.1E-01	1.3E-10	4.5E-03	NA
AT3G45730	0.80	2.91	0.85	4.8E-03	1.3E-14	9.0E-03	NA
AT3G15630	1.41	2.51	0.97	3.9E-12	1.0E-33	4.8E-06	NA
AT2G17880	0.84	2.18	0.64	3.5E-03	8.9E-09	3.0E-02	DnaJ-domain superfamily protein
AT4G32480	1.46	2.04	0.13	1.8E-08	4.1E-14	5.3E-01	Protein of unknown function (DUF506)
AT5G14120	0.80	1.73	0.42	3.2E-03	1.9E-08	8.0E-02	Major facilitator superfamily protein
AT2G25460	0.34	1.66	0.72	9.8E-02	1.8E-16	5.1E-04	NA
AT1G52110	0.20	1.61	0.73	4.2E-01	2.8E-04	3.2E-02	Mannose-binding lectin superfamily protein
AT5G19120	0.93	1.61	0.22	7.6E-05	3.1E-12	2.7E-01	Eukaryotic aspartyl protease family protein
AT2G32150	0.53	1.61	0.40	1.1E-02	2.4E-15	4.0E-02	Haloacid dehalogenase-like hydrolase (HAD) superfamily protein
AT1G11185	-0.21	1.56	0.43	4.3E-01	1.5E-05	9.6E-02	other RNA
AT1G35830	0.48	1.55	0.34	5.6E-02	2.6E-04	1.7E-01	VQ motif-containing protein
AT4G19980	0.48	1.46	0.63	3.8E-02	3.4E-09	8.1E-03	NA
AT3G26240	0.96	1.44	0.56	2.8E-04	9.9E-08	2.2E-02	Cysteine/Histidine-rich C1 domain family protein
AT3G49790	0.82	1.37	0.61	1.5E-03	1.5E-07	1.2E-02	Carbohydrate-binding protein
AT1G02060	0.77	1.35	0.45	5.2E-03	2.6E-05	7.6E-02	Tetratricopeptide repeat (TPR)-like superfamily protein
AT4G19160	0.87	1.34	0.31	3.9E-07	1.2E-16	6.0E-02	NA
AT1G73750	0.39	1.33	0.66	1.2E-01	5.8E-05	2.4E-02	Uncharacterised conserved protein UCPO31088
AT4G34419	-0.50	-1.33	-0.45	3.6E-02	2.7E-03	1.0E-01	NA

AT1G75700	-0.54	-1.33	-0.65	3.5E-02	1.5E-03	4.2E-02	HVA22-like protein G (HVA22G)
AT5G55650	-0.41	-1.34	-0.27	1.0E-01	1.2E-03	2.4E-01	NA
AT1G67920	-0.73	-1.36	-0.50	7.1E-03	3.9E-05	5.6E-02	NA
AT5G13880	-0.39	-1.38	-0.32	1.3E-01	3.0E-04	1.8E-01	NA
AT2G18969	-0.78	-1.38	-0.18	6.2E-03	6.3E-04	4.0E-01	NA
AT5G57345	-0.81	-1.38	-0.34	3.5E-03	1.9E-05	1.4E-01	NA
AT3G25795	-0.34	-1.40	-0.67	1.6E-01	1.4E-03	4.1E-02	other RNA
AT1G54530	-0.70	-1.45	-0.32	7.9E-03	2.8E-06	1.6E-01	putative calcium-binding EF hand family protein
AT5G26790	-0.51	-1.45	-0.24	4.3E-02	2.4E-05	2.8E-01	NA
AT1G62045	-0.56	-1.51	-0.46	3.1E-02	2.2E-05	7.4E-02	NA
AT4G37608	-0.73	-1.52	-0.61	8.6E-03	4.1E-05	3.7E-02	NA
AT2G30230	-0.92	-1.53	-0.44	3.4E-04	8.3E-09	5.0E-02	NA
AT2G15020	-0.20	-1.53	-0.06	2.7E-01	4.1E-03	7.8E-01	NA
AT1G54540	-0.54	-1.53	-0.51	5.4E-04	2.2E-28	1.4E-04	Late embryogenesis abundant (LEA) hydroxyproline-rich glycoprotein family
AT1G61930	-0.66	-1.54	-0.57	1.1E-02	1.6E-06	3.2E-02	Protein of unknown function. DUF584
AT4G33145	-0.47	-1.56	-0.51	3.2E-02	2.7E-03	8.0E-02	NA
AT3G07425	-0.71	-1.57	-0.57	9.0E-03	8.3E-04	6.2E-02	NA
AT2G43340	-0.94	-1.60	-0.75	1.3E-04	1.3E-10	1.8E-03	Protein of unknown function (DUF1685)
AT1G13670	-0.76	-1.61	-0.58	1.3E-03	7.8E-12	7.5E-03	NA
AT5G15725	-0.76	-1.64	-0.69	6.9E-03	5.9E-05	2.9E-02	NA
AT1G76220	-0.63	-1.64	-0.40	1.9E-02	4.5E-05	1.1E-01	Arabidopsis protein of unknown function (DUF241)
AT4G28088	-0.24	-1.67	-0.63	-	3.7E-03	5.4E-02	Low temperature and salt responsive protein family
AT2G02300	-0.34	-1.70	-0.81	1.8E-01	2.2E-06	8.5E-03	phloem protein 2-B5 (PP2B5)
AT5G20790	-0.94	-1.73	-0.34	2.3E-04	8.2E-11	1.1E-01	NA
AT1G72240	-1.03	-1.73	-0.10	2.9E-04	5.8E-08	6.4E-01	NA
AT1G55230	-0.15	-1.80	-0.47	5.6E-01	1.6E-03	9.5E-02	Family of unknown function (DUF716)
AT3G63160	-0.33	-1.80	-0.11	1.1E-01	1.5E-03	6.1E-01	NA
AT3G52900	-0.92	-1.81	-0.81	1.9E-03	6.4E-07	9.8E-03	Family of unknown function (DUF662)
AT5G37550	-1.02	-1.88	-0.83	2.4E-04	8.3E-10	3.2E-03	NA
AT4G04745	-1.11	-1.94	-1.00	1.2E-04	1.4E-09	1.0E-03	NA
AT3G18470	-0.24	-1.95	-0.19	-	2.7E-03	3.2E-01	PLAC8 family protein (PCR7)
AT3G21680	-0.82	-2.00	-0.94	1.4E-03	4.7E-13	3.7E-04	NA
AT4G08555	-0.95	-2.02	-0.67	1.6E-03	1.0E-07	2.5E-02	NA
AT2G17972	-0.31	-2.20	-0.45	2.1E-01	4.3E-05	9.9E-02	NA
AT3G56290	-1.16	-2.26	-1.11	1.1E-06	3.4E-19	8.6E-06	NA
AT1G04800	-0.16	-2.51	0.02	3.3E-01	1.2E-03	9.1E-01	glycine-rich protein
AT3G22235	-0.14	-2.70	-0.68	5.1E-01	5.7E-04	4.5E-02	NA
AT4G27657	-0.54	-3.04	-1.27	2.6E-02	1.4E-05	6.7E-03	NA

<sup>A</sup> Differentially expressed genes (DEG) in 5-do *kor1-4* roots relative to WT samples. Each genotype was first normalized to the WT (cutoff: logFC =  $\pm 1.32$ , p-value < 0.01), and *kor1-4* DEGs were classified as JA-dependent if their value remained at least 50% changed in *kor1-4 aos* with respect to *kor1-4*. DEGs are organized by gene ontology (GO) functional classes and implemented manually. In many cases genes may fall into more than one category. DEGs highlighted in magenta were selected for further analyses.

<sup>B</sup> Logarithmic Fold Change of the means of two biological replicated experiments. A negative number indicates down regulated genes.

<sup>C</sup> False Discovery rate (FDR) corrected p-value in comparison to WT.

NA: not annotated

**Table S3: Differentially expressed JA-independent genes in *kor1-4* roots**

AGI code <sup>A</sup>	logFC <sup>B</sup>			p-value <sup>C</sup>			Description
	<i>aos</i>	<i>kor1-4</i>	<i>kor1-4 aos</i>	<i>aos</i>	<i>kor1-4</i>	<i>kor1-4 aos</i>	
<b>Cell wall organization &amp; biogenesis</b>							
AT1G64160	-0.01	9.55	9.63	9.1E-01	1.7E-12	3.5E-12	Disease resistance-responsive (dirigent-like protein) family protein (DIR5)
<b>AT4G28850</b>	0.10	5.99	6.78	4.3E-01	2.4E-06	5.9E-07	xyloglucan endotransglucosylase/hydrolase 26 (XTH26)
AT1G06520	0.06	5.96	6.66	7.2E-01	4.7E-09	1.8E-10	glycerol-3-phosphate acyltransferase 1 (GPAT1)
AT1G61080	0.62	4.70	4.42	8.4E-03	1.0E-07	1.8E-06	Hydroxyproline-rich glycoprotein family protein
AT2G20520	0.55	4.09	4.31	3.1E-02	2.1E-36	6.1E-40	FASCICLIN-like arabinogalactan 6 (FLA6)
AT2G01610	0.15	3.42	4.00	5.7E-01	2.0E-15	3.6E-20	Plant invertase/pectin methylesterase inhibitor superfamily protein
<b>AT4G13390</b>	0.67	3.10	3.32	1.4E-02	5.9E-12	7.7E-13	Proline-rich extension 12 (EXT12)
AT5G20230	0.33	2.81	2.86	1.9E-01	9.0E-10	1.8E-09	blue-copper-binding protein (BCB)
AT1G54970	0.54	2.81	3.09	3.0E-02	7.8E-19	5.9E-22	proline-rich protein 1 (PRP1)
AT3G27400	0.36	2.60	3.16	1.4E-01	6.9E-17	6.4E-24	Pectin lyase-like superfamily protein
AT5G06640	0.79	2.60	2.45	5.4E-03	1.1E-10	2.9E-09	Proline-rich extensin-like family protein
<b>AT1G11920</b>	0.18	2.58	3.03	4.8E-01	9.8E-10	4.0E-12	Pectin lyase-like superfamily protein (PLL6)
AT2G24980	0.71	2.56	2.58	9.4E-03	2.1E-11	4.5E-11	Proline-rich extensin-like family protein
AT5G06630	0.74	2.53	2.77	6.9E-03	8.8E-12	4.2E-13	proline-rich extensin-like family protein
AT3G45960	0.39	2.35	3.33	1.2E-01	1.8E-06	5.1E-10	expansin-like A3 (EXLA3)
AT5G48070	0.29	1.94	1.98	9.2E-02	1.6E-35	9.7E-37	xyloglucan endotransglucosylase/hydrolase 20 (XTH20)
AT5G57560	0.02	1.92	2.77	9.5E-01	1.0E-12	7.3E-24	Xyloglucan endotransglucosylase/hydrolase family protein (XTH22)
AT1G09460	1.11	1.92	1.02	1.6E-08	7.9E-23	3.7E-07	Carbohydrate-binding X8 domain superfamily protein
AT2G45220	0.68	1.91	2.09	9.9E-03	5.1E-09	6.2E-10	Plant invertase/pectin methylesterase inhibitor superfamily (PME17)
AT4G11655	0.34	1.71	2.27	1.4E-01	5.1E-04	1.6E-04	CASP-LIKE PROTEIN 4A4 (CASPL4A4)
AT4G22080	0.27	1.71	1.94	1.8E-01	1.1E-20	6.0E-26	root hair specific 14 (RSH14)
AT5G19800	0.40	1.61	1.64	3.1E-02	1.8E-21	1.1E-21	hydroxyproline-rich glycoprotein family protein
AT2G43620	-0.08	1.60	2.32	7.4E-01	1.3E-16	1.3E-32	Chitinase family protein
AT1G76930	0.87	1.60	1.59	8.5E-04	4.2E-09	1.4E-08	extensin 4 (EXT4)
AT4G07960	0.40	1.47	1.52	3.0E-02	8.4E-18	2.0E-18	Cellulose-synthase-like C12 (CSLC12)
AT3G22800	0.63	1.42	1.14	5.3E-03	1.1E-10	6.5E-07	Leucine-rich repeat (LRR) family protein (LRX6)
AT5G04310	0.37	1.39	1.07	1.2E-01	3.4E-07	1.7E-04	Pectin lyase-like superfamily protein
AT2G31220	0.19	1.34	1.30	4.4E-01	8.3E-04	2.3E-03	basic helix-loop-helix (bHLH) DNA-binding superfamily protein (BHLH10)
AT3G15370	-0.13	1.33	1.83	5.8E-01	4.5E-09	2.5E-15	expansin 12 (EXPA12)
AT5G65390	-0.20	-1.33	-1.06	1.9E-01	7.8E-22	9.7E-14	arabinogalactan protein 7 (AGP7)
AT4G26490	-0.16	-1.38	-1.29	5.4E-01	5.0E-06	4.6E-05	Late embryogenesis abundant (LEA) hydroxyproline-rich glycoprotein family
AT4G03540	-0.50	-1.39	-0.88	3.1E-02	2.9E-08	4.7E-04	CASP-likeprotein 1C1 (CASPL1C1)
AT5G19730	0.20	-1.45	-1.03	4.2E-01	4.3E-07	3.4E-04	Pectin lyase-like superfamily protein (PME53)
AT2G43050	-0.06	-1.45	-1.00	8.0E-01	1.2E-10	8.6E-06	Plant invertase/pectin methylesterase inhibitor superfamily (PME16)
AT2G21100	-0.63	-1.46	-0.76	1.6E-02	4.3E-06	9.4E-03	Disease resistance-responsive (dirigent-like protein) family protein (DIR23)
AT2G46570	0.07	-1.49	-0.76	8.0E-01	5.1E-06	9.1E-03	laccase 6 (LAC6)
AT5G40730	-0.78	-1.51	-0.77	2.9E-03	6.4E-08	4.0E-03	arabinogalactan protein 24 (AGP24)
AT5G03170	-0.43	-1.52	-1.06	3.1E-02	2.7E-14	2.0E-07	FASCICLIN-like arabinogalactan-protein 11 (FLA11)

AT3G49330	-0.53	-1.61	-1.40	1.1E-02	1.3E-14	4.2E-11	Plant invertase/pectin methylesterase inhibitor superfamily protein
AT4G25830	-0.45	-1.61	-1.13	5.4E-02	2.1E-08	7.7E-05	CASP-LIKE PROTEIN 2C1
AT1G65310	-0.27	-1.66	-0.91	3.8E-02	7.2E-45	1.8E-14	xyloglucan endotransglucosylase/hydrolase 17 (XTH17)
AT5G24105	-0.85	-1.76	-1.21	1.5E-03	4.1E-09	3.6E-05	arabinogalactan protein 41 (AGP41)
AT5G26730	-0.74	-1.77	-1.32	7.7E-03	8.7E-06	6.8E-04	Fasciclin-like arabinogalactan family protein
AT1G43790	-0.85	-2.00	-1.32	2.5E-03	5.1E-09	8.4E-05	tracheary element differentiation-related 6 (TED6)
AT4G26320	-0.80	-2.25	-2.02	2.9E-03	5.8E-13	1.3E-10	arabinogalactan protein 13 (AGP13)
AT5G53250	-0.69	-2.27	-1.59	1.9E-04	1.4E-40	8.0E-21	arabinogalactan protein 22 (AGP22)
AT4G25250	-0.52	-2.32	-1.30	1.6E-03	4.3E-55	2.6E-19	Plant invertase/pectin methylesterase inhibitor superfamily protein (PMEI4)
AT5G44130	-0.34	-2.38	-2.52	6.6E-02	2.1E-35	2.2E-38	FASCICLIN-like arabinogalactan protein 13 precursor (FLA13)
AT1G55330	-0.93	-2.44	-1.58	3.8E-04	6.2E-18	1.5E-08	arabinogalactan protein 21 (AGP21)
AT2G18800	-0.64	-2.53	-2.38	6.7E-03	3.4E-22	1.6E-19	xyloglucan endotransglucosylase/hydrolase 21 (XTH21)
AT2G33790	0.04	-2.63	-1.61	8.7E-01	1.6E-32	8.8E-14	arabinogalactan protein 30 (AGP30)
AT5G15290	0.21	-3.31	-2.65	4.0E-01	2.9E-18	1.2E-13	Casparian strip membrane domain protein 5 (CASP5)

#### Oxidation-reduction process

AT5G05340	0.44	8.40	9.48	7.2E-02	2.7E-62	3.0E-79	Peroxidase 52 (PER52)
AT4G22710	0.11	6.50	7.31	6.0E-01	6.0E-18	5.2E-22	cytochrome P450, family 706, subfamily A, polypeptide 2 (CYP706A2)
AT4G26260	1.17	5.23	2.72	1.2E-04	1.5E-51	3.9E-14	myo-inositol oxygenase 4 (MIOX4)
AT2G18150	0.20	5.16	6.34	4.2E-01	3.7E-84	9.0E-128	Peroxidase superfamily protein (PER15)
AT5G52400	0.10	4.71	5.01	3.9E-01	8.6E-05	2.3E-04	cytochrome P450, family 715, subfamily A, polypeptide 1 (CYP715A1)
AT1G49570	0.02	4.32	4.01	9.5E-01	8.5E-23	3.7E-19	Peroxidase superfamily protein (PER10)
AT4G36430	-0.17	4.15	5.27	4.6E-01	4.2E-75	1.1E-120	Peroxidase superfamily protein (PER49)
AT5G44400	0.05	3.65	3.96	8.6E-01	1.1E-40	2.7E-47	FAD-binding Berberine family protein
AT1G34510	0.67	3.61	2.96	6.0E-03	3.7E-48	1.3E-31	Peroxidase superfamily protein (PER8)
AT5G06720	-0.29	3.61	4.11	2.4E-01	1.4E-38	1.3E-49	Peroxidase superfamily protein (PER53)
AT5G39580	0.80	3.51	3.66	6.1E-06	3.5E-113	1.1E-122	Peroxidase superfamily protein (PER62)
AT2G19800	1.06	2.88	1.74	6.2E-06	5.0E-33	4.5E-13	myo-inositol oxygenase 2 (MIOX2)
AT5G19880	0.33	2.84	5.46	1.2E-01	1.7E-05	6.2E-14	Peroxidase superfamily protein (PER58)
AT4G22690	0.29	2.82	3.34	2.6E-01	2.3E-15	1.5E-20	cytochrome P450, family 706, subfamily A, polypeptide 1 (CYP706A1)
AT5G06730	-0.10	2.81	3.52	6.7E-01	3.8E-49	7.9E-78	Peroxidase superfamily protein (PER54)
AT4G21840	0.16	2.66	2.09	5.5E-01	1.0E-12	3.0E-08	methionine sulfoxide reductase B8 (MSRB8)
AT5G19890	0.02	2.50	2.13	9.5E-01	2.5E-05	4.1E-04	Peroxidase superfamily protein (PER59)
AT1G30730	0.78	2.36	1.79	7.1E-05	2.3E-38	1.5E-22	FAD-binding Berberine family protein
AT3G30775	0.89	2.18	1.32	2.4E-07	3.6E-40	2.4E-15	Methylenetetrahydrofolate reductase family protein (POX1)
AT1G34540	0.02	2.17	2.45	9.6E-01	3.0E-07	4.6E-08	cytochrome P450, family 94, subfamily D, polypeptide 1 (CYP94D1)
AT4G08780	0.13	1.63	1.83	5.2E-01	3.6E-22	3.3E-27	Peroxidase superfamily protein (PER38)
AT4G08770	-0.43	1.52	1.81	1.8E-02	2.2E-19	2.5E-26	Peroxidase superfamily protein (PER37)
AT2G42850	0.01	1.39	1.62	9.8E-01	5.4E-09	3.5E-11	cytochrome P450, family 718 (CYP718)
AT1G14520	-0.15	-1.34	-1.08	5.8E-01	1.8E-04	2.6E-03	myo-inositol oxygenase 1 (MIOX1)
AT4G10040	-0.79	-1.37	-0.71	2.2E-03	3.4E-07	5.5E-03	cytochrome c-2 (CYTC2)
AT1G72230	-0.36	-1.40	-1.05	5.1E-02	6.8E-15	1.2E-08	Cupredoxin superfamily protein
AT2G02050	-1.01	-1.48	-0.87	1.3E-03	8.4E-05	1.1E-02	NADH-ubiquinone oxidoreductase B18 subunit, putative
AT5G15180	0.02	-1.59	-1.22	9.5E-01	1.8E-13	3.6E-08	Peroxidase superfamily protein (PER56)

AT3G01190	-0.23	-1.64	-1.18	1.1E-01	1.4E-37	1.2E-19	Peroxidase superfamily protein (PER27)
AT4G04840	-0.41	-1.69	-1.69	8.6E-03	4.9E-32	8.2E-32	methionine sulfoxide reductase B6 (MSRB6)
AT2G47380	-1.01	-1.69	-1.12	1.5E-03	3.0E-05	3.3E-03	Cytochrome c oxidase subunit Vc family protein
AT2G34810	-0.34	-1.77	-1.57	1.3E-01	7.9E-13	3.5E-10	FAD-binding Berberine family protein
AT2G23910	-0.32	-2.20	-1.57	2.0E-01	2.6E-11	1.5E-06	NAD(P)-binding Rossmann-fold superfamily protein

### Secondary metabolism

AT3G60120	0.21	7.22	8.71	9.6E-02	9.2E-08	4.9E-10	beta glucosidase 27 (BGLU27)
AT1G69920	-0.21	4.71	5.61	3.9E-01	1.9E-27	1.6E-38	glutathione S-transferase TAU 12 (GSTU12)
AT5G36150	1.10	4.34	3.73	7.3E-04	1.0E-24	7.5E-18	putative pentacyclic triterpene synthase 3 (PEN3)
AT4G02520	0.06	2.56	3.44	7.8E-01	1.3E-41	5.5E-74	glutathione S-transferase PHI 2 (GSTF2)
AT1G18570	0.33	2.48	3.10	1.1E-01	3.8E-35	1.1E-54	myb domain protein 51 (MYB51)
AT2G44460	0.58	2.41	1.47	1.3E-02	2.3E-04	6.5E-03	beta glucosidase 28 (BGLU28)
AT1G21130	0.38	1.97	2.40	7.0E-02	8.2E-22	1.3E-31	O-methyltransferase family protein (IGMT4)
AT1G02930	0.00	1.83	2.94	9.9E-01	4.8E-13	1.1E-29	glutathione S-transferase 6 (GSTF6)
AT1G21120	0.04	1.83	2.18	8.8E-01	8.1E-14	1.6E-18	O-methyltransferase family protein
AT1G59870	0.75	1.73	1.50	6.0E-03	1.9E-07	1.1E-05	ABC-2 and Plant PDR ABC-type transporter family protein (ABCG36)
AT1G61820	0.50	1.60	1.31	8.8E-03	1.7E-19	4.2E-13	beta glucosidase 46 (BGLU46)
AT5G28510	0.30	1.47	1.66	2.2E-01	5.1E-04	4.9E-04	beta glucosidase 24 (BGLU24)
AT3G56400	0.29	1.39	1.95	2.2E-01	7.4E-08	3.2E-13	WRKY DNA-binding protein 70 (WRKY70)
AT5G48850	-0.48	-1.38	-1.10	2.5E-02	7.5E-10	1.6E-06	Tetratricopeptide repeat (TPR)-like superfamily protein
AT4G25700	-0.20	-1.43	-0.86	3.9E-01	7.1E-09	4.4E-04	beta-hydroxylase 1 (BETA-OHASE1)
AT4G14090	-0.35	-1.46	-0.90	8.7E-02	3.9E-03	2.5E-02	UDP-Glycosyltransferase superfamily protein (UGT75C1)
AT1G04770	-0.82	-1.53	-1.04	1.2E-03	1.8E-09	5.8E-05	Tetratricopeptide repeat (TPR)-like superfamily protein
AT4G38620	-0.87	-1.64	-1.05	2.3E-06	1.5E-20	5.9E-09	myb domain protein 4 (MYB4)
AT1G07590	-1.13	-2.22	-1.82	7.4E-04	6.4E-07	4.4E-05	Tetratricopeptide repeat (TPR)-like superfamily protein

### Response to stress

AT4G33720	0.04	6.70	3.80	7.2E-01	5.9E-07	1.1E-03	CAP (Cysteine-rich secretory proteins, Antigen 5, and Pathogenesis-related 1 protein) superfamily protein (CAPE3)
AT3G23250	0.20	5.10	5.85	4.3E-01	1.5E-31	6.4E-41	myb domain protein 15 (MYB15)
AT1G19250	0.51	4.41	3.93	4.6E-02	3.5E-27	4.1E-21	flavin-dependent monooxygenase 1 (FMO1)
AT1G73805	0.08	3.85	4.64	7.6E-01	1.1E-10	2.5E-14	Calmodulin binding protein-like (SARD1)
AT1G19610	0.06	3.77	2.88	7.6E-01	3.4E-06	3.6E-04	Arabidopsis defensin-like protein (PDF1.4)
AT1G56060	0.04	3.66	6.67	7.3E-01	3.5E-04	3.9E-06	Cysteine-rich transmembrane module 3 (ATHCYSTM3)
AT4G12480	0.20	3.42	3.49	3.9E-01	6.1E-55	1.1E-56	Bifunctional inhibitor/lipid-transfer protein/seed storage 2S albumin superfamily protein (EARLI1)
AT1G72520	0.01	3.35	2.72	9.8E-01	1.7E-11	1.2E-07	PLAT/LH2 domain-containing lipoxygenase family protein (LOX4)
AT1G80840	0.79	3.33	2.59	2.3E-03	4.1E-36	2.6E-21	WRKY DNA-binding protein 40 (WRKY40)
AT1G07135	-0.06	3.11	3.95	8.4E-01	3.0E-14	8.7E-22	glycine-rich protein
AT3G04220	0.29	3.08	3.33	2.5E-01	9.0E-23	7.3E-26	Disease resistance protein (TIR-NBS-LRR class) family
AT5G01900	0.53	3.03	3.00	2.7E-02	1.9E-06	1.1E-05	WRKY DNA-binding protein 62 (WRKY62)
AT2G18700	1.63	3.01	1.73	3.7E-10	7.0E-30	8.1E-11	trehalose phosphatase/synthase 11 (TPS11)
AT1G32960	0.00	2.85	3.42	1.0E+00	3.6E-11	7.5E-15	Subtilase family protein (SBT3.3)
AT3G07350	1.03	2.67	1.70	4.2E-05	1.7E-25	4.6E-11	Protein of unknown function (DUF506)
AT3G50930	-0.16	2.65	3.40	4.7E-01	2.5E-40	6.2E-66	cytochrome BC1 synthesis (HSR4)
AT1G66090	-0.07	2.52	3.83	7.7E-01	4.7E-06	2.0E-10	Disease resistance protein (TIR-NBS class)

AT3G54150	0.13	2.30	3.31	6.2E-01	1.7E-18	7.7E-37	S-adenosyl-L-methionine-dependent methyltransferases superfamily protein
AT3G44260	0.09	2.23	3.11	7.5E-01	2.2E-07	1.1E-11	Polynucleotidyl transferase. ribonuclease H-like superfamily protein (CAF1-9)
AT4G35480	0.18	2.17	2.18	4.9E-01	2.3E-11	4.5E-11	RING-H2 finger A3B (ATL45)
AT2G46400	-0.24	2.14	3.53	3.5E-01	1.9E-07	3.8E-16	WRKY DNA-binding protein 46 (WRKY46)
AT1G59620	0.46	2.13	2.32	6.4E-02	5.3E-06	4.0E-06	Disease resistance protein (CC-NBS-LRR class) family (CW9)
AT4G12470	1.07	1.94	1.90	1.3E-05	8.7E-15	6.8E-14	azelaic acid induced 1 (AZI1)
AT1G60140	1.00	1.90	1.19	6.9E-10	1.8E-33	2.4E-13	trehalose phosphate synthase (TPS10)
AT2G40000	0.90	1.86	1.64	1.6E-06	8.9E-26	4.1E-20	ortholog of sugar beet HS1 PRO-1 2 (HSPRO2)
AT5G49520	0.38	1.70	1.78	8.5E-02	5.3E-14	9.8E-15	WRKY DNA-binding protein 48 (WRKY48)
AT1G15010	0.20	1.65	1.91	2.7E-01	2.7E-03	4.2E-03	mediator of RNA polymerase II transcription subunit
AT4G12490	-0.13	1.60	1.19	6.2E-01	1.9E-04	4.0E-03	Bifunctional inhibitor/lipid-transfer protein/seed storage 2S albumin superfamily protein
AT2G01340	0.22	1.56	1.63	3.9E-01	7.3E-07	8.5E-07	NA
AT4G25790	0.38	1.53	1.99	3.1E-02	1.4E-23	8.0E-39	CAP (Cysteine-rich secretory proteins. Antigen 5. and Pathogenesis-related 1 protein) superfamily protein
AT3G50950	0.27	1.49	1.75	1.0E-01	4.4E-24	3.1E-32	HOPZ-ACTIVATED RESISTANCE 1 (RPP13L4)
AT1G53990	0.30	1.45	1.18	1.9E-01	2.3E-09	3.3E-06	GDSL-motif lipase 3 (GLIP3)
AT1G31290	-0.13	1.41	3.21	2.9E-01	3.8E-03	9.3E-05	ARGONAUTE 3 (AGO3)
AT3G04070	0.55	1.39	1.84	1.0E-02	1.0E-11	2.8E-19	NAC domain containing protein 47 (NAC47)
AT1G69150	-0.03	1.35	0.71	9.2E-01	3.6E-06	1.0E-02	CYL-CoA-binding domain3 (ACBP3)
AT1G15890	0.54	1.35	0.76	1.9E-02	1.5E-08	1.6E-03	Disease resistance protein (CC-NBS-LRR class) family
AT3G03270	-0.52	-1.34	-1.09	3.3E-02	2.3E-06	2.0E-04	Adenine nucleotide alpha hydrolases-like superfamily protein
AT3G28210	-0.69	-1.38	-0.76	9.5E-03	1.8E-05	9.8E-03	zinc finger (AN1-like) family protein (SAP12)
AT3G05880	-0.60	-1.46	-1.62	1.6E-02	6.5E-07	1.6E-07	Low temperature and salt responsive protein family (RCI2A)
AT1G20450	-0.58	-1.47	-0.96	5.3E-05	1.2E-32	3.9E-14	Dehydrin family protein (ERD10)
AT3G07230	-1.04	-1.51	-0.80	9.4E-04	4.9E-05	1.4E-02	wound-responsive protein-related
AT1G52690	-0.02	-1.55	-0.87	9.5E-01	6.3E-05	9.9E-03	Late embryogenesis abundant protein (LEA) family protein (LEA7)
AT1G20440	-0.56	-1.55	-0.91	1.2E-03	6.2E-25	3.6E-09	cold-regulated 47 (COR47)
AT3G05890	-0.65	-1.64	-1.26	3.8E-03	2.5E-13	3.8E-08	Low temperature and salt responsive protein family (RCI2B)
AT5G23750	-0.72	-1.89	-1.40	6.2E-03	3.5E-09	1.3E-05	Remorin family protein
AT1G07500	-0.75	-2.09	-1.13	5.9E-03	2.2E-08	6.1E-04	Siamese related 5 (SMR5)
AT2G47770	-0.21	-2.28	-2.02	4.2E-01	8.4E-07	1.2E-05	TSPO(outer membrane tryptophan-rich sensory protein)-related (TSPO)
AT5G12020	-0.38	-2.60	-2.60	1.1E-01	2.1E-05	7.8E-05	17.6 kDa class II heat shock protein (HSP17.6)
AT5G47450	-0.27	-2.81	-2.34	2.1E-01	2.0E-32	5.3E-23	tonoplast intrinsic protein 2;3 (TIP2-3)

#### Ethylene biosynthesis and signalling

AT5G61890	0.10	6.26	5.95	5.6E-01	1.1E-09	2.3E-08	Integrase-type DNA-binding superfamily protein (ERF114)
AT2G44840	0.08	4.56	3.83	7.3E-01	2.2E-12	1.5E-08	ethylene-responsive element binding factor 13 (ERF13)
AT3G49700	0.20	4.19	4.97	1.1E-01	1.9E-04	2.6E-04	1-aminocyclopropane-1-carboxylate synthase 9 (ACS9)
AT5G07310	-0.01	3.57	4.36	9.1E-01	3.1E-04	4.0E-04	Integrase-type DNA-binding superfamily protein (ERF115)
AT5G21120	0.35	3.18	3.54	1.3E-01	1.8E-07	4.7E-08	ETHYLENE-INSENSITIVE3-like 2 (EIL2)
AT5G64750	0.34	3.09	1.81	1.7E-01	3.9E-10	1.2E-04	Integrase-type DNA-binding superfamily protein (ABR1)
AT4G08040	0.15	2.90	3.05	5.9E-01	1.1E-17	8.3E-19	1-aminocyclopropane-1-carboxylate synthase 11 (ACS11)
AT5G47220	0.21	2.67	2.13	3.6E-01	3.0E-06	1.9E-04	ethylene responsive element binding factor 2 (ERF2)
AT2G44940	-0.46	-1.47	-0.89	1.5E-03	1.4E-32	1.3E-12	Integrase-type DNA-binding superfamily protein (ERF034)

AT5G52020	-1.07	-1.95	-1.03	5.3E-04	1.3E-07	2.3E-03	Integrase-type DNA-binding superfamily protein (ERF025)
<b>Calcium signalling</b>							
AT2G41100	0.81	5.01	5.56	1.9E-04	1.1E-140	2.0E-173	Calcium-binding EF hand family protein TOUCH3 (TCH3)
AT3G22910	0.45	2.98	4.11	8.0E-02	1.7E-13	2.5E-24	ATPase E1-E2 type family protein / haloacid dehalogenase-like hydrolase family protein (ACA13)
AT3G17690	0.45	2.57	2.41	3.8E-02	2.4E-33	4.4E-29	cyclic nucleotide gated channel 19 (CNGC19)
AT3G47480	-0.01	2.44	3.62	9.8E-01	2.2E-09	4.3E-18	Calcium-binding EF-hand family protein (CML47)
AT4G01010	0.33	2.11	2.09	1.9E-01	1.4E-10	5.7E-10	cyclic nucleotide-gated channel 13 (CNGC13)
AT5G39670	0.02	2.07	3.22	9.6E-01	1.2E-06	5.2E-12	Calcium-binding EF-hand family protein (CML46)
AT5G26920	0.72	2.01	1.42	2.4E-03	2.2E-18	1.4E-09	Cam-binding protein 60-like G (CBP60G)
AT1G08860	0.09	1.44	2.31	4.1E-01	5.8E-03	5.3E-03	Calcium-dependent phospholipid-binding Copine family protein (BON3)
AT2G22300	0.47	1.38	1.05	4.6E-03	4.2E-22	1.0E-12	signal responsive 1 (CAMTA3)
AT2G44310	-0.91	-1.78	-1.26	2.9E-03	1.6E-05	1.5E-03	Calcium-binding EF-hand family protein
AT1G24620	-0.58	-1.78	-1.08	2.5E-02	4.6E-07	1.2E-03	EF hand calcium-binding protein family (CML25)
<b>Response to water deprivation</b>							
AT3G54820	0.08	1.73	1.47	7.6E-01	4.1E-11	4.0E-08	plasma membrane intrinsic protein 2;5 (PIP2-5)
AT3G13437	-0.58	-1.43	-1.59	2.6E-02	5.7E-04	6.9E-04	Enhancer of vascular wilt resistance 1 (EWR1)
AT2G37180	-0.12	-1.49	-1.57	3.4E-01	4.7E-43	3.3E-47	Aquaporin-like superfamily protein (PIP2-3)
AT3G24500	-0.72	-1.50	-1.12	6.7E-03	1.7E-06	4.0E-04	multi-protein bridging factor 1C (MBF1C)
AT5G52300	0.06	-1.53	-1.79	8.5E-01	1.9E-04	1.4E-04	CAP160 protein (LTI65)
AT3G50980	-0.30	-1.65	-1.15	2.2E-01	4.3E-04	6.5E-03	dehydrin xero 1 (XERO1)
AT4G20260	-0.78	-1.69	-1.15	1.1E-03	8.6E-13	2.0E-06	plasma-membrane associated cation-binding protein 1 (PCAP1)
AT5G15960	-0.54	-1.74	-1.20	3.6E-02	9.8E-07	6.0E-04	stress-responsive protein / stress-induced protein (KIN1)
AT1G67360	-0.72	-1.82	-1.21	5.4E-03	6.0E-10	4.3E-05	Rubber elongation factor protein (REF)
AT5G06760	-0.86	-3.50	-2.62	3.7E-03	2.5E-13	2.8E-08	Late Embryogenesis Abundant 4-5 (LEA4-5)
<b>Membrane ligands and receptors</b>							
AT1G70130	0.15	7.02	7.04	2.3E-01	2.1E-07	8.0E-07	Concanavalin A-like lectin protein kinase family protein (LECRK52)
AT4G11480	0.23	5.25	6.42	7.0E-02	3.2E-05	7.2E-06	cysteine-rich RECEPTOR-like protein kinase 32 (CRK32)
AT3G23120	-0.08	5.17	7.01	6.3E-01	2.0E-09	7.6E-16	receptor like protein 38 (RLP38)
AT2G34930	0.56	3.73	2.22	2.3E-02	2.3E-37	6.8E-14	disease resistance family protein / LRR family protein
AT3G46340	0.48	3.45	3.84	4.2E-02	2.2E-08	2.9E-09	Leucine-rich repeat protein kinase family protein
AT5G18470	-0.14	3.12	3.85	6.0E-01	6.5E-32	1.2E-47	Curculin-like (mannose-binding) lectin family protein
AT5G46330	0.04	2.97	4.09	8.2E-01	1.1E-04	1.3E-05	Leucine-rich receptor-like protein kinase protein (FLS2)
AT1G53440	0.58	2.69	2.25	1.2E-02	1.1E-27	1.5E-19	Leucine-rich repeat transmembrane protein kinase
AT4G23180	0.32	2.45	3.28	2.0E-01	3.3E-09	2.0E-14	cysteine-rich RECEPTOR-like protein kinase 10 (CRK10)
AT4G23260	0.31	2.37	2.42	2.2E-01	4.1E-08	7.4E-08	cysteine-rich RECEPTOR-like protein kinase 18 (CRK18)
AT2G32660	0.99	2.24	2.36	1.5E-03	8.0E-08	5.9E-08	receptor like protein 22 (RLP22)
AT3G59740	0.13	2.19	1.42	6.4E-01	1.9E-07	4.6E-04	Concanavalin A-like lectin protein kinase family protein (LECRK57)
AT1G33790	0.44	2.12	1.15	4.7E-02	5.7E-19	2.6E-06	jacalin lectin family protein (JAL4)
AT2G29000	-0.04	2.05	1.71	8.6E-01	6.9E-04	4.2E-03	Leucine-rich repeat protein kinase family protein
AT1G66920	0.01	1.92	2.48	9.9E-01	1.2E-04	2.2E-05	Protein kinase superfamily protein (LRK10L-2.4)
AT1G66830	0.01	1.88	3.20	9.8E-01	3.2E-04	2.0E-06	Leucine-rich repeat protein kinase family protein
AT1G78830	0.77	1.86	1.52	3.5E-03	2.3E-10	3.3E-07	Curculin-like (mannose-binding) lectin family protein
AT4G11470	0.18	1.71	2.82	4.2E-01	5.8E-04	1.7E-05	cysteine-rich RECEPTOR-like protein kinase 31 (CRK31)

AT1G51810	0.04	1.66	1.32	7.3E-01	4.0E-03	1.6E-02	Leucine-rich repeat protein kinase family protein
AT1G05700	0.25	1.64	1.29	2.0E-01	1.1E-18	1.7E-11	Leucine-rich repeat transmembrane protein kinase protein
AT1G45616	0.21	1.54	1.04	1.8E-01	4.4E-03	2.2E-02	receptor like protein 6 (RLP6)
AT2G29220	0.10	1.52	1.07	5.3E-01	4.7E-03	2.2E-02	Concanavalin A-like lectin protein kinase family protein (LECRK31)
AT5G40170	0.39	1.49	1.54	5.1E-02	5.6E-14	1.8E-14	receptor like protein 54 (RLP54)
AT1G71400	0.70	1.48	1.26	9.7E-04	4.7E-14	5.1E-10	receptor like protein 12 (RLP12)
AT3G15356	0.39	1.48	1.11	1.1E-01	2.5E-07	1.7E-04	Legume lectin family protein (LEC)
AT4G22730	0.54	1.47	1.83	3.2E-02	4.6E-07	1.8E-09	Leucine-rich repeat protein kinase family protein
AT5G01540	0.01	1.43	2.68	9.8E-01	5.5E-07	5.2E-19	lectin receptor kinase a4.1 (LECRK62)
AT5G49770	0.15	1.39	1.26	5.6E-01	2.7E-07	9.0E-06	Leucine-rich repeat protein kinase family protein
AT5G44700	0.28	1.39	1.26	2.4E-01	2.6E-08	1.4E-06	Leucine-rich repeat transmembrane protein kinase (GSO2)
AT4G21400	0.49	1.39	0.88	1.6E-02	2.1E-12	1.7E-05	cysteine-rich RECEPTOR-like protein kinase 28 (CRK28)
AT1G70520	0.54	1.36	1.47	3.0E-03	8.8E-18	4.0E-20	cysteine-rich RECEPTOR-like protein kinase 2 (CRK2)
AT1G16110	0.54	1.32	0.78	2.5E-02	5.3E-07	3.0E-03	wall associated kinase-like 6 (WAKL6)
AT1G73165	-0.34	-1.38	-1.84	1.4E-01	2.3E-03	1.3E-03	CLAVATA3/ESR-RELATED 1 (CLE1)
AT4G14010	-0.83	-1.56	-1.22	2.1E-03	1.3E-07	5.8E-05	ralf-like 32 (RALFL32)
AT5G09978	-0.82	-1.75	-1.68	1.5E-03	1.3E-10	1.3E-09	elicitor peptide 7 precursor (PEP7)
AT3G19320	-0.24	-2.06	-1.86	2.8E-01	4.7E-14	6.5E-12	Leucine-rich repeat (LRR) family protein
AT3G29780	-0.72	-2.15	-1.51	8.7E-03	5.5E-08	7.2E-05	ralf-like 27 (RALFL27)

#### Transport

AT5G52710	-0.01	6.83	7.79	9.1E-01	3.9E-07	3.6E-08	Copper transport protein family
AT5G52760	-0.01	5.18	7.21	9.1E-01	3.9E-05	6.0E-07	Copper transport protein family (HIPPI4)
AT5G52700	-0.01	4.77	6.67	9.1E-01	7.6E-05	3.5E-06	Copper transport protein family
AT5G52720	-0.01	3.99	6.86	9.1E-01	2.2E-04	1.7E-06	Copper transport protein family
AT1G77380	0.80	3.97	3.93	3.7E-04	2.2E-87	2.0E-85	amino acid permease 3 (AAP3)
AT5G52680	-0.14	3.41	4.98	2.3E-01	1.2E-04	4.5E-06	Copper transport protein family
AT4G01830	0.17	3.01	1.83	5.3E-01	3.4E-12	2.0E-05	P-glycoprotein 5 (ABCB5)
AT1G09930	-0.06	2.97	4.10	6.1E-01	3.5E-04	1.5E-04	oligopeptide transporter 2 (OPT2)
AT5G52670	-0.47	2.89	4.00	2.7E-02	9.9E-09	1.5E-14	Copper transport protein family
AT4G13420	-0.10	2.84	4.03	4.0E-01	1.7E-04	1.9E-05	high affinity K <sup>+</sup> transporter 5 (POT5)
AT4G18197	0.26	2.68	2.51	2.8E-01	1.5E-07	2.3E-06	purine permease 7 (PUP7)
AT4G18205	0.37	2.45	1.70	1.5E-01	1.5E-09	2.1E-05	Nucleotide-sugar transporter family protein (PUP22)
AT4G21120	1.16	2.24	1.98	8.4E-05	1.8E-11	4.4E-09	amino acid transporter 1 (CAT1)
AT4G19680	0.43	1.88	1.83	3.8E-02	5.2E-20	6.7E-19	iron regulated transporter 2 (IRT2)
AT4G27730	0.53	1.80	1.71	1.8E-02	7.9E-16	3.9E-14	oligopeptide transporter 1 (OPT6)
AT3G13100	0.54	1.74	1.86	2.5E-02	2.3E-10	4.3E-11	multidrug resistance-associated protein 7 (ABCC7)
AT5G26690	0.10	1.63	1.56	6.6E-01	1.4E-03	4.1E-03	Heavy metal transport/detoxification superfamily protein (HIPPO2)
AT5G26340	0.33	1.60	1.34	3.0E-02	2.8E-32	1.5E-22	Major facilitator superfamily protein (STP13)
AT1G12950	0.11	1.52	1.59	5.0E-01	2.1E-31	3.8E-34	root hair specific 2 (DTX31)
AT4G27970	0.07	1.51	1.32	7.8E-01	1.7E-13	4.3E-10	SLAC1 homologue 2 (SLAH2)
AT3G07040	0.51	1.51	1.41	4.1E-02	4.4E-07	6.4E-06	NB-ARC domain-containing disease resistance protein (RPM1)
AT3G62150	0.16	1.51	1.36	5.2E-01	1.1E-08	8.1E-07	P-glycoprotein 21 (ABCB21)
AT2G04080	0.16	1.50	1.07	3.6E-01	3.6E-03	1.9E-02	MATE efflux family protein (DTX2)
AT4G35180	-0.08	1.46	1.75	7.8E-01	3.1E-06	1.6E-07	LYS/HIS transporter 7 (LHT7)



AT5G40780	0.62	1.45	1.54	9.3E-03	7.1E-09	3.3E-09	LYS/HIS transporter 1 (LHT1)
AT3G20660	0.62	1.44	0.91	9.0E-03	8.0E-09	3.1E-04	organic cation/carnitine transporter4 (OCT4)
AT1G62280	0.38	1.41	0.82	9.1E-02	5.3E-09	7.0E-04	SLAC1 homologue 1 (SLAH1)
AT4G23700	0.87	1.39	0.92	2.6E-05	1.4E-12	5.6E-06	cation/H+ exchanger 17 (CHX17)
AT1G13210	0.64	1.37	0.80	1.3E-02	6.0E-06	5.8E-03	autoinhibited Ca2+/ATPase II (ALA11)
AT5G01760	0.25	1.35	0.97	2.5E-01	3.0E-03	1.8E-02	ENTH/VHS/GAT family protein (TOL7)
AT5G64410	0.37	1.35	1.48	8.6E-03	3.4E-30	1.4E-35	oligopeptide transporter 4 (OPT4)
AT1G60050	0.17	1.35	2.75	3.6E-01	5.2E-03	7.5E-04	Nodulin MtN21 /EamA-like transporter family protein (UMAMIT35)
AT3G21080	-0.01	1.34	1.04	9.1E-01	7.0E-03	2.3E-02	ABC transporter-related
AT5G46050	0.14	1.32	0.69	5.5E-01	2.1E-10	1.1E-03	peptide transporter 3 (NPF5.2)
AT5G08040	-0.67	-1.34	-0.71	1.2E-02	1.8E-03	3.7E-02	mitochondrial import receptor subunit TOM5 homolog (TOM5)
AT3G48970	-0.48	-1.37	-1.56	5.3E-02	1.1E-03	1.2E-03	Heavy metal transport/detoxification superfamily protein (HIPP31)
AT4G23710	-0.88	-1.46	-0.79	2.5E-03	1.9E-05	1.1E-02	vacuolar ATP synthase subunit G2 (VHA-G2)
AT5G46600	-0.56	-1.63	-0.88	2.7E-02	7.3E-07	4.1E-03	Aluminium activated malate transporter protein (ALMT13)
AT4G35060	-0.83	-1.78	-1.30	1.9E-03	1.4E-09	1.3E-05	Heavy metal transport/detoxification superfamily protein (HIPP25)
AT2G39510	0.14	-3.35	-2.70	5.4E-01	1.2E-34	1.1E-24	nodulin MtN21 /EamA-like transporter family protein (UMAMIT14)

#### Transferases

AT1G01680	0.04	6.43	6.80	7.3E-01	2.1E-06	2.7E-06	plant U-box 54 (PUB54)
AT1G05675	0.16	2.72	3.63	4.2E-01	8.1E-05	1.0E-05	UDP-Glycosyltransferase superfamily protein (UGT74E1)
AT1G34520	0.10	2.05	1.58	4.4E-01	2.2E-03	1.1E-02	MBOAT (membrane bound O-acyl transferase) family protein
AT3G61210	0.48	1.68	0.95	6.1E-02	9.4E-06	6.6E-03	S-adenosyl-L-methionine-dependent methyltransferases superfamily protein
AT5G49690	0.87	1.45	1.57	1.5E-03	4.3E-07	1.8E-07	UDP-Glycosyltransferase superfamily protein (UGT91C1)
AT5G38200	-0.09	1.41	1.53	6.7E-01	4.6E-16	2.1E-18	Class I glutamine amidotransferase-like superfamily protein
AT5G42830	-0.06	1.33	1.93	7.8E-01	1.6E-15	9.4E-31	HXXXD-type acyl-transferase family protein
AT4G31310	-0.91	-1.34	-0.78	1.5E-03	2.6E-05	8.9E-03	AIG2-like (avirulence induced gene) family protein
AT5G02890	-0.37	-1.36	-1.73	4.8E-02	5.9E-13	1.3E-18	HXXXD-type acyl-transferase family protein
AT4G12545	-0.45	-1.41	-1.74	6.7E-02	2.0E-06	4.3E-08	Bifunctional inhibitor/lipid-transfer protein/seed storage 2S albumin superfamily protein
AT2G38920	-0.44	-1.43	-0.77	8.2E-02	1.3E-04	1.6E-02	SPX (SYG1/Pho81/XPR1) domain-containing protein / zinc finger (C3HC4-type RING finger) protein-related (RF178)
AT1G02950	-0.53	-1.49	-0.82	3.5E-02	1.5E-06	5.0E-03	glutathione S-transferase F4 (GSTF4)
AT4G12520	-0.34	-1.49	-1.44	9.0E-02	4.2E-13	6.8E-12	Bifunctional inhibitor/lipid-transfer protein/seed storage 2S albumin superfamily protein
AT4G22460	-0.01	-1.61	-1.34	9.6E-01	5.8E-24	8.0E-17	Bifunctional inhibitor/lipid-transfer protein/seed storage 2S albumin superfamily protein
AT1G48750	-0.84	-1.69	-1.35	2.9E-03	3.5E-07	6.6E-05	Bifunctional inhibitor/lipid-transfer protein/seed storage 2S albumin superfamily protein
AT3G29630	-0.52	-1.86	-1.40	1.2E-02	5.2E-19	2.1E-11	UDP-Glycosyltransferase superfamily protein (UGT79B4)
AT2G03370	-0.63	-2.15	-1.80	5.4E-03	9.5E-17	7.2E-13	Glycosyltransferase family 61 protein
AT5G46890	-0.01	-2.15	-2.10	9.7E-01	3.2E-29	1.4E-27	Bifunctional inhibitor/lipid-transfer protein/seed storage 2S albumin superfamily protein
AT4G12510	-0.34	-2.20	-1.72	1.8E-01	6.0E-07	5.6E-05	Bifunctional inhibitor/lipid-transfer protein/seed storage 2S albumin superfamily protein
AT5G46900	0.02	-2.39	-2.47	9.4E-01	6.7E-20	1.3E-20	Bifunctional inhibitor/lipid-transfer protein/seed storage 2S albumin superfamily protein
AT2G37870	-0.48	-2.81	-2.05	4.3E-02	4.0E-20	5.0E-12	Bifunctional inhibitor/lipid-transfer protein/seed storage 2S albumin superfamily protein
AT4G33550	-0.73	-2.91	-1.51	4.9E-03	7.1E-22	3.2E-07	Bifunctional inhibitor/lipid-transfer protein/seed storage 2S albumin superfamily protein

Regulation of transcription							
AT4G00130	-0.01	6.08	6.99	9.1E-01	5.0E-06	1.2E-06	DNA-binding storekeeper protein-related transcriptional regulator
AT4G18170	0.93	4.20	4.37	2.2E-03	1.2E-25	3.2E-27	WRKY DNA-binding protein 28 (WRKY28)
AT4G17980	0.14	3.94	5.98	2.3E-01	2.5E-04	2.9E-05	NAC domain containing protein 71 (ANAC71)
AT5G43175	-0.01	3.27	5.36	9.1E-01	5.5E-04	1.3E-04	basic helix-loop-helix (bHLH) DNA-binding superfamily protein (BHLH139)
AT5G24110	0.63	3.19	4.08	1.7E-02	2.2E-11	2.6E-17	WRKY DNA-binding protein 30 (WRKY30)
AT1G29860	0.03	3.03	4.95	9.1E-01	4.4E-06	2.7E-12	WRKY DNA-binding protein 71 (WRKY71)
AT5G01380	0.14	2.41	3.23	5.4E-01	1.7E-05	3.8E-07	Homeodomain-like superfamily protein (GT-3A)
AT4G14860	0.28	2.26	3.14	1.3E-01	6.5E-04	3.6E-04	ovate family protein 11 (OFP11)
AT1G32510	0.28	2.23	2.12	2.2E-01	3.5E-05	1.9E-04	NAC domain containing protein 11 (ANAC11)
AT2G28500	-0.02	2.20	3.56	9.5E-01	1.5E-04	6.4E-07	LOB domain-containing protein 11 (LBD11)
AT3G12977	0.93	1.84	1.61	9.7E-05	4.1E-15	1.6E-11	NAC (No Apical Meristem) domain transcriptional regulator superfamily protein
AT3G03660	0.31	1.80	1.98	2.2E-01	2.2E-05	1.8E-05	WUSCHEL related homeobox 11 (WOX11)
AT5G46590	0.14	1.70	1.31	5.8E-01	1.5E-11	5.4E-07	NAC domain containing protein 96 (ANAC96)
AT4G25410	-0.02	1.69	1.48	9.6E-01	1.1E-12	1.5E-09	basic helix-loop-helix (bHLH) DNA-binding superfamily protein (BHLH126)
AT5G07100	0.87	1.60	1.34	5.7E-04	2.1E-10	2.8E-07	WRKY DNA-binding protein 26 (WRKY26)
AT4G15690	0.12	1.55	1.81	3.5E-01	4.8E-03	8.5E-03	Thioredoxin superfamily protein (GRXS5)
AT2G40200	0.32	1.42	1.06	1.8E-01	9.7E-04	9.3E-03	basic helix-loop-helix (bHLH) DNA-binding superfamily protein (BHLH51)
AT3G09290	-0.50	-1.48	-1.21	3.5E-02	2.7E-07	3.3E-05	telomerase activator1 (TAC1)
AT1G65330	-0.11	-1.49	-0.86	-	3.5E-03	2.8E-02	MADS-box transcription factor family protein (PHE1)
AT5G50820	-0.54	-1.52	-1.28	3.4E-02	3.5E-06	1.5E-04	NAC domain containing protein 97 (ANAC97)
AT4G30410	-0.84	-1.64	-1.06	1.6E-03	1.2E-08	2.2E-04	sequence-specific DNA binding transcription factors (IBL1)
AT3G27360	-1.32	-1.88	-1.59	5.7E-04	8.9E-05	9.9E-04	Histone superfamily protein (HTR2)
AT3G49760	-0.44	-2.28	-1.29	8.0E-02	4.0E-10	1.4E-04	basic leucine-zipper 5 (BZIP5)
Response to nutrient levels or nutrient starvation							
AT4G25220	0.78	3.69	3.98	4.4E-03	7.9E-30	5.4E-34	root hair specific 15 (RHS15)
AT2G02990	-0.10	2.96	3.53	7.2E-01	1.1E-24	4.3E-34	ribonuclease 1 (RNS1)
AT1G13300	0.60	1.72	1.32	3.8E-03	2.7E-19	1.5E-11	myb-like transcription factor family protein (HRS1)
AT4G08620	0.22	1.51	1.21	4.0E-01	4.0E-05	1.3E-03	sulphate transporter 1;1 (SULTR1;1)
AT2G41240	-0.30	-1.34	-3.06	2.4E-01	3.9E-04	7.4E-08	basic helix-loop-helix protein 100 (BHLH100)
AT1G47400	-0.33	-1.48	-1.26	1.8E-01	4.2E-04	2.9E-03	Fe-uptake-inducing peptide 3 (FEP3)
AT3G56970	-0.42	-1.91	-2.53	9.7E-02	6.3E-07	1.6E-09	basic helix-loop-helix (bHLH) DNA-binding superfamily protein (ORG2)
AT5G24655	-0.64	-1.90	-0.39	1.5E-02	1.5E-04	1.3E-01	response to low sulfur 4 (LSU4)
AT3G49570	-0.73	-1.94	-1.71	7.9E-03	2.1E-07	6.5E-06	response to low sulfur 3 (LSU3)
AT3G49580	-0.70	-2.19	-2.34	9.9E-03	1.1E-08	4.9E-09	response to low sulfur 1 (LSU1)
AT5G66815	-0.67	-2.19	-1.66	1.1E-02	1.4E-09	2.8E-06	C-terminally encoded peptide 5 (CEP5)
AT1G47395	-0.78	-2.49	-2.31	6.0E-03	6.2E-09	1.2E-07	Fe-uptake-inducing peptide 2 (FEP2)
Other cellular processes							
AT1G56250	0.10	7.44	8.51	3.9E-01	4.2E-08	1.4E-09	phloem protein 2-B14 (PP2B14)
AT1G56240	-0.07	6.08	7.50	5.2E-01	1.9E-06	2.9E-08	phloem protein 2-B13 (PP2B13)
AT5G64870	0.20	4.81	5.71	2.9E-01	4.8E-08	3.6E-10	SPFH/Band 7/PHB domain-containing membrane-associated protein family (FLOT3)
AT2G02320	-0.01	4.00	5.60	9.1E-01	2.3E-04	7.9E-05	phloem protein 2-B7 (PP2B7)
AT4G30430	0.24	3.83	5.83	5.9E-02	3.0E-04	5.3E-05	tetraspanin9 (TET9)

AT5G25260	0.50	3.11	2.46	3.9E-02	9.2E-08	3.0E-05	SPFH/Band 7/PHB domain-containing membrane-associated protein family (FLOT2)
AT5G39120	-0.01	2.62	4.83	9.2E-01	1.1E-03	2.1E-04	RmlC-like cupins superfamily protein
AT1G25240	0.02	2.61	2.21	9.5E-01	1.6E-06	6.6E-05	ENTH/VHS/GAT family protein
AT5G39130	0.04	2.35	5.32	7.3E-01	1.6E-03	1.3E-04	RmlC-like cupins superfamily protein
AT2G22880	0.04	1.97	2.28	9.0E-01	3.0E-07	1.9E-08	VQ motif-containing protein
AT1G59850	0.45	1.83	2.02	5.3E-02	5.5E-14	1.7E-16	ARM repeat superfamily protein (TOR1L5)
AT4G37220	0.12	1.79	2.78	6.7E-01	2.2E-05	5.9E-09	Cold acclimation protein WCOR413 family
AT2G02340	-0.07	1.52	3.87	5.9E-01	4.4E-03	2.2E-04	phloem protein 2-B8 (PP2B8)
AT5G38940	0.02	1.48	1.27	9.6E-01	7.2E-11	5.7E-08	RmlC-like cupins superfamily protein
AT5G24100	-0.37	-1.38	-0.97	3.8E-02	4.0E-16	2.3E-08	Leucine-rich repeat protein kinase family protein
AT1G73630	-0.76	-1.40	-0.71	3.8E-03	1.5E-06	8.7E-03	EF hand calcium-binding protein family (CML26)
AT3G44590	-0.89	-1.43	-1.00	3.0E-03	1.8E-04	6.1E-03	60S acidic ribosomal protein family (RPP2D)
AT4G02810	-0.17	-1.43	-1.00	5.0E-01	3.5E-07	2.8E-04	Protein of unknown function (DUF3049)
AT5G45010	-0.92	-1.43	-0.80	2.5E-03	1.6E-04	1.7E-02	DSS1 homolog on chromosome V (DSS1V)
AT4G26230	-1.00	-1.45	-0.74	1.0E-03	3.2E-05	1.7E-02	Ribosomal protein L31e family protein (RPL31B)
AT2G34160	-0.94	-1.47	-0.84	1.9E-03	4.8E-05	1.1E-02	Alba DNA/RNA-binding protein
AT5G04750	-1.09	-1.47	-0.76	2.0E-04	2.5E-06	8.4E-03	F1FO-ATPase inhibitor protein, putative
AT3G56020	-1.13	-1.58	-0.87	7.0E-04	8.0E-05	1.3E-02	Ribosomal protein L41 family (RPL41G)
AT5G09520	-0.12	-1.73	-1.47	5.1E-01	5.6E-30	9.1E-22	hydroxyproline-rich glycoprotein family protein (PELPK2)
AT1G78230	0.01	-1.74	-1.57	9.7E-01	2.4E-08	8.2E-07	Outer arm dynein light chain 1 protein
AT3G08520	-1.15	-1.78	-0.98	6.0E-04	1.7E-05	7.3E-03	Ribosomal protein L41 family (RPL41G)
AT4G23496	-0.56	-4.74	-4.34	3.3E-02	8.5E-18	7.3E-16	SPIRAL1-like5 (SP1L5)

#### Other metabolic processes

AT1G68290	0.07	6.47	7.19	5.8E-01	3.9E-07	8.3E-08	endonuclease 2 (ENDO2)
AT2G02010	0.44	5.51	6.60	6.8E-02	1.2E-22	6.0E-32	glutamate decarboxylase 4 (GAD4)
AT3G28580	-0.04	5.49	6.69	8.8E-01	2.4E-22	1.7E-32	P-loop containing nucleoside triphosphate hydrolases superfamily protein
AT5G40000	-0.13	5.44	6.43	4.8E-01	1.9E-14	1.9E-19	P-loop containing nucleoside triphosphate hydrolases superfamily protein
AT3G57460	-0.01	4.64	3.39	9.1E-01	1.0E-04	1.8E-03	catalytics;metal ion binding
AT5G39190	-0.07	3.92	5.51	5.2E-01	2.0E-04	4.5E-05	germin-like protein 2 (GLP5A)
AT1G09932	0.24	3.76	4.38	3.3E-01	8.9E-52	1.8E-70	Phosphoglycerate mutase family protein
AT3G28600	0.04	3.73	4.43	8.7E-01	1.2E-06	7.7E-08	P-loop containing nucleoside triphosphate hydrolases superfamily protein
AT1G08080	-0.01	3.71	6.43	9.1E-01	3.2E-04	7.2E-06	alpha carbonic anhydrase 7 (ACA7)
AT3G60420	0.21	3.32	3.37	3.2E-01	1.6E-06	6.3E-06	Phosphoglycerate mutase family protein
AT2G39400	0.11	2.65	2.16	7.0E-01	8.4E-17	2.8E-11	alpha/beta-Hydrolases superfamily protein
AT3G28540	0.27	2.47	5.16	1.4E-01	3.4E-04	1.4E-08	P-loop containing nucleoside triphosphate hydrolases superfamily protein
AT5G43590	0.33	2.46	1.78	1.9E-01	8.3E-08	7.9E-05	Acyl transferase/acyl hydrolase/lysophospholipase superfamily protein
AT2G35990	-0.09	2.46	3.33	6.8E-01	4.8E-05	2.4E-06	Putative lysine decarboxylase family protein (LOG2)
AT3G28510	0.27	2.44	4.21	3.0E-01	4.3E-11	6.7E-30	P-loop containing nucleoside triphosphate hydrolases superfamily protein
AT5G65158	0.02	2.34	2.31	9.2E-01	9.4E-04	3.2E-03	Lipase/lipoxygenase. PLAT/LH2 family protein (PLAT13)
AT5G41080	1.31	2.26	1.30	3.8E-13	2.4E-35	1.7E-12	PLC-like phosphodiesterases superfamily protein (GDPG2)
AT4G14365	0.12	2.21	2.88	6.5E-01	1.6E-14	4.2E-23	XB3 ortholog 4 in Arabidopsis thaliana (XBAT34)
AT2G28210	0.36	2.09	2.46	1.2E-01	1.0E-16	3.3E-22	alpha carbonic anhydrase 2 (ATACA2)
AT3G29670	-0.09	2.07	1.22	7.6E-01	1.2E-13	1.8E-05	HXXXD-type acyl-transferase family protein (PMAT2)

AT3G55840	0.29	2.05	2.32	2.5E-01	1.7E-06	4.6E-07	Hs1pro-1 protein (HSPRO1)
AT5G10380	0.00	1.65	1.52	9.9E-01	3.3E-04	1.5E-03	RING/U-box superfamily protein (ATL55)
AT4G22470	0.75	1.65	0.94	3.1E-03	1.7E-10	3.3E-04	protease inhibitor/seed storage/lipid transfer protein (LTP) family protein
AT2G30660	0.00	1.57	2.96	1.0E+00	6.9E-04	1.5E-06	ATP-dependent caseinolytic (Clp) protease/crotonase family protein
AT1G23390	0.48	1.57	1.25	3.4E-02	7.8E-11	5.7E-07	Kelch repeat-containing F-box family protein
AT4G32300	0.74	1.57	1.52	2.5E-03	2.3E-10	2.1E-09	S-domain-2 5 (SD25)
AT3G21500	0.18	1.52	2.13	3.0E-01	3.7E-03	3.0E-03	1-deoxy-D-xylulose 5-phosphate synthase 1 (DXPS1)
AT5G57190	0.32	1.51	0.99	1.3E-01	4.1E-14	2.6E-06	phosphatidylserine decarboxylase 2 (PSD2)
AT5G64000	0.24	1.51	2.43	3.4E-01	1.9E-07	8.8E-16	Inositol monophosphatase family protein (SAL2)
AT5G65140	0.55	1.48	1.46	1.1E-02	1.6E-12	1.3E-11	Haloacid dehalogenase-like hydrolase (HAD) superfamily protein (TPPJ)
AT5G58830	0.16	1.43	2.67	-	5.8E-03	3.7E-03	Subtilisin-like serine endopeptidase family protein (SBT4.8)
AT1G33700	0.49	1.43	1.32	2.7E-02	3.3E-10	2.2E-08	Beta-glucosidase. GBA2 type family protein
AT3G18930	0.30	1.41	1.19	2.3E-01	5.2E-06	2.3E-04	RING/U-box superfamily protein (ATL65)
AT3G47800	0.54	1.35	1.00	9.6E-03	3.2E-11	2.0E-06	Galactose mutarotase-like superfamily protein
AT5G11320	0.19	1.34	2.83	1.1E-01	6.9E-03	3.1E-03	Flavin-binding monooxygenase family protein (YUC4)
AT2G38600	0.13	-1.47	-2.12	6.2E-01	3.5E-07	5.3E-11	HAD superfamily. subfamily IIIB acid phosphatase
AT3G57010	-0.50	-1.50	-1.00	2.6E-02	3.0E-10	4.2E-05	Calcium-dependent phosphotriesterase superfamily protein (SSL8)
AT5G58770	-0.77	-1.51	-1.39	4.7E-03	2.4E-06	2.8E-05	Undecaprenyl pyrophosphate synthetase family protein
AT5G62480	-0.58	-1.55	-1.24	1.2E-02	1.3E-10	5.2E-07	glutathione S-transferase tau 9 (GSTU9)
AT4G38690	-0.44	-1.62	-1.09	7.3E-02	1.0E-06	7.3E-04	PLC-like phosphodiesterases superfamily protein
AT2G23000	-0.25	-1.67	-1.26	2.2E-01	7.5E-14	1.7E-08	serine carboxypeptidase-like 10 (SCPL10)
AT1G66460	-0.22	-1.80	-1.47	3.8E-01	2.7E-07	2.6E-05	Protein kinase superfamily protein
AT4G39000	0.03	-2.67	-2.35	9.2E-01	1.4E-06	2.0E-05	glycosyl hydrolase 9B17 (GH9B17)

#### Other hormonal responses

AT5G13320	0.03	5.29	4.28	9.0E-01	4.4E-17	4.2E-11	Auxin-responsive GH3 family protein (PBS3)
AT1G30040	0.32	2.33	2.67	1.9E-01	1.5E-17	4.3E-22	gibberellin 2-oxidase (GA2OX2)
AT4G08950	0.46	1.86	2.41	3.1E-02	5.0E-18	9.0E-29	Phosphate-responsive 1 family protein (EXO)
AT2G39980	-0.43	1.81	2.39	6.0E-02	6.0E-15	2.2E-24	HXXXD-type acyl-transferase family protein
AT3G55720	0.18	1.49	1.74	4.3E-01	7.3E-12	3.7E-15	Protein of unknown function (DUF620)
AT4G37390	0.10	1.41	0.98	6.8E-01	7.4E-12	4.0E-06	Auxin-responsive GH3 family protein (YDK1)
AT5G20820	-0.04	1.40	1.48	8.9E-01	1.6E-03	2.7E-03	SAUR-like auxin-responsive protein family (SAUR76)
AT1G75590	-0.51	-1.43	-1.20	3.9E-02	2.0E-06	1.1E-04	SAUR-like auxin-responsive protein family
AT5G55250	-0.38	-1.43	-1.79	8.5E-02	2.2E-09	7.0E-13	IAA carboxymethyltransferase 1 (IAMT1)
AT1G72430	-0.30	-1.47	-0.91	6.4E-02	8.5E-23	1.5E-09	SAUR-like auxin-responsive protein family (SAUR78)
AT2G16580	-0.64	-1.78	-1.04	7.8E-03	1.6E-11	5.9E-05	SAUR-like auxin-responsive protein family
AT1G75750	-0.29	-1.86	-1.44	2.4E-02	9.4E-62	2.0E-37	GAST1 protein homolog 1 (GASA1)
AT4G12550	-0.35	-2.19	-2.64	1.6E-01	1.4E-10	1.3E-13	Auxin-Induced in Root cultures 1 (AIR1)

#### Other signalling processes

AT5G66640	0.10	3.75	4.56	6.6E-01	1.3E-07	8.1E-10	DA1-related protein 3 (DAR3)
AT3G56380	0.04	2.47	3.91	7.3E-01	1.4E-03	1.0E-03	response regulator 17 (ARR17)
AT2G32140	0.31	2.40	3.08	2.0E-01	9.1E-07	5.3E-09	transmembrane receptors
AT2G20142	0.12	2.23	2.66	6.7E-01	3.6E-15	1.3E-20	Toll-Interleukin-Resistance (TIR) domain family protein
AT5G18350	0.15	2.09	2.26	3.8E-01	1.2E-03	2.7E-03	Disease resistance protein (TIR-NBS-LRR class) family
AT4G17660	0.04	2.04	4.99	7.3E-01	2.3E-03	2.5E-04	Protein kinase superfamily protein (PBL20)

AT5G41750	0.57	1.95	2.21	1.2E-02	2.9E-17	2.4E-21	Disease resistance protein (TIR-NBS-LRR class) family
AT5G61560	0.39	1.65	1.98	1.1E-01	9.1E-09	2.9E-11	U-box domain-containing protein kinase family protein
AT5G38344	0.71	1.65	0.93	7.9E-03	1.0E-03	2.0E-02	Toll-Interleukin-Resistance (TIR) domain family protein
AT2G44080	0.07	1.64	2.38	8.0E-01	4.1E-11	8.8E-21	ARGOS-like (ARL)
AT4G11170	0.43	1.61	2.11	9.0E-02	5.0E-05	2.2E-06	Disease resistance protein (TIR-NBS-LRR class) family
AT1G72900	0.07	1.56	1.66	7.9E-01	6.5E-14	3.0E-15	Toll-Interleukin-Resistance (TIR) domain-containing protein
AT2G26530	-0.03	1.55	1.33	9.1E-01	3.7E-13	1.7E-09	Protein of unknown function (DUF1645)
AT2G19330	-0.01	1.45	3.59	9.1E-01	5.7E-03	1.5E-03	plant intracellular ras group-related LRR 6 (PIRL6)
AT1G63750	0.11	1.44	1.38	6.9E-01	2.9E-06	2.0E-05	Disease resistance protein (TIR-NBS-LRR class) family
AT1G79860	0.06	1.36	1.65	8.3E-01	1.4E-07	8.3E-10	RHO guanyl-nucleotide exchange factor 12 (ROPGEF12)
AT4G23510	0.12	1.33	1.17	5.0E-01	9.4E-19	4.1E-14	Disease resistance protein (TIR-NBS-LRR class) family
AT4G40010	-0.41	-1.35	-0.78	2.1E-02	1.4E-15	4.0E-06	SNF1-related protein kinase 2.7 (SRK2F)
AT2G22000	-0.80	-1.42	-0.87	3.2E-03	2.5E-06	2.9E-03	elicitor peptide 6 precursor (PEP6)
AT5G44610	-0.89	-1.53	-0.94	2.8E-03	4.8E-05	6.9E-03	microtubule-associated protein 18 (PCAP2)
AT5G45810	-0.72	-1.77	-0.92	3.2E-03	1.1E-11	2.8E-04	CBL-interacting protein kinase 19 (CIPK19)
AT1G01380	-0.61	-2.37	-1.15	2.2E-02	9.5E-07	3.6E-03	Homeodomain-like superfamily protein (ETC1)

#### Unclassified or unknown

AT1G65500	0.18	6.09	7.85	1.4E-01	4.1E-06	2.8E-08	NA
AT5G22530	-0.01	4.70	7.03	9.1E-01	8.7E-05	1.2E-06	NA
AT5G60350	0.33	4.40	5.29	8.2E-02	3.6E-07	5.9E-09	NA
AT2G24600	0.08	4.35	4.30	7.7E-01	7.0E-50	2.7E-48	Ankyrin repeat family protein
AT3G48640	0.04	4.35	2.51	7.3E-01	1.7E-04	4.3E-03	NA
AT5G54710	-0.11	3.96	4.65	6.9E-01	7.5E-18	1.0E-23	Ankyrin repeat family protein
AT5G22520	-0.01	3.52	5.84	9.1E-01	4.3E-04	5.3E-05	NA
AT5G52390	0.74	3.47	4.24	8.1E-03	3.6E-18	4.0E-26	PAR1 protein
AT5G54720	0.09	3.44	4.60	5.8E-01	1.2E-04	2.2E-05	Ankyrin repeat family protein
AT4G16008	0.26	3.39	3.08	2.1E-01	7.8E-07	2.1E-05	NA
AT4G20160	0.19	2.90	3.14	3.9E-01	7.1E-06	9.3E-06	NA
AT2G33850	0.36	2.67	3.07	1.5E-01	1.6E-18	1.3E-23	NA
AT3G46110	0.02	2.65	3.18	9.5E-01	1.3E-10	5.2E-14	Domain of unknown function (DUF966)
AT3G02840	-0.09	2.63	4.49	6.5E-01	5.2E-05	2.9E-09	ARM repeat superfamily protein
AT1G27020	0.36	2.62	2.32	1.3E-01	8.1E-18	5.4E-14	NA
AT1G75160	0.19	2.60	2.86	4.7E-01	2.1E-10	1.2E-11	Protein of unknown function (DUF620)
AT1G10340	0.42	2.49	2.38	6.5E-02	8.5E-25	3.5E-22	Ankyrin repeat family protein
AT3G01175	0.86	2.43	1.69	3.7E-03	5.3E-08	1.1E-04	Protein of unknown function (DUF1666)
AT1G59865	0.13	2.15	4.01	2.5E-01	2.0E-03	9.7E-04	NA
AT1G19380	-0.18	2.11	2.42	4.7E-01	2.6E-14	7.9E-18	Protein of unknown function (DUF1195)
AT2G05510	0.09	1.96	2.38	7.1E-01	7.5E-18	6.4E-25	Glycine-rich protein family
AT1G01453	0.29	1.70	2.33	2.5E-01	1.9E-08	1.7E-13	NA
AT2G18690	0.46	1.52	1.91	9.3E-03	2.9E-22	5.8E-34	NA
AT1G13480	0.17	1.50	1.91	5.1E-01	1.2E-08	2.8E-12	Protein of unknown function (DUF1262)
AT1G78460	0.23	1.49	1.14	3.7E-01	7.6E-06	8.3E-04	SOUL heme-binding family protein
AT1G33840	-0.40	1.47	1.86	1.1E-01	3.7E-05	1.9E-06	Protein of unknown function (DUF567)
AT5G36925	-0.53	1.46	2.07	3.1E-02	8.7E-05	9.3E-07	NA
AT3G43930	0.39	1.45	2.34	1.2E-01	3.5E-04	2.0E-06	BRCT domain-containing DNA repair protein

AT5G48190	0.14	1.38	2.57	5.0E-01	3.2E-03	2.6E-04	Domain of unknown function (DUF23)
AT5G57340	0.39	1.37	1.22	6.2E-02	3.8E-11	1.2E-08	NA
AT5G44568	0.05	1.35	2.20	8.4E-01	3.5E-03	7.6E-04	NA
AT4G30460	-0.37	-1.32	-1.38	2.5E-02	1.8E-18	1.6E-19	glycine-rich protein
AT4G13615	-0.89	-1.34	-0.78	3.0E-03	2.5E-04	1.7E-02	Uncharacterised protein family SERF
AT1G47410	-0.69	-1.35	-0.81	7.4E-03	3.6E-06	3.8E-03	NA
AT2G24040	-0.56	-1.35	-0.72	2.3E-02	3.2E-06	8.0E-03	Low temperature and salt responsive protein family
AT1G36622	-0.78	-1.35	-0.93	5.3E-03	8.3E-05	4.8E-03	NA
AT4G30670	-0.51	-1.35	-0.71	2.0E-02	2.0E-09	1.2E-03	Putative membrane lipoprotein
AT5G54145	-0.85	-1.35	-1.01	3.3E-03	9.4E-05	3.2E-03	NA
AT1G72510	-0.79	-1.35	-1.37	4.9E-03	8.0E-05	1.9E-04	Protein of unknown function (DUF1677)
AT1G58070	-0.36	-1.35	-1.15	9.8E-02	1.5E-08	3.0E-06	NA
AT1G47820	-0.94	-1.36	-1.10	2.0E-03	2.1E-04	2.8E-03	NA
AT5G08050	-0.65	-1.36	-0.69	1.3E-03	4.3E-13	1.7E-04	Protein of unknown function (DUF1118)
AT3G15357	-0.85	-1.36	-0.87	3.8E-03	3.0E-04	1.2E-02	NA
AT3G62400	-0.84	-1.36	-0.89	3.9E-03	1.7E-04	8.8E-03	NA
AT4G39235	-0.64	-1.37	-0.80	1.5E-02	1.1E-03	2.3E-02	NA
AT1G31935	-0.86	-1.38	-1.16	1.9E-03	4.6E-06	2.0E-04	other RNA
AT3G55420	-0.50	-1.38	-0.96	4.9E-03	1.8E-17	4.9E-09	NA
AT2G37530	-0.54	-1.38	-0.82	2.9E-02	4.0E-06	4.0E-03	NA
AT1G67785	-1.01	-1.39	-0.74	9.7E-04	7.3E-05	1.8E-02	NA
AT1G18290	-0.52	-1.41	-0.77	3.6E-02	6.5E-06	7.3E-03	NA
AT2G41170	-0.41	-1.42	-1.26	4.0E-02	1.3E-12	7.2E-10	F-box family protein
AT4G30450	-0.47	-1.42	-1.35	4.0E-02	3.4E-08	4.4E-07	glycine-rich protein
AT5G25240	-0.22	-1.43	-2.93	3.8E-01	1.2E-03	1.8E-05	NA
AT2G34585	-0.85	-1.44	-1.13	3.1E-03	2.1E-05	9.7E-04	NA
AT5G07322	-0.83	-1.45	-1.08	2.9E-03	6.1E-06	8.5E-04	other RNA
AT1G68300	-0.82	-1.45	-1.09	4.4E-03	5.8E-05	2.3E-03	Adenine nucleotide $\alpha$ -hydrolases-like superfamily protein
AT4G14380	-0.57	-1.45	-0.77	2.6E-02	1.1E-05	9.2E-03	NA
AT3G41761	-0.65	-1.45	-0.94	1.2E-02	1.7E-03	1.8E-02	other RNA
AT1G75335	-0.94	-1.46	-0.82	2.7E-03	6.0E-04	2.2E-02	NA
AT3G07470	-0.77	-1.46	-0.86	3.6E-03	4.8E-07	2.3E-03	Protein of unknown function. DUF538
AT3G57062	-0.75	-1.46	-1.11	4.8E-03	1.7E-06	3.6E-04	NA
AT1G29520	-0.59	-1.47	-1.08	1.7E-02	4.0E-07	2.5E-04	AWPM-19-like family protein
AT2G30930	-0.92	-1.50	-1.08	6.7E-04	1.3E-07	1.9E-04	NA
AT3G11600	-0.70	-1.50	-1.26	7.1E-03	7.7E-07	5.9E-05	NA
AT1G12080	-0.96	-1.51	-0.88	5.5E-04	3.9E-07	2.4E-03	Vacuolar calcium-binding protein-related
AT5G18150	-0.88	-1.52	-1.05	3.1E-03	7.2E-05	4.1E-03	Methyltransferase-related protein
AT1G11700	-0.84	-1.52	-0.95	1.7E-03	9.9E-08	7.6E-04	Protein of unknown function. DUF584
AT2G45860	-1.28	-1.52	-0.97	1.8E-04	5.5E-05	5.9E-03	NA
AT3G52790	-0.67	-1.56	-0.92	1.1E-02	2.5E-06	3.4E-03	peptidoglycan-binding LysM domain-containing protein
AT3G22540	-0.38	-1.56	-1.25	1.3E-01	1.1E-04	1.7E-03	Protein of unknown function (DUF1677)
AT5G57785	-0.63	-1.58	-1.06	1.5E-02	4.9E-07	7.1E-04	NA
AT4G01140	-0.15	-1.58	-1.21	3.7E-01	8.4E-26	7.5E-16	Protein of unknown function (DUF1191)
AT3G52920	-0.64	-1.62	-1.02	6.6E-03	5.2E-11	4.7E-05	Family of unknown function (DUF662)

AT4G22666	-0.81	-1.66	-0.84	2.8E-04	9.0E-15	8.7E-05	Bifunctional inhibitor/lipid-transfer protein/seed storage 2S albumin superfamily protein
AT4G23870	-0.77	-1.69	-0.90	3.8E-03	2.5E-08	1.8E-03	NA
AT5G62150	-1.09	-1.71	-0.88	7.4E-05	8.2E-09	1.6E-03	peptidoglycan-binding LysM domain-containing protein
AT5G66985	-0.88	-1.71	-1.20	2.0E-03	2.5E-07	2.9E-04	NA
AT2G27740	-0.69	-1.73	-1.18	1.1E-02	4.1E-06	1.1E-03	Family of unknown function (DUF662)
AT2G17300	-0.49	-1.74	-0.97	1.8E-02	1.8E-15	8.0E-06	NA
AT4G24130	-0.66	-1.75	-1.39	6.0E-03	1.4E-11	1.5E-07	Protein of unknown function. DUF538
AT2G41312	-0.35	-1.76	-2.08	1.6E-01	4.3E-05	1.6E-05	other RNA
AT4G37700	-0.62	-1.77	-1.98	1.4E-02	4.6E-09	3.2E-10	NA
AT1G79075	-0.99	-1.77	-1.00	2.2E-03	1.4E-04	1.1E-02	other RNA
AT5G26720	-0.87	-1.78	-0.92	3.3E-03	7.6E-06	7.7E-03	NA
AT1G61667	-0.77	-1.82	-1.21	5.5E-03	3.2E-07	5.1E-04	Protein of unknown function. DUF538
AT1G28815	-0.70	-1.83	-1.40	1.0E-02	7.3E-07	1.3E-04	NA
AT1G75550	-0.32	-1.87	-1.21	2.0E-01	9.3E-07	6.9E-04	glycine-rich protein
AT2G28410	-0.57	-1.93	-1.53	1.6E-02	1.4E-12	1.8E-08	NA
AT3G18450	-0.18	-1.95	-1.48	4.4E-01	5.0E-14	5.3E-09	PLAC8 family protein
AT3G19030	-0.83	-1.97	-1.37	4.4E-03	4.2E-06	8.3E-04	NA
AT1G17090	-0.69	-1.98	-1.14	1.0E-02	9.8E-08	1.0E-03	NA
AT5G06190	-0.51	-1.99	-1.07	4.6E-02	1.7E-05	6.0E-03	NA
AT3G51750	-0.76	-1.99	-1.25	6.2E-03	4.2E-07	7.1E-04	NA
AT3G53980	-0.46	-2.03	-1.02	2.5E-02	4.8E-23	1.1E-06	Bifunctional inhibitor/lipid-transfer protein/seed storage 2S albumin superfamily protein
AT4G09890	-1.08	-2.05	-1.51	8.8E-05	2.3E-11	5.1E-07	Protein of unknown function (DUF3511)
AT3G59370	-0.96	-2.12	-1.64	1.5E-03	7.9E-08	2.9E-05	Vacuolar calcium-binding protein-related
AT1G04778	-0.53	-2.14	-1.37	3.6E-02	3.0E-05	2.4E-03	NA
AT4G18422	-0.49	-2.23	-1.39	4.0E-02	1.2E-04	4.3E-03	NA
AT1G02700	-0.25	-2.35	-2.75	2.9E-01	8.6E-05	9.3E-05	NA
AT1G11740	-0.54	-2.38	-1.88	3.8E-02	5.5E-07	5.1E-05	ankyrin repeat family protein
AT3G59930	-0.41	-2.50	-2.11	1.0E-01	4.2E-11	3.1E-08	NA
AT2G36295	-0.90	-2.67	-1.67	2.5E-03	1.7E-10	2.4E-05	NA
AT3G48940	-0.68	-2.77	-2.28	9.3E-03	4.3E-14	2.2E-10	Remorin family protein
AT1G23110	-0.19	-2.88	-2.81	4.3E-01	2.9E-05	1.1E-04	NA
AT4G11020	-0.50	-4.04	-3.68	4.8E-02	3.0E-09	2.6E-08	NA
AT5G33355	-0.26	-6.47	-4.85	3.0E-01	3.4E-30	2.9E-30	Defensin-like (DEFL) family protein

<sup>A</sup> Differentially expressed genes (DEG) in 5-do *kor1-4* roots relative to WT samples. Each genotype was first normalized to the WT (cutoff: logFC =  $\pm 1.32$ , p-value < 0.01), and *kor1-4* DEGs were classified as JA-independent if their value remained at least 50% unchanged in *kor1-4 aos* with respect to *kor1-4*. DEGs are organized by gene ontology (GO) functional classes and implemented manually. In many cases genes may fall into more than one category. DEGs highlighted in magenta were selected for further analyses.

<sup>B</sup> Logarithmic Fold Change of the means of two biological replicated experiments. A negative number indicates down regulated genes.

<sup>C</sup> False Discovery rate (FDR) corrected p-value in comparison to WT.

NA: not annotated

**Table S4: List of oligonucleotides used in this study.**

Name	5' → 3' sequence	Objective
<b>Primers for cloning</b>		
MST-093	TTCCCCCCCCGGgatgatgctctctgataaagc	<i>KOR1</i> promoter of 2132bp flanked by <i>XmaI</i> and <i>KpnI</i> sites
MST-094	CGGGGTACCaagtctttgggagctgcaa	
MST-151	TTCCCCCCCCGGGatcgacagatctcaatctc	<i>ESMD1</i> promoter of 2168 bp flanked by <i>XmaI</i> and <i>KpnI</i> sites
MST-152	CGGGGTACCGgacgaggacatccttgga	
MST-096	AAAAGCAGGCTGatgtacggaagagatccatg	<i>KOR1</i> CDS* of 1866 bp flanked by attB1 and attB2 sites
MST-095	GAAAGCTGGGTTtcaaggtttccatggtgctg	
MST-098	GTACAAAGTGGTTatgtacggaagagatccatg	<i>KOR1</i> CDS* of 1866 bp flanked by attB2r and attB3 sites
MST-097	GTATAATAAAGTTGtcaaggtttccatggtgctg	
MST-150	AAAAGCAGGCTGatgctagcgaagaatcgg	<i>ESMD1</i> CDS no* of 1587 bp flanked by attB1 and attB2 sites
MST-149	GAAAGCTGGGTTggtggcaggaggtggtctc	
<b>Primers for genotyping</b>		
KOR2.F	ttgatttaactcgccttg	<i>kor1-4</i> and WT amplicons of 513bp, digested with <i>HinfI</i> result in WT (459 bp + 54 bp) and <i>kor1-4</i> (289 bp + 170 bp + 54 bp)
KOR1.R	tcacacccaaatccttcttacc	
KOR.3F	tgcatgagagagtaattctgg	<i>kor1-5</i> and WT amplicons of 516bp, digested with <i>NcoI</i> result in WT (516 bp) and <i>kor1-5</i> (401 bp + 115 bp)
327A.1R	agatgctgaagccagagcag	
MST-226	gtgggttaatgcttagaggaatg	<i>esmd1-1</i> and WT amplicons of 439bp, digested with <i>ApeKI</i> result in WT (439 bp) and <i>esmd1-1</i> (269 bp + 170 bp)
MST-227	ccgatgttgattgtcaagag	
MST-143	tctcctgttgcattttgatgg	<i>esmd1-3</i> and WT amplicons of 491 bp, digested with <i>HaeIII</i> result in WT (290 bp + 107 bp + 94 bp) and <i>esmd1-3</i> (384 bp + 107 bp)
MST-144	tctggaacaacaccaggaa	
DG070	tcgtttccaattgggttt	<i>the1-1</i> and WT amplicons of 208 bp, digested with <i>HinfI</i> result in WT (184 bp + 14 bp + 10 bp) and <i>the1-1</i> (153 bp + 31 bp + 14 bp + 10 bp)
DG071	tggagtgaatctggaacaaga	
MST-321	cgccatctttgttcaacaatcagatcc	<i>ein2-1</i> and WT amplicons of 149 bp, digested with <i>BsrBI</i> result in WT (113 bp + 36 bp) and <i>ein2-1</i> (149 bp)
MST-322	ccagaggaaagagagttggatgtaaagtactctaccgct	
MST-362	gagaacaactcctggatttcgtaactac	<i>dek1-4</i> and WT amplicons of 181 bp, digested with <i>DdeI</i> result in WT (181 bp) and <i>dek1-4</i> (151 bp + 30 bp)
MST-363	gtcaagaaccatttcacatgaaatctctc	
aos.F	gggagcgattgagaaaatgg	For genotyping of <i>aos</i> . Amplifies 449 bp in WT and ca. 200 bp in <i>aos</i> .
aos.R	cgacgagaaattaacggagc	
P337	cgggcctaacttttggtgatgatgct	For genotyping of <i>JGP</i> insertions 1 & 2
P26	ggtttcgcctcatgtgttgagca	
P83	ttttgctttctgcagcaactg	For genotyping of <i>JGP</i> insertion 1 together with P26. Amplifies 533 bp in WT and 721 bp in <i>JGP</i> .
P84	ttttgctttctgcagcaactg	
P85	gagcaggcgggtggtactgg	For genotyping of <i>JGP</i> insertion 2 together with P26. Amplifies 784 bp in WT and 551 bp in <i>JGP</i> .
P86	caaaagcaaaggccagttga	
KOR.KO1.F	tagctgccatattttcgg	<i>kor1-6</i> (SALK_075812)
KOR.KO1.R	cagtcagacgaagatcttgc	



**Table S4 (continued)**

<b>Name</b>	<b>5' → 3' sequence</b>	<b>Objective</b>
DG-054	tctccctgcatcattcaaac	For genotyping of <i>rop2-12</i> (WiscDsLox441B8)
DG-055	ttgtttgtttccgatcttg	
MST-112	tttatcaacgccgttgaaatc	For genotyping of <i>eru-2</i> (SALK_o83442)
MST-113	atthtgtgtcgggtctgtag	
DGo17	gcttcttggtcattctgctg	For genotyping of <i>wak1-1</i> (SALK_107175)
DGo18	ttgtgctgacaagatgtgacc	
DGo58	cctgcgaaaatgagtgaagag	For genotyping of <i>wak2-12</i> (SALK_12_D05C)
DGo59	attcattgatgtctggccaag	
DGo56	atgtgacttgggagttcgtg	For genotyping of <i>herk1-1</i> (SALK_o08043)
DGo57	tgcagatttcacgtctctgtg	
DGo23	actggtcacaatgctactgcc	For genotyping of <i>herk2-1</i> (SALK_105055)
DGo24	cttaccaaaccctccaactcc	
DGo68	gatttccggctttgtaggag	For genotyping of <i>mri-2</i> (GK_820D05)
DGo69	atgaaaatcatcccatgatcg	
DGo62	attcactcccaagtccaatc	For genotyping of <i>rlp44-3</i> (SAIL_596_E12)
DGo63	aatggatggcatgattaggatc	
MST-134	tcgaacgaatcagtttatcg	For genotyping of <i>mik1</i> (SALK_095005)
MST-135	aatggccttgagattaatgg	
MST-126	aacggatcgattccttctga	For genotyping of <i>mik2-1</i> (SALK_061769)
MST-127	ttttgcctgatagccgattc	
MST-335	ttgtttgagtgacagggac	For genotyping of <i>sub-9</i> (SAIL_1158_D09)
MST-336	gatgttgtgtggttcagtg	
MST-329	gctgcacgagtactgcttttc	For genotyping of <i>mca1-3</i> (SALK_206846)
MST-330	tctctatcaacaatgccgtcc	
MST-345	gttggtttctgggttaagcc	For genotyping of <i>msl10-1</i> (SALK_076254)
MST-346	tacttgagtaaccgggtgctg	
MST-331	taaccattcagttgggttcg	For genotyping of <i>osca1-2</i> (SAIL_607_F09)
MST-332	attggacaacaacgagttgg	
MST-333	aaagacgaagctgcagaactg	For genotyping of <i>osca1-4</i> (SAIL_1172_D02)
MST-334	tcgcatgccaatagtcttag	
MST-276	ctgaagatcagctttgtccg	For genotyping of <i>tch3-2</i> (SALK_090554)
MST-277	ttgtggaatccctcagatcag	
MST-274	gacactaacgacaaaactccg	For genotyping of <i>aca13</i> (SAIL_878_Bo6)
MST-275	tctgccgtgaaaatgttatc	
MST-268	accaggtgtgtgtgaaccttc	For genotyping of <i>per52-1</i> (SALK_081257)
MST-269	agtagggagcttacggctacg	
MST-270	tatgcagtatgcaacgagacg	For genotyping of <i>xth26-2</i> (SALK_055758)
MST-271	ctgaccagtcgcatttcttag	
MST-278	agtacacaccacaccagagc	For genotyping of <i>ext12</i> (SAIL_1249_F11)
MST-279	agatgtatggtggtggaggag	
MST-304	gtctaaccgtcgtgcactagc	For genotyping of <i>pll6-1</i> (GK_033D05)
MST-305	aaacgtctttggacgttctcc	
SALK.LBb1.3	atthtggcatttcggaac	For genotyping of all SALK T-DNA insertion lines

**Table S4 (continued)**

Name	5' → 3' sequence	Objective
GABI.LB	atattgaccatcatactcattgc	For genotyping of all GK T-DNA insertion lines
SAIL.LB3	tagcatctgaatttcataaccaatctcgatacac	For genotyping of all SAIL T-DNA insertion lines
WiscDsLox.LB	aacgtccgcaatgtgttattaagtgtgc	For genotyping of all WiscDsLox T-DNA insertion lines
<b>Primers for qRT-PCR</b>		
JAZ10.qF	atcccgatttctccggtcca	— <i>JAZ10</i> (At5g13220) 222 bp fragment
JAZ10.qR	actttctccttgcatgggaaga	
UBQ.qF	cagtctgtgtgtagagctatcatagcat	— <i>UBC21</i> (At5g25760) 83 bp fragment
UBQ.qR	agaagattccctgagtcgcagtt	
MST-258	gggtgaccaaattcagatgctgag	— <i>JOX3</i> (At3g55970) 124 bp fragment
MST-259	aggaacattgcccttgggttg	
VSP2F	catcatagagctcgggattgaaccc	— <i>VSP2</i> (At5g24770) 111 bp fragment
VSP2R	agatgcttcagtaggtcacgc	
MST-147	tttgctgcttcgacgcac	— <i>PDF1.2</i> (At5g44420) 144 bp fragment
MST-148	gcatgatccatgtttggctcc	

Note, for genotyping of T-DNA lines, sizes of amplification products are given by T-DNA express (<http://signal.salk.edu/cgi-bin/tdnaexpress>). Three primer reactions will target a bigger WT amplicon (forward + reverse primer) and a smaller mutant amplicon (T-DNA left border primer + forward or reverse primer).

## Acknowledgements

This work was only possible with the support of many special people, for which I would like to thank all of you very much!

First of all I want to thank Dr. Debora Gasperini who gave me the opportunity to conduct my thesis on this fascinating and challenging topic. Debora, I am especially thankful for all the discussions we had over the years that enabled me to develop confidence in my own work, evolve my critical thinking skills, and establish my own ideas in order to drive this project forward. You dedicated a lot of time in improving my scientific and non-scientific skills. I truly benefited from your knowledge and drive and now feel more than ready for whatever task may come during my professional life.

Next I want to thank Prof. Dr. Bettina Hause for accompanying and supporting me as my mentor during this thesis. My scientific life as well as my first steps in the Jasmonate world started in your lab and definitely contributed to my current development. My PhD work truly benefited from having you as another Jasmonate and cell biology expert onboard. I also want to thank you for being my University supervisor and for reviewing my thesis.

I furthermore want to thank Prof. Dr. Marcel Quint and Dr. Marco Trujillo for their advice during the early stages of my PhD project. Our discussions led me to see my project from different perspectives and to develop and test new hypotheses. Also I want to thank Marcel Quint for reviewing my thesis - I am looking forward to your opinion on my findings.

I am also glad that Prof. Dr. Elizabeth Haswell accepted to review my thesis. I gained a lot of scientific input from your publications and I very much look forward to discuss my project with you.

Now I want to thank a number of people that contributed practically to my thesis. A big thank you goes out to Dr. Rene' Dreos for performing the RNA-seq and NGS analyses. Also thank you for getting me started with the PlantSeg software. Thank you also to Dr. Cătălin Voiniciuc for performing the cell wall analyses according to my needs and for all the fruitful discussions that led me to advance my project. Next I want to thank Hagen Stellmach for performing the oxylipin profiling and sharing his enormous knowledge in microscopy techniques. I am also thankful to my lab colleagues Dr. Mukesh Meena and Marlene Zimmer. Mukesh, thank you for helping me with the big number of sections and segmentations. It was a struggle to get this pipeline established but we did it! Marlene, thank you for all your support and technical

help, especially your superb grafting skills. I don't know how far I would have come without you. You are the best!

Since I now have started with my lab colleagues - I want to thank all of you (Marlene, Adina, Andi, Mukesh, Yunjing and Ronny). Thanks for all the scientific and non-scientific discussions. Thanks for sharing your thoughts during joyful and difficult times. I am really glad having you as friends and colleagues around me!

I also don't want to forget all of my colleagues from the MSV department and around the IPB. Thank you for all the critical discussions during my presentations, the pleasant atmosphere, and so many hours of fun during work. Especially I want to mention my fellow PhD student and friend Micha. We always shared the ups and downs of our project and it was nice to see both of us advance during all those years! Of course I will always remember our dominant quiz duel victory against our bosses 😊

Ein großes Dankeschön auch an all die helfenden Hände am IPB, welche ein großartiges Arbeitsumfeld ermöglichten. Ein besonderer Dank geht hierbei an Eberhard Warkus für die Konstruktion der Bioassay-Boxen.

Ich bedanke mich bei all meinen Freunden für Ihre Unterstützung und die vielen gemeinsamen Erlebnisse. Es tat immer gut in Eurer Gegenwart einmal Abschalten zu können.

Ein großes Dankeschön geht an meine gesamte Familie, die mich immer auf jede erdenkliche Weise unterstützt hat. Ein besonderer Dank gilt meiner lieben Frau Mandy und unseren beiden tollen Kinder. Ich weiß, ihr habt in den letzten Jahren wegen mir auf viele Dinge verzichten müssen, und es hat mir oft sehr wehgetan für euch. Umso glücklicher bin ich, in dieser Phase dennoch so viel Unterstützung und Liebe von euch erfahren zu haben.

Thank You! Dankeschön!

## Curriculum vitae

Name: Stefan Mielke

Nationality: German

Day of birth: 13.11.1987

Place of birth: Forst (Lausitz), Germany

### *Education and research experience*

---

*02/2016 – present*

#### **Doctorate**

Faculty of Natural Science – Biological Sciences Martin-Luther University of Halle-Wittenberg  
Dissertation thesis  
**“Interplay between plant cell walls and Jasmonate production”**

Jasmonate signalling group

Supervisor: Dr. Debora Gasperini

Leibniz Institute of Plant Biochemistry, Halle (Saale)

*09/2015 – 01/2016*

#### **Research assistant**

Protein recognition and degradation group

Supervisor: Prof. Dr. Nico Dissmeyer

Leibniz Institute of Plant Biochemistry, Halle (Saale)

*08/2013 – 01/2014*

#### **Internship**

Protein recognition and degradation group

Supervisor: Prof. Dr. Nico Dissmeyer

Leibniz Institute of Plant Biochemistry, Halle (Saale)

*10/2012 – 03/2015*

#### **Master student**

Martin-Luther University of Halle-Wittenberg

Graduation: Master of Science, final grade 1.3

*08/2010 – 04/2013*

#### **Internship and follow-up Research assistant**

Jasmonate function and mycorrhiza group

Supervisor: Prof. Dr. Bettina Hause

Leibniz Institute of Plant Biochemistry, Halle (Saale)

*10/2007 – 09/2012*

#### **Bachelor student**

Martin-Luther University of Halle-Wittenberg

Graduation: Bachelor of Science, final grade 2.8

*08/2000 – 07/2007*

#### **High-School education**

Friedrich-Ludwig-Jahn Gymnasium Forst

Graduation: Abitur, final grade 1.9

## Conference attendances

---

- "*9<sup>th</sup> International PhD school Plant Development*", Zelllingen-Retzbach, GER, 05. - 07.10.2016; Winner of Best Poster Award
- "*Plant Science student conference 2017*", Halle (Saale), GER, 06. - 09.06.2017
- "*International Plant Immunity Symposium 2018*", Göttingen, GER, 14. - 15.06.2018
- "*29<sup>th</sup> International Conference on Arabidopsis Research* ", Turku, FIN, 25. - 29.06.2018
- "*Regulatory Oxylipins conference*", Ghent, BEL, 01. - 04.04.2019; Winner of Best Poster Award
- "*Plant Science Student Conference*", Halle (Saale), GER, 18. - 21.06.2019

Halle (Saale), April 2021

Stefan Mielke

## List of publications

- **Mielke S**, Zimmer M, Meena MK, Dreos R, Stellmach H, Hause B, Voiniciuc C, Gasperini D (2021). Jasmonate biosynthesis arising from altered cell walls is prompted by turgor-driven mechanical compression *Science Advances* 7, doi: 10.1126/sciadv.abf0356
  - Preprint at [bioRxiv](#)
  - Recommended by [Faculty Opinions](#)
- **Mielke S**, Gasperini D (2020). Plant-Insect bioassay for testing Arabidopsis resistance to the generalist herbivore *Spodoptera littoralis*. *Methods in Molecular Biology* 2085, 69-78, doi: 10.1007/978-1-0716-0142-6\_5.
- Schulze A, Zimmer M, **Mielke S**, Stellmach H, Melnyk CW, Hause B, Gasperini D (2019). Wound-induced shoot-to-root relocation of JA-Ile precursors coordinates Arabidopsis growth. *Molecular Plant* 12, 1383-1394, doi: 10.1016/j.molp.2019.05.013.
  - Preprint at [bioRxiv](#)
- **Mielke S**, Gasperini D (2019). Interplay between plant cell walls and jasmonate production. *Plant & Cell Physiology* 60, 2629-2637, doi: 10.1093/pcp/pcz119.
  - Editor's Choice [highlight](#)
- Faden F, **Mielke S**, Dissmeyer N (2019). Modulating protein stability to switch toxic protein function on and off in living cells. *Plant Physiology* 179, 929-942, doi: 10.1104/pp.18.01215.
  - Preprint at [bioRxiv](#)
- Faden F, Ramezani T, **Mielke S**, Almudil I, Nairz K, Froehlich MS, Höckendorff J, Brandt W, Hoehenwarter W, Dohmen RJ, Schnittger A, Dissmeyer N (2016). Phenotypes on demand via switchable target protein degradation in multicellular organisms. *Nature Communications* 7, 12202, doi: 10.1038/ncomms12202.
- Faden F, **Mielke S**, Lange D, Dissmeyer N (2014). Generic tools for conditionally altering protein abundance and phenotypes on demand. *Biological Chemistry* 395, 737-762, doi: 10.1515/hsz-2014-0160.

## Eidesstattliche Erklärung (Statutory declaration)

Hiermit erkläre ich an Eides statt, dass ich mich mit der vorliegenden wissenschaftlichen Arbeit erstmals um die Erlangung des Doktorgrades bewerbe, die Arbeit selbstständig und ohne fremde Hilfe verfasst, nur die angegebenen Quellen und Hilfsmittel genutzt und die den benutzten Werken wörtlich oder inhaltlich entnommenen Stellen als solche kenntlich gemacht habe.

Halle (Saale), den \_\_\_\_\_

\_\_\_\_\_  
Stefan Mielke